

# Self-Propelled Particles with Inhomogeneous Activity

Dissertation  
zur Erlangung des akademischen Grades  
Doctor rerum naturalium (Dr. rer. Nat.)

Vorgelegt  
dem Bereich Mathematik und Naturwissenschaften  
Fakultät Physik  
Institut für Theoretische Physik  
der Technischen Universität Dresden

Von  
Hidde Derk Vuijk  
Geboren am 11-09-1989 in Naarden

Gutachter:  
Prof. Dr. Jens-Uwe Sommer  
Prof. Dr. Joseph Brader  
Dr. Abhinav Sharma

Eingereicht am  
17-08-2022



# Summary

Movement is an essential feature of life. It allows organisms to move towards a more favorable environment and to search for food. There are many biological systems that fall under the category *active matter*, from molecular motors walking on microtubules inside cells to flocks of birds. What these systems have in common is that each of its constituents converts energy into directed motion, that is, they propel themselves forward. Besides the many biological examples, there is also synthetic active matter, these are self-propelled particles made in a laboratory. These are typically colloidal sized particles that can propel themselves forward by self-phoresis. In this work the focus is on the low Reynolds number regime, meaning that the typical size of the constituents is less than a few micrometers. The models that are used to describe such active matter can be viewed as nonequilibrium extensions to Brownian motion (the thermal motion of small particles dissolved in a fluid).

In many systems the self-propulsion speed (activity) is not homogeneous in space: the particles swim faster in some areas than in others. The main topic of this dissertation is how a single active particle, or a few active particles tied together by a potential, behave in such systems. It is known that a single active particle without any steering mechanism spends most time in the regions where it moves slowly, or in other words, they spend most time in regions where they are less active. However, it is shown in Chapter 5 that, even though they spend most time in the less active regions, dynamical properties, such as the probability to move towards the more active regions is higher than moving towards the less active regions.

Furthermore, when the active particles are connected to a passive Brownian "cargo" particle, chained together to form a colloidal sized polymer (Chapter 6), or fixed to another active particle (Chapter 7), the resulting active dimers or polymers either accumulate in the high activity regions or the low activity regions, depending on the friction of the cargo particle, the number of monomers in the polymer, or the relative orientation of

active particles.

Lastly, when the activity is both time- and space-dependent, a steady drift of active particles can be induced, without any coupling between the self-propulsion direction and the gradient in the activity (Chapter 8). This phenomenon can be used to position the particles depending on their size.

Part I introduces the basic physics and mathematical models of active matter. The new research is shown in Part II. While dissertation focuses on inhomogeneous active matter, other publications completed as part of my doctoral research, mainly on odd-diffusion and liquid-state theory, are listed on page 205.



# Acknowledgement

I would like to thank Abhi for his guidance, and his unbounded enthusiasm and curiosity. I am grateful professor Jens-Uwe Sommer for the opportunity to work at the IPF, and for the many discussion on active matter. I wish to thank professor Holger Merlitz for our collaboration. Many thanks to Iman. I learned a lot from our discussions on diffusion with Lorentz force. I would like to thank Erik Kalz. It was a great joy working together and exploring the physics of odd-diffusion. Furthermore, many thanks to Sophie for our collaboration on active colloidal molecules. Finally, I would also like to thank all my colleagues for discussion in the PhD seminars.



# Contents

<b>I</b>	<b>Introduction</b>	<b>1</b>
<b>1</b>	<b>Brownian Motion</b>	<b>3</b>
1.1	Brownian motion . . . . .	4
1.1.1	The Overdamped Limit . . . . .	12
1.2	Stochastic Differential Equations . . . . .	13
1.2.1	The Fokker-Planck Equation . . . . .	14
1.3	Examples . . . . .	18
1.3.1	Diffusion in a Potential . . . . .	18
1.3.2	Diffusion in Inhomogeneous Media . . . . .	19
1.3.3	Rotational Brownian Motion . . . . .	21
1.A	Appendix . . . . .	25
<b>2</b>	<b>Active matter</b>	<b>29</b>
2.1	Biological Active Matter . . . . .	30
2.1.1	Propulsion by Beating Flagella . . . . .	32
2.1.2	Run-and-Tumble Motion . . . . .	36
2.2	Synthetic Active Matter . . . . .	37
2.2.1	Self-Diffusiophoresis . . . . .	37
2.3	Inhomogeneous Activity . . . . .	45
2.3.1	Inhomogeneous Activity in Biological Systems . . . . .	45
2.3.2	Inhomogeneous Activity in Synthetic Systems . . . . .	46
2.4	Active Colloidal Molecules and Polymers . . . . .	46
<b>3</b>	<b>Modeling Active Matter</b>	<b>49</b>
3.1	Models . . . . .	50
3.1.1	Run-And-Tumble Particles . . . . .	50
3.1.2	Active Brownian Particles . . . . .	52
3.1.3	Active Ornstein-Uhlenbeck Particles . . . . .	53
3.2	Basic Results . . . . .	54
3.2.1	Enhanced Diffusion . . . . .	54
3.2.2	Coarse-Grained Fokker-Planck Equation . . . . .	56

3.2.3	Wall Accumulation . . . . .	62
3.2.4	Sedimentation . . . . .	64
3.2.5	Inhomogeneous Activity . . . . .	66
<b>II</b>	<b>Inhomogeneous Activity</b>	<b>71</b>
<b>4</b>	<b>Introduction</b>	<b>73</b>
<b>5</b>	<b>pseudochemotaxis</b>	<b>77</b>
5.1	Model and Theory . . . . .	79
5.2	Target Finding Probability . . . . .	82
5.3	Mean First Passage Time to Target . . . . .	83
5.4	Pseudochemotaxis . . . . .	85
5.5	Conclusion . . . . .	86
5.A	Appendix . . . . .	88
5.A.1	The Backwards Fokker-Planck Equation . . . . .	88
5.A.2	Mean First Passage Time . . . . .	90
5.A.3	Exit Probability . . . . .	90
5.A.4	MFTP and Exit Probability . . . . .	91
<b>6</b>	<b>Cargo-Carrying Particles</b>	<b>93</b>
6.1	The Model . . . . .	95
6.2	Chemotaxis of Active Dimers . . . . .	97
6.3	Other Potentials . . . . .	100
6.3.1	Run-and-Tumble Dimer in One Dimension . . . . .	100
6.4	Chemotaxis of Active Polymers . . . . .	103
6.5	Discussion . . . . .	104
6.A	Appendix . . . . .	106
6.A.1	Coarse Graining The Active-Passive Dimer . . . . .	106
6.A.2	The Active-Passive Dimer Model . . . . .	107
6.A.3	Eliminating the Orientational Degrees of Freedom . . . . .	108
6.A.4	Elimination of the Internal Degree of Freedom . . . . .	110
6.A.5	The Born-Oppenheimer Approximation . . . . .	116
6.A.6	Average Position of the Dimer . . . . .	120
6.A.7	Comparison to Active Temperature . . . . .	121
6.A.8	Run-and-Tumble Dimer in One Dimension . . . . .	123
6.A.9	Coarse Graining the RTP Dimer . . . . .	125
6.A.10	Numerical Solution . . . . .	128

<b>7</b>	<b>Active Colloidal Molecules</b>	<b>129</b>
7.1	The Model . . . . .	130
7.2	Results and Discussion . . . . .	132
7.A	Appendix . . . . .	139
7.A.1	Active Dimer Model . . . . .	139
7.A.2	Small Gradient Approximation . . . . .	140
7.A.3	Odd Diffusion . . . . .	144
7.A.4	Steady State . . . . .	144
7.A.5	Torque . . . . .	146
7.A.6	Mapping to Experimental Dimer . . . . .	147
<b>8</b>	<b>Time-Varying Activity Fields</b>	<b>149</b>
8.1	The Model . . . . .	150
8.2	Polarization . . . . .	151
8.3	Density . . . . .	152
8.4	Drift Velocity . . . . .	154
8.5	Confined Particles . . . . .	156
8.6	Conclusion . . . . .	157
8.A	Appendix: Linear-Response Theory . . . . .	158
8.A.1	Polarization . . . . .	159
8.A.2	Density . . . . .	162
<b>III</b>	<b>Appendix</b>	<b>165</b>
<b>A</b>	<b>Hydrodynamics</b>	<b>167</b>
A.1	The Navier-Stokes Equation . . . . .	167
A.2	The Stokes Equation . . . . .	169
A.3	Friction of a Rotating Sphere . . . . .	170
A.4	Friction of a Translating Sphere . . . . .	171
A.5	Friction of a Rod . . . . .	174
A.6	Lorentz's Reciprocal Theorem . . . . .	176
	<b>Bibliography</b>	<b>178</b>
	<b>List of Publications</b>	<b>205</b>
	<b>Eidesstattliche Erklärung</b>	<b>207</b>

**Part I**  
**Introduction**



# **Chapter 1**

## **Brownian Motion**



In 1828, the botanist Robert Brown observed with a microscope the irregular motion of dissolved granules from pollen grains. He was not the first to observe this (the first was Ingen-Housz [1]); however, he was the first to systematically investigate its origin. Initially he thought the irregular motion was due to the organic nature of the granules. He found, however, that this motion was not limited to organic substances. With this observation, Brown showed that this motion is not only of interest to biologists, but also to physicists. Besides showing that Brownian motion is not limited to organic molecules, Brown disproved that the motion he observed was due to other physical processes, such as the evaporation of the fluid.

What follows is a short history of the theory of Brownian motion. This serves as an introduction to the mathematical models used to describe Brownian motion and forms the basis of models later in this work. Only those methods on which later models are build are explained; therefore, many important theoretical contributions (in particular those of M. Smoluchowski [2, 3]) are omitted.

## 1.1 Historical Development of the Theory of Brownian Motion

### Fick's Laws

If the solute in an ideal solution is inhomogeneously distributed, the solute diffuses in such a way as to decrease the inhomogeneity. Fick's first law states that the flux due to this diffusion is proportional to the gradient of the density [4]:

$$\mathbf{J}(\mathbf{r}, t) = -D\nabla\rho(\mathbf{r}, t), \quad (1.1)$$

where the proportionality constant  $D$  is called the diffusion constant. The flux is the amount of solute moving through a unit area per unit time.

If the solute is locally conserved, the density obeys a continuity equation [4]:

$$\partial_t\rho(\mathbf{r}, t) = -\nabla \cdot \mathbf{J}(\mathbf{r}, t). \quad (1.2)$$

This equation is also known as Fick's second law. Using the divergence theorem, one can show that this equation ensures local particle conservation because the change in particle number at location  $\mathbf{r}$  is equal to the net flow out of the infinitesimal volume centered at  $\mathbf{r}$ . Combining Fick's first

and second laws gives

$$\partial_t \rho(\mathbf{r}, t) = D \nabla^2 \rho(\mathbf{r}, t), \quad (1.3)$$

which is called the diffusion equation.

### Einstein's theory of Brownian motion

The first explanation of Brownian motion came from Einstein [5]. What follows is a short summary of his theory based on his original article [5] and a later, more didactic article [6] (see Ref. [7] for English translations).

In the classical theory of thermodynamics (that is, before the atomistic theory of matter was accepted), the free energy of a system consisting of a number of large suspended bodies in a fluid does not depend on the positions of the suspended bodies. Therefore, according to this theory, the suspended bodies do not exert an osmotic pressure on a membrane that is only permeable to the fluid. Einstein realized that in contrast to the classical theory of thermodynamics, according to the molecular kinetic theory of heat [5]

" ... unterscheidet sich ein gelöstes Molekül von einem suspendierten Körper *lediglich* durch die Größe, und man sieht nicht ein, warum einer Anzahl suspendierter Körper nicht derselbe osmotische Druck entsprechen sollte, wie der nämlichen Anzahl gelöster Moleküle. Man wird anzunehmen habe, daß die suspendierten Körper infolge der Molekularbewegung der Flüssigkeit eine wenn auch sehr langsame ungeordnete Bewegung in der Flüssigkeit ausführen ..."<sup>1</sup>

In other words, suspended bodies exert the same osmotic pressure as dissolved molecules, and because of this they must perform irregular motion due to the motion of the fluid molecules.

The osmotic pressure of an ideal solution of  $N$  particles in a volume  $V$  is given by Van 't Hoff's law  $\Pi = T\rho$ , where  $\Pi$  is the osmotic pressure,  $T$  is the temperature in units such that the Boltzmann constant is unity<sup>2</sup> and  $\rho = N/V$  is the density of Brownian particles. When there is

---

<sup>1</sup>" ... a dissolved molecule differs from a suspended body only in size, and one cannot see why a number of suspended bodies would not exert the same osmotic pressure as the same number of dissolved molecules. One must take for granted that as a result of the molecular movement of the fluid, the suspended body must move irregularly, albeit very slowly... "

<sup>2</sup>Temperature then has units of energy. Room temperature ( $\approx 300\text{K}$ ) corresponds to  $T_{\text{room}} = 1.4 \times 10^{-23} \times 300 \approx 4 \times 10^{-21}\text{J}$ .

a gradient in the osmotic pressure (due to a gradient in the density) the corresponding thermodynamic force density is  $\nabla\Pi = -T\nabla\rho$ . This force is balanced by the frictional force on the Brownian particle. The frictional force is proportional to the velocity of the particle and can be written as  $\gamma\mathbf{v}$ , where  $\mathbf{v}$  is the velocity and  $\gamma$  the friction constant of the particle. The force balance equation is  $\gamma\mathbf{v}\rho = -T\nabla\rho$ . The flux of particles is equal to  $\mathbf{v}\rho$ , which, according to Fick's law (Eq. 1.1), is equal to  $-D\nabla\rho$ . Substituting this for  $\mathbf{v}\rho$  in the force balance equation gives  $-\gamma D\nabla\rho = -T\nabla\rho$ . This gives for the diffusion constant

$$D = \frac{T}{\gamma}. \quad (1.4)$$

For a spherical particle the friction constant is given by Stokes' law:  $\gamma = 6\pi a\eta_s$ , where  $a$  is the radius of the particle and  $\eta_s$  is the dynamic viscosity of the surrounding fluid [8] (see App. A.4 for a derivation). Together with the previous equation for the diffusion constant, this gives the Stokes-Einstein relation:

$$D = \frac{T}{6\pi a\eta_s}. \quad (1.5)$$

Subsequently, Einstein related this macroscopic description to the irregular movement of the Brownian particle. For simplicity, only one spatial dimension is considered. Because he assumed that the Brownian particles are independent, the probability density of a single particle is  $p(x, t) = \rho(x, t)/N$ . Then he considers a time interval that is small compared to the time between observations of the particle, but large enough such that the displacements in each time interval are independent. This means that the time interval should be longer than the velocity autocorrelation time of the particle. If  $\phi(\Delta)$  is the probability that the particle displaces  $\Delta$  in a time interval  $\tau$ , then

$$p(x, t + \tau) = \int_{-\infty}^{\infty} d\Delta \phi(\Delta) p(x + \Delta, t). \quad (1.6)$$

Because the time interval  $\tau$  and the displacement are small, one can use a

Taylor expansion for the probability on both sides:

$$\begin{aligned}
 p(x, t) + \partial_t p(x, t)\tau &= p(x, t) \int_{-\infty}^{\infty} d\Delta \phi(\Delta) \\
 &+ \partial_x p(x, t) \int_{-\infty}^{\infty} d\Delta \phi(\Delta)\Delta \\
 &+ \frac{1}{2} \partial_x^2 p(x, t) \int_{-\infty}^{\infty} d\Delta \phi(\Delta)\Delta^2. \quad (1.7)
 \end{aligned}$$

Because the particle must make some displacement, the first integral is unity. The second integral is zero because a displacement in the positive and negative direction are equally likely, and therefore  $\phi(\Delta) = \phi(-\Delta)$ . Collecting the remaining terms of the previous equation, and multiplying by  $N$  gives

$$\partial_t \rho(x, t)\tau = \left[ \frac{1}{2\tau} \int_{-\infty}^{\infty} d\Delta \phi(\Delta)\Delta^2 \right] \partial_x^2 \rho(x, t). \quad (1.8)$$

Comparing this with the diffusion equation (Eq. 1.1) shows that

$$D = \frac{1}{2\tau} \int_{-\infty}^{\infty} d\Delta \phi(\Delta)\Delta^2. \quad (1.9)$$

This relates the diffusion constant to  $\phi(\Delta)$ , which is determined by microscopic dynamics of the Brownian particle.

From this equation one can deduce the corresponding equation for higher dimensions. Because the displacements in each dimension is independent, the equation for the time evolution of  $\rho(\mathbf{r}, t)$  in  $d$  dimensions is

$$\partial_t \rho(\mathbf{r}, t) = \sum_{i=1}^d \partial_{x_i}^2 \rho(\mathbf{r}, t) = D \nabla^2 \rho(\mathbf{r}, t), \quad (1.10)$$

which is just the diffusion equation of Fick's second law in Eq. 1.1.

The fundamental solution to the diffusion equation is readily obtained using Fourier transformation methods. When the initial density is a delta distribution at the origin, the solution is

$$\rho(\mathbf{r}, t) = \frac{e^{-\frac{\mathbf{r}^2}{4Dt}}}{(4\pi Dt)^{\frac{d}{2}}}, \quad (1.11)$$

where  $d$  is the number of spatial dimensions.

From the solution to the diffusion equation one can find the average and mean squared displacement:

$$\langle \mathbf{r} \rangle = \int d\mathbf{r} \mathbf{r} \rho(\mathbf{r}, t) = 0, \quad (1.12)$$

$$\langle \mathbf{r}^2 \rangle = \int d\mathbf{r} \mathbf{r}^2 \rho(\mathbf{r}, t) = 2dDt. \quad (1.13)$$

This shows that taking many small steps in random directions (a random walk) gets you nowhere on average, that is, your average end point is your starting point; however, the typical traveled distance (the mean squared displacement) grows in time:

$$\sqrt{\langle \mathbf{r}^2 \rangle} = \sqrt{2dDt} \propto \sqrt{t}. \quad (1.14)$$

That the mean squared displacement grows as  $\sqrt{t}$  is typical for diffusive processes.

One can use the Stokes-Einstein relation (Eq. 1.5) to calculate estimate the order of magnitude of the diffusion constant for a colloid. A colloid has a size of about  $0.1 \mu m$ , at room temperature  $T \approx 4 \times 10^{-21} J$ , and the viscosity of water is  $1 mPa \cdot s$ . This gives for the diffusion constant  $D \approx 2 \times 10^{-11} m^2/s$ . The typical distance a colloid moves in a second is  $\sqrt{\langle \mathbf{r}^2 \rangle} = \sqrt{6D} \approx 10^{-5} m$ , so it moves about 100 times its own size per second.

On the other hand, a granular particle with a typical size of  $1 mm$  diffuses very little. Its diffusion constant is about  $D \approx 2 \times 10^{-15} m^2/s$ . The typical distance it diffuses in a second is approximately  $\sqrt{6D} \approx 10^{-7} m$ , which is  $10^{-4}$  times its own size per second. This shows that diffusion (that is, thermal motion) becomes less important when the length scale increases.

### Langevin's theory of Brownian motion

A few years after Einstein's theory of Brownian motion, Paul Langevin derived the same results, but using a completely different method, which is, in his own words, "infinitely more simple"[9]<sup>3</sup>. His method is based on Newton's second law of motion, according to which the acceleration of the Brownian particle is governed by the forces acting on it:

$$m \partial_t^2 x(t) = F_{fluid}, \quad (1.15)$$

---

<sup>3</sup>See Ref. [10] for an English translation of Langevin's paper.

where  $m$  is the mass of the Brownian particle, and  $F_{fluid}$  is the force of the surrounding fluid on the particle. This force accounts for the friction force,  $-\gamma\partial_t x$ , which is the average of the fluid force. In addition to this, there is a fluctuating force, with zero average, on the particle due to the discrete nature of the fluid. Indicating the fluctuating force by  $\zeta(t)$ , the equation of motion becomes

$$m\partial_t^2 x(t) = -\gamma\partial_t x + \zeta. \quad (1.16)$$

Multiplying this equation by  $x$  and using  $x\partial_t x = \partial_t x^2/2$ , and  $x\partial_t^2 x = \partial_t^2 x^2/2 - (\partial_t x)^2$ , this becomes

$$\frac{1}{2}m\partial_t^2 x^2 - m(\partial_t x)^2 = -\frac{1}{2}\gamma\partial_t x^2 + x\zeta. \quad (1.17)$$

This is an equation for the motion of a single particle. For many noninteracting dissolved particles, one can take an ensemble average over the noise, indicated by  $\langle \cdot \rangle$ . According to Langevin, the average noise term,  $x\zeta$ , is zero because of the irregularity of the fluctuating force  $\zeta$ . Using the equipartition theorem,  $m\langle(\partial_t x)^2\rangle = T$ , and defining  $z = \partial_t\langle x^2\rangle$ , the equation becomes

$$\frac{1}{2}m\partial_t z - T = -\frac{1}{2}\gamma z. \quad (1.18)$$

The solution to this equation is

$$z(t) = 2\frac{T}{\gamma} + Ce^{-t/\tau}, \quad (1.19)$$

where  $C$  is a constant, and  $\tau = m/\gamma$ . For a colloid this time scale is of the order of  $10^{-8}s$ .<sup>4</sup> The time scales of interest for the mean squared displacement are much larger than this, so the second term of the previous equation can be ignored. Using  $z(t) = \partial_t\langle x^2\rangle$  and integrating once more, gives for the mean square displacement

$$\langle x^2 \rangle = 2\frac{T}{\gamma}t, \quad (1.20)$$

---

<sup>4</sup>For a spherical colloid of radius  $a$  the friction is given by Stokes law (Eq. A.30)  $\gamma = 6\pi a\eta_s$ . The mass of a colloid is its volume,  $4\pi a^3/3$ , times its mass density. The mass density of a colloid is about twice that of water:  $\rho_{colloid} \approx 2 \times 10^3 kg m^{-3}$ . The typical size of a colloid is of the order of  $a \approx 10^{-7}m$ , and the viscosity of water is  $\eta_s \approx 10^{-3}Pa s$ . With this the time scale becomes  $\tau = m/\gamma = (4\pi a^3\rho_{colloid}/3)/(6\pi a\eta_s) \approx 5 \times 10^{-9} s$ .

where it is assumed the particle started at  $x = 0$ . By comparison with Eq. 1.13, one finds the same diffusion constant as with Einsteins method  $D = \frac{T}{\gamma}$ .

### Ornstein and Uhlenbeck's theory

Ornstein and Uhlenbeck extended Langevin's theory of diffusion by solving the Langevin equation also for  $t < m/\gamma$ , and make explicit under which conditions the assumptions underlying Einstein's and Langevin's theory are valid [11]. The Langevin equation is

$$m\partial_t v = -\gamma v + \zeta, \quad (1.21)$$

where  $v = \partial_t x$  is the velocity and  $\zeta$  is the random force.

The random force is rapidly fluctuating with zero mean. This force fluctuates rapidly because the positions of the fluid molecules change rapidly. The time scale of the fluctuations in the positions of the fluid molecules is called the fluid relaxation time  $\tau_{fluid}$  and is much smaller than any other relevant time scale in the problem.<sup>5</sup> From these considerations one can conclude that the average of the fluctuation force is zero:  $\langle \zeta(t) \rangle = 0$ , and the random force autocorrelation function  $\phi(|t'|) = \langle \zeta(t'+t)\zeta(t) \rangle$  is only nonzero for  $t' < \tau_{fluid}$  because  $\phi(|t'| \gg \tau_{fluid}) = \langle \zeta(t'+t) \rangle \langle \zeta(t) \rangle = 0$ .

The solution to the Langevin equation is

$$v = v_0 e^{-t/\tau} + \frac{1}{m} e^{-t/\tau} \int_0^t dt' e^{t'/\tau} \zeta(t'), \quad (1.22)$$

where  $v_0 = v(t=0)$ , and  $\tau = m/\gamma$ . Averaging over the noise and using

---

<sup>5</sup>A rough estimate of the fluid relaxation time can be obtained as follows [12]. As the typical speed of a fluid molecule one can take the root mean square velocity  $\sqrt{\langle v^2 \rangle}$ , which by the equipartition theorem is of the order  $\sqrt{T/m}$ , where  $m$  is the mass of the molecule. The molecules in the surrounding fluid are all close together. Therefore, they collide with other fluid particles when they move about their own size. The fluid equilibrates due to these collisions, so the time between collision is of the same order as the fluid relaxation time:  $\tau_{fluid} \approx a/\sqrt{\langle v^2 \rangle}$ , where  $a$  is the size of a fluid molecule. For water  $a \approx 2 \times 10^{-1} \text{ nm}$ ,  $m \approx 3 \times 10^{-26} \text{ kg}$ , and at room temperature  $T \approx 4 \times 10^{-21} \text{ J}$ . This gives  $\tau_{fluid} \approx 5 \times 10^{-13} \text{ s}$ . This is some what larger than the  $10^{-14} \text{ s}$  from what is known from experiments [13, Ch. 2]; however it is still orders of magnitude smaller than the velocity relaxation time of a Brownian particle  $\tau \approx 5 \times 10^{-9} \text{ s}$ .

$\langle \xi(t) \rangle = 0$  gives the mean velocity:

$$\langle v \rangle = v_0 e^{-t/\tau}. \quad (1.23)$$

The mean squared velocity is

$$\begin{aligned} \langle v^2 \rangle &= v_0^2 e^{-2t/\tau} + \frac{1}{m^2} e^{-2t/\tau} \int_0^t ds \int_0^t ds' e^{(s+s')/\tau} \phi(s-s'), \\ &= v_0^2 e^{-2t/\tau} + \frac{A\tau}{2m^2} (1 - e^{-2t/\tau}), \end{aligned} \quad (1.24)$$

where

$$\int_{-t}^t dt' \phi(t') \approx \int_{-\infty}^{\infty} dt' \phi(t') \equiv A, \quad (1.25)$$

was used. This is valid because for any time difference  $t$  of interest,  $\phi(t)$  is zero. The equipartition theorem states that  $\lim_{t \rightarrow \infty} \langle v^2 \rangle = T/m$ . This requires that  $A = 2T\gamma$ , and therefore

$$\langle v^2 \rangle = v_0^2 e^{-2t/\tau} + \frac{T}{m} (1 - e^{-2t/\tau}). \quad (1.26)$$

Integrating Eq. 1.22 once more, gives the solution for the position of the particle:

$$x(t) = v_0 \tau (1 - e^{-t/\tau}) + \frac{1}{m} \int_0^t ds e^{-s/\tau} \int_0^s ds' e^{-s'/\tau} \xi(s'), \quad (1.27)$$

for  $x(0) = 0$ . The mean is  $\langle x \rangle = v_0 \tau (1 - e^{-t/\tau})$ , and, using the same methods as before, the mean squared displacement becomes

$$\langle x^2 \rangle = 2Dt + v_0^2 \tau^2 (1 - e^{-t/\tau})^2 - D\tau (3 + e^{-2t/\tau} - 4e^{-t/\tau}), \quad (1.28)$$

where  $x(t=0) = 0$ . A plot of this result is shown in Fig. 1.1.

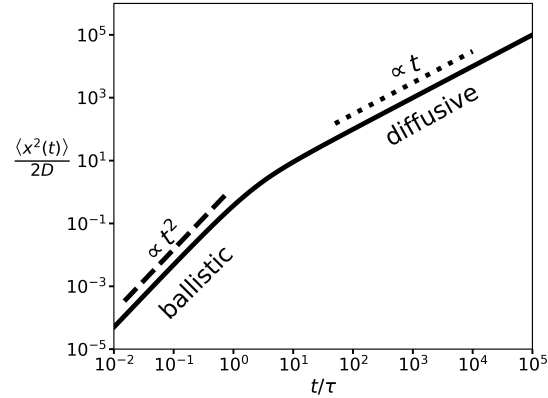
This solution captures both the  $t \gg \tau$  as well as the  $t \ll \tau$  behavior, see Fig. 1.1. In these limits

$$\langle x^2 \rangle \sim \begin{cases} v_0^2 t^2 & \text{as } t/\tau \rightarrow 0, \\ 2Dt & \text{as } t/\tau \rightarrow \infty. \end{cases} \quad (1.29)$$

This reproduces the  $t/\tau \rightarrow \infty$  behavior from Einstein's and Langevin's theories. So these theories are valid for time increments longer than the



**Figure 1.1:** The mean squared displacement on a log-log scale with  $x(0) = 0$ , and  $v_0^2 = \langle v_0^2 \rangle = T/m = D/\tau = 1$ . For  $t/\tau \ll 1$  the displacement increases ballistically, that is,  $x(t) \propto t$ , so  $\langle x^2(t) \rangle \propto t^2$ . For  $t/\tau \gg 1$  the mean squared displacement increases diffusively, that is,  $\langle x^2(t) \rangle \propto t$ .



velocity autocorrelation time  $\tau$ . In addition, it shows that for short times  $\sqrt{\langle x^2 \rangle} = \langle x \rangle = v_0 t$ . There are two kinds of behavior, on time scales shorter than the velocity autocorrelation time the typical displacement grows linearly in time (ballistic behavior), and for time scales longer than the velocity autocorrelation time the typical displacement grows as  $\sqrt{t}$  (diffusive behavior).

### 1.1.1 The Overdamped Limit

The reason for the absence of the short time behavior in Einstein's treatment (see Sec. 1.1), is that Einstein only considered the position variable and assumed that the increments in the position are independent. On a time scale shorter than the velocity autocorrelation time  $\tau = m/\gamma$ , the changes in position are *not* independent, but are correlated, and therefore Einstein's assumption is not valid on those time scales.

If one is only interested in time scales much larger than  $\tau$ , it is not necessary to consider the velocity degree of freedom. Equation 1.22 can be rewritten as an equation for the position variable:

$$\partial_t x = v = v_0 e^{-t/\tau} + \frac{2}{\gamma} \int_0^t dt' \frac{1}{2\tau} e^{-(t-t')/\tau} \zeta(t'). \quad (1.30)$$

If one is only interested in  $t \gg \tau$ , one can take the  $\tau \rightarrow 0$  limit of this equation. Using that in this limit  $v_0 e^{-t/\tau} \rightarrow 0$ , and  $e^{-(t-t')/\tau} / (2\tau) \rightarrow \delta(t-t')$ , the equation becomes

$$\partial_t x = \frac{2}{\gamma} \int_0^t dt' \delta(t-t') \zeta(t') = \frac{1}{\gamma} \zeta(t). \quad (1.31)$$

One would obtain the same result by setting  $m\partial_t v = 0$  in Eq. 1.21. This is only allowed if the noise strength is not dependent on the variable  $x$ , otherwise a more careful limiting procedure is needed (see Sections 1.3.2 and 1.A).

This limit is called the overdamped limit. In all problems considered in this work  $\tau$  is shorter than any other time scale of interest, and therefore only the overdamped limit is considered.

## 1.2 Stochastic Differential Equations

The Langevin equation (Eq. 1.16) is an example of a stochastic differential equation (SDE). Stochastic differential equations are used to model a wide variety of phenomena, from natural sciences such as physics, chemistry, and biology [14–20], to social sciences, economy and finance [21–23]. In order to describe such a wide variety of phenomena, a more general SDE than the Langevin equation is needed. The more general version of the Langevin equation is

$$\partial_t x(t) = a(x(t)) + b(x(t)) \zeta(t), \quad (1.32)$$

where  $x(t)$  does not necessarily represent the position of a particle. The functions  $a$  and  $b$  can also have explicit time dependence. This would not change any of the results shown in this section. Here a simple, nonrigorous explanation is given, a more rigorous treatment see for example Ref. [14].

In the discussion on the Ornstein-Uhlenbeck theory of Brownian motion, it was assumed that the random force  $\zeta$  fluctuates on a time scale shorter than any other time scale in the problem. In the limit that the time scale of fluctuations goes to zero, the noise autocorrelation function becomes a delta function:  $\langle \zeta(t' + t)\zeta(t) \rangle \propto \delta(t')$ . The proportionality constant can be set to unity, and the strength of the noise is changed by changing the factor  $b$  in Eq. 1.32. The Langevin equation for the Brownian particle can then be written as  $m\partial_t v = -\gamma v + \sqrt{2T/m}\zeta$ , where  $\sqrt{2T/m}$  is the noise strength  $A$  in Eq. 1.25. The time scale of the noise fluctuation is  $m/\gamma$ . In the limit that this time scale goes to zero, the Langevin equation becomes  $\partial_t x = \sqrt{2D}\zeta$ . The increment of the variable  $x$  is  $dx = \sqrt{2D}dW$ , where  $dW = \zeta dt$ . Because  $dx$  obeys a Gaussian distribution (Eq. 1.11), with  $\langle dx \rangle = 0$  and  $\langle dx^2 \rangle = 2D dt$ , the distribution of  $dW$  is also Gaussian but with  $\langle dW \rangle = 0$  and  $\langle dW^2 \rangle = dt$ . The stochastic process  $W(t)$  is called a Wiener process [14]. Because the distribution of  $dW$  is Gaussian with

zero mean,  $\langle dW^{2n} \rangle = \mathcal{O}(dt^n)$  are all negligible. One can view the SDE 1.32 as an other way of writing

$$dx = a(x)dt + b(x)dW. \quad (1.33)$$

The equation  $\langle dW^2 \rangle = dt$  also holds without the average. The following explanation of this is based on Ref. [24]. Consider the integral

$$I = \int_0^t dW^2 = \lim_{N \rightarrow \infty} I_N \quad (1.34)$$

where  $I_N = \sum_{i=1}^N (\Delta W_i)^2$ , and  $N = t/\Delta t$ . Because  $\langle (\Delta W_i)^2 \rangle = \Delta t$ , the average is  $\langle I_N \rangle = N \Delta t$ , and  $\langle I \rangle = t$ . The average of the square is

$$\langle I_N^2 \rangle = \sum_{i,j=1}^N \langle (\Delta W_i)^2 (\Delta W_j)^2 \rangle. \quad (1.35)$$

Because  $dW$  is Gaussian distributed, Isserlis's formula holds [25]:

$$\langle (\Delta W_i)^2 (\Delta W_j)^2 \rangle = \langle (\Delta W_i)^2 \rangle \langle (\Delta W_j)^2 \rangle + 2 \langle \Delta W_i \Delta W_j \rangle^2.$$

Because the increments are independent  $\langle \Delta W_i \Delta W_j \rangle^2 = \langle (\Delta W_i)^2 \rangle^2 \delta_{ij}$ . With this

$$\langle I_N^2 \rangle = \sum_{i,j=1}^N (\Delta t)^2 + 2(\Delta t)^2 \delta_{ij} = N^2 \Delta t^2 + 2N \Delta t^2, \quad (1.36)$$

and using  $I = \lim_{N \rightarrow \infty} I_N$  with  $\Delta t = t/N$  gives  $\langle I^2 \rangle = t^2$ . So the mean of the integral is  $I = t$ , and its variance is  $\langle I^2 \rangle - \langle I \rangle^2 = 0$ . Because the variance is zero  $I$  is not a stochastic variable at all, but  $I = \int_0^t dW^2 = t$ . Taking the differential on both sides gives

$$dW^2 = dt. \quad (1.37)$$

What this means is that any SDE with  $dW^2$  has the same properties as the same SDE with  $dW^2$  replaced by  $dt$ .

### 1.2.1 The Fokker-Planck Equation

Because of the stochastic nature of SDEs, the quantities of interest are usually averages and not particular solutions to the equation. Therefore, one

can study the probability density corresponding the stochastic variable instead of the SDE itself. The partial differential equation for the time evolution of the probability density corresponding to the SDE in Eq. 1.32 is called a Fokker-Planck equation (FPE). The relation between the SDE and the corresponding FPE is explained in this section. The cases with  $x$  independent  $b$  and  $x$  dependent  $b(x)$  are treated separately.

### Additive Noise

When the function  $b$  is not dependent on the stochastic variable, as in

$$\partial_t x(t) = a(x(t)) + b\zeta(t), \quad (1.38)$$

the noise in the SDE is called additive noise. The discretized version of the previous equation is

$$dx = a(x)dt + b dW(t), \quad (1.39)$$

where  $x = x(t)$ . Note that the value of  $x$  at time  $t$  is independent of  $dW$  at time  $t$ . The differential of a function of the stochastic variable  $f(x(t))$  is

$$\begin{aligned} df(x) &= dx\partial_x f(x) + (dx)^2 \frac{1}{2} \partial_x^2 f(x) \\ &= \left[ a(x)\partial_x f(x) + \frac{1}{2} b^2 \partial_x^2 f(x) \right] dt + b dW \partial_x f(x), \end{aligned} \quad (1.40)$$

where  $dW_t^2 = dt$  was used and terms of order  $dt^{3/2}$  were ignored. The average of this is

$$\begin{aligned} \frac{\langle df(x) \rangle}{dt} &= \int dx P(x, t) \left[ a(x)\partial_x f(x) + \frac{1}{2} b^2 \partial_x^2 f(x) \right], \\ &= \int dx f(x) \left[ -\partial_x (a(x)P(x, t)) + \frac{1}{2} b^2 \partial_x^2 P(x, t) \right]. \end{aligned} \quad (1.41)$$

The time differential can be moved into the average:

$$\frac{\langle df(x) \rangle}{dt} = \left\langle \frac{df(x)}{dt} \right\rangle = \int dx f(x) \partial_t P(x, t). \quad (1.42)$$

Because the function  $f(x)$  is arbitrary, the integrands of the last two integrals are equal. This gives the FPE corresponding to the SDE 1.38:

$$\partial_t P(x, t) = -\partial_x [a(x)P(x, t)] + \frac{1}{2}b^2\partial_x^2 P(x, t). \quad (1.43)$$

The extension to multiple dimensions is straightforward. The multidimensional equivalent of Eq. 1.38 is

$$\partial_t \mathbf{r} = \mathbf{A}(\mathbf{r}) + \mathbf{B} \cdot \boldsymbol{\zeta}, \quad (1.44)$$

where  $\mathbf{A}(\mathbf{r})$  is a  $d$ -dimensional vector,  $\mathbf{B}$  is  $d \times n$ -dimensional matrix, and  $\boldsymbol{\zeta}$  is an  $n$ -dimensional vector, where  $d$  is the number of elements of  $\mathbf{r}$  and  $n \leq d$ . The corresponding FPE is

$$\partial_t P(\mathbf{r}, t) = -\nabla \cdot \left[ \mathbf{A}(\mathbf{r})P(\mathbf{r}, t) - \frac{1}{2}\mathbf{B} \cdot \mathbf{B}^T \cdot \nabla P(\mathbf{r}, t) \right]. \quad (1.45)$$

### Multiplicative Noise

When the noise strength in an SDE is dependent on the stochastic variable, as in Eq. 1.32, it is called multiplicative noise. When this occurs, the integral of this equation is not uniquely defined. This somewhat technical concept is explained in detail in Ref. [14]. What follows is a short summary of the basic properties of such an SDE.

When an SDE has multiplicative noise, one must specify how to integrate the equation. Two of the most used choices are Itô and Stratonovich integration. The difference lies in how the noise term is evaluated. With the Itô rule the function  $b$  is evaluated at the left side of the time interval. The discrete version of the SDE is

$$dx_{t_i} = a(x_{t_i}) dt + b(x_{t_i}) dW_{t_i}. \quad (1.46)$$

With the Stratonovich rule the function  $b$  is evaluated at the average of  $x_{t_i}$  and  $x_{t_{i+1}}$ :

$$dx_{t_i} = a(x_{t_i}) dt + b\left(\frac{x_{t_i} + x_{t_{i+1}}}{2}\right) dW_{t_i}. \quad (1.47)$$

The advantage of the Itô integration is that  $b(x(t), t)$  and  $\boldsymbol{\zeta}(t)$  are not correlated. However, a downside of this choice is that the 'normal' rules of calculus no longer apply, that is  $df \neq f'dx$ , where  $f' = \partial_x f(x)$ . Instead

one has to use Itô's formula

$$df(x(t)) = \left[ a(x(t), t) f'(x(t)) + \frac{1}{2} b^2(x(t), t) f''(x(t)) \right] dt + b(x(t), t) f'(x(t)) dW(t), \quad (1.48)$$

where  $dW(t) = \int_t^{t+dt} dx \zeta(s)$ . With the Stratonovich rule the normal rules of calculus apply:

$$df(x(t)) = f'(x(t)) dx. \quad (1.49)$$

However,  $b(x(t), t)$  and  $\zeta(t)$  are correlated. Which integration rule should be used is either indicated in the text, or by (I) or (S) before the SDE for, respectively, the Itô and Stratonovich rule.

When Eq. 1.32 is an Itô SDE, the corresponding FPE is

$$\partial_t P(x, t) = -\partial_x [a(x, t) P(x, t)] + \frac{1}{2} \partial_x^2 [b^2(x, t) P(x, t)]. \quad (1.50)$$

When Eq. 1.32 is a Stratonovich SDE, the corresponding FPE is

$$\begin{aligned} \partial_t P(x, t) = & -\partial_x [a(x, t) P(x, t)] \\ & + \frac{1}{2} \partial_x \{ b(x, t) \partial_x [b(x, t) P(x, t)] \}. \end{aligned} \quad (1.51)$$

Comparing the two FPEs shows that

$$(I) \partial_t x = a + b \zeta(t), \quad (1.52)$$

and

$$(S) \partial_t x = a - \frac{1}{2} b b' + b \zeta(t), \quad (1.53)$$

have the same FPE, and therefore correspond to the same stochastic process. This means that there is no "right" integration rule for a physical process, but the same process can be described by different SDEs with different integration rules. The correspondence between the Itô and Stratonovich SDEs can be used to transform from one to the other, if that is more expedient for the problem at hand.

The same holds for the d-dimensional SDE

$$\partial_t \mathbf{r} = \mathbf{A}(\mathbf{r}, t) + \mathbf{B}(\mathbf{r}, t) \cdot \boldsymbol{\zeta}(t), \quad (1.54)$$

where  $\mathbf{A}$  is a  $d$ -dimensional vector,  $\mathbf{B}$  is a  $d \times n$ -dimensional matrix, and  $\boldsymbol{\zeta}$  is an  $n$ -dimensional vector. The vector  $\mathbf{r}$  are the degrees of freedom, which are not necessarily the position coordinates but can be the velocity or other degrees of freedom. If this is an Itô SDE, the corresponding FPE is

$$\partial_t P(\mathbf{r}, t) = -\nabla_i [A_i P(\mathbf{r}, t)] + \frac{1}{2} \nabla_i \nabla_j [B_{ik} B_{jk} P(\mathbf{r}, t)], \quad (1.55)$$

and if it is a Stratonovich SDE, the corresponding FPE is

$$\partial_t P(\mathbf{r}, t) = -\nabla_i [A_i P(\mathbf{r}, t)] + \frac{1}{2} \nabla_i \{B_{ik} \nabla_j [B_{jk} P(\mathbf{r}, t)]\}. \quad (1.56)$$

### 1.3 Examples

To elucidate the concept of Brownian motion further, three examples are worked out. These examples will be part of more complicated models that are introduced later in Part II.

#### 1.3.1 Diffusion in a Potential

A Brownian particle in force field  $\mathbf{F}$  can be described by the SDE

$$m \partial_t \mathbf{v} = -\gamma \mathbf{v} + \mathbf{F} + \sqrt{2T\gamma} \boldsymbol{\zeta}, \quad (1.57)$$

this is the Langevin equation (Eq. 1.16) with a force term added to the force balance. If only time scales much larger than  $m/\gamma$  are considered, the left-hand side is negligible, and the SDE becomes

$$\partial_t \mathbf{r} = \frac{1}{\gamma} \mathbf{F} + \sqrt{2D} \boldsymbol{\zeta}. \quad (1.58)$$

If the force field  $\mathbf{F}$  is conservative, it is the gradient of a potential  $\mathbf{F} = -\nabla U$ , as is the case for, for example, a Brownian particle in an optical trap [26]. The corresponding FPE is

$$\partial_t P(\mathbf{r}, t) = -\nabla \cdot \mathbf{J}, \quad (1.59)$$

with

$$\mathbf{J} = -\frac{1}{\gamma} \nabla U P(\mathbf{r}, t) - D \nabla P(\mathbf{r}, t). \quad (1.60)$$

In steady state the flux  $J$  must be a constant vector. Because the probability is normalized, it and its derivatives must vanish as  $|\mathbf{r}| \rightarrow \infty$ , so  $J = 0$  in this limit, and because it is a constant, it must be zero everywhere.

Integrating the expression of the flux gives

$$P(\mathbf{r}) \propto \exp[-U(\mathbf{r})/T]. \quad (1.61)$$

The proportionality constant can be obtained from the normalization condition. This solution is nothing but the Boltzmann distribution of the particle.

In case of colloids of radius  $a$  in a gravitational field  $U(x) = mgh$ , where  $m = \frac{3}{4}\pi a^3(\rho_{colloid} - \rho_{solvent})$  is the Archimedean weight of the colloid,  $g$  is the gravitational acceleration, and  $h$  is the height of the colloid. Then, for an ideal solution,

$$\rho(h) = \rho(0) \exp[-mgh/T], \quad (1.62)$$

which is the same as the barometric law for gases.

### 1.3.2 Diffusion in Inhomogeneous Media

Brownian motion can be generalized to diffusion with a space dependent temperature and friction [27–32]. This introduces certain complications that can already be seen in Fick's laws [Eqs. 1.2 and 1.1]:  $\partial_t \rho = D \nabla^2 \rho$ . If  $D$  is constant, there are (at least) two generalizations of this equation:  $\partial_t \rho = \nabla \cdot [D(x) \nabla \rho]$  and  $\partial_t \rho = \nabla^2 D(x) \rho$ . The other option  $\partial_t \rho = D(x) \nabla^2 \rho$  is not possible because it violates particle conservation. If the temperature and friction are space dependent, the diffusion constant is space dependent. It is not obvious how one should generalize Fick's law in this case and which, if any, of the generalizations of Fick's law is correct.

The Langevin equation (Eq. 1.21) with space dependent temperature and friction is

$$m \partial_t v = -\gamma(x)v + \sqrt{2T(x)\gamma(x)}\xi, \quad (1.63)$$

where the noise is normalized such that  $\langle \xi(t)\xi(t') \rangle = \delta(t - t')$ . Note that this equation does not have multiplicative noise (it is the equation of motion for  $v$  and the noise strength depends on  $x$ ) so it is irrelevant how (Itô or Stratonovich) one integrates this equation. The equation for the position variable is  $\partial_t x = v$ . If one takes the overdamped limit of this equation (that is, one sets  $(m/\gamma)\partial_t v = 0$ ), just as one would do for



constant  $T$  and  $\gamma$ , a problem arises. The equation would be

$$\partial_t x = \sqrt{2T(x)/\gamma(x)}\xi, \quad (1.64)$$

which has multiplicative noise, and therefore, one should specify how this equation should be integrated. However, which integration rule should be used does not follow from the derivation. A more careful derivation (see 1.A) shows that, the Itô SDE

$$\partial_t x = -\frac{\gamma'(x)T(x)}{\gamma^3(x)} + \sqrt{2\frac{T(x)}{\gamma(x)}}\xi, \quad (1.65)$$

where  $\gamma'(x) = \partial_x \gamma(x)$ . The corresponding FPE is

$$\partial_t P(x, t) = -\partial_x J, \quad (1.66)$$

$$J = \frac{1}{\gamma(x)}\partial_x [T(x)P(x, t)]. \quad (1.67)$$

This shows that if only  $T$  is space dependent the correct generalization of Fick's law is  $\partial_t \rho = \partial_x^2 D(x)\rho$  (for a single particle the difference between the probability  $P$  and the density  $\rho$  is a constant), and if only  $\gamma$  is space dependent the correct generalization of Fick's law is  $\partial_t \rho = \partial_x [D(x)\partial_x \rho]$ , and if both  $T$  and  $\gamma$  are space dependent, neither of the suggested generalizations is correct.

The generalization of Fick's law in case of space dependent  $\gamma$  and constant  $T$  could be obtained from physical arguments. Because the temperature is constant, this is an equilibrium system, and therefore obeys a Boltzmann distribution in steady state, which leads to the only generalization  $\partial_t \rho = \partial_x [D(x)\partial_x \rho]$ .

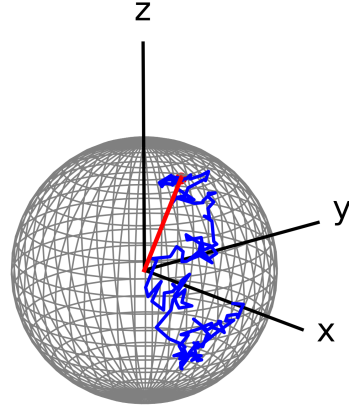
If  $T$  is space dependent and  $\gamma$  is constant, the steady-state probability density is

$$P(x) \propto \frac{1}{T(x)}. \quad (1.68)$$

The probability is larger in regions where the temperature is small. The temperature is what causes the motion of the fluid and the particle, in other words, it is what agitates the particle. So the particle moves to regions where it is less agitated.

This mechanism also explains an other, perhaps more familiar, phenomenon. In the Autumn fallen leaves accumulate at the edges of streets.

**Figure 1.2:** Rotational Brownian motion of the unit vector  $\mathbf{n}$  (red) in three dimensions. The wire mesh represents the unit sphere. The start point is  $\mathbf{n}_0 = \hat{x}$ , and the blue line represents the history of the orientation. One can view this both as rotational Brownian motion of a unit vector, as well as Brownian motion of a particle on the unit sphere where the particle's position is indicated by the end of the unit vector.



When the leaves are in the middle of the street, cars will move them around (i.e. agitate them). The cars do not drive, or at least less often, right along the edge of the street, so when a leaf is moved near the edge, it is not moved again and will stay there.

One could argue that the friction also appears in the noise strength in Eq. 1.63 in the same way as the temperature. However, it also appears in the dissipative term  $(-\gamma(x)v)$ , so when the friction constant is space dependent, the noise (fluctuations) is space dependent, but the dissipation is space dependent as well. These two effects cancel each other in steady state and therefore result in a Boltzmann distribution.

### 1.3.3 Rotational Brownian Motion

Rotational diffusion of a unit vector  $\mathbf{n}$  can be written down by analogy with the diffusion equation (Eq. 1.1). In two dimensions, rotational diffusion describes the diffusive motion of a unit vector  $\mathbf{n}$ . This vector is a function of the angle  $\phi$ . The corresponding SDE is

$$\partial_t \phi = \sqrt{2D_r} \zeta, \quad (1.69)$$

or in Cartesian coordinates this becomes

$$\partial_t \mathbf{n} = \sqrt{2D_r} \mathbf{n} \cdot \boldsymbol{\epsilon} \cdot \zeta, \quad (1.70)$$

where

$$\boldsymbol{\epsilon} = \begin{bmatrix} 0 & 1 \\ -1 & 0 \end{bmatrix}.$$

It may seem odd that in contrast to the SDE for  $\phi$ , this SDE has mul-

tiplicative noise. However, the equation should be supplemented with the condition  $\partial_t |\mathbf{n}| = 0$  because it is a unit vector. With this condition, the difference between the Itô and Stratonovich integration for the SDE vanishes.

Because  $\mathbf{n}$  is a unit vector, its increments are always perpendicular to  $\mathbf{n}$  itself and therefore the radial component of the probability flux is zero. The FPE for two dimensional rotational diffusion is

$$\partial_t P(\phi, t) = D_r \partial_\phi^2 P(\phi, t), \quad (1.71)$$

where  $D_r$  is the rotational diffusion constant (with units of inverse time), and  $\partial_\phi^2$  is the Laplacian on the unit circle. This can also be written in Cartesian coordinates:

$$\partial_t P(\mathbf{n}, t) = -D_r \mathcal{R} \cdot \mathbf{J}, \quad (1.72)$$

where  $\mathbf{J}$  is the flux

$$\mathbf{J} = -\mathcal{R} P(\mathbf{n}, t), \quad (1.73)$$

where  $\mathcal{R} = (\mathbf{1} - \mathbf{nn}) \cdot \nabla_{\mathbf{n}}$  is the nabla operator projected onto the direction perpendicular to  $\mathbf{n}$ .

In three dimensions, rotational diffusion describes the diffusion of a unit vector  $\mathbf{n}$  that depends on two angles:  $\mathbf{n} = \mathbf{n}(\theta, \phi)$ , where  $\theta$  and  $\phi$  are the polar and azimuthal angle, respectively (see Fig. 1.2). Because the change of the unit vector, the radial component of the probability flux is zero, and therefore the FPE for rotational Brownian motion of the unit vector  $\mathbf{n}$  is

$$\partial_t P(\mathbf{n}, t) = \mathcal{R} \cdot \mathbf{J}, \quad (1.74)$$

where  $\mathbf{J} = D_r \mathcal{R} P(\mathbf{n}, t)$ ,  $D_r$  is the rotational diffusion constant (with units of inverse time), and  $\mathcal{R}$  is the angular part of the nabla operator, which in Cartesian coordinates can be written as  $\mathcal{R} = \mathbf{n} \times \nabla_{\mathbf{n}} = (\mathbf{1} - \mathbf{nn}) \cdot \nabla_{\mathbf{n}}$ . For a sphere of radius  $a$ , the rotational diffusion constant is  $D_r = T / (8\pi\eta_s a^3)$  (see Chapter A, Eq. A.14).

Using the Cartesian expression for the FPE of  $\mathbf{n}$ , and comparing with Eq. 1.56, shows that the corresponding Stratonovich SDE for  $\mathbf{n}$  is

$$\partial_t \mathbf{n} = \sqrt{2D_r} \mathbf{n} \times \boldsymbol{\eta}. \quad (1.75)$$

And, just as in the two dimensional case, the constraint  $\partial_t |\mathbf{n}| = 0$  should

be added to this equation. With this the difference between the Itô and Stratonovich integration of the SDE vanishes.

The FPE for both two and three dimension can be written as

$$\partial_t P(\mathbf{n}, t) = \mathcal{L}P(\mathbf{n}, t), \quad (1.76)$$

where the Fokker-Planck operator is

$$\mathcal{L} = D_r \mathcal{R}^2 = D_r [(\mathbf{1} - \mathbf{n}\mathbf{n}) \cdot \nabla_{\mathbf{n}}]^2. \quad (1.77)$$

The formal solution to this equation is  $P(\mathbf{n}, t|\mathbf{n}) = e^{\mathcal{L}t}P(\mathbf{n}, 0|\mathbf{n}_0)$ , where  $P(\mathbf{n}, t|\mathbf{n}_0)$  is the probability of  $\mathbf{n}$  at time  $t$  given that  $\mathbf{n} = \mathbf{n}_0$  at  $t = 0$ .

The mean square displacement of the unit vector  $\mathbf{n}$  is

$$\langle (\mathbf{n}(t) - \mathbf{n}_0)^2 \rangle = 2 - 2 \langle \mathbf{n}(t) \cdot \mathbf{n}_0 \rangle. \quad (1.78)$$

For a fixed initial orientation, the vector  $\mathbf{n}_0$  can be taken out of the average:  $\langle \mathbf{n}(t) \cdot \mathbf{n}_0 \rangle = \mathbf{n}_0 \cdot \langle \mathbf{n}(t) \rangle$ . The average can be calculated using the solution to the FPE:

$$\begin{aligned} \langle \mathbf{n}(t) \rangle &= \int d\Omega \mathbf{n}(\Omega) P(\mathbf{n}(\Omega), t|\mathbf{n}_0), \\ &= \int d\Omega \mathbf{n}(\Omega) e^{\mathcal{L}t} P(\mathbf{n}(\Omega), 0|\mathbf{n}_0), \end{aligned} \quad (1.79)$$

where  $\Omega$  is the solid angle in  $d$  dimensions. The Fokker-Planck operator  $\mathcal{L}$  is self-adjoint, so the operator can be made to act on  $\mathbf{n}(\Omega)$  instead of the probability. The vector  $\mathbf{n}$  is an eigen function of this Fokker-Planck operator with eigenvalue  $-(d-1)D_r$ . With this the integral becomes

$$\langle \mathbf{n}(t) \rangle = \int d\Omega P(\mathbf{n}(\Omega), 0|\mathbf{n}_0) e^{-(d-1)D_r t} \mathbf{n}(\Omega). \quad (1.80)$$

The exponential can be taken out of the integral, and the remaining integral is equal to  $\mathbf{n}_0$ , so  $\langle \mathbf{n}(t) \rangle = \mathbf{n}_0 e^{-(d-1)D_r t}$ . The autocorrelation function is

$$\langle \mathbf{n}(t) \cdot \mathbf{n}_0 \rangle = e^{-(d-1)D_r t}, \quad (1.81)$$

which defines the autocorrelation time

$$\tau = \frac{1}{(d-1)D_r}. \quad (1.82)$$

Because of isotropy, this can also be written as

$$\langle \mathbf{n}(t) \mathbf{n}_0 \rangle = \frac{1}{d} e^{-t/\tau} \mathbf{1}, \quad (1.83)$$

where  $\mathbf{1}$  is the identity matrix.

The mean squared displacement is

$$\langle (\mathbf{n}(t) - \mathbf{n}_0)^2 \rangle = 2 - 2 \cdot \langle \mathbf{n}(t) \cdot \mathbf{n}_0 \rangle = 2 - 2e^{-(d-1)D_r t}. \quad (1.84)$$

Expanding the exponential in the mean-square displacement shows that

$$\langle (\mathbf{n}(t) - \mathbf{n}_0)^2 \rangle = 2(d-1)D_r t \quad \text{as } t \rightarrow 0. \quad (1.85)$$

This is the same as ordinary diffusion (in flat space) in one dimension lower because on short time scales the particle on the sphere ( $d = 3$ ) or circle ( $d = 2$ ) does not move far enough to probe the curvature of the space.

## 1.A Appendix: The Small-Mass Limit With Space-Dependent Friction and Temperature

When a  $m \rightarrow 0$  limit results in a SDE with multiplicative noise, one cannot set the acceleration term in the Ornstein-Uhlenbeck process to zero, as was done in Sec. 1.1.1. The following nonrigorous derivation is based on Ref. [30]. For a more rigorous derivation using methods of stochastic calculus see Refs. [31–33], for a rigorous derivation using the Fokker-Planck equation see [27–29], or for a derivation based on path integrals, see Ref. [34]. Alternatively, one can view diffusion with space-dependent friction and temperature as a limiting case of run-and-tumble motion (see Sec. 3.1.1), which is explained in Ref. [35].

The Ornstein-Uhlenbeck process with space dependent friction and temperature is

$$m\partial_t v(t) = -\gamma(t)\partial_t x(t) + \sqrt{2T(t)\gamma(t)}\zeta(t), \quad (1.86)$$

where  $\gamma(t) = \gamma(x(t))$ , and  $T(t) = T(x(t))$ . To fix the noise term, it is assumed that locally the fluctuation dissipation theorem still holds. Furthermore, it was assumed that the velocity distribution is the equilibrium distribution with the temperature replaced by the space-dependent temperature:

$$p(v|x) = \sqrt{\frac{m}{2\pi T(x)}} \exp\left[-\frac{mv^2}{2T(x)}\right], \quad (1.87)$$

which is a valid approximation as long as the persistence length  $vm/\gamma$  is much smaller than the gradient in the temperature.

In the previous SDE it does not matter whether it is integrated with the Itô or Stratonovich rule. The equation after the small-mass limit has multiplicative noise, and therefore it does matter how that equation is integrated. Because it simplifies the derivation, I use the Itô integration rule.

Rearranging Eq. 1.86 gives for the position increment

$$dx(t) = \frac{F(t)}{\gamma(t)}dt + \sqrt{2T(t)/\gamma(t)}dW(t) - \frac{m}{\gamma(t)}dv(t). \quad (1.88)$$

Next  $dx$  is integrated from  $t$  to  $t + \Delta t$ , where  $\Delta t \gg m/\gamma$ . Note that in the limit  $m \rightarrow 0$  the time increment  $\Delta t$  can be made arbitrarily small while still satisfying  $\Delta t \gg m/\gamma$ . Therefore  $\Delta t$  can be treated as a differential.

The position increment becomes

$$\begin{aligned}\Delta x(t) &= \int_t^{t+\Delta t} dt' \frac{F(t')}{\gamma(t')} + \int_t^{t+\Delta t} dW(t') \sqrt{2T(t)/\gamma(t)} \\ &\quad - \int_t^{t+\Delta t} dv(t') \frac{m}{\gamma(t)}, \\ &= \frac{F(t)}{\gamma(t)} \Delta t + \sqrt{2T(t)/\gamma(t)} \Delta W(t) - \int_t^{t+\Delta t} dv(t') \frac{m}{\gamma(t)},\end{aligned}\quad (1.89)$$

where for the integral over the noise the Itô rule was used:

$$\int_t^{t+\Delta t} dW(t') \sqrt{2T(t)/\gamma(t)} = \sqrt{2T(t)/\gamma(t)} \int_t^{t+\Delta t} dW(t'),$$

in the limit  $\Delta t \rightarrow 0$ .

The last integral in  $\Delta x(t)$  can be rearranged as follows:

$$\begin{aligned}dv(t) \frac{m}{\gamma(t)} &= d \left[ \frac{mv(t)}{\gamma(t)} \right] + mv(t) \frac{1}{\gamma^2(t)} d\gamma(t), \\ &= d \left[ \frac{mv(t)}{\gamma(t)} \right] + mv(t) \frac{\gamma'(t)}{\gamma^2(t)} dx(t) + mv(t) \frac{\gamma''(t)}{2\gamma^2(t)} [dx(t)]^2, \\ &= d \left[ \frac{mv(t)}{\gamma(t)} \right] + mv^2(t) \frac{\gamma'(t)}{\gamma^2(t)} dt + m \frac{\gamma''(t)T(t)}{\gamma^3(t)} dx(t),\end{aligned}\quad (1.90)$$

where for the last line  $[dx(t)]^2 = 2T(t)dt/\gamma(t)$  and  $dx(t) = v(t)dt$  was used. The first and last term vanish in the small-mass limit when integrated from  $t$  to  $t + \Delta t$ . Therefore

$$\begin{aligned}\int_t^{t+\Delta t} dv(t') \frac{m}{\gamma(t')} &= \int_t^{t+\Delta t} dt' mv^2(t') \frac{\gamma'(t')}{\gamma^2(t')}, \\ &= \frac{\gamma'(t)}{\gamma^2(t)} \int_t^{t+\Delta t} dt' mv^2(t').\end{aligned}\quad (1.91)$$

Because the integral extends over a time interval  $\Delta t \gg m/\gamma$ , the integral sums over many uncorrelated samples of  $mv^2(t)$  because  $m/\gamma$  is the correlation time of the velocity  $v$ . By the law of large numbers the result is equal to the mean. Therefore,  $\int_t^{t+\Delta t} dt' mv^2(t') = \int_t^{t+\Delta t} dt' \langle mv^2(t') \rangle = T(t)\Delta t$  because it is assumed that the velocity distribution is the equilibrium distribution with the local temperature  $T(x)$ . With this the space

increment becomes

$$\Delta x(t) = \frac{F(t)}{\gamma(t)} \Delta t + \sqrt{2T(t)/\gamma(t)} \Delta W(t) - \frac{\gamma'(t)T(t)}{\gamma^3(t)} \Delta t. \quad (1.92)$$

The  $\Delta$ s can be replaced by infinitesimal differentials because the time increments  $\Delta t$  can be made arbitrarily small as  $m \rightarrow 0$ . The corresponding (Itô) SDE then becomes

$$\partial_t x = \frac{F(x)}{\gamma(x)} - \frac{\gamma'(x)T(x)}{\gamma^3(x)} + \sqrt{\frac{2T(x)}{\gamma(x)}} \xi. \quad (1.93)$$

The corresponding Fokker-Planck equation is

$$\partial_t P(x, t) = -\partial_x \left[ \frac{F(x)}{\gamma(x)} P(x, t) \right] + \partial_x \left[ \frac{1}{\gamma(x)} \partial_x [T(x) P(x, t)] \right]. \quad (1.94)$$





## **Chapter 2**

### **Active matter**

Active matter are particles that convert energy (either stored or absorbed from the environment) into directed motion [36]. This means that these particles are driven out of equilibrium on a local level. This can be contrasted with systems that are driven out of equilibrium in a global way. For example, a sheared liquid is driven out of equilibrium due to the energy input at the boundaries. Much work is done on the collective effects emerging from a large number of active particles [36–39]; this work, however, focuses on the behavior of a single or a few particles.

There are many biological examples of active matter. This class covers a wide range of length scales, from molecular motors walking on filaments inside cells [40, 41], and active proteins [42–46], to moving animals such as birds and fish [47]. Here the focus is on micrometer scale. On this scale, biological active matter are also referred to as microswimmers [48]. Two prominent examples are the bacterium *e. coli* and sperm cells, both of which swim by deforming their bodies.

Besides the many biological examples of active matter, there is active matter that can be made in a laboratory. This, so called synthetic active matter, are typically micrometer sized particles that can propel themselves forward by different phoretic mechanisms [49]. Besides the phoretic self-propulsion, there are synthetic active particles that can propel themselves forward by changing their shape much like, and inspired by, biological active matter [50–52]. Furthermore, there are active particles whose activity can be tuned by light [53–58].

Because the typical self-propulsion mechanism of biological and synthetic active matter is often different, each is discussed separately. To get a basic understanding of how biological and synthetic active matter can propel itself forward, one simplified model system of each type of active matter is explained in the following two sections.

## 2.1 Biological Active Matter

Movement is essential for life. For example, it allows organisms to move towards more favorable conditions or to escape predators. Prokaryotic and eukaryotic micro-organisms<sup>1</sup> can move by a variety of methods; for example, they can crawl on a substrate, or propel themselves forward by

---

<sup>1</sup>Eukaryotes and prokaryotes are two classes of living cells. Eukaryotes are organisms consisting of cell that have their DNA enclosed in its nucleus. Examples are fungi, algae, plants and animals. Prokaryotes are organisms that do not keep their DNA enclosed in its nucleus. Most prokaryotes are simple, single-celled organisms. The most prominent example of prokaryotes are bacteria [64].

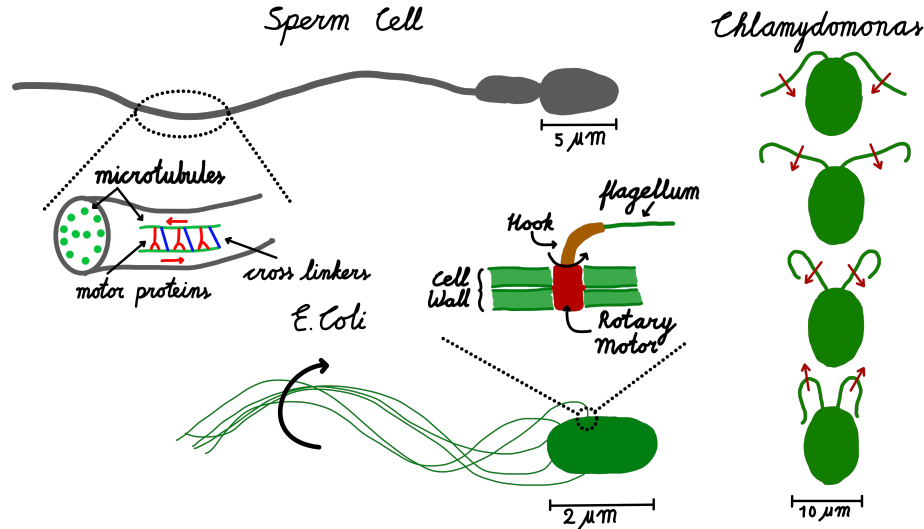


**Figure 2.1:** Examples of biological microswimmers. Each organism has its own scale bar. The sperm cell [59] and the algae *chlamydomonas* [60] are eukaryotes. Their flagella are deformed by motor proteins (dynein) inside the flagellum (see zoomed-in image with the sperm cell). The motors (red) slide the microtubules (green) along their length. Because the sliding is hindered by the cross linkers (blue), the flagellum bends. The sperm cell swims by wave-like beating of its flagellum. The different drawings of *chlamydomonas* show stages of the swim stroke. It swims upward, and time increases from bottom to top, red arrows indicate the direction of movement of the flagella. This stroke is similar to the breast-stroke swimming [61]. The prokaryote *E. coli* has passive flagella that are rotated by a rotary motor in the cell membrane [62, 63]. This rotary motor rotates a rigid hook to which the flagellum is attached (see zoomed-in image with *e. coli*). When the motor rotates counter-clockwise, the flagella of *e. coli* form a helical bundle.

deforming their body, by movement of cilia on their membrane, and, one much studied example, by moving flagella [65–68]. The latter will be used to introduce the basics of self-propulsion of micro-organisms.

The flagella of prokaryotic cells and those of eukaryotic cells are very different. The prokaryotic flagellum is a rigid filament, which has roughly a diameter of 20 nm. The movement of this flagellum is caused by a molecular motor in the cell membrane that rotates the flagellum [63]. An organism can have a single flagellum, for example *pseudomonas aeruginosa*, or multiple flagella, for example *e. coli* (see Fig. 2.1). When the flagella of *e. coli* rotate counter clockwise, they form a helical bundle. The rotation of this bundle results in a propulsive force, the origin of which is explained

in the next section.

Although seemingly very similar, the origin of this force is not the same as a propeller on a boat (which is in the high Reynolds number regime and needs momentum), but is more similar to a corkscrew being pulled into the cork when it is rotated.

The eukaryotic flagellum is flexible. Its core consists of microtubules, between which there are molecular motors that slide the microtubules with respect to each other along their length. Besides the molecular motors there are cross linkers that prevent the microtubules from sliding far, which, together with the molecular motors, causes the flagellum to bend [64]. Two examples of prokaryotic microswimmers, a sperm cell and the algae *chlamydomonas*, are shown in Fig. 2.1.

### 2.1.1 Propulsion by Beating Flagella

Swimming at the micrometer scale is governed by different mechanics as swimming on the meter scale (that is, swimming by humans). The difference can be quantified by the Reynolds number (see Appendix A), which is the ratio of the inertial and viscous forces:

$$Re = \frac{\rho V L}{\eta_s}, \quad (2.1)$$

where  $\rho$  is the density of the medium (for water  $\rho = 10^3 \text{ kg m}^{-3}$ ),  $V$  the typical velocity,  $L$  the length scale, and  $\eta_s$  is the viscosity of the medium (for water  $\eta_s = 10^{-3} \text{ kg m}^{-1} \text{ s}^{-1}$ ). For a bacterium such as *e. coli*, with a length  $L \approx 2 \mu\text{m}$  and a velocity of  $V \approx 20 \mu\text{m s}^{-1}$ , the Reynolds number is approximately  $Re \approx 4 \times 10^{-5}$ . A swimming human ( $L \approx 2 \text{ m}$ ,  $V \approx 1 \text{ m s}^{-1}$ ) has a Reynolds number of  $Re \approx 2 \times 10^6$ . This shows that, unlike for a swimming human, for a swimming bacterium momentum is not important<sup>2</sup>. Low Reynolds swimmers make use of the viscosity of the medium to swim. In particular, a common method is to use the fact that

---

<sup>2</sup>This becomes especially clear when one considers the coasting time and coasting distance, that is, the time it takes for the swimmer's momentum to dissipate and the distance it would move after the swimmer stops swimming [69]. This time is  $\tau_m = m/\gamma$ , where  $m$  is its mass and  $\gamma$  is its friction constant. Assuming that the density of the swimmer is the same order of magnitude as that of water, one obtains  $m \approx \rho_{\text{water}} 4\pi L^3/3$ , where  $L$  is its linear size. Its friction follows from the Stokes equation (Eq. A.8),  $\gamma \approx 6\pi\eta_s L$ . With this, coasting time of *e. coli* is  $\tau_m \approx \times 10^{-6} \text{ s}$ . The coasting distance is  $V\tau_m \approx 2 \times 10^{-12} \text{ m}$ . So if an *e. coli* bacterium would decide to stop swimming, it would come to rest within microseconds and move for about an Ångström. (Of course it would still move due to thermal fluctuations.)

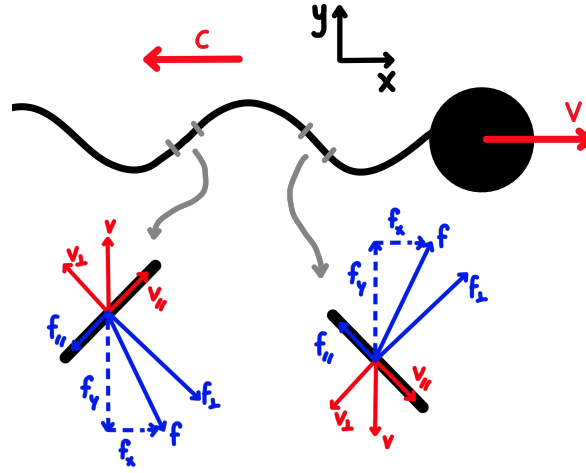


**Figure 2.2:** Self-propulsion due to a beating flagellum. The flagellum has a sinusoidal form with a wave velocity  $c$  in the negative  $x$  direction. The propulsion mechanism can be explained by considering two segments of the flagellum that are separated by half a wave length (gray segments). In this case the left segment moves up. This velocity can be decomposed in a velocity parallel to the segment ( $\mathbf{v}_{\parallel}$ ) and a velocity perpendicular to the segment ( $\mathbf{v}_{\perp}$ ). The friction force parallel to the segment is  $\mathbf{f}_{\parallel} = -\gamma_{\parallel}\mathbf{v}_{\parallel}$ , and friction force perpendicular to the segment is  $\mathbf{f}_{\perp} = -\gamma_{\perp}\mathbf{v}_{\perp}$ . Because  $\gamma_{\parallel} \approx 2\gamma_{\perp}$ , the total friction force on the segment  $\mathbf{f} = \mathbf{f}_{\parallel} + \mathbf{f}_{\perp}$  is not opposite to the velocity  $\mathbf{v}$  and has a non-zero, positive  $x$  component. Similarly, the friction force on the right segment has a non-zero, positive  $x$  component. The  $y$  components of both segments cancel. This can be done for each pair of segments separated by half a period. The net friction force of each pair of segments is zero in the  $y$  direction (if the flagellum is long enough to ignore end effects) and positive and non-zero in the  $x$  direction, resulting in movement of the organism in the positive  $x$  direction with velocity  $V$ .

the viscosity of slender rod moving along its long axis is about half the viscosity when it moves perpendicular to its long axis. The following simple model shows how a microswimmer can exploit this to swim.

In this model the head is modeled as a sphere with a beating flagellum attached to it (see Fig. 2.2). The analysis below is based on Refs. [70–73]. This is a model of the beating flagellum of a sperm cell (see Fig. 2.1), but the principles for the helical flagellum of *e. coli* are the same. The simplest method to calculate the velocity is resistive-force theory [73–76] (for more accurate methods see Refs. [77, 78]). The viscous force per unit length on the flagellum is  $\mathbf{f}_{fric} = -\tilde{\gamma}_{\perp}\mathbf{nn} \cdot \mathbf{v} - \tilde{\gamma}_{\parallel}\mathbf{tt} \cdot \mathbf{v}$ , where  $\mathbf{v}$  is the velocity of an infinitesimal segment of the flagellum with unit normal vector

$\hat{\mathbf{n}}$  and unit tangent vector  $\hat{\mathbf{t}}$ , and  $\tilde{\gamma}_{\parallel}$  and  $\tilde{\gamma}_{\perp}$  are the parallel and perpendicular friction coefficients per unit length of a rod with the same radius as the flagellum. In appendix A.5 it is shown that the friction coefficients of a rod with length  $L$  and radius  $R$  are approximately

$$\gamma_{\parallel} = \frac{2\pi\eta_s L}{\ln\left(\frac{L}{2R}\right)}, \quad \gamma_{\perp} = \frac{4\pi\eta_s L}{\ln\left(\frac{L}{2R}\right)}, \quad (2.2)$$

where  $\eta_s$  is the viscosity of the medium. The friction coefficients per unit length are  $\tilde{\gamma}_{\parallel} = \gamma_{\parallel}/L$  and  $\tilde{\gamma}_{\perp} = \gamma_{\perp}/L$ . Using that  $\mathbf{nn} = \mathbf{1} - \mathbf{tt}$ , the friction force can be written as  $\mathbf{f}_{fric} = -\tilde{\gamma}_{\perp}\mathbf{v} - (\tilde{\gamma}_{\parallel} - \tilde{\gamma}_{\perp})\mathbf{tt} \cdot \mathbf{v}$ . The method that the micro-organisms use to swim uses the anisotropy in the friction constants  $\tilde{\gamma}_{\perp} \neq \tilde{\gamma}_{\parallel}$ ; see Fig. 2.2.

The flagellum moves up and down to produce a traveling wave such that the shape of the flagellum in the comoving frame is given by  $y(x, t) = A \sin(kx + \omega t)$ , where  $A$  is the amplitude,  $2\pi/k$  is the wave length, and  $\omega$  its frequency. The wave propagates with a velocity  $c = \omega/k$  in the negative  $x$  direction. If the head moves with velocity  $V$ , the velocity of the flagellum is given by  $\mathbf{v} = V\hat{\mathbf{e}}_x + \partial_t y \hat{\mathbf{e}}_y$ . The unit tangent vector to the flagellum is

$$\hat{\mathbf{t}} = \frac{\hat{\mathbf{e}}_x + \partial_x y \hat{\mathbf{e}}_y}{\sqrt{1 + (\partial_x y)^2}} = \hat{\mathbf{e}}_x + \partial_x y \hat{\mathbf{e}}_y + \mathcal{O}(A^2 k^2), \quad (2.3)$$

where it is assumed that the amplitude is much smaller than the wave length, and therefore terms of the order  $A^2 k^2$  can be ignored.

The total frictional force on the flagellum is  $\mathbf{F} = \int_0^L ds \mathbf{f}_{fric}$ , where  $ds$  is the arc length of the flagellum and  $L$  its contour length, which is  $L = N2\pi/k$ , where  $N$  is the number of simultaneous waves in the tail. Because the  $Ak \ll 1$ , one can approximate  $ds \approx dx$ . If one ignores the end effects of the flagellum, there is no vertical motion. The horizontal force is balanced by the friction force on the head:

$$0 = -\gamma_{head}V - \hat{\mathbf{e}}_x \cdot \int_0^{N2\pi/k} dx \tilde{\gamma}_{\perp}\mathbf{v} + (\tilde{\gamma}_{\parallel} - \tilde{\gamma}_{\perp})\mathbf{tt} \cdot \mathbf{v}, \quad (2.4)$$

where  $\gamma_{head}$  is the friction coefficient of the head. Evaluating the integral

using the expression for  $y$ ,  $\mathbf{v}$  and  $\mathbf{t}$ , gives

$$V = \frac{1}{2}A^2k^2c \left( \frac{\tilde{\gamma}_\perp}{\tilde{\gamma}_\parallel} - 1 \right) \frac{1}{1 + \frac{\gamma_{head}}{L\tilde{\gamma}_\parallel}}. \quad (2.5)$$

The speed is proportional to the square of the ratio of the amplitude and the wavelength ( $A^2k^2$ ) and the wave velocity ( $c$ ). Furthermore, it depends on the ratio of the perpendicular and parallel friction constants per unit length of the flagellum ( $\tilde{\gamma}_\perp/\tilde{\gamma}_\parallel$ ), and the ration of the friction of the head  $\gamma_{head}$  and the parallel friction of the straight flagellum  $L\tilde{\gamma}_\parallel$ . Note that, for large  $L$ ,  $\gamma_\perp/\gamma_\parallel \approx 2$ , so the velocity is positive, that is, it swims in the opposite direction of the wave propagation.

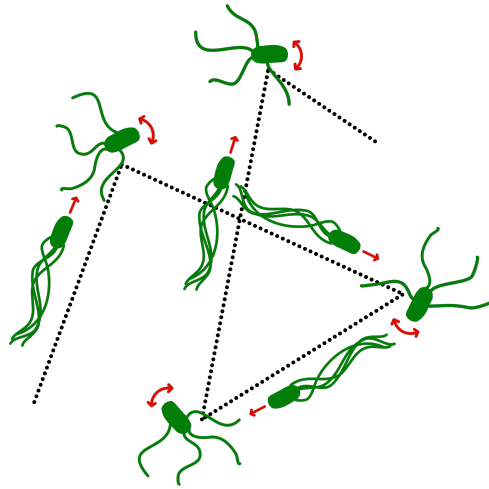
The spermatozoa *P. Miliaris* uses a beating flagellum to propel itself forward. Its beating amplitude is  $A = 4 \mu m$ , its wave number  $k = 0.26 \mu m^{-1}$ , it has  $N = 1.3$  waves, its angular velocity is  $\omega = 22 s^{-1}$ , the radius of its head is  $R_{head} = 0.5 \mu m$ , and the radius of its flagellum is  $a = 0.2 \mu m$  [74]. Equation 2.5 and the Stokes equation (Eq. A.30) for the friction of the head gives  $V \approx 380 \mu m/s$ , which is about double the actual value. The reason is that the assumption that the amplitude is small compared to the wave length is violated, but  $Ak \approx 1$ . A calculation without the assumption of small amplitudes gives the correct value of  $V \approx 190 \mu m/s$  [74].

The self-propulsion due to a single helical flagellum of, for example, *e. coli*, is governed by the same mechanism as the beating flagellum of a eukaryotic cell. In matter of fact, this mechanism might be more familiar. Because the friction constant of corresponding to motion parallel to the long axis of a rod is smaller than the friction constant corresponding to motion perpendicular to a rod, a corkscrew is pulled into a cork when it is rotated, so due to the anisotropy of the friction, rotational motion is coupled to translational motion. The torque due to the rotation of the flagellum must be balanced. The only way this is possible is to rotate the body of the bacterium in the opposite direction.

Note that, even though, this mechanism looks similar to the propulsion due to a propeller of a motor boat, it is governed by completely different physics. The bacterium is governed by low Reynolds number hydrodynamics (the Stokes equation) and it uses the viscosity of the medium to propel itself forward; the propeller of a boat is governed by high Reynolds number hydrodynamics and it uses momentum to propel itself forward.



**Figure 2.3:** Run-and-tumble motion of *e. coli*. When the rotary motors in the membrane rotate counter clock wise, the flagella form a helical bundle and the bacterium is swims forward in a straight line. This is called a run, which lasts a bout 1 s. It swims with a speed of about  $30 \mu\text{m}/\text{s}$  making the run length  $\approx 30 \mu\text{m}$ . When the rotary motors rotate clock wise, the bundle disentangles and spreads out. Due to this, the bacterium rotates. This is called a tumble and lasts about 0.1 s. After a tumble the bacterium has a random, approximately uncorrelated new direction for the next run.



### 2.1.2 Run-and-Tumble Motion

Biological swimmers do not swim in a straight line. Firstly, there is rotational diffusion due to the thermal noise of the fluid. This causes the swimmer to change its direction continuously. Secondly, some swimmers have their own mechanism to re-orient. The most prominent example of the latter is the run-and-tumble motion of *e. coli* [79]. When *e. coli* is in the run phase, its flagella rotate counter clockwise and the flagella form a helical bundle that propels it forward. After some time of swimming in an almost straight line, a tumble event occurs. When this happens one or more of the motors driving the flagella reverses its direction. This causes the bundle of flagella to spread out, which in turn results in the re-orientation of the bacterium. After the tumble event, the run phase starts again and the bacterium moves in a new direction. The run time of *e. coli* is roughly a second. Because the time it takes to tumble is only about one tenths of that, the tumble time is often approximated by zero. The speed of *e. coli* is about  $30 \mu\text{m}/\text{s}$ , so the distance traveled in a single run is roughly ten times its own length.

Eukaryotic swimmers can also perform run-and-tumble motion. For example *Chlamydomonas* (see Fig. 2.1) swims in a straight run by beating its two flagella synchronously, and tumbles by asynchronously beating its flagella [80].

## 2.2 Synthetic Active Matter

A much used strategy for self-propulsion of synthetic active matter is self-phoresis. Phoresis is the motion of a particle due to an externally imposed gradient such as a gradient in the electric potential (electrophoresis), a gradient in the temperature (thermophoresis), or a gradient in the concentration of a dissolved solute (diffusiophoresis) [81–83]. When these gradients are created by the particle itself, it is called self-phoresis. The detailed mechanism behind the motion of a self-diffusiophoretic particle is explained in the next section.

### 2.2.1 Self-Diffusiophoresis

Diffusiophoresis is the movement of a colloid due to a gradient in the solute [82, 84]. When a colloid produces solute molecules in such a way that there is a local gradient in the solute concentration around the colloid, the colloid moves due to self-diffusiophoresis. The gradient in solute concentration around the particle is typically maintained by covering half of the particle’s surface with a catalyst for a chemical reaction. For example, a polystyrene particle with half of its surface covered with platinum in a solution of hydrogen peroxide ( $H_2O_2$ ) and water. The platinum is a catalyst for the reaction  $2 H_2O_2 \rightarrow 2 H_2O + O_2$ . Because the hydrogen peroxide has a similar interaction with the colloid as water, the platinum is effectively a source of  $O_2$  and the water and hydrogen peroxide can be ignored (see Fig. 2.4).

The analysis presented here is based on Refs. [85–88]. The solute is assumed to be dilute, and is therefore considered as an ideal solution<sup>3</sup>. The equation for the time evolution of the solute concentration  $c(\mathbf{r})$  is governed by a continuity equation:

$$\partial_t c + \nabla \cdot \mathbf{J} = 0, \quad (2.6)$$

where  $\mathbf{J}$  is the flux of solute, which is

$$\mathbf{J} = c\mathbf{v} - D\nabla c + \beta Dc\mathbf{f}, \quad (2.7)$$

where  $\mathbf{v}$  is the fluid velocity,  $D$  is the diffusion constant of the solute, and  $\beta$  is the inverse of the temperature, and  $\mathbf{f}$  is the force of between solute and the colloid (for example, steric repulsion and van der Waals forces

---

<sup>3</sup>Correlations due to the interactions between the solute molecules can affect the self-propulsion velocity, and even reverse its direction [89].

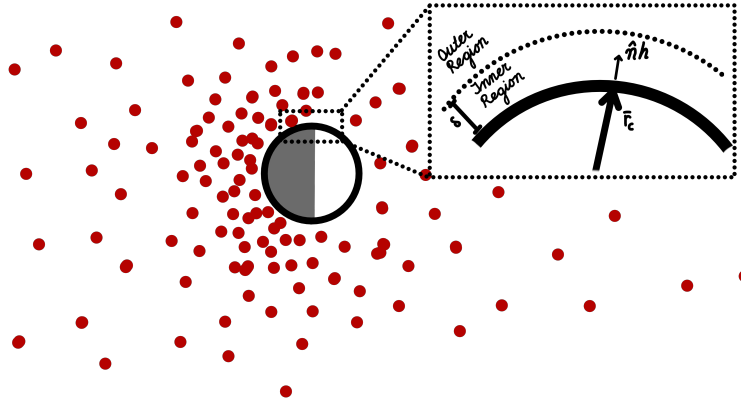


**Figure 2.4:** Diffusiophoresis of a colloidal particle. Gray part of the surface is a catalyst for a chemical reaction. Here it is assumed that the reaction effectively produces a single species of solute molecules (red particles). The inhomogeneous distribution of the catalytic surface on the colloid results in a self-generated solute gradient. The gradient in the solute concentration causes the particle to move due to diffusiophoresis. The zoomed-in figure shows the inner and outer region, and the coordinates used in the analysis of the inner region. The interaction range of the solute is  $\delta$ ,  $\hat{\mathbf{n}}$  indicates the unit normal vector to the surface of the colloid,  $h$  is the distance between the solute and the surface of the colloid, and  $\mathbf{r}_c$  a vector pointing to a location the surface of the colloid. The position of a solute molecule in the inner region is determined by  $\mathbf{r}_c$  and  $h$ .

[49]). The first term accounts for the convection of the solute due to the flow of the fluid. The second and third terms are, respectively, the flux due to diffusion and the force.

The dynamics of the fluid is governed by the Stokes equation (see Section A.2):

$$\nabla \cdot \Sigma + c\mathbf{f} = 0, \quad (2.8)$$

where  $\Sigma = -p\mathbf{1} + \eta_s [\nabla \mathbf{v} + (\nabla \mathbf{v})^T]$  is the stress tensor with pressure  $p$  and viscosity  $\eta_s$ . The force on the solute appears in this equation because the force on the solute is transmitted to the fluid. With the incompressibility equation  $\nabla \cdot \mathbf{v} = 0$ , the gradient of the stress tensor can be written as  $\nabla \cdot \Sigma = -p\mathbf{1} + \eta_s \nabla^2 \mathbf{v}$ . The boundary conditions for the fluid are no

slip at the surface of the colloid and zero velocity at infinity:

$$\mathbf{v}(\mathbf{r}) = \mathbf{V} \text{ for } \mathbf{r} \in S_c, \quad (2.9)$$

$$\mathbf{v}(\mathbf{r}) = 0 \text{ as } |\mathbf{r}| \rightarrow \infty, \quad (2.10)$$

where  $S_c$  is the surface of the colloid and  $\mathbf{V}$  is the self-propulsion velocity of the colloid. The goal of the following calculation is to find an expression for  $\mathbf{V}$ .

The equation for the solute and the equation for the fluid dynamics are coupled:  $\mathbf{v}$  appears in the equation for  $c$ , and  $c$  appears in the equation for  $\mathbf{v}$ . This complication can be overcome because on the length scale of the colloid ( $\sim \mu m$ ) diffusion of molecules in water is more efficient than convection. The time it takes a molecule to diffuse a distance equal to the radius of a colloid, is  $t_{diff} = a^2/(2D)$  where  $a$  is the radius of the colloid, and  $D$  is the diffusion constant of a solute molecule (see Eq. 1.13). The time it takes for convection with velocity  $V = |\mathbf{V}|$  to transport a molecule the same distance is  $t_{conv} = a/V$ . The ratio of these times is called the Péclet number:  $Pe = (t_{diff})/(t_{conv}) = (Va)/(2D)$ . If this number is small diffusion is more important than convection. The diffusion constant of a solute molecule in water is  $D \approx 10^{-9} m^2/s$ <sup>4</sup>, the size of a colloid is of the order of a micrometer, and a typical self-propulsion velocity of a self-phoretic colloid is about ten times its size per second [90]. This results in  $Pe \approx 5 \times 10^{-3}$ . Because the Péclet number is small, the convection in the equation for the solute concentration can be ignored. The case of nonvanishing Péclet number makes the treatment much more complicated [91].

As the colloid moves it sets up a gradient in solute concentration which is constant in the coordinate frame that moves along with the colloid. The time dependence only comes from the boundary conditions, which depend on the position of the colloid; therefore, in the comoving frame, the time derivative  $\partial_t c$  is zero. In the comoving frame, the equation for the solute concentration reduces to  $0 = \nabla \cdot \mathbf{J}$ , with  $\mathbf{J} = -D\nabla c + \beta Dc\mathbf{v}$ . The boundary conditions are a constant concentration far away from the colloid,  $c(\mathbf{r}) \sim c_0$  as  $|\mathbf{r}| \rightarrow \infty$ , and on the surface of the particle  $\hat{\mathbf{n}} \cdot \mathbf{J} = \alpha(\mathbf{r})$  for  $\mathbf{r} \in S_c$ , where  $\hat{\mathbf{n}}$  is the unit normal vector of the surface of the

---

<sup>4</sup>The diffusion constant can be calculated using the Stokes-Einstein equation (Eq. A.31)  $D = T/(6\pi\eta_s a_m)$ , where  $a_m$  is the linear size of the molecule (for oxygen  $a_m \approx 10^{-10} m$ ). The viscosity of water is  $\eta_s = 10^{-3} Pa s$ , and at room temperature  $T \approx 4 \times 10^{-21} J$ . This gives  $D \approx 2 \times 10^{-3} m^2/s$ . The Stokes equation used to derive the Stokes-Einstein equation is not applicable to such small length scales, because the fluid cannot be considered a continuum; it does however give roughly the correct value for the diffusion constant.

colloid, and  $\alpha(\mathbf{r})$  is called the surface activity [92], which accounts for the source of solute particles at the surface of the colloid (the  $O_2$  production in the example above). This is what drives the system out of equilibrium. For a self-phoretic colloid  $\alpha$  is not constant on the surface, and therefore the solute concentration is not uniform on the surface of the colloid. Because the solute concentration no longer depends on the fluid dynamics, it can be solved independently, and the result can subsequently be used in the calculation of the fluid velocity.

Furthermore, the hydrodynamic problem of the fluid flow can be split in solving the flow near the boundary of the colloid (called the inner region) and solving the flow in the region far from the colloid (called the outer region); see Fig. 2.4. The width of the inner region is equal to the interaction range of the solute and the colloid  $\delta$ .

Because the inner region has a width equal to the interaction range of the colloid and the solute, the curvature of the colloid is much larger than this length and can therefore be ignored:  $\delta/a \approx 0$ . The coordinates in the inner region are then the location on the surface of the colloid  $\mathbf{r}_c$  and the distance to the surface  $h$  (see Fig. 2.4). The goal of the calculation of inner problem is to find the fluid flow at the boundary between the inner and outer region ( $h = \delta$ ). This flow is called the slip velocity and serves as a boundary condition for the fluid flow in the outer region.

The equation for the solute concentration in the inner region is

$$0 = \nabla \cdot \mathbf{J} = -D\nabla^2 c_{in} - Dc_{in} \nabla(\beta U), \quad (2.11)$$

where  $c_{in} = c_{in}(\mathbf{r}_c, h)$  is the solute concentration in the inner region, and  $U$  is the potential that gives rise to the force  $\mathbf{f} = -\nabla U$ . The boundary condition is

$$[\hat{\mathbf{n}} \cdot (-D\nabla c_{in} - Dc_{in} \nabla \beta U)]_{h=0} = \alpha(\mathbf{r}_c). \quad (2.12)$$

The gradients occur on a length scale  $\delta$ , and the typical value of the concentration in the inner region, obtained by solving the problem without a potential, is  $c_{in} = \alpha a/D$ , where  $\alpha$  is the typical value of  $\alpha(\mathbf{r}_c)$ . Defining the dimensionless quantities  $\tilde{h} = h/\delta$ ,  $\tilde{\nabla} = \delta \nabla$ , and  $\tilde{c}_{in} = c_{in} D / (\alpha a)$  turns the boundary condition into  $\hat{\mathbf{n}} \cdot [\tilde{\nabla} \tilde{c}_{in} + \tilde{c}_{in} \tilde{\nabla} \beta U]_{\tilde{h}=0} = -\delta/a$ . This shows that up to zeroth order in  $\delta/a$ , the boundary condition becomes  $\hat{\mathbf{n}} \cdot [\nabla c_{in} + c_{in} \nabla \beta U]_{h=0} = 0$ . The solution to Eq. 2.11 can then be obtained by integration:

$$c_{in}(\mathbf{r}_c, h) = c_{out}(\mathbf{r}_c) e^{-\beta U(h)}, \quad (2.13)$$

where  $c_{out}(\mathbf{r}_c)$  is the solute concentration in the outer region evaluated at the position  $(\mathbf{r}_c, h + \delta)$ . Note that this is just the Boltzmann distribution.

The equation for the fluid flow in the  $h$  direction in the inner region is

$$-\partial_h p_{in} + \eta_s \nabla^2 v_h = c_{in} \partial_h U. \quad (2.14)$$

Because the boundary of the colloid is impenetrable for the fluid,  $v_h$  is zero at the boundary, and because the inner region has a small width it can be ignored in the whole inner region. In the outer region the pressure is a constant, and because of the incompressibility condition this constant is irrelevant and can be set to zero. The remaining equation can be integrated with the boundary condition  $p_{in}(\mathbf{r}_c, h = \delta) = p_{out} = 0$ :

$$p_{in}(\mathbf{r}_c, h) = \frac{1}{\beta} c_{out}(\mathbf{r}_c) \left[ e^{-\beta U(h)} - 1 \right] \quad (2.15)$$

Because of the no-slip condition on the surface of the colloid, at this surface the fluid flows with the same velocity as the colloid. This determines the boundary condition for the fluid flow parallel to the surface:

$$\mathbf{v}_{\parallel} = \mathbf{V}_{\parallel}, \quad (2.16)$$

where  $\mathbf{V}$  is the velocity of the colloid.

The force on the fluid parallel to the surface  $\mathbf{f}_{\parallel} = 0$ , so equation for the fluid flow parallel to the surface is

$$-\nabla_{\parallel} p_{in} + \eta_s \partial_h^2 v_{\parallel} = 0, \quad (2.17)$$

where the approximation  $\nabla^2 \approx \partial_h^2$  was used, which holds if  $\delta/a \ll 1$ , and  $\nabla_{\parallel} = (\mathbf{1} - \hat{\mathbf{n}}\hat{\mathbf{n}}) \cdot \nabla$  is the gradient in the direction parallel to the surface. Using Eq. 2.14 for  $p_{in}$  gives

$$\partial_h^2 v_{\parallel} = \frac{1}{\beta \eta_s} \left( \nabla_{\parallel} c_{out} \right) \left[ e^{-\beta U} - 1 \right]. \quad (2.18)$$

The solution can be obtained by asymptotic matching of the fluid flow in the inner and outer region  $\mathbf{v}_{in}(\mathbf{r}_p, h \rightarrow \infty) = \mathbf{v}_{out}(\mathbf{r}_p) = \mathbf{v}_{slip}$ , where  $\mathbf{v}_{slip}$  is the so called slip velocity. The boundary conditions are  $v_{\parallel} = 0$  at  $h = 0$  (no slip at the surface), and  $v_{\parallel} = v_{slip}$  for  $h \rightarrow \infty$  (no external shear rate) [88]. Multiplying the previous equation by  $h$  and integrating from zero to

infinity results in

$$\mathbf{v}_{slip} = \frac{\lambda_D^2}{\beta\eta_s} (\mathbf{1} - \hat{\mathbf{n}}\hat{\mathbf{n}}) \cdot \nabla c_{out}(\mathbf{r}_c), \quad (2.19)$$

where

$$\lambda_D^2 = \int_0^\infty dh 1 - e^{-\beta U(h)}, \quad (2.20)$$

is called the Derjaguin length [88]. Note that  $\lambda_D^2$  can be both positive and negative. If the interaction between the particle and the solute is repulsive  $\lambda_D^2 > 0$ , and if the interaction is attractive  $\lambda_D^2 < 0$ .

The problem in the outer region consists of a particle moving with velocity  $\mathbf{V}$ . The radius of the spherical surface separating the inner and outer region is  $a + \delta$ , where  $a$  is the radius of the colloid. Because the fluid at the boundary between the inner and outer region moves with velocity  $\mathbf{v}_{slip}$  relative to the colloid, the boundary condition is  $\mathbf{v} = \mathbf{V} + \mathbf{v}_{slip}$  at the boundary between the inner and outer region.

To calculate  $\mathbf{V}$ , one can use Lorentz's reciprocal theorem (see Sec. A.6). According to this theorem  $\int_{S_c^+} dS \hat{\mathbf{n}} \cdot \Sigma' \cdot \mathbf{v} = \int_{S_c^+} dS \hat{\mathbf{n}} \cdot \Sigma \cdot \mathbf{v}'$ , where  $(\Sigma, \mathbf{v})$  and  $(\Sigma', \mathbf{v}')$  are both solutions to the Stokes equation in the same domain, but with different boundary conditions. The integrals are over a spherical surface  $S_c^+$  with radius  $a + \delta$ . For  $(\Sigma', \mathbf{v}')$  a known solution can be used, in this case the fluid flow around a particle dragged with a force  $\mathbf{F}'$  and with no-slip boundary condition. This problem is solved in Appendix A.4. The solution is that the particle moves with velocity  $\mathbf{V}' = \mathbf{F}' / (6\pi\eta_s a)$ . At the surface the fluid moves with the particle, so  $\mathbf{v}' = \mathbf{V}'$  at the surface of the particle is constant. Then  $\int_{S_c^+} dS \hat{\mathbf{n}} \cdot \Sigma \cdot \mathbf{v}' = \mathbf{V}' \cdot \int_{S_c^+} dS \hat{\mathbf{n}} \cdot \Sigma$ .

Integrating the Stokes equation  $\nabla \cdot \Sigma + c\mathbf{f} = 0$  over the volume of the inner region

$$\begin{aligned} 0 &= - \int_{a < r < a + \delta} dV \hat{\mathbf{n}} \cdot \Sigma + c\mathbf{f} \\ &= \int_{S_c} dS \hat{\mathbf{n}} \cdot \Sigma - \int_{S_c^+} dS \hat{\mathbf{n}} \cdot \Sigma - \int_{a < r < a + \delta} dV c\mathbf{f}, \end{aligned} \quad (2.21)$$

where  $S_c$  is the surface of the colloid, and the normal vectors  $\hat{\mathbf{n}}$  are directed out of the spherical surfaces. The first integral is the hydrodynamic force on the colloid. The third integral is the force of the solute particles on the colloid ( $\mathbf{f}$  is the force of the colloid on the solute). The sum of the first and third integral is the total force, which must be zero because there

is no external force acting on the system. Therefore, the second integral vanishes, and because of that  $\int_{S_c^+} dS \hat{\mathbf{n}} \cdot \Sigma' \cdot \mathbf{v} = 0$ .

The force on the colloid in the primed system is  $\mathbf{F}' = \int_{S_c^+} dS \hat{\mathbf{n}} \cdot \Sigma'$ . This force is constant over the surface of the colloid, so  $\hat{\mathbf{n}} \cdot \Sigma' = \mathbf{F}' / (4\pi a^2)$ . Using this,  $\int_{S_c^+} dS \hat{\mathbf{n}} \cdot \Sigma' \cdot \mathbf{v} = 0$ , and  $\mathbf{v} = \mathbf{V} + \mathbf{v}_{slip}$  on the surface gives

$$\mathbf{V} \cdot \mathbf{F}' = -\frac{1}{4\pi a^2} \mathbf{F}' \cdot \int_{S_c^+} dS \mathbf{v}_{slip}. \quad (2.22)$$

Because the force  $\mathbf{F}'$  is arbitrary

$$\mathbf{V} = -\frac{1}{4\pi a^2} \int_{S_c^+} dS \mathbf{v}_{slip} = -\frac{\lambda_D^2}{\beta\eta_s} \frac{1}{4\pi a^2} \int_{S_c^+} dS (\mathbf{1} - \hat{\mathbf{n}}\hat{\mathbf{n}}) \cdot \nabla c_{out}. \quad (2.23)$$

What remains is to calculate the concentration in the outer region, which is governed by  $\nabla^2 c(\mathbf{r}) = 0$  with boundary conditions  $\hat{\mathbf{n}} \cdot \nabla c(\mathbf{r}) = -\alpha(\mathbf{r})/D$  for  $r \equiv |\mathbf{r}| = a + \delta \approx a$  and  $c(\mathbf{r}) = 0$  as  $|\mathbf{r}| \rightarrow \infty$ . The solution to these equations is [92]

$$c(\mathbf{r}) = c(r, \theta) = \frac{a}{D} \sum_{l=0}^{\infty} \frac{\alpha_l}{l+1} \left(\frac{a}{r}\right)^{l+1} P_l(\cos \theta), \quad (2.24)$$

where  $\theta$  is the angle with the  $x$ -axis,  $P_l(x)$  are the Legendre polynomials and  $\alpha_l$  are the coefficients of the expansion of the surface activity in Legendre polynomials:  $\alpha(\mathbf{r}_c) = \alpha(\theta) = \sum_{l=0}^{\infty} \alpha_l P_l(\cos \theta)$ .

As an example, a so called Janus particle is considered. Such a particle has half its surface covered with a catalyst (see Refs. [85, 92, 93] for other patterns of the catalytic surface). If the part of the colloid with  $x > 0$  in the comoving frame is covered with the catalyst, as shown in Fig. 2.4, the surface activity can be expressed as  $\alpha(\mathbf{r}_c) = \alpha(\cos \theta) = \bar{\alpha} [1 - H(\cos \theta)]$ , where  $\bar{\alpha}$  is the number of solute molecules produced per unit time per unit area, and  $H(x)$  is the Heaviside step function. The coefficients of the expansion in Legendre polynomials are then  $\alpha_0 = \bar{\alpha}/2$  and  $\alpha_{l>0} = \bar{\alpha} (P_{l+1}(0) - P_{l-1}(0)) / 2$ .

Using this in Eq. 2.23 gives [85, 94]

$$\mathbf{V} = \frac{\lambda_D^2}{\beta\eta_s} \frac{\bar{\alpha}}{4D} \hat{\mathbf{e}}_x. \quad (2.25)$$

If the interaction between the colloid and the solute is repulsive then  $\lambda_D^2 > 0$ , and the particle "swims" in the positive  $x$  direction. That is, it swims



with the catalytic side behind. If the interaction between the colloid and the solute is attractive it swims with the catalytic side in front.

The constant  $\bar{\alpha}$  is the number of produced solute molecules ( $O_2$  in the example reaction) per unit area per unit time. This depends on the number of fuel molecules ( $H_2O_2$  in the example reaction) that are converted to water and solute molecules. If the reaction is diffusion limited, that is the limiting factor is the time it takes for fuel to diffuse towards the reaction site and not the time it takes to convert the fuel to solute, this scales as  $\sim a^{-1}$ . This scaling can be obtained as follows. The surface activity  $\bar{\alpha}$  is proportional to the total number of produced solute molecules per unit time. This is equal to the number of fuel molecules converted to water and solute per unit time:  $N_s = \int dS \hat{\mathbf{n}} \cdot \mathbf{J}_f$ , where  $\mathbf{J}_f = -D_f \nabla c_f$  is the flux of fuel molecules, with  $D_f$  the diffusion constant of a fuel molecule, and  $c_f$  the fuel concentration. The integral is over the catalytic surface of the colloid with unit normal vector  $\hat{\mathbf{n}}$ . However, for the scaling one can approximate the Janus colloid by a colloid that is fully covered by the catalyst and extend the integral over the full surface. The fuel concentration obeys the diffusion equation  $\nabla^2 c_f = 0$ , with boundary conditions  $c_f(r \rightarrow \infty) = c_f^\infty$  and  $c_f(a) = 0$  because as soon as a fuel molecule reaches the catalytic surface it is converted to water and solute. The solution to this equation is obtained by integration, which gives  $c_f(r) = c_f^\infty (1 - a/r)$ , which in turn results in  $N_s = D_f c_f^\infty / a$ . If only a part of the colloid is covered with a catalytic surface, this result does not hold. It does, however, still give the correct scaling  $N_s \sim a^{-1}$ . The self-propulsion speed of this Janus colloid is proportional to  $\bar{\alpha}$  which is proportional to  $N_s$ , and therefore  $|V| \sim a^{-1}$ . That is, smaller particles have a higher self-propulsion velocity than larger particles. For a more detailed analysis of the dependence of the self-propulsion velocity on the particle's size, see Refs. [95, 96].

The Janus colloid does not swim in the same direction forever, but, because the colloid rotates due to rotational Brownian motion (see Sec. 1.3.3), it changes its direction continuously. The rotational diffusion constant is also affected by the activity. However, this effect is usually much weaker than the effect of the self-propulsion [97]. Note that the rotational diffusion constant is also dependent on the radius of the particle.

### Light-Activated Self-Diffusiophoresis

There are many other ways to self-propel besides the self-phoretic active mechanism described in the previous section. In particular, there are mechanisms that need a light source, resulting in so called light-activated active particles. One of such methods is based on locally demixing a fluid

[54]. In this case half of the colloid is covered with a light absorbing material such as gold [54] or carbon [57]. When such a particle is illuminated, one side heats up, creating a local temperature gradient. If such a particle is placed in a (near) critical binary mixture, for example lutidine in water [54], and is illuminated, the cap heats up and locally demixes the mixture. If the cap is hydrophobic, the water rich phase depletes the region near the cap, and the solute (e.g. lutidine) rich phase absorbs at the hydrophobic cap. The colloid moves in the resulting gradient due to self-diffusiophoresis, as described in the previous section. The rotational diffusion of the colloid, and with that the orientational correlation time of the self-propulsion direction, is independent of the illumination intensity, and therefore, independent of the swim speed [54].

One advantage of this method of self-propulsion is that the energy source is the light source, which can be supplied externally. In case of self-diffusiophoresis due to a catalytic cap (as in the previous section), a constant source of fuel is needed to keep the particles moving.

## 2.3 Inhomogeneous Activity

The particular behavior of active matter manifests itself when the particles interact either with other active particles [36, 37, 98, 99], when they interact with walls or other obstacles [90, 100, 101], or when is inhomogeneous; that is, their self-propulsion speed is space, and possibly time, dependent. This is the main topic of the work presented in Part II. Some examples of biological and synthetic active matter systems with inhomogeneous activity are given below.

### 2.3.1 Inhomogeneous Activity in Biological Systems

Nucleus centering is essential for the proper functioning of a cell. In most cells the centrosome takes care of this [102]. Recently, it has been discovered that in certain cells that do not have a centrosome (for example mouse oocytes) the nucleus is centered by active diffusion [103–105]. Inside these cells there are molecular motors (myosin) that walk on a network of filaments (actin). These molecular motors interact with the cell nucleus by pushing against it. The speed with which the motors move is larger near the cell cortex than in the center. This gradient in the self-propulsion speed of the motors results in an effective pressure gradient [106]. The corresponding effective force pushes the nucleus down the pressure gradient towards the center of the cell.

Bacteria, such as *e. coli*, can also have a space dependent activity. In general *e. coli* needs oxygen to drive its rotary motor [107, 108]. Certain strains of *e. coli* can also drive their motor when there is no oxygen available. This alternative mechanism uses photons [109, 110]. The self-propulsion speed of these bacteria is proportional to the light intensity [111]. Because one can easily control the illumination pattern in time and space [58, 111, 112], light-powered *e. coli* are an excellent system to test theories of active matter with inhomogeneous activity.

### 2.3.2 Inhomogeneous Activity in Synthetic Systems

The self-diffusiophoretic active particles described earlier have a swim speed proportional to the number of produced solute molecules. This means that as long as the number of fuel molecules reaching the catalytic cap of the colloid is the limiting factor, the more fuel is present the faster they propel themselves forward (up to a saturation speed). This was used in Ref. [113] to study experimentally active colloidal rods with space dependent swim speed. The gradient in the fuel was created by placing a hydrogel soaked with the fuel in the experimental setup. The fuel is slowly released resulting in a concentration gradient of fuel. This corresponds to a swim speed gradient because the particles move slower if there is less fuel. This method is not difficult to implement; however, it does not give much control over the shape of the swim speed profile, as the resulting swim speed gradient depends on the diffusion of the fuel.

In case of light-activated self-diffusiophoresis, it is straight forward to impose any desired activity pattern by patterning the illumination intensity [54, 57, 114]. Furthermore, one can change the illumination pattern in time as well.

The gradient in the swim speed due to a gradient in the fuel concentration or light intensity (or other source for the driving mechanism) can cause a torque on the particle such that it aligns its self-propulsion direction along the gradient in the swim speed [57, 114, 115]; however, there are methods that avoid this [116–119]

## 2.4 Active Colloidal Molecules and Polymers

Atoms can form chemical bonds with other atoms to form molecules. The typical size of molecules is several Ångström. The constituent atoms and how they are arranged determine the properties of the resulting material.

Similarly, one can bind colloidal sized particles together, to form colloidal molecules [120–124]. When at least one of the colloids is active, the resulting molecule is called an active colloidal molecule [125]. The active colloidal “atoms” can be bound together by the same mechanisms as for passive colloids. Here a few mechanisms are mentioned that can be used to make active dimers and polymers, for more details see Ref. [125]. Colloids can be chained together by DNA [126]. The persistence length of the colloidal polymer can be controlled by changing the length of the DNA between the colloids. Furthermore, active colloids can be configured into different collective states. For example, when the two sides of the active colloids have opposite charge, they assemble in chains, that is active polymers [127]. Lastly, diffusiophoretic active particles can self-assemble into dimers [128, 129].



## **Chapter 3**

# **Modeling Active Matter**

There are several models for active matter, all of which have two defining features: local energy input and persistent motion. Here three of the most common models of active particles – namely, run-and-tumble, active Brownian and active Ornstein-Uhlenbeck particles – are presented. In order to understand how activity affects these systems, several basic properties are discussed.

## 3.1 Models

### 3.1.1 Run-And-Tumble Particles

Run-and-tumble (RT) motion is a commonly used model for the dynamics of a large group of bacteria [35]. The behavior of RT particles is characterized by two states: the run state, in which it moves (roughly) in a straight line with constant speed  $v_s$ , and the tumble state in which it re-orient its direction (see Fig. 2.3). For bacteria such as *e. coli* the run state lasts about 1 s and the tumble state about 0.1 s. Because the tumble state lasts much shorter than the run state, it is approximated as instantaneous. Furthermore, it is assumed that after a tumble the orientation is uncorrelated with the previous orientation.

The autocorrelation function of the orientation in the RT process can be obtained from the master equation. The master equation for the RT process is

$$\partial_t P(\mathbf{n}, t | \Omega_0) = -\alpha P(\mathbf{n}, t | \Omega_0) + \frac{\alpha}{\Omega_d}, \quad (3.1)$$

where  $\mathbf{n} = \mathbf{n}(\Omega)$ ,  $\Omega_d$  is the solid angle in  $d$  dimensions,  $\Omega_0$  is the orientation at  $t = 0$ ,  $\alpha$  is the tumble rate, and  $\Omega_d$  is the surface area of a  $d$  dimensional unit sphere ( $\Omega_2 = 2\pi$  and  $\Omega_3 = 4\pi$ ). The first term on the right-hand side accounts for the tumbling from orientation  $\mathbf{n}(\Omega)$  to any other orientation. The second term on the right-hand side accounts for the tumbling from any orientation to an orientation  $\mathbf{n}(\Omega)$ . The solution to this equation can be obtained by integration:

$$P(\mathbf{n}, t | \Omega_0) = \delta^{(d-1)}(\mathbf{n}(t) - \Omega_0) e^{-\alpha t} + \frac{1 - e^{-\alpha t}}{\Omega_d}, \quad (3.2)$$

where  $\mathbf{n}(\Omega_0)$  is the orientation at time  $t = 0$ .

This can be used to obtain the autocorrelation function for the orienta-

tion vector:

$$\langle \mathbf{n}(0) \cdot \mathbf{n}(t) \rangle = \mathbf{n}(0) \cdot \int d\Omega \mathbf{n}(\Omega) P(\Omega, t | \Omega_0) = e^{-\alpha t}, \quad (3.3)$$

where  $\int d\Omega \mathbf{n}(\Omega) = 0$  was used. Just as for the rotational diffusion (see Eq. 1.83), the autocorrelation function decays exponentially. For the RT process the autocorrelation time is

$$\tau = \frac{1}{\alpha}. \quad (3.4)$$

For RT motion, that is a RT particle that moves with speed  $v_s$  in the direction of its orientation, there are also the spatial degrees of freedom. The master equation corresponding to RT motion is

$$\partial_t P(t) = -v_s \mathbf{n} \cdot \nabla P(t) - \alpha P(t) + \frac{\alpha}{\Omega_d} \rho(t), \quad (3.5)$$

where  $P(t) = P(\mathbf{r}, \Omega, t)$ , and  $\rho(t) = \rho(\mathbf{r}, t) \equiv \int d\Omega P(t)$  is the local density of particles, irrespective of their orientation. The first term on the right-hand side accounts for the drift in the direction  $\mathbf{n}$  due to the active motion, and the last two terms account for the tumble dynamics and are the same as in Eq. 3.1.

From the master equation one can obtain the long-time mean squared displacement (MSD) corresponding to RT motion [130]. Here, however, a method based on the ideas from ideal chains in polymer physics is used [131, 132]. If the particle tumbles with rate  $\alpha$ , the time intervals  $\Delta t$  between tumbles are distributed according to a Poisson distribution<sup>1</sup>  $P_\alpha(\Delta t) = \alpha e^{-\alpha \Delta t}$ . The first two moments of this distribution are  $\langle \Delta t \rangle = \alpha^{-1}$  and  $\langle (\Delta t)^2 \rangle = 2\alpha^{-2}$ .

The length of a straight run between tumbles is  $l_i = v_s \mathbf{n}_i$ , where  $v_s$  is the swim speed, and  $\mathbf{n}_i$  the unit vector in that points in the swimming direction. The position after  $N$  runs is  $\sum_i^N l_i \Delta t_i$ , which leads to

$$\langle \mathbf{r}^2(t) \rangle = \left\langle \sum_{i,j}^N l_i l_j \mathbf{n}_i \cdot \mathbf{n}_j \right\rangle \quad (3.6)$$

---

<sup>1</sup>The probability of to tumble in  $dt$  is  $\alpha dt$ . Therefor the probability of a run time  $\Delta t$ , where this time can be separated in  $n \rightarrow \infty$  infinitesimal intervals  $\Delta t = n dt$ , is the probability not to tumble  $n - 1$  times in a time interval  $dt$  and to tumble once at the end in a time interval  $dt$ :  $P_\alpha(\Delta t) dt = (1 - \alpha dt)^{n-1} \alpha dt$ . For  $n \rightarrow \infty$  this becomes the Poisson distribution shown in the main text.



for the mean-squared displacement. The run length (or time) and the orientation are independent, therefore the average over the orientation vectors can be performed independently, which gives  $\langle \mathbf{n}_i \cdot \mathbf{n}_j \rangle = \delta_{ij}$  because each orientation is independent. Due to the delta function, only one of the sums remain:

$$\langle \mathbf{r}^2(t) \rangle = \left\langle \sum_i^N l_i^2 \right\rangle. \quad (3.7)$$

The number of runs is given implicitly by  $t = \sum_i^N \Delta t_i$ . If the number of runs is large, this becomes  $t = N \langle \Delta t \rangle$ , by the law of large numbers. Using this to replace  $N$  in the average of the MSD gives

$$\langle \mathbf{r}^2(t) \rangle = \frac{t}{\langle \Delta t \rangle} \langle l_i^2 \rangle = \frac{t}{\langle \Delta t \rangle} v_s^2 \langle (\Delta t)^2 \rangle = 2dD_a t, \quad (3.8)$$

with diffusion constant

$$D_a = \frac{v_s^2}{d\alpha}. \quad (3.9)$$

The bacterium *e. coli* swims with a speed of  $v_s \approx 30 \mu\text{ms}^{-1}$ , and has a tumble rate of  $\alpha \approx 1 \text{ s}^{-1}$  [62]. The diffusion constant due to the active motion is<sup>2</sup>  $D_a = 300 \mu\text{m}^2\text{s}^{-1}$ . If this bacterium would stop swimming, it would move around due to the thermal motion. Using the Stokes-Einstein relation (Eq. 1.5) with the size  $2 \mu\text{m}$  of the bacterium for the radius gives  $D = 0.1 \mu\text{m}^2\text{s}^{-1}$ . This shows that for this bacterium the active motion is much more important than the motion due to thermal agitation.

More on the mean-squared displacement of active particles, in particular their short and intermediate time behavior, is discussed in Sec. 3.2.1.

### 3.1.2 Active Brownian Particles

Synthetic active particles (see Section 2.2.1) propel themselves forward and are subject to thermal noise. This thermal noise affects both the translational as well as the rotational motion. Unlike the RT model, in the active Brownian particle (ABP) model the change in orientation is continuous, in particular it is modeled as rotational Brownian motion(see Section 1.3.3).

---

<sup>2</sup>The diffusion constant of *e. coli* is actually some what larger than this because when it tumbles its new orientation is correlated with the previous orientation and other details that are ignored in the model used here [18].

The Langevin equation corresponding to the translational motion of this model is

$$\partial_t \mathbf{r} = v_s \mathbf{n} + \sqrt{2D} \boldsymbol{\zeta}, \quad (3.10)$$

where  $v_s$  is the swim speed,  $\mathbf{n}$  the instantaneous orientation,  $D$  the passive diffusion constant, and  $\boldsymbol{\zeta}$  is a random Gaussian vector with  $\langle \boldsymbol{\zeta}(t) \rangle = 0$  and  $\langle \boldsymbol{\zeta}(t) \boldsymbol{\zeta}(t') \rangle = \delta(t - t') \mathbf{1}$ . The orientation vector  $\mathbf{n}$  undergoes rotational diffusion. In two dimensions this corresponds to

$$\partial_t \theta = \sqrt{2D_r} \eta, \quad (3.11)$$

where  $\mathbf{n} = (\cos(\theta), \sin(\theta))$ ,  $D_r$  is the rotational diffusion constant, and  $\eta$  is a random Gaussian number with mean  $\langle \eta(t) \rangle = 0$ , and  $\langle \eta(t) \eta(t') \rangle = \delta(t - t')$ . In three dimensions, rotational Brownian motion is described by

$$\partial_t \mathbf{n} = \sqrt{2D_r} \mathbf{n} \times \boldsymbol{\eta}, \quad (3.12)$$

where  $\boldsymbol{\eta}$  is a random Gaussian vector with mean  $\langle \boldsymbol{\eta}(t) \rangle = 0$  and  $\langle \boldsymbol{\eta}(t) \boldsymbol{\eta}(t') \rangle = \delta(t - t') \mathbf{1}$ .

### 3.1.3 Active Ornstein-Uhlenbeck Particles

The active Ornstein-Uhlenbeck model was originally proposed as an approximation to ABPs [133]. However, it has become a much used model in its own right [134–139]. In this model, the self-propulsion in the equation for the translational degrees of freedom,  $v_s \mathbf{n}$ , is replaced by a Gaussian noise that has the same first two moments:

$$\partial_t \mathbf{r} = \boldsymbol{\chi} + \sqrt{2D} \boldsymbol{\zeta}, \quad (3.13)$$

where  $\langle \boldsymbol{\chi}(t) \rangle = \langle v_s \mathbf{n}(t) \rangle = 0$  and

$$\langle \boldsymbol{\chi}(t) \boldsymbol{\chi}(t') \rangle = \langle v_s \mathbf{n}(t) v_s \mathbf{n}(t') \rangle = \frac{1}{d} v_s^2 e^{-(t-t')/\tau} \mathbf{1} \quad (3.14)$$

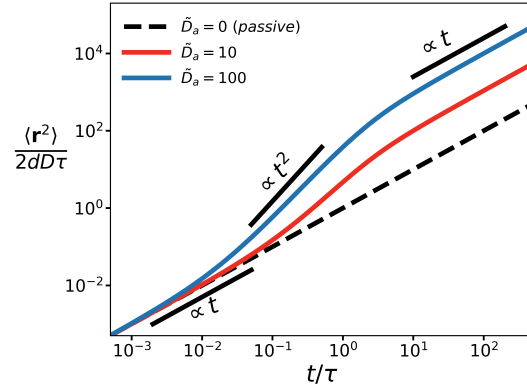
where the correlation function of  $\mathbf{n}$  is given in Eq. 1.83, and  $\tau = (d - 1)D_r$ .

The time correlated stochastic processes  $\boldsymbol{\chi}$  is related to an uncorrelated stochastic process  $\boldsymbol{\eta}$  by

$$\tau \partial_t \boldsymbol{\chi} = -\boldsymbol{\chi} + \sqrt{2D_a} \boldsymbol{\eta}, \quad (3.15)$$

where  $\boldsymbol{\eta}$  is a random Gaussian vector with  $\langle \boldsymbol{\eta}(t) \rangle = 0$  and  $\langle \boldsymbol{\eta}(t) \boldsymbol{\eta}(t') \rangle =$

**Figure 3.1:** The MSD of an ABP normalized by the MSD of a passive Brownian particle in time equal to the orientational correlation time  $\tau$  for different active diffusion constants  $\tilde{D}_a = D_a/D$ . For  $t/\tau < 2D/D_a$  the behavior is dominated by passive diffusion, and scales linearly with time. Between  $t/\tau = 2D/D_a$  and  $t/\tau = 2$  the behavior is ballistic due to the persistent active motion. For  $t/\tau > 2$  the behavior is diffusive again, but with an enhanced diffusion constant  $D + D_a$ . The active diffusion constant  $D_a$  can be orders of magnitude larger than the thermal diffusion constant.



$\delta(t - t')$ . Because both Eq. 3.13 and 3.15 are Gaussian processes, the active Ornstein-Uhlenbeck process has many advantages regarding analytical calculations [135]. In this work, however, the active Ornstein-Uhlenbeck model is only used as an approximation in Chapter 5.

## 3.2 Basic Results

Even though, on a long time scale the behavior of a free active particle is diffusive, and therefore similar to the behavior of an equilibrium Brownian particle, as already shown in Sec. 3.1.1. Due to the inherently nonequilibrium nature of active particles, their behavior in more complex environments can be quite different from equilibrium Brownian particles. In this section some of the basic features of active particles are discussed. These examples serve as an introduction to the methods that are used throughout the rest of this work.

### 3.2.1 Enhanced Diffusion

In Section 3.1.1 it was shown that on long times scales the RT process is diffusive. On shorter time scales, however, active particles have richer behavior. The following theory holds for run-and-tumble, active Brownian and active Ornstein-Uhlenbeck particles because it only uses the first two moments of the active force.

The time integral of the stochastic differential equation for an active

particle is

$$\mathbf{r}(t) = \int_0^t dt' \left[ v_s \mathbf{n}(t') + \sqrt{2D} \boldsymbol{\zeta}(t') \right], \quad (3.16)$$

with  $\mathbf{r}(0) = 0$ . The mean squared displacement is

$$\begin{aligned} \langle \mathbf{r}(t)^2 \rangle = \int_0^t dt' \int_0^t dt'' \langle & \left[ v_s \mathbf{n}(t') + \sqrt{2D} \boldsymbol{\zeta}(t') \right] \cdot \\ & \left[ v_s \mathbf{n}(t'') + \sqrt{2D} \boldsymbol{\zeta}(t'') \right] \rangle. \end{aligned} \quad (3.17)$$

The passive thermal noise  $\boldsymbol{\zeta}$  and the orientation vector are uncorrelated, therefore  $\langle \mathbf{n}(t') \cdot \boldsymbol{\zeta}(t'') \rangle = 0$ . The thermal noise autocorrelation is  $\langle \boldsymbol{\zeta}(t') \cdot \boldsymbol{\zeta}(t'') \rangle = \delta(t' - t'')$ , and the autocorrelation of the orientation vector is  $\langle \mathbf{n}(t') \cdot \mathbf{n}(t'') \rangle = \exp(-|t' - t''|/\tau)$ , where  $\tau = 1/(\alpha + (d-1)D_r)$  is the correlation time (see Eqs. 3.4 and 1.82). Using this gives [94]

$$\frac{\langle \mathbf{r}(t)^2 \rangle}{2dD\tau} = \frac{t}{\tau} + \frac{D_a}{D} \frac{t}{\tau} + \frac{D_a}{D} \left( e^{-t/\tau} - 1 \right), \quad (3.18)$$

where the MSD is divided by the MSD due to thermal noise in a time  $\tau$ , and

$$D_a \equiv \frac{1}{d} \tau v_s^2, \quad (3.19)$$

is the active diffusion constant.

The MSD has three regimes (see Fig. 3.1). The first two regimes can be obtained by expanding in  $t/\tau$ :

$$\frac{\langle \mathbf{r}(t)^2 \rangle}{2dD\tau} = \frac{t}{\tau} + \frac{1}{2} \frac{D_a}{D} \left( \frac{t}{\tau} \right)^2 + \mathcal{O} \left( \frac{t^3}{\tau^3} \right). \quad (3.20)$$

This shows that for short times the MSD is diffusive and only the thermal diffusion is important:

$$\frac{\langle \mathbf{r}(t)^2 \rangle}{2dD\tau} \sim \frac{t}{\tau}. \quad (3.21)$$

At intermediate times the MSD behaves ballistically, that is  $MSD \sim t^2$ .

$$\frac{\langle \mathbf{r}(t)^2 \rangle}{2dD\tau} \sim \frac{1}{2} \frac{D_a}{D} \left( \frac{t}{\tau} \right)^2. \quad (3.22)$$

Note that this ballistic behavior is not a consequence of momentum, but is a result of the self-propulsion of the ABP.

For long times the exponential in Eq. 3.18 vanishes, which results in diffusive behavior again:

$$\frac{\langle \mathbf{r}(t)^2 \rangle}{2dD\tau} \sim \left(1 + \frac{D_a}{D}\right) \frac{t}{\tau}. \quad (3.23)$$

On time scales longer than the orientational correlation time  $\tau$ , an ABP is diffusive with an effective diffusion constant  $D_{eff} = D + D_a$ . On this time scale the ABP behaves like a "hot" passive Brownian particle with temperature  $T_{eff} = T + T_a$ , where  $T_a = \gamma D_a = \gamma \tau v_s^2 / d$ . This effective temperature may be a useful quantity for noninteracting ABPs without obstacles. With interactions, either with other ABPs or obstacles, the effective temperature can most often not be used to describe the system.

The crossover time between the first diffusive regime and the ballistic regime can be obtained from:

$$\frac{t_{\times}^{(1)}}{\tau} \approx \frac{1}{2} \frac{D_a}{D} \left(\frac{t_{\times}^{(1)}}{\tau}\right)^2 \rightarrow \frac{t_{\times}^{(1)}}{\tau} \approx \frac{2D}{D_a}. \quad (3.24)$$

The crossover time between the ballistic regime and the long time diffusive regime can be obtain in the same way:

$$\frac{1}{2} \frac{D_a}{D} \left(\frac{t_{\times}^{(2)}}{\tau}\right)^2 \approx \left(1 + \frac{D_a}{D}\right) \frac{t_{\times}^{(2)}}{\tau} \rightarrow \frac{t_{\times}^{(2)}}{\tau} \approx 2, \quad (3.25)$$

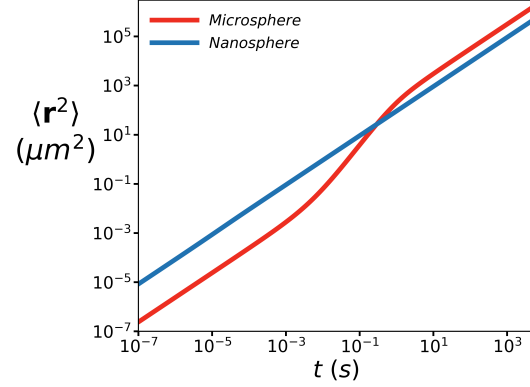
where it is assumed that  $D_a/D \gg 1$ .

The thermal translational diffusion constant is inversely proportional to the size of the particle  $D \propto a^{-1}$  (see Eq. A.31); the rotational diffusion constant, on the other hand, is inversely proportional to the cube of the size of the particle  $D_r \propto a^{-3}$  (see Eq. A.14). This means that the behavior on the MSD strongly depends on the size of the particle [96, 141] (see Fig. 3.2).

### 3.2.2 Coarse-Grained Fokker-Planck Equation

Properties of the spatial distribution of active particles can be obtained from the equation of motion of the active particles. For this a coarse-graining method is introduced. This method is used extensively in the

**Figure 3.2:** The MSD of two active particles with different sizes. The microsphere has a radius of  $0.5 \mu\text{m}$  and a swim speed of  $v_s = 20 \mu\text{m}/\text{s}$ , which is the same as the ABP in Ref. [90]. This corresponds to  $D = 0.4 \mu\text{m}^2/\text{s}$ ,  $D_a = 52 \mu\text{m}^2/\text{s}$ , and  $\tau = 0.4\text{s}$ . The nanosphere has a radius of  $15 \text{nm}$  and a swim speed of  $v_s = 600 \mu\text{m}/\text{s}$ , which is the same as the ABP in Ref. [140]. This corresponds to  $D = 14 \mu\text{m}^2/\text{s}$ ,  $D_a = 1.3 \mu\text{m}^2/\text{s}$ , and  $\tau = 10^{-5}\text{s}$ .



In case of the microsphere, one can clearly observe the transition between motion dominated by passive diffusion and ballistic motion at time  $t_{\times}^{(1)} \approx 6 \times 10^{-3} \text{s}$ , and the transition to diffusion with diffusion constant  $D + D_a \approx D_a$  at time  $t_{\times}^{(2)} \approx 0.8 \text{s}$ . For the nanosphere there is no ballistic regime because  $t_{\times}^{(1)} > t_{\times}^{(2)}$ . At time  $t_{\times}^{(2)} = 2 \times 10^{-5}$  there is a transition between thermal diffusion and active diffusion; however, as  $D_a \approx 0.1D$ , the effect of the activity is not visible in the log-log plot.

rest of this work.

The equation of motion of an active Brownian particle subjected to a force  $\mathbf{F}$  is

$$\partial_t \mathbf{r} = -\frac{1}{\gamma} \mathbf{F} - v_s \mathbf{n} + \sqrt{2D} \boldsymbol{\xi} \quad (3.26)$$

and the rotational dynamics is governed by

$$\partial_t \mathbf{n} = \sqrt{2D_r} \mathbf{n} \times \boldsymbol{\eta}, \quad (3.27)$$

in three dimensions, or

$$\partial_t \theta = \sqrt{2D_r} \boldsymbol{\eta}, \quad (3.28)$$

in two dimensions. Instead of, or in addition to, the rotational diffusion of the orientation vector  $\mathbf{n}$ , one can have tumble motion, which can be added to the Fokker-Planck equation (FPE). The FPE corresponding to these stochastic differential equations is

$$\partial_t P(\mathbf{r}, \mathbf{n}, t) = -\nabla \cdot \mathbf{J}_{\mathbf{r}}^P + D_r \mathcal{R}^2 P(t) - \alpha P(t) + \frac{\alpha}{\Omega_d} \rho(t), \quad (3.29)$$

where

$$\mathbf{J}_{\mathbf{r}}^P = \left( \frac{1}{\gamma} \mathbf{F} + v_s \mathbf{n} \right) P(t) - D \nabla P(t), \quad (3.30)$$

is the probability flux in position space, and  $\mathcal{R}^2$  is the rotation operator (see Section 1.3.3). The terms with  $\alpha$  account for the tumble motion with rate  $\alpha = \alpha(\mathbf{r})$ , and  $\rho(t) = \rho(\mathbf{r}, t) = \int d\Omega P(\mathbf{r}, \mathbf{n}(\Omega), t)$ . Here the swim speed, the rotational diffusion constant, and the tumble rate are taken to be space dependent.

This equation can be coarse grained by integrating out the orientational degrees of freedom. This results in an equation for the particle density  $\rho(\mathbf{r}, t)$ . To this end, the probability density  $P(\mathbf{r}, \mathbf{n}, t)$  can be expanded in eigenfunctions of  $\mathcal{R}^2$ . In two dimensions the eigenfunctions are  $\sin(\theta l)$  and  $\cos(\theta l)$ , for  $l = 0, 1, 2, \dots$ , and in three dimensions the eigenfunctions are the spherical harmonics  $Y_{lm}(\Omega) = Y_{lm}(\theta, \phi)$  [142]. In the case at hand it is more convenient to use a so called Cartesian multipole expansion [143]. In two dimensions the Cartesian eigenfunctions of  $\mathcal{R}^2$  are

$$T^{(l)} = \frac{(-1)^l}{l!} (l + \delta_{l,0}) \nabla^{\otimes l} [1 - \ln(r)] \Big|_{\mathbf{r}=\mathbf{n}}, \quad (3.31)$$

where  $T^{(l)}$  is a symmetric rank  $l$  tensor. The first three tensors are

$$T^{(0)} = \mathbf{1}, \quad T^{(1)} = \mathbf{n}, \quad T^{(2)} = 2\mathbf{nn} - \mathbf{1}. \quad (3.32)$$

One can easily see that the components of  $T^{(l)}$  are linear combinations of  $\sin(\theta l)$  and  $\cos(\theta l)$ . Because of this, it is clear that the eigenvalues of  $T^{(l)}$  are  $-l^2$ .

In three dimensions the Cartesian eigenfunctions of  $\mathcal{R}^2$  are

$$T^{(l)} = \frac{(-1)^l}{l!} \nabla^{\otimes l} \frac{1}{r} \Big|_{\mathbf{r}=\mathbf{n}}. \quad (3.33)$$

The first three are

$$T^{(0)} = \mathbf{1}, \quad T^{(1)} = \mathbf{n}, \quad T^{(2)} = \frac{1}{2} (3\mathbf{nn} - \mathbf{1}), \quad (3.34)$$

where  $T^{(l)}$  is a symmetric rank  $l$  tensor. Again, it is clear that the elements of  $T^{(l)}$  are linear combinations of  $Y_{lm}(\theta, \phi)$ , and therefore the eigenvalues

are  $-l(l+1)$ . Note the eigenvalues for both two and three dimensions can be written as  $-l(l+d-2)$ .

In all that follows, at most the first three eigenfunctions are used. The probability density  $P(\mathbf{r}, \mathbf{n}, t)$  can be expanded in the tensors  $T^{(l)}$  defined above; however it is more convenient to define

$$T^{(2)} = \mathbf{nn} - \frac{1}{d}\mathbf{1}, \quad (3.35)$$

for both two and three dimensions. The expansion is

$$P(\mathbf{r}, \mathbf{n}, t) = \rho(\mathbf{r}, t) + \boldsymbol{\sigma}(\mathbf{r}, t) \cdot \mathbf{n} + \omega(\mathbf{r}, t) : \left( \mathbf{nn} - \frac{1}{d}\mathbf{1} \right) + \Theta(P), \quad (3.36)$$

where  $\Theta(P)$  is the projection onto the third and higher order eigenfunctions. Note that because  $(\mathbf{nn} - \mathbf{1}/d)$  is traceless symmetric tensor, this expansion only defines the traceless symmetric part of  $\omega$ . Therefore the isotropic part  $\text{Tr}[\omega] \delta_{ij}/d$  and the antisymmetric part can be taken to be zero [143].

In order to obtain expressions for the coefficients  $(\rho, \sigma, \omega)$  of the expansion,

$$\langle f(\mathbf{n}) \rangle = \frac{1}{\Omega_d} \int d\Omega f(\mathbf{n}(\Omega)) \quad (3.37)$$

is defined<sup>3</sup>. Note that  $\langle g(\mathbf{n})\mathcal{R}^2 f(\mathbf{n}) \rangle = \langle f(\mathbf{n})\mathcal{R}^2 g(\mathbf{n}) \rangle$ . Clearly  $\langle 1 \rangle = 1$ , and because of isotropy  $\langle \mathbf{n} \rangle = 0$ . Again because of isotropy the elements of  $\langle \mathbf{nn} \rangle$  must be invariant under rotations of the coordinates. This means that it must be an isotropic rank two tensor [143]. Because the only isotropic rank two tensor is the identity  $\langle \mathbf{nn} \rangle = a\mathbf{1}$ , where  $a$  is a constant, which can be obtained by contracting both sides with the identity. The left-hand side becomes  $\mathbf{1} : \langle \mathbf{nn} \rangle = \langle \mathbf{n} \cdot \mathbf{n} \rangle = 1$ , and the right-hand side becomes  $a\mathbf{1} : \mathbf{1} = a d$ . Therefore,  $\langle \mathbf{nn} \rangle = \mathbf{1}/d$ . Similarly, one gets  $\langle \mathbf{nnn} \rangle = 0$ , and

$$\langle n_i n_j n_k n_l \rangle = \frac{1}{d(d+2)} (\delta_{ij}\delta_{kl} + \delta_{ik}\delta_{jl} + \delta_{il}\delta_{jk}). \quad (3.38)$$

---

<sup>3</sup>The angle brackets are used for both this integral over the orientations as well as the average over the noise. Which is meant is clear from context.



With this, one can show that the eigenfunctions are orthogonal:

$$\langle \mathbf{1n} \rangle = 0, \quad (3.39)$$

$$\left\langle \mathbf{1} \left( \mathbf{nn} - \frac{1}{d} \mathbf{1} \right) \right\rangle = 0, \quad (3.40)$$

$$\left\langle \mathbf{n} \left( \mathbf{nn} - \frac{1}{d} \mathbf{1} \right) \right\rangle = 0. \quad (3.41)$$

Furthermore,  $\langle \mathbf{1}\Theta(P) \rangle = 0$ ,  $\langle \mathbf{n}\Theta(P) \rangle = 0$ , and  $\left\langle \left( \mathbf{nn} - \frac{1}{d} \mathbf{1} \right) \Theta(P) \right\rangle = 0$ . The coefficients can now be obtained by projecting out the eigenfunctions:

$$\langle P(t) \rangle = \rho, \quad (3.42)$$

$$\langle \mathbf{n}P(t) \rangle = \frac{1}{d} \boldsymbol{\sigma}, \quad (3.43)$$

$$\left\langle \left( \mathbf{nn} - \frac{1}{d} \mathbf{1} \right) P(t) \right\rangle = \frac{2}{d(d+2)} \boldsymbol{\omega}, \quad (3.44)$$

where the derivation of the last equation relies on the traceless symmetric properties of  $\boldsymbol{\omega}$ .

With these results about the properties of integrals over the orientational degrees of freedom, it is straightforward to determine the equations for the coefficients in Eq. 3.36. The equation for the density is

$$\partial_t \rho(\mathbf{r}, t) = \langle \partial_t P(t) \rangle = -\nabla \cdot \mathbf{J}, \quad (3.45)$$

with

$$\mathbf{J} = \frac{1}{\gamma} \mathbf{F}\rho(\mathbf{r}, t) + \frac{1}{d} v_s \boldsymbol{\sigma}(\mathbf{r}, t) - D \nabla \rho(\mathbf{r}, t). \quad (3.46)$$

The equation for  $\boldsymbol{\sigma}$  is

$$\partial_t \boldsymbol{\sigma} = d \langle \mathbf{n} \partial_t P(t) \rangle. \quad (3.47)$$

The nontrivial orientational integrals are

$$\begin{aligned} d \langle n_i n_j P(t) \rangle &= d \langle (n_i n_j - \delta_{ij}/d) P(t) \rangle + \delta_{ij} \langle P(t) \rangle \\ &= \frac{2}{d+2} \omega_{ij} + \delta_{ij} \rho(\mathbf{r}, t), \end{aligned} \quad (3.48)$$

and

$$\begin{aligned} d \langle D_r \mathbf{n} \mathcal{R}^2 P(t) \rangle &= d D_r \langle P(t) \mathcal{R}^2 \mathbf{n} \rangle = -d(d-1) D_r \langle \mathbf{n} P(t) \rangle \\ &= -(d-1) D_r \sigma. \end{aligned} \quad (3.49)$$

With this the equation for  $\sigma$  becomes

$$\begin{aligned} \partial_t \sigma_i &= -\partial_j \left[ \frac{1}{\gamma} F_j \sigma_i \right] - \frac{2}{d+2} \partial_j [v_s \omega_{ij}] - \partial_i [v_s \rho(\mathbf{r}, t)] \\ &\quad + D \nabla^2 \sigma_i - \tau^{-1} \sigma_i, \\ &= -\partial_j J_{ji}^{(\sigma)} - \tau^{-1} \sigma_i, \end{aligned} \quad (3.50)$$

with  $\tau^{-1} = (d-1)D_r + \alpha$  is the orientational correlation time, and

$$\begin{aligned} J_{ji}^{(\sigma)} &= d \langle n_i J_j \rangle \\ &= \frac{1}{\gamma} F_j \sigma_i + \frac{2}{d+2} v_s \omega_{ji} + v_s \rho(\mathbf{r}, t) \delta_{ij} - D \partial_j \sigma_i, \end{aligned} \quad (3.51)$$

is the first moment of the flux.

Instead of the coefficient  $\sigma(\mathbf{r}, t)$ , one can define the polarization, that is the average orientation per particle:

$$\mathbf{p}(\mathbf{r}, t) = \frac{\langle \mathbf{n}(t) \delta(\mathbf{r}(t) - \mathbf{r}) \rangle}{\langle \delta(\mathbf{r}(t) - \mathbf{r}) \rangle} = \frac{\sigma(\mathbf{r}, t)}{d \rho(\mathbf{r}, t)}. \quad (3.52)$$

Lastly, the equation for  $\omega$  can be derived by the same methods, which results in

$$\begin{aligned} \partial_t \omega_{ij} &= -\partial_k \left[ \frac{1}{\gamma} F_k \omega_{ij} \right] - \frac{1}{2} \partial_k [v_s \chi_{ijkl} \sigma_l] - \partial_k [v_s Y_{ijk}] \\ &\quad + D \nabla^2 \omega_{ij} - [2dD_r + \alpha] \omega_{ij}, \end{aligned} \quad (3.53)$$

where

$$\chi_{ijkl} = \frac{1}{d(d+2)} \left( \delta_{ik} \delta_{jl} + \delta_{il} \delta_{jk} - \frac{2}{d} \delta_{ij} \delta_{kl} \right). \quad (3.54)$$

and  $Y_{ijk}$  comes from the projection onto  $\Theta(P)$ . Clearly this procedure results in an infinite hierarchy of equations, where the equation of  $T^{(l)}$  depends on  $T^{(l+1)}$ . In order to use these equations an approximation is needed to truncate the hierarchy at a finite order. Here, it is assumed that

$\omega = 0$ , that is, the quadrupole moment is zero. The reasoning behind and limitations of this approximation will be explained by considering three examples of active matter systems.

Equation 3.50 show that, if  $\omega$  is negligible, then an active Brownian particle with rotational diffusion constant  $D_r$  is equivalent to a run-and-tumble particle with tumble rate  $\alpha = (d - 1)D_r$ . When  $\omega$  cannot be neglected. Equation 3.53 shows that the correlation time of  $\omega$  is  $2dD_r + \alpha$ . To make a run-and-tumble particle equivalent to an active Brownian particle both this correlation time and the correlation time of  $\sigma$  should be equal. Clearly it is not possible to satisfy both  $\alpha = (d - 1)D_r$  and  $\alpha = 2d$ . Therefore, whenever  $\omega$  is not negligible, active Brownian particles and run-and-tumble particles are not equivalent. For more on the similarities and differences between active Brownian particles and run-and-tumble particles under different conditions, see Refs. [144, 145].

### 3.2.3 Wall Accumulation

One of the interesting features of active matter is that the steady-state density does not (necessarily) obey a Boltzmann distribution because it is not an equilibrium system. This is particularly notable for an active particle near a wall [100, 146, 147]. Here as system with a hard wall at  $x = 0$  and periodic boundary conditions in the other two directions is studied. The potential of the wall is

$$U(\mathbf{r}) = \begin{cases} 0, & \text{for } x > 0, \\ \infty, & \text{for } x < 0. \end{cases} \quad (3.55)$$

In an equilibrium system the density would follow a Boltzmann distribution,  $\rho(\mathbf{r}) \propto e^{-U/T}$ , so the density would be uniform for  $x > 0$ .

In case of an active particle, Eq. 3.29 needs to be solved in steady state with the appropriate boundary conditions. The force of the wall is only present at  $x = 0$ , and therefore it only affects the boundary conditions. The probability flux  $J_{\mathbf{r}}^P$  (Eq. 3.30) in the direction perpendicular to the wall ( $\hat{e}_x$ ) is zero at  $x = 0$ . This means that all its moments are zero. In particular,  $\hat{e}_x \cdot \langle J_{\mathbf{r}}^P \rangle = \hat{e}_x \cdot J = 0$  and  $\hat{e}_x \cdot \langle \mathbf{n} J_{\mathbf{r}}^P \rangle = \hat{e}_x \cdot J^{(\sigma)} = 0$ . At infinite distance from the wall the density is equal to the bulk density  $\rho(x \rightarrow \infty) = \rho_b$ .

In steady state the particle flux in the  $x$  direction is constant because of the symmetry of the problem, and because  $\hat{e}_x \cdot J|_{x=0} = 0$ , it must be zero

everywhere:

$$0 = \hat{e}_x \cdot \mathbf{J} = \frac{1}{d} v_s \sigma - D \partial_x \rho, \quad (3.56)$$

where  $\sigma = \hat{e}_x \cdot \boldsymbol{\sigma}$ . The first moment of the probability flux, that is  $\mathbf{J}^{(\sigma)}$  is not zero everywhere. In steady state the equation for  $\partial_t \sigma = 0$  (Eq. 3.50) gives

$$0 = -v_s \partial_x \rho + D \partial_x^2 \sigma - \tau^{-1} \sigma. \quad (3.57)$$

The solutions for the density and polarization can be obtained by substituting Eq. 3.56 in Eq. 3.57 and integrating, which gives

$$\frac{\rho(x)}{\rho_b} = 1 + \frac{D_a}{D} e^{-x/l_w}, \quad (3.58)$$

$$p(x) = \frac{\sigma(x)}{d\rho(x)} = -\frac{D_a}{v_s l_w} \frac{e^{-x/l_w}}{1 + \frac{D_a}{D} e^{-x/l_w}}, \quad (3.59)$$

with decay length

$$l_w = \sqrt{\frac{\tau D}{1 + D_a/D}}. \quad (3.60)$$

These results are an approximation because it is assumed that  $\omega \approx 0$ . The value of the density at the wall, however, turns out to be exact [146]. See Fig. 3.3 for a comparison between theory and simulations.

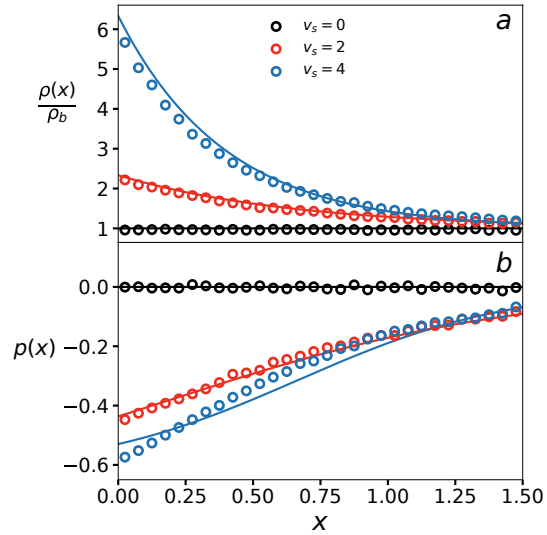
From the Stokes-Einstein relation for the translational and rotational diffusion constants (Eqs. A.31 and A.14) gives

$$l_w = a \sqrt{\frac{4}{3(d-1)}} \frac{1}{\sqrt{1 + D_a/D}}, \quad (3.61)$$

where  $a$  is the particle's radius. This shows that the decay length is at most of the order of the particle's radius.

Note that the density increases towards the wall ( $x = 0$ ) (see Fig. 3.3 a) even though there is no attractive potential between the wall and the particle. Furthermore, the polarization near the wall (see Fig. 3.3 b) is in the direction of the wall, without any torque exerted by the wall on the particle. This is a common feature in active matter that can be summarized as follows: active particles accumulate in regions where the active

**Figure 3.3:** (a) Accumulation and (b) polarization of ABPs at a hard wall ( $x = 0$ ). The symbols show simulation results. The solid lines show the theoretical prediction of Eqs. 3.58 and 3.59 in, respectively, a and b. Without activity ( $v_s = 0$ , black symbols) the density is homogeneous. The ABPs (red and blue), on the other hand, have a higher density at the wall. (b) Near the wall, the ABPs are on average oriented in the direction of the wall. The active accumulation and polarization near the wall can be explained as follows: The particles that swim to the left are stopped by the wall, which decreases their swim speed, thereby increasing the density. The particles that swim to the right can swim away, therefore, the remaining particles have an average orientation towards the wall. The units are such that  $D = \tau = 1$ .



motion is hindered.

As before, the size of the active particle matters for the magnitude of the wall accumulation. For the micro sphere from the previous section  $l_w = 0.07 \mu m$  (about 0.14 times the particle's radius) and  $\rho(0)/\rho_b = 124$ . For the nanosphere  $l_w = 0.01 \mu m$  (about 0.8 times the particle's radius) and  $\rho(0)/\rho_b = 1.09$ . For both particles the decay length is smaller than the particle's radius. The increase of density at the wall of the nanosphere is about 10 %, and for the micro sphere 123 % because the active diffusion constant of the micro sphere is much larger and the thermal diffusion constant much smaller.

### 3.2.4 Sedimentation

As a second example, the sedimentation of active particles is considered. The problem of sedimentation of active particles has been considered theoretically in refs. [145, 148–151] and experimentally in ref. [152]. Here, following ref. [148], passive diffusion is ignored ( $D = 0$ ) and the details of the interaction with the bottom are ignored, meaning that the results hold for  $z > l_w$ , where  $z$  is the distance from the bottom and  $l_w$  is the length scale of the wall accumulation given in Eq. 3.60.

As with the previous example, due to symmetry there is no particle flux in the steady state:

$$0 = -v\rho + \frac{1}{d}v_s\sigma, \quad (3.62)$$

and,

$$0 = v\partial_z\sigma - v_s\partial_z\rho(\mathbf{r}, t) - \tau^{-1}\sigma, \quad (3.63)$$

which comes from Eq. 3.50 with  $\partial_t\sigma = 0$ . Note that the no-flux boundary condition for the first moment of the probability flux  $\hat{e}_z \cdot \langle \mathbf{n}\mathbf{J}^P \rangle|_{z=0} = 0$ , is *not* imposed. The reason is that if  $D = 0$ , that boundary condition and the boundary condition on the particle flux  $\hat{e}_z \cdot \mathbf{J}|_{z=0} = \hat{e}_z \cdot \langle \mathbf{J}^P \rangle|_{z=0} = 0$  cannot both be obeyed. This inconsistency arises because of the vanishing decay length of the wall accumulation if  $D = 0$  (see Eq. 3.60), and results in a boundary layer  $0 < z < l_w \rightarrow 0$  within which the theory breaks down.

The solutions to Eqs. 3.62 and 3.63 up to first order in  $v/v_s$  are

$$\rho(z) = \rho_0 e^{-z/l_s}, \quad (3.64)$$

$$p(z) = \frac{\sigma(z)}{d\rho(z)} = \frac{v}{v_s}, \quad (3.65)$$

where  $\rho_0$  is a normalization constant,  $p$  is the polarization, and

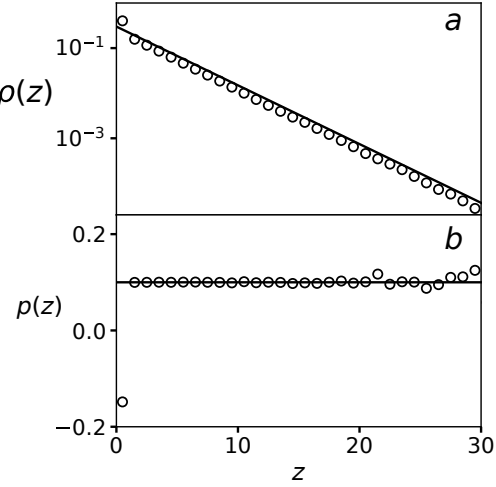
$$l_s = \frac{\tau v_s^2}{dv} = \frac{D_a}{v}, \quad (3.66)$$

is the sedimentation length; see Fig. 3.4. Theories including thermal diffusion and higher order correction in  $v/v_s$  exist but the calculations are more involved [145, 148–150].

This density profile has the same form as passive, thermal sedimentation (Eq. 1.62), but with a different sedimentation length. In equilibrium the sedimentation length is  $l_s^{(eq)} = D/v$ , where  $D = T/\gamma$  is the thermal diffusion constant. In case of active particles  $l_s = D_a/v$ , with  $D_a = \tau v s^2/d$ , only in the limit  $v \ll v_s$ . Beyond this limit, ABPs and RTPs are not equivalent, indicating that  $\omega$  and higher order expansion coefficients are not negligible.

The  $v \ll v_s$  limit corresponds to the experiments on active colloids reported in Ref. [152]. In that experiment the colloids had a passive diffusion constant of  $D = 0.33 \mu\text{m}^2\text{s}^{-1}$ , an active diffusion constant up to

**Figure 3.4:** Sedimentation of an ABP with swim speed  $v_s = 1$ , sedimentation speed  $v = 1/10$ , and persistence time  $\tau = 1$  without thermal diffusion. Figure a shows the theoretical prediction (solid line, Eq. 3.64) together with simulation data (symbols) on a semi-log plot. Figure b shows the theoretical prediction for the polarization (solid line, Eq. 3.65) together with the simulation data (symbols). The effect of the hard repulsion of the bottom is not taken into account in the theoretical prediction. This occurs on a length scale  $l_w = 0$  (Eq. 3.60 with  $D = 0$ ) and is therefore only present in the left most simulation data point.



$D_a = 1.57 \mu\text{m}^2\text{s}^{-1}$ , a persistence time of  $\tau = 0.9 \text{ s}$ , and a sedimentation velocity of  $v = 0.05 \mu\text{m}\text{s}^{-1}$ . In this case  $D_a/v \gg \tau v/d$ , resulting in a sedimentation length of  $l_s = D_a/v = 31 \mu\text{m}$ . In the limit  $v_s \gg v$  the effect of passive diffusion is to increase the sedimentation length:  $l_s = v/(D + D_a)$ , which gives  $l_s = 38 \mu\text{m}$  for the values above, and is in good agreement with experimental results [152].

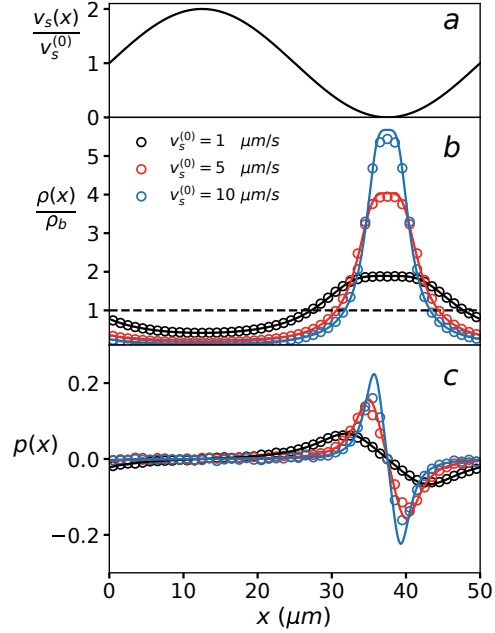
### 3.2.5 Inhomogeneous Activity

As a last example, an active particle with space dependent activity without an external force is considered. In ref. [153] a similar system was considered, but with interacting active particles. For completion, both the swim speed and the orientational diffusion constant are space dependent. The equation for  $\sigma$  is

$$\begin{aligned} \partial_t \sigma(\mathbf{r}, t) = & -\nabla [v_s(\mathbf{r})\rho(\mathbf{r}, t)] - \tau^{-1}\sigma(\mathbf{r}, t) \\ & + D\nabla^2\sigma(\mathbf{r}, t) - \frac{2}{d+2}\nabla \cdot [v_s(\mathbf{r})\omega(\mathbf{r}, t)]. \end{aligned} \quad (3.67)$$

The vector  $\sigma$  is not conserved, as indicated by the  $\tau^{-1}\sigma$  term in the previous equation. This means that the relaxation time is at least  $\tau$ . The equation for  $\rho$  (Eq. 3.45) clearly shows that it is a locally conserved quantity that relaxes on a time scale  $\sim \mathcal{O}(\nabla^{-1})$ . So when gradients are small  $\sigma$  relaxes much faster than  $\rho$ , and therefore on time scales longer than  $\tau$  one can set  $\partial_t \sigma = 0$ .

**Figure 3.5:** Density and polarization of ABPs in three dimensions with inhomogeneous activity. Symbols represent simulation results, and solid lines theoretical predictions (Eq. 3.71 in panel a, and Eq. 3.73 in panel b). Where the swim speed (panel a) is small, the density (panel b) large. The density accumulation becomes more pronounced for increasing swim speed. The polarization (panel c) points in the direction antiparallel to the swim-force gradient, which coincides with the direction parallel to the density gradient. As the gradient in the swim force increases, the theoretical prediction starts to deviate from the simulation results (see the blue symbols). When this happens the higher order coefficients of the expansion of the probability density (Eq. 3.36) become significant (see Fig. 3.6).



When the system is homogeneous,  $\omega = 0$  because of the system is isotropic. This shows that  $\omega$  is at least of first order in the gradient. Retaining terms up to and including  $\sim \mathcal{O}(\nabla)$  in the equation for  $\sigma$  results in

$$\sigma(\mathbf{r}, t) = -\tau(\mathbf{r})\nabla [v_s(\mathbf{r})\rho(\mathbf{r}, t)]. \quad (3.68)$$

Note that  $\sigma(\mathbf{r}, t)$  is still time dependent, but only through the time dependence of the density. Using this for the particle flux (Eq. 3.46) gives

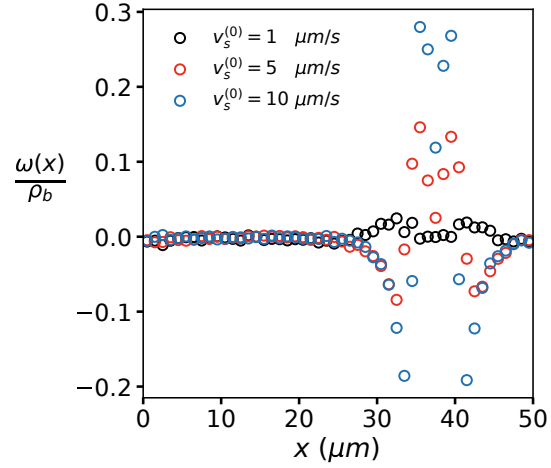
$$\mathbf{J} = -\frac{1}{d}\tau(\mathbf{r})v_s(\mathbf{r})\nabla [v_s(\mathbf{r})\rho(\mathbf{r}, t)] - D\nabla\rho(\mathbf{r}, t). \quad (3.69)$$

As shown in Ref. [35], this flux can be related to the flux of thermal diffusion (Eq. 1.67) with space dependent friction and/or space dependent temperature by choosing  $\tau(\mathbf{r})$  and  $v_s(\mathbf{r})$  appropriately. In particular, if both  $\tau$  and  $v_s$  constant in space, the flux becomes  $\mathbf{J} = -(D_a + D)\nabla\rho(\mathbf{r}, t)$ , which is just Fick's law (Eq. 1.1) with an effective space-dependent diffusion constant  $D_a + D$ . This is consistent with the calculation of the long-time mean-squared displacement Eq. 3.23.

From here on only space-independent rotational correlation times are



**Figure 3.6:** The expansion coefficient  $\omega$  of the probability density (see Eq. 3.36) measured in simulations for the same parameters as Fig. 3.5. When the gradient of the swim speed becomes larger,  $\omega$  becomes more important. When it becomes significant, Eq. 3.71 starts to deviate from the simulation results ( $v_s^{(0)} = 10 \mu\text{m}/\text{s}$  in Fig. 3.5). Furthermore, it indicates that the correspondence between ABPs and RTs break down.



considered. The particle flux (Eq. 3.46) then becomes

$$J = -\frac{1}{2} [\nabla D_a(\mathbf{r})] \rho(\mathbf{r}, t) - [D_a(\mathbf{r}) + D] \nabla \rho(\mathbf{r}, t), \quad (3.70)$$

where, as before,  $D_a(\mathbf{r}) = \tau v_s^2(\mathbf{r})/d$  is the active diffusion constant. The flux-free steady-state solution is

$$\rho(\mathbf{r}) \propto \left[ 1 + \frac{D_a(\mathbf{r})}{D} \right]^{-\frac{1}{2}}, \quad (3.71)$$

where the proportionality constant is determined by normalization. In absence of passive diffusion the steady-state density is

$$\rho(\mathbf{r}) \propto \frac{1}{\sqrt{D_a(\mathbf{r})}} \propto \frac{1}{v_s(\mathbf{r})}. \quad (3.72)$$

The steady-state density is large where  $D_a$  is small, which means that the active particles accumulate where the swim speed  $v_s(\mathbf{r})$  is small. This phenomena is akin to the accumulation of leaves at the side of the road in the fall. The leaves are moved around on the road due to the driving cars (that is, due to "active" noise). Because there are more cars driving near the middle of the road than right along the side of road, the "active" noise at the side of the road is smaller than in the middle, which causes the accumulation of the leaves near the sides of the road.

The corresponding polarization is

$$\mathbf{p}(\mathbf{r}) = \frac{\sigma(\mathbf{r})}{d\rho(\mathbf{r})} = -\frac{\tau}{d} \frac{D}{D + D_a} \nabla v_s(\mathbf{r}). \quad (3.73)$$

That is, the active particles have an average polarization in the direction of smaller activity. Note that in absence of thermal diffusion ( $D = 0$ ), the polarization vanishes.

The theoretical prediction compares well with simulations for experimentally relevant values of the parameter; see Fig. 3.5. When the gradient in the swim speed increases, higher order expansion coefficients in the expansion of the probability density (Eq. 3.36) become more important and may not be negligible (see Fig. 3.6). When this happens active Brownian particles and run-and-tumble particles are no longer equivalent [144, 145].



**Part II**

**Inhomogeneous Activity**



# **Chapter 4**

## **Introduction**

Many biological microswimmers have the ability to perform chemotaxis [154–158]. Chemotaxis is directed motion of an organism towards a more favorable environment where there is a larger concentration of a certain chemical  $c(\mathbf{r})$ , for example, its energy source. The most straightforward method for chemotaxis would rely on the difference of the chemical concentration at the back and front end of the organism. However, as *e. coli* has a length of about  $2 \mu\text{m}$  the fluctuations in the chemical concentration are typically too large to give a reliable estimate of the local gradient [159–161]. Therefore *e. coli* uses a different strategy [162–166]. It measures the concentration as it swims, and it has a way to integrate the measured concentrations with a kernel  $K(t)$ . This kernel has a maximum near  $t = 0$  and a minimum at  $t > 1/\alpha_0$ , where  $\alpha_0$  is its tumble rate for  $\nabla c = 0$  (see Fig. 4.1). Note that  $1/\alpha_0 = \tau_0$  is the time of a run if the concentration is uniform. If this integral is positive (negative), it decreases (increases) its tumble rate  $\alpha$ :

$$\alpha(t) = \alpha_0 - \int_{-\infty}^t dt' K(t-t') c(x(t')), \quad (4.1)$$

where  $x(t)$  is the position of the bacterium at time  $t$ . This means that it effectively compares a weighted average of the concentration it measured in the previous run to a weighted average of the concentration measured in the current run. With this it can estimate the gradient in the concentration in its run direction. This strategy leads to a net drift up the concentration gradient, see Fig. 4.1.

The mechanism for chemotaxis that *e. coli* and other organisms rely on requires complicated biochemical mechanism to a) measure the local chemical concentration  $c(\mathbf{r})$  in its neighborhood, b) integrate the measured concentration over time, which requires a form of memory, and c) change its behavior, that is, its tumble rate, depending on the result of the integral [167–173]. These mechanism are not available to synthetic active particles.

Besides chemotaxis (or other kinds of taxis) particle migration can be caused by kinesis. Kinesis is the migration due to inhomogeneous kinetics of the active particle, that is migration due to a space dependent swim speed, called *orthokinesis*, or space-dependent orientational dynamics, called *klinokinesis*, such as the rotational diffusion constant. Unlike taxis, which depends on a space-dependent vector field (i.e. gradient of a concentration of a chemical), kinesis relies on a space-dependent scalar field (i.e. local concentration of a chemical), and therefore does not have an obvious direction. Furthermore, because kinesis relies on the local

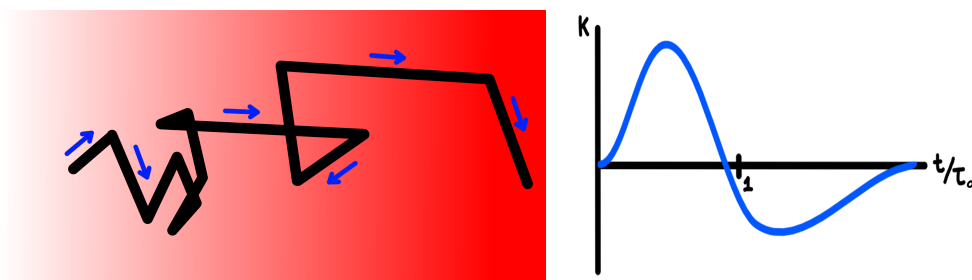


**Figure 4.1:** Left: Schematic of chemotaxis of *e. coli*. The red color gradient indicates the concentration of the chemical the bacterium is attracted to (e.g. its fuel), the black line indicates the path of the bacterium, and the blue arrows the direction of the self-propulsion. As the bacterium performs run-and-tumble motion, it integrates the local concentration in time with the kernel  $K(t)$  shown in the right figure. It effectively compares a weighted sum of the concentration measured in a previous run ( $t/\tau_0 > 1$ ) with a weighted sum of the concentration measured in the current run ( $t/\tau_0 < 1$ ). If the integral in Eq. 4.1 is positive, meaning that there is a higher concentration in the current run than in the previous run, the tumble rate decreases resulting in longer runs, as shown in the left figure. This strategy results in a net drift up the concentration gradient.

value of a scalar field, it does not need an estimate of the gradient, and therefore no memory or any other complicated mechanism that for example *e. coli* relies on to perform chemotaxis. Taxis and kinesis can both play a role in biological active matter such as microswimmers [164].

Active matter has a wide range of applications [174–177]: material science [178], environmental science (e.g. clean up of pollutants [179–181]), transport of cargo [182–185], and biomedical science [186–188] (e.g. drug delivery [189–197]). For many applications it is important to steer the active particles towards the correct target zone. Steering of active particles has been realized experimentally by feedback mechanisms, where the state of the active particle (position and orientation) are measured and accordingly the external stimuli are modified [118, 119]. However, since it is not always be possible to externally measure the state and tune the behavior of active particles, an autonomous approach is desirable where an active particle senses the local environment and adjusts its behavior accordingly [198], similar to the complex behavior of biological active microswimmers such as *e. coli* [199].

Two possible autonomous approaches to steer the particles are taxis and kinesis. Because synthetic active particles do not have any mechanisms from memory, they can only rely on the local measurement of



the gradient. For example, self-diffusiophoretic active particles experience a torque proportional to the local fuel gradient [115]. Similarly, light driven particles experience a torque due to a gradient in the light intensity [57, 114]. This torque orients the particle either parallel (or antiparallel) to the fuel or light intensity gradient, resulting in chemotaxis (antichemotaxis) in case of the self-diffusiophoretic particles or phototaxis (antiphototaxis) in case of the light driven particles. Whether the particle orients parallel or antiparallel to the gradient can, for example, be controlled by the patterning of the catalytic surface on the colloid [115].

Besides the tactic response, there is also a kinetic response. If for example there is a fuel gradient, the active particle moves faster where there is more fuel present than in areas with less fuel resulting in klinokinesis. Furthermore, the orientational dynamics, that is the rotational diffusion constant, can change due to the different amount of fuel.

Besides the relevance to artificial active matter, studying inhomogeneous activity could shed light on the evolution of early life forms or catalytic enzymes [42–45] that do not have any complicated biochemical mechanism of bacteria such as *e. coli* (integrating a concentration over time and adjusting the orientational dynamics accordingly). The results of this section could help understand the movement of life forms in activity gradients. For example, if food or fuel is the limiting factor for the movement of these organisms, they would move faster where there is more fuel. The results of the following part of the thesis could help explain how this strategy can still lead to movement towards the regions with higher food concentration.

The remainder of this thesis concerns active particles with inhomogeneous activity. In particular orthokinetic particles are studied. That is, there is no torque on the orientation of the particle, and the rotational diffusion constant is assumed to be independent of the activity. In Section 3.2.5 it was shown that such particles accumulate where the activity is small. The next four chapters explain active system where the behavior of active particles is different, that is, where the particles are moving towards regions of higher activity, and the physics that determines the behavior of these particles.

## Chapter 5

# Pseudochemotaxis of Active Brownian Particles

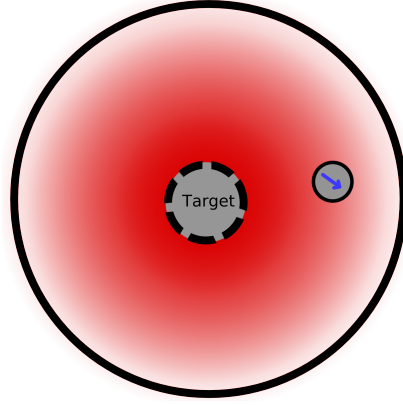
This chapter contains results which have been published in ref. [200].  
Reprinted (adapted) with permission from H.D. Vuijk, A. Sharma, D. Mondal, J.-U. Sommer, and H. Merlitz. *Physical Review E* 96, 042612, 2018.  
Copyright (2018) by the American Physical Society.

In Chapter 3.2.5 it was shown that in steady state active particles accumulate where they are less active, that is, where they move slowly. If one assumes that the activity is positively correlated with the fuel available to the active particle, the regions of low activity correspond to regions with less fuel. The accumulation in low activity regions then mimics antichemotactic behavior as the active particles move away from regions where the fuel concentration is high. However, as there is no torque on the particle due to the gradient in the activity, the accumulation should not be called antichemotaxis, but is a result from orthokinesis.

In this chapter we investigate if orthokinesis can lead to chemotactic like behavior, that is movement toward regions of higher activity without directional cues. A first step towards an answer is the inspection of a most simple system which features both activity and a primitive concept for a "food-source" namely an increasing activity towards the source caused by a gradient of available food in the proximity of the source. Motivated by this, we consider in this chapter systems for which the activity varies in space, focusing on two dynamical properties of an active system: target finding probability and the mean first passage time (MFPT) to the target. The target finding probability is the probability that a particle introduced at a given location, exits through a specified boundary representing the target. The MFPT to target is a measure of average reaction time in finite domains [201].

Here we show that both these dynamical properties are strongly dependent on the spatial distribution of activity. In particular, we find that the insights gained from steady-state inhomogeneous active systems, such as preferential accumulation in the low-activity regions and orientation of particles antiparallel to the activity gradient (see Chapter 3.2.5), cannot be used to understand the dynamical properties of an inhomogeneous active system. When the activity is distributed such that high-activity zone is located between the target and the starting location, the target finding probability is increased and the passage time is decreased in comparison to a uniformly active system. Moreover, for a continuously distributed profile, the activity gradient results in a drift of active particle up the gradient bearing resemblance to chemotaxis. The theoretical predictions are based on an approximate Fokker-Planck equation (FPE) and are shown to be in good agreement with the Brownian dynamics simulations.

**Figure 5.1:** Schematic of the inhomogeneous active system. The sketch shows a two dimensional cut through the spherical set up. The target zone (sphere with radius  $r_0$ ) in the center has an absorbing boundary and is assumed to be the source of the fuel of the active particles. The fuel distribution in the spherical geometry is shown in red, which results in a swim speed that of the form  $r^{-\alpha}$ , where  $r$  is the distance to the center. The active particle is shown as a gray circle with an orientation vector (blue). For the MFPT calculation the active particle starts at the outer boundary (with radius  $R$ ), which in this case is reflective. For the target finding probability calculation the particle starts where the probability to be absorbed by the target zone is  $1/2$  if there is no activity ( $c = 0$ ). In this case the outer boundary is an absorbing boundary.



## 5.1 Model and Theory

We consider a three dimensional system of active, noninteracting, spherical Brownian particles with position  $\mathbf{r}$  and orientation specified by an embedded unit vector  $\mathbf{n}(t)$  (see Fig. 5.1). A space-dependent self-propulsion speed  $v_0(\mathbf{r})$  acts in the direction of orientation. Omitting hydrodynamic interactions the motion can be modeled by the Langevin equations

$$\begin{aligned}\partial_t \mathbf{r} &= v_0(\mathbf{r}) \mathbf{n} + \sqrt{2D} \boldsymbol{\zeta}, \\ \partial_t \mathbf{n} &= \sqrt{2D_r} \mathbf{n} \times \boldsymbol{\eta}.\end{aligned}\tag{5.1}$$

The stochastic vectors  $\boldsymbol{\zeta}(t)$  and  $\boldsymbol{\eta}(t)$  are Gaussian distributed with zero mean and have time correlations  $\langle \boldsymbol{\zeta}(t) \boldsymbol{\zeta}(t') \rangle = \mathbf{1} \delta(t - t')$  and  $\langle \boldsymbol{\eta}(t) \boldsymbol{\eta}(t') \rangle = \mathbf{1} \delta(t - t')$ . The (passive) translational and rotational diffusion coefficients,  $D$  and  $D_r$ , are treated as independent parameters. The set of equations in 5.1 are used for the Brownian dynamics simulations to compare the theoretical predictions.

To make further analytical progress, we replace the active noise term ( $v_0(\mathbf{r}) \mathbf{n}$ ) in the equation of motion for  $\mathbf{r}$  with a noise term with the same mean and autocorrelation [133, 202–205]. The mean of  $\mathbf{n}$  is zero, and the autocorrelation is  $\langle \mathbf{n}(t + t') \mathbf{n}(t') \rangle = \frac{1}{3} e^{-t'/\tau}$ , where  $\tau = 1/(2D_r)$  (see Sec.

1.3.3). The equation of motion for  $\mathbf{r}$  then becomes

$$\partial_t \mathbf{r} = v_0(\mathbf{r})\chi + \sqrt{2D}\xi, \quad (5.2)$$

where  $\langle \chi(\mathbf{r}, t + t')\chi(\mathbf{r}, t') \rangle = \frac{1}{3}e^{-|t|/\tau}$ . This approximation transforms the active Brownian particle into an active Ornstein-Uhlenbeck particle (see Sec. 3.1.3).

Because this equation has colored noise, there is no corresponding FPE. If in the limit that the autocorrelation time vanishes ( $\tau \rightarrow 0$ ), the active noise  $\chi$  becomes white noise with autocorrelation  $\langle \chi(\mathbf{r}, t + t')\chi(\mathbf{r}, t') \rangle = \frac{2\tau}{3}\delta(t)$ . After this limit the equation for  $\mathbf{r}$  has multiplicative white noise, so one should specify the integration rule for the SDE. If multiplicative white noise is the limit of multiplicative colored noise, the correct integration rule is the Stratonovich rule. After rescaling the noise the equation for the position becomes

$$\partial_t \mathbf{r} = \sqrt{2D_a(\mathbf{r})}\boldsymbol{\eta} + \sqrt{2D}\xi = \sqrt{2(D_a(\mathbf{r}) + D)}\boldsymbol{\zeta}, \quad (5.3)$$

where

$$D_a(\mathbf{r}) = \frac{1}{6}\tau v_0^2(\mathbf{r}) = \frac{v_0^2(\mathbf{r})}{6D_r}, \quad (5.4)$$

is the space dependent active diffusion coefficient. This Stratonovich SDE is equivalent to the Itô SDE

$$\partial_t \mathbf{r} = \frac{1}{2}\nabla D_a(\mathbf{r}) + \sqrt{2(D_a(\mathbf{r}) + D)}\boldsymbol{\zeta}, \quad (5.5)$$

where the  $\nabla D_a(\mathbf{r})/2$  is called the noise-induced drift.

We use this equation to derive Fokker-Planck equation for  $P(\mathbf{r}, t)$ , defined as the probability density of finding an active particle at position  $\mathbf{r}$  at time  $t$ :

$$\partial_t P(\mathbf{r}, t) = -\nabla \cdot \left[ \frac{1}{2}P(\mathbf{r}, t)\nabla D_a(\mathbf{r}) \right] + \nabla^2 [(D_t + D_a(\mathbf{r}))P(\mathbf{r}, t)]. \quad (5.6)$$

We note that  $D_a(r)$  can be much larger than  $D_t$  and hence, the diffusion of a particle may be governed predominantly by the activity. For non-interacting particles, the enhanced diffusivity of active particles is reminiscent of Brownian particles at an increased effective temperature [144]. In fact, Eq. 5.6 describes a nonequilibrium process which breaks detailed

balance and can be interpreted as describing a passive system with spatially varying temperature. The Fokker-Planck equation obtained above is based on the Markovian process in Eq. 5.5. However, even for the non Markovian process in Eq. 5.2, there exist different schemes [204, 206, 207], following which an approximate FPE can be derived. These schemes yield an FPE with first order correction in the persistence time of the particle [133, 208]. However, the correction is coupled to a potential term [133, 208], which is not present in our model, and therefore the error in the white-noise approximation of  $\chi(\mathbf{r})$  is of the order  $\tau^2$ .

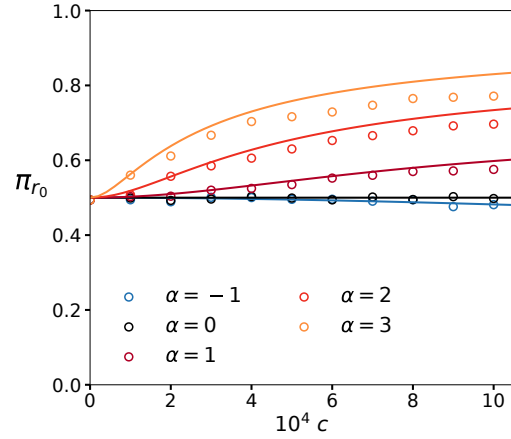
We consider activity to be distributed spherically symmetric, continuously varying with distance  $r$  from the center as

$$v_0(r) = \frac{c}{r^\alpha} \left[ \int_{r_0}^R dr 4\pi r^2 \frac{1}{r^\alpha} \right]^{-1}, \quad (5.7)$$

where the exponent  $\alpha$  is varied to obtain different distributions. We consider  $\alpha \geq -1$ . The volume integral of the activity is  $c$  which can be interpreted as the ‘total activity’ available in the spherical geometry between  $r_0$  and  $R$ . The region  $0 < r \leq r_0$  may represent a source of fuel for the active particles [209] (see Fig. 5.1). We assume that the activity (i.e., the self-propulsion speed of an active particle) is proportional to the local concentration of the fuel. The total activity is, in this sense, proportional to the total amount of fuel present in the system. If one considers that the fuel source is emitting fuel at a constant rate which then diffuses isotropically in the surroundings, one obtains the steady state fuel distribution as  $1/r$  which corresponds to  $\alpha = 1$ . If the source emits a constant number of fuel particles per unit time which travel ballistically radially outwards, the corresponding steady state fuel is distributed as  $1/r^2$ . Since our focus in this study the effect of different distributions, we do not concern ourselves with the specific details of how a particular fuel distribution is obtained. In order to compare the effect of different distributions, we impose the constraint of fixed total activity (fuel)  $c$  for all values of  $\alpha$ .

In Brownian dynamics simulations, we consider noninteracting particles with translational diffusion constant  $D_t = 1/30$ . The rotational diffusion constant  $D_r = 1/2$ . This corresponds to a quick rotation of the particle as compared to translation in the spirit of our approximation of short reorientation times made above. Based on the choice of parameters, the radius  $a$  of the particle can be calculated using the Stokes-Einstein  $D_r/D_t \sim a^{-2} \approx 1/4$ . The total activity  $c$  is a free parameter. The trajectory of each particle is generated by integrating the Langevin equations

**Figure 5.2:** Target finding probability  $\pi_{r_0}$  of active particles as a function of the total activity  $c$ . The activity profiles considered are of the form  $v_0(r) \propto r^{-\alpha}$ . Each profile is normalized such that the total activity is same for all values of  $\alpha$ . Simulation data are shown as symbols and were obtained from Brownian dynamics simulation of Eqs. 5.1. The lines correspond to the theoretical prediction of Eq. 5.8 in. The target finding probability  $\pi_{r_0}(r)$  is calculated for  $r = 50/3$ , which yields equiprobable exit from  $r = r_0$  or  $r = R$  for  $c = 0$ .  $\pi_{r_0}(r)$  does not change when the system is uniformly active (circles). However, when the same amount of total activity is distributed such that it increases towards the target  $r = r_0$ , the probability is strongly biased.



in Eq. 5.1 using a time step  $dt = 3 \times 10^{-3} \tau_D$ , where  $\tau_D = 1/D_t$  is the time scale of translational diffusion over a unit length. We fix the inner boundary of the spherical geometry as  $r_0 = 10$ . The outer boundary is fixed to  $R = 50$ . With these parameters the distance between the inner and outer boundary is much larger than the particle's diameter.

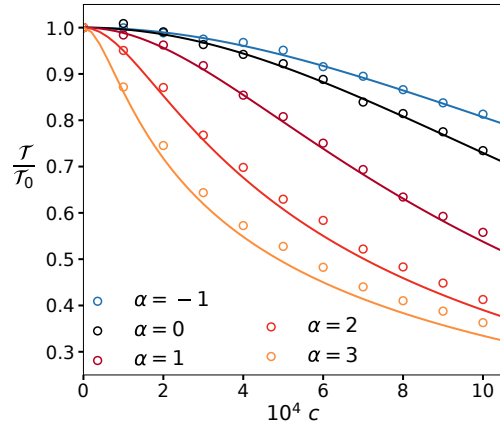
## 5.2 Target Finding Probability

We first consider target finding probability,  $\pi_{r_0}(r)$ , defined as the probability that a particle that is introduced at  $r$  at time  $t = 0$  reaches the specified target, i.e., exits through the inner boundary  $r_0$  before it vanishes through the outer boundary. This is shown in Fig. 5.2 as a function of the total activity  $c$  and can be calculated from Eq. 5.6 as (see Appendix 5.A)

$$\pi_{r_0}(r) = \frac{\int_r^R dz z^{-2} (D_t + D_a(z))^{-\frac{1}{2}}}{\int_{r_0}^R dz z^{-2} (D_t + D_a(z))^{-\frac{1}{2}}}. \quad (5.8)$$

The scenarios considered are (i) the activity increases as one moves away from the target  $v_0(r) \propto r$ , corresponding to  $\alpha = -1$ , (ii) uniformly distributed activity as corresponding to  $\alpha = 0$  and (iii) activity distributed such that it increases towards the inner boundary  $r_0$  (target) correspond-

**Figure 5.3:** Mean first passage time to target  $\mathcal{T}$  relative to the MFPT with  $c = 0$  of active particles as a function of the total activity  $c$ . The activity profiles considered are of the form  $v_0(r) \propto r^{-\alpha}$ . Each profile is normalized such that the total activity is same for all values of  $\alpha$ . Simulation data are shown as symbols and were obtained from Brownian dynamics simulation of Eqs. 5.1. The lines correspond to the theoretical prediction Eq. 5.9. The mean first passage time to target ( $r = r_0$ ) in is calculated for a particle starting at the outer boundary, that is at  $r = R$ . It is normalized to its corresponding value  $\mathcal{T}_0$  in a passive system. Inhomogeneously distributed activity leads to a larger decrease in MFPT in comparison to a uniformly active system.



ing to  $\alpha = 1, 2, 3$  (Eq. 5.7). The target finding probability does not change in the case of uniform activity, see Fig. 5.2. Only when the activity is increases towards the target the probability is strongly biased to reach the target at  $r_0$ . As can be seen in Fig. 5.2, the theoretical predictions are in good agreement with the simulation data. The starting location  $r = 50/3$  is chosen as it corresponds to an equally likely exit from either of the two boundaries in a passive or a uniformly active system. We note that the qualitative behavior remains the same for any other starting location, i.e., probabilities to exit from either of the boundaries do not change in presence of uniform activity whereas in the case of inhomogeneous activity, the probability increases at the end where the activity increases. Although, here we consider smoothly distributed activity as in Eq. 5.7, the same qualitative behavior is obtained for piecewise distributed activity. For instance, if the activity is assumed to be uniform between  $r_0$  and  $R$  except a step-like larger activity of arbitrary length anywhere between  $r_0$  and  $r$ , the probability of escaping through the target boundary increases.

### 5.3 Mean First Passage Time to Target

The MFPT of an active particle starting at the outer boundary  $r = R$  to reach the target at  $r = r_0$  is shown in Fig. 5.3. Considering  $r = R$  as a reflecting boundary, MFPT to target of a particle,  $\mathcal{T}(r)$ , is the average



time taken by a particle starting at  $r$  to reach the target  $r = r_0$ . This can be calculated from the Fokker-Planck Eq. 5.6 as (see Appendix 5.A)

$$\mathcal{T}(r) = \int_{r_0}^r dz \frac{z^{-2}}{\sqrt{D_t + D_a(z)}} \int_z^R dy \frac{y^2}{\sqrt{D_t + D_a(y)}}. \quad (5.9)$$

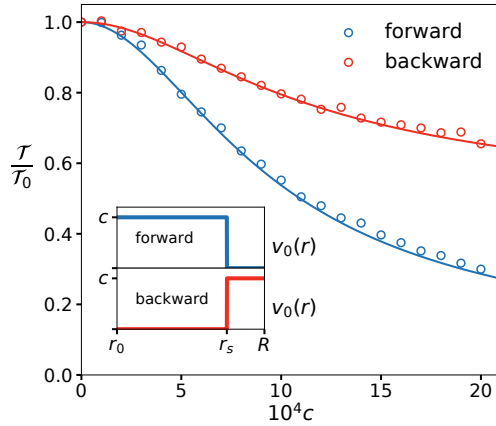
We normalize the MFPT with its corresponding value in a passive system ( $\mathcal{T}_0$ ). Increasing activity always decreases the MFPT. However, the decrease in MFPT is much more pronounced when the activity is spatially distributed such that it increases towards the target. As can be seen in Fig. 5.3, the theoretical predictions are in good agreement with the simulation data. In our coarse-grained approach, it can be easily seen from Eq. 5.6 that a uniformly active system is equivalent to a passive system with an effective diffusion constant ( $D_t + D_a$ ). The decrease in the MFPT can thus be simply attributed to the increased diffusivity of the particle. However, when the activity is inhomogeneously distributed, the decrease in MFPT is more pronounced.

As in the case of target finding probability, the spatial distribution of the activity strongly influences the MFPT. A particularly simple but instructive case that illustrates the role of the spatial distribution of activity can be constructed as follows. We consider two scenarios, called the forward and the backward scenario. In the forward scenario, the region  $r_0 < r < r_s$  is uniformly active and  $r_s < r < R$  passive. In the backward scenario, the situation is reversed with the active region becoming passive and vice versa. The intermediate distance  $r_s = \sqrt[3]{(r_0^3 + R^3)}/2$  is chosen such that the total activity in both scenarios is the same (see inset of Fig. 5.4). The activity gradient is everywhere zero except at  $r = r_s$  implying that the noise-induced drift of the particle occurs only at  $r = r_s$  towards  $r_0$  in the forward scenario and  $R$  in the backward scenario. In Fig. 5.4, we plot the MFPT as a function of the total activity  $c$  for the forward ( $\mathcal{T}_f(R)$ ) and backward ( $\mathcal{T}_b(R)$ ) scenarios. Clearly, the forward scenario yields a much faster passage to the target. One can show in a straightforward calculation that the difference between the MFPTs of the backward and the forward scenario,  $\delta\mathcal{T} = \mathcal{T}_b(R) - \mathcal{T}_f(R)$  is given as

$$\delta\mathcal{T} = \frac{D_a}{6(D_t + D_a)} \left[ \frac{2r_s^3}{r_0} - \frac{2R^3}{r_s} + 3R^2 - 4r_s^2 + r_0^2 \right], \quad (5.10)$$

where  $D_a = c^2/(6D_r)$ . It can be easily shown that  $\delta\mathcal{T}$  is always positive. This simple case serves to illustrate the strong influence of the spa-

**Figure 5.4:** Mean first passage time to target for stepwise uniform activity as shown in the inset. Symbols denote data from Brownian dynamics simulations and the lines to the theoretical predictions of Eq. 5.9. The forward scenario corresponds to the active region close to the target whereas in the backward scenario, the active region is away from the target towards the outer boundary. Both scenarios have the same total activity. The forward scenario yields a much faster passage to the target.



tial distribution of activity on the MFPT. With the active region closer to the absorbing boundary, the MFPT in the forward scenario is significantly smaller than in the backward scenario.

The agreement between the theoretical predictions and the simulations decreases with increasing  $\alpha$  as can be seen in Fig. 5.3. The theoretical description based on Eqs. 5.2 and 5.5 ignores the coupling between fluctuations in orientation and positional degrees of freedom. With increasing  $\alpha$ , the activity increases near the target and the position of the particle can change significantly during orientational relaxation. Ignoring this coupling between orientation and position is the main reason for the disagreement between theory and simulations.

## 5.4 Pseudochemotaxis

The increase in likelihood of escaping through the target boundary is reminiscent of the chemotaxis phenomenon [62]. Chemotaxis is a fundamental sensory mechanism by which bacteria and other single- or multicellular organisms monitor the concentration gradients of specific chemicals, translating the information into motion either uphill or downhill to the gradient. The increased likelihood of escaping from the inner boundary, where activity increases, can be likened to an active particle climbing up the fuel gradient. This chemotactic behavior has been recently realized in experiments on supramolecular nanomotors which climb up the hydrogen peroxide concentration gradient [209].

Considering that the stationary distribution of active particles in an

inhomogeneous activity profile tends to accumulate in the low activity region, the chemotactic behavior of active particles appears paradoxical. Recently, Ghosh *et. al* [210] addressed this paradox by emphasizing the distinction between the dynamical and stationary behavior of inhomogeneous active systems. The stationary distribution is obtained under the assumption that the active particle is trapped between two reflecting boundaries. The target finding probability, in contrast, is the likelihood of reaching a target boundary. In a stationary scenario, the drift of the particle towards the end where activity increases, is a dynamical effect and does not impact the stationary distribution. Because of this, and that the particle does not experience a torque due to the gradient in the activity, this increase in the target finding probability is not due to chemotaxis, but is called pseudochemotaxis [35, 210].

## 5.5 Conclusion

In this chapter we studied the dynamical properties of noninteracting active particles in an inhomogeneous activity profile. Using Brownian dynamics simulations, we calculated the probability to reach a fixed target and the mean first passage time to the target of an active particle. We showed that both these quantities are strongly dependent on the spatial distribution of the activity. When the activity is distributed such that high-activity zone is located between the target and the starting location, the target finding probability is increased and the passage time is decreased in comparison to a uniformly active system. Moreover, for a continuously distributed profile, the activity gradient results in a drift of active particle up the gradient bearing resemblance to chemotaxis [210, 211].

We found that the insights gained from steady-state inhomogeneous active systems, such as preferential accumulation in the low-activity regions and orientation of particles antiparallel to the activity gradient, cannot be used to understand the dynamical properties of an inhomogeneous active system. The noise-induced drift emerges naturally in a system with spatially varying noise and it points in the direction of the activity gradient. As a consequence, a particle starting anywhere in the system drifts towards higher activity. The particle moves increasingly faster as it gets closer to the target. The drift aids the passage of the particle to the target giving rise to the observed increase in target finding probability. However, this does not mean that the particle has a larger residence time in the high activity regions. If the particle is reflected from the target, it can move into low activity regions where it resides for a longer time than in

the high activity regions.

Finally, considering activity profiles in general the following interesting questions arise: Which activity profile, for a given total activity  $c$ , yields the minimum mean first passage time? Which profile yields the maximum target finding probability? In a recent study [158] on chemotaxis, the authors have considered a source emitting a chemical signal which develops a spatio-temporal distribution.

## 5.A Appendix

The calculations of the MFTP and exit probability are shown here for the one dimensional FPE of the form  $\partial_t p(x, t|x_0, t_0) = Lp(x, t|x_0, t_0)$ , where  $p(x, t|x_0, t_0)$  is the probability density for  $x$  at time  $t$  given that it was  $x_0$  at time  $t_0$ , and the operator can be written as

$$L = \frac{\partial}{\partial x}A(x) + \frac{\partial^2}{\partial x^2}B(x). \quad (5.11)$$

The adjoint of this operator is

$$L^\dagger = -A(x)\frac{\partial}{\partial x} + B(x)\frac{\partial^2}{\partial x^2}, \quad (5.12)$$

where the adjoint is defined by  $\int dx f(x)Lg(x) = \int dx g(x)L^\dagger f(x)$ . Note that the adjoint in curvilinear coordinates needs to be defined with the appropriate integral. The analysis presented in the remainder of this appendix is based on refs. [14, 16].

### 5.A.1 The Backwards Fokker-Planck Equation

The stochastic process in Eqs. 5.1 is a Markov process [212]. This means that the process has no "memory", and that the state of the process at time  $t + dt$  only depends on the state at time  $t$ . The probability density for the system to be at position  $x_1$  at time  $t_1$  given that it was at  $x_2$  at time  $t_2$ ,  $x_3$  at time  $t_3$ , and so on, where  $t_1 > t_2 > t_3 > \dots$ , is  $p(x_1, t_1|x_2, t_2; x_3, t_3, \dots)$ . If the process is a Markov process than  $p(x_1, t_1|x_2, t_2; x_3, t_3, \dots) = p(x_1, t_1|x_2, t_2)$ . Using this, one can write the three point probability density as

$$p(x_1, t_1; x_2, t_2; x_3, t_3) = p(x_1, t_1|x_2, t_2)p(x_2, t_2|x_3, t_3)p(x_3, t_3). \quad (5.13)$$

Integrating this over  $x_2$  and dividing by  $p(x_3, t_3)$  results in the Chapman-Kolmogorov equation:

$$p(x_1, t_1|x_3, t_3) = \int dx_2 p(x_1, t_1|x_2, t_2)p(x_2, t_2|x_3, t_3), \quad (5.14)$$

where  $p(x_1, t_1; x_3, t_3)/p(x_3, t_3) = p(x_1, t_1|x_3, t_3)$  was used.

The backwards Fokker-Planck equation can be derived from the Chapman-

Kolmogorov equation by taking the derivative with respect to  $t_2$ :

$$\begin{aligned}
0 &= \frac{\partial}{\partial t_2} p(x_1, t_1 | x_3, t_3) \\
&= \int dx_2 \left[ p(x_2, t_2 | x_3, t_3) \frac{\partial}{\partial t_2} p(x_1, t_1 | x_2, t_2) \right. \\
&\quad \left. + p(x_1, t_1 | x_2, t_2) \frac{\partial}{\partial t_2} p(x_2, t_2 | x_3, t_3) \right]. \tag{5.15}
\end{aligned}$$

The time derivative in the last line can be replaced by the Fokker-Planck operator, and by using the definition of the adjoint this becomes

$$0 = \int dx_2 p(x_2, t_2 | x_3, t_3) \left[ \frac{\partial}{\partial t_2} p(x_1, t_1 | x_2, t_2) + L^\dagger(x_2) p(x_1, t_1 | x_2, t_2) \right], \tag{5.16}$$

where  $L^\dagger(x_2)$  depends and acts on  $x_2$ . The term in the square brackets must be zero because  $p(x_2, t_2 | x_3, t_3) \geq 0$ , and therefore

$$\frac{\partial}{\partial t_2} p(x_1, t_1 | x_2, t_2) = -L^\dagger(x_2) p(x_1, t_1 | x_2, t_2). \tag{5.17}$$

If  $A(x)$  and  $B(x)$  are independent of time, the probability is invariant under time translations, and therefore

$$\begin{aligned}
\frac{\partial}{\partial t_2} p(x_1, t_1 | x_2, t_2) &= \frac{\partial}{\partial t_2} p(x_1, 0 | x_2, t_2 - t_1) \\
&= -\frac{\partial}{\partial t_1} p(x_1, 0 | x_2, t_2 - t_1) \\
&= -\frac{\partial}{\partial t_1} p(x_1, t_1 | x_2, t_2). \tag{5.18}
\end{aligned}$$

This together with Eq. 5.17 gives the backwards FPE:

$$\frac{\partial}{\partial t_1} p(x_1, t_1 | x_2, t_2) = L^\dagger(x_2) p(x_1, t_1 | x_2, t_2). \tag{5.19}$$

### 5.A.2 Mean First Passage Time

The probability that  $a \leq x \leq b$  at time  $t$  given that it was at  $x$  at time  $t = 0$  is

$$P_{a,b}(x, t) = \int_a^b dx' p(x', t|x, 0). \quad (5.20)$$

If  $p(x', t|x, 0)$  obeys the backwards FPE, so does  $P_{a,b}(x, t)$ :

$$\partial_t P_{a,b}(x, t) = L^\dagger P_{a,b}(x, t) \quad (5.21)$$

The probability  $P_{a,b}(x, t)$  is equal to the probability that  $x$  leaves the interval  $a \leq x \leq b$  at a time later than  $t$ . The probability distribution of exit times is then equal to minus the time derivative of  $P_{a,b}(x, t)$ . The first moment of this distribution gives the MFPT:

$$\mathcal{T}(x) = - \int_0^\infty dt t \partial_t P_{a,b}(x, t) = \int_0^\infty dt P_{a,b}(x, t). \quad (5.22)$$

By applying the backwards Fokker-Planck operator on both side one obtains a differential equation for the mean first passage time

$$L^\dagger \mathcal{T}(x) = \int_0^\infty dt L^\dagger P_{a,b}(x, t) = \int_0^\infty dt \partial_t P_{a,b}(x, t). \quad (5.23)$$

Using that  $P_{a,b}(x, t = \infty) = 0$  and  $P_{a,b}(x, 0) = 1$  gives

$$L^\dagger \mathcal{T}(x) = -1, \quad (5.24)$$

which can be solved for a particular operator to yield the MFPT.

### 5.A.3 Exit Probability

In this case both the  $a$  and  $b$  boundaries of the interval  $(a, b)$  are absorbing. The probability of exiting the interval through boundary  $a$  given that it started at  $x$  is

$$\pi_a(x) = - \int_0^\infty dt' J(a, t'|x, 0), \quad (5.25)$$

where  $J$  is the flux, which for the general FPE

$$\partial_{t'} p(a, t'|x, 0) = L p(a, t'|x, 0) = -\partial_a J(a, t'|x, 0) \quad (5.26)$$

can be written as

$$J(a, t'|x, 0) = -A(a)p(a, t'|x, 0) - \partial_a [B(a)p(a, t'|x, 0)], \quad (5.27)$$

for some  $A$  and  $B$ . Using this for the exit probability  $\pi_a$  gives

$$\pi_a(x) = \int_0^\infty dt' [A(a)p(a, t'|x, 0)] + \partial_a [B(a)p(a, t'|x, 0)]. \quad (5.28)$$

Acting with the adjoint Fokker-Planck operator gives

$$\begin{aligned} L^\dagger(x)\pi_a(x) &= \int_0^\infty dt' [A(a) + \partial_a B(a)] L^\dagger p(a, t'|x, 0) \\ &= \int_0^\infty dt' \partial_{t'} [A(a) + \partial_a B(a)] p(a, t'|x, 0) \\ &= -J(a, 0|x, 0). \end{aligned} \quad (5.29)$$

Because  $p(a, 0|x, 0) = \delta(a - x)$ , the flux on the right-hand side vanishes for  $a \neq x$ , which gives the differential equation for the probability to exit through boundary  $a$ :

$$L^\dagger \pi_a(x) = 0. \quad (5.30)$$

The boundary conditions are  $\pi_a(a) = 1$  because it is immediately absorbed at  $a$ , and  $\pi_a(b) = 0$  because it is immediately absorbed at  $b$ .

#### 5.A.4 MFTP and Exit Probability

The probability density corresponding to the FPE in Eq. 5.6 only depends on the radial coordinate  $r = |\mathbf{r}|$ . Integrating out the angular dependence results in

$$\partial_t P(r, t) = LP(r, t), \quad (5.31)$$

where the Fokker-Planck operator is

$$Lf(r) = -\frac{1}{2} \frac{1}{r^2} \frac{\partial}{\partial r} \left[ r^2 \frac{\partial D_a}{\partial r} f(r) \right] + \frac{1}{r^2} \frac{\partial}{\partial r} \left[ r^2 \frac{\partial}{\partial r} [(D_a + D)f(r)] \right]. \quad (5.32)$$



In spherical coordinates the adjoint of an operator acting only on the radial coordinate is defined by

$$\int dr r^2 f(r) Lg(r) = \int dr r^2 g(r) L^\dagger f(r), \quad (5.33)$$

which gives

$$L^\dagger f(r) = \frac{1}{2} \frac{\partial D_a}{\partial r} \frac{\partial}{\partial r} f(r) + \frac{1}{r^2} (D_a + D) \frac{\partial}{\partial r} \left[ r^2 \frac{\partial}{\partial r} f(r) \right]. \quad (5.34)$$

The equation for the exit probability for the system in Sec. 5.2 with this operator is

$$\phi(r) \partial_r \pi_{r_0}(r) + \partial_r^2 \pi_{r_0}(r) = 0, \quad (5.35)$$

where

$$\phi(r) = \frac{1}{2} \partial_r [\ln(D + D_a(a))] + \frac{2}{r}. \quad (5.36)$$

The boundary conditions are  $\pi_{r_0}(r_0) = 1$  because the particle is immediately absorbed at the target, and  $\pi_{r_0}(R) = 0$  because the particle is immediately absorbed at the outer boundary. Equation 5.8 can be obtained from Eq. 5.35 by integration.

Using the adjoint Fokker-Planck operator (Eq. 5.34), the equation for the mean first passage time (Eq. 5.24) for the system in Sec. 5.2 can be written as

$$\phi(r) \partial_r \mathcal{T}(r) + \partial_r^2 \mathcal{T}(r) = -\frac{1}{D_a(r) + D}. \quad (5.37)$$

The boundary conditions are  $\mathcal{T}(r_0) = 0$  as the particle is immediately absorbed at the target, and  $\partial_r \mathcal{T}(r)|_{r=R} = 0$  because of the reflecting outer boundary with radius  $R$ . Equation 5.9 is obtained by integrating the previous equation with the appropriate boundary conditions.

## Chapter 6

# Chemotaxis of Cargo-Carrying Self-Propelled Particles

This chapter contains results which have been published in ref. [185].  
Reprinted (adapted) with permission from H.D. Vuijk, H. Merlitz, M. Lang,  
A. Sharma, and J.-U. Sommer. *Physical Review Letters* 126, 208102, 2021.  
Copyright (2018) by the American Physical Society.

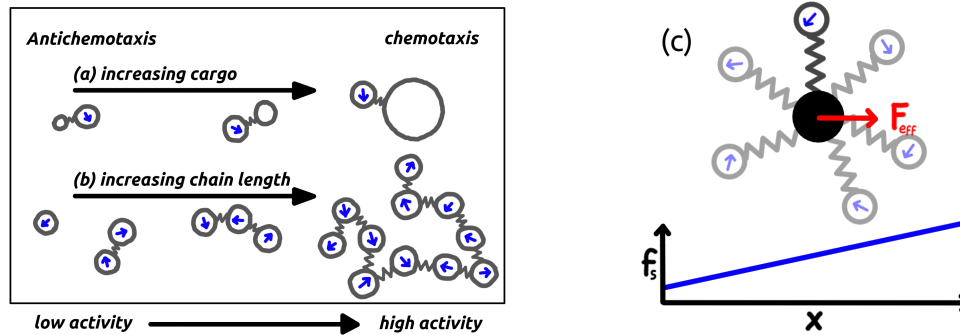


**Figure 6.1:** Crossover from anti-chemotactic to chemotactic behavior. ABPs are sketched as circles with arrows. Cargo particles (sketched as empty circles) are bound to ABPs. (a) When the cargo is small, that is, its friction coefficient is small, the dimer accumulates in low activity regions (anti-chemotaxis). When the cargo is large, the dimer accumulates in the high activity regions (chemotaxis). (b) Self emergence of cargo in active chains. When active particles are connected in a chain, one observes the crossover from anti-chemotactic to chemotactic behavior with increasing chain length. (c) A sketch of the Born-Oppenheimer approximation. A single ABP is connected to a cargo (black circle) with a fixed position. Because the cargo is fixed in space, the ABP (open circle with arrow) is able to explore the space around the cargo (translucent ABPs) and sense the gradient in the swim force ( $f_s$ ). On average the ABP pulls on the cargo in the direction of the gradient of the swim force, which results in an effective force ( $F_{eff}$ ) on the cargo. The bottom graph shows the swim force in the neighborhood of the cargo.

Although active particles can display interesting transient behavior in fuel gradients, called pseudochemotaxis [200, 209, 210, 213, 214], as shown in the previous chapter, activity does not lead to an advantage in the search for fuel sources as compared to passive diffusion on long time scales (see Section 3.2.5). These observations have led to the general belief that chemotaxis, by which we mean the migration to regions of higher activity (or fuel), a prominent feature of living systems, cannot be reflected by uninformed moving objects, in particular not by active particles without a coupling between the gradient in the activity and a torque on the orientation. In this chapter, we demonstrate that active Brownian particles (ABPs) can show chemotactic behavior in activity gradients when they are bound to a passive cargo particle. With increasing size of the cargo, the active-passive complex switches its behavior from anti-chemotactic like to chemotactic and accumulates in regions with a large fuel concentration (see Fig. 6.1). Furthermore, we show that an explicit distinction between cargo and active particles is not fundamental to our proposed mechanism

and can self-emerge in an active system. We demonstrate this in a system of ABPs connected in a chain: with increasing chain length there is a crossover from anti-chemotactic like behavior to chemotaxis.

## 6.1 The Model

The dimer model consists of an ABP (see Section 3.1.2) attached to a passive cargo. All results hold for both  $d = 2$  and  $d = 3$  dimensions. Results for  $d = 1$  are shown App. 6.A.8. The equations of motion for the dimer are

$$\partial_t \mathbf{r}_1 = \frac{1}{\gamma} \mathbf{F} + \frac{1}{\gamma} f_s(\mathbf{r}_1) \mathbf{n} + \sqrt{2T/\gamma} \boldsymbol{\xi}_1, \quad (6.1)$$

$$\partial_t \mathbf{n} = \sqrt{2D_r} \mathbf{n} \times \boldsymbol{\eta} \quad (6.2)$$

$$\partial_t \mathbf{r}_2 = -\frac{1}{q\gamma} \mathbf{F} + \sqrt{2T/q\gamma} \boldsymbol{\xi}_2, \quad (6.3)$$

where  $\mathbf{r}_1$  is the coordinate of the active particle and  $\mathbf{r}_2$  the coordinate of the (passive) cargo particle,  $\mathbf{n}$  is the orientation of the active particle, and  $\mathbf{F}$  is the force the cargo particle exerts on the active particle (the force on the passive particle is  $-\mathbf{F}$ ). The orientation vector changes because of rotational Brownian motion (see Section 1.3.3). The results in this chapter also hold if the particle tumbles – that is, with a certain rate the active particle completely randomizes its orientation abruptly (see Section 3.1.1) – in addition to the continuous diffusion of the orientation vector.  $T$  is the temperature in units such that the Boltzmann constant  $k_b$  is unity. The friction of the active particle is  $\gamma$ . The friction of the passive cargo particle is  $q$  times that of the active particle. The swim force of the active particle is  $f_s$ , which makes the swim speed is  $v_s = f_s/\gamma$ . The vectors  $\boldsymbol{\xi}_1$ ,  $\boldsymbol{\xi}_2$  and  $\boldsymbol{\eta}$  are random, Gaussian vectors with zero mean and autocorrelation  $\langle \boldsymbol{\xi}_1(t) \boldsymbol{\xi}_1(t') \rangle = \langle \boldsymbol{\xi}_2(t) \boldsymbol{\xi}_2(t') \rangle = \langle \boldsymbol{\eta}(t) \boldsymbol{\eta}(t') \rangle = \mathbf{1} \delta(t - t')$ , where  $\mathbf{1}$  is the identity matrix. Note that in this model the rotation of the active particle is not hindered by the bond. In the next chapter a dimer is considered of which the active particles have a fixed orientation with respect to the bond vector, see also ref. [215].

The potential holding the two particles together is

$$U(\mathbf{r}_1, \mathbf{r}_2) = \frac{1}{2} k (|\mathbf{r}_1 - \mathbf{r}_2| - l_0)^2, \quad (6.4)$$

where  $k$  is the spring constant, and  $l_0$  is the rest length. We consider two

cases theoretically: i) A rigid bond, which we model by taking the limit  $k \rightarrow \infty$ . ii) A harmonic spring with zero rest length ( $l_0 = 0$ ) and general spring constant  $k$ . The force on the active particle is  $\mathbf{F} = -\nabla_1 U = -k(r' - l_0)\hat{\mathbf{r}}'$ , where  $\mathbf{r}' = \mathbf{r}_1 - \mathbf{r}_2$ ,  $r' = |\mathbf{r}'|$ , and  $\hat{\mathbf{r}}' = \mathbf{r}'/r'$ . Other potentials are considered numerically.

The activity of the ABP is characterized by its persistence time  $\tau = (d-1)D_r$  (characteristic time of rotation of the active particle) and a space-dependent swim force  $f_s(\mathbf{r})$ , which we assume to be proportional to the local fuel concentration. Regions where the swim force is large (small) we call high (low) activity regions.

The Fokker-Planck equation (FPE) corresponding to the probability density of this system is

$$\begin{aligned} \partial_t P(t) = & -\frac{1}{\gamma} \nabla_1 \cdot [\mathbf{F}P(t) + f_s \mathbf{n}P(t) - T \nabla_1 P(t)] \\ & + \frac{1}{q\gamma} \nabla_2 \cdot [\mathbf{F}P(t) + T \nabla_2 P(t)] + \frac{1}{(d-1)\tau} \mathcal{R}^2 P(t), \end{aligned} \quad (6.5)$$

where  $P(t) = P(\mathbf{r}_1, \mathbf{n}, \mathbf{r}_2, t)$ , and  $\mathcal{R} = \mathbf{p} \times \nabla_{\mathbf{p}}$  is the rotation operator [216].

We coarse grain Eq. 6.5 in two steps. First we expand  $P(t)$  in eigenfunctions of  $\mathcal{R}^2$  (see Sec. ). and transform to the 'center-of-friction' coordinate  $\mathbf{R} = \frac{1}{1+q}\mathbf{r}_1 + \frac{q}{1+q}\mathbf{r}_2$ , which we take as the position of the dimer, and the internal coordinate  $\mathbf{r}' = \mathbf{r}_1 - \mathbf{r}_2$ . Then we integrate out the orientational degrees of freedom  $\mathbf{p}$  and the internal coordinate and ignore terms  $\mathcal{O}(\nabla^3)$ . In Appendix 6.A details are shown of the derivation and the approximation. This approximation is valid when the separation between the ABP and the passive particle and the persistence length of the ABP are small compared to gradients in the system. This results in the following equation for the probability density of the dimer:

$$\partial_t \rho(\mathbf{R}, t) = -\nabla \cdot \mathbf{J}, \quad (6.6)$$

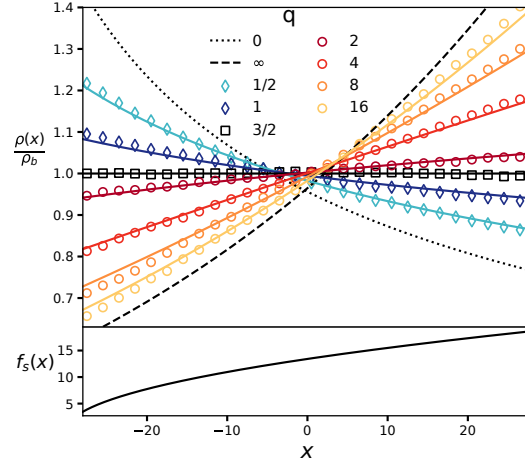
where the flux of the dimers is

$$\mathbf{J} = -\frac{1}{2}\epsilon\rho(\mathbf{R}, t)\nabla D(\mathbf{R}) - D(\mathbf{R})\nabla\rho(\mathbf{R}, t), \quad (6.7)$$

with

$$\epsilon = 1 - q\frac{d-1}{d}, \quad (6.8)$$

**Figure 6.2:** Density distributions of ABPs relative to the bulk density  $\rho_b = \frac{1}{56} \int_{-28}^{28} dx \rho(x)$  bound to a passive cargo particle with different friction (top figure). The bond length of the dimer is unity,  $d = 3$ ,  $\tau = 1/40$ , and the swim force is  $f_s(x) = \sqrt{6(x+30)}$  (bottom figure). The dimensions of the simulation box are  $60 \times 60 \times 60$ . The particles interact with the confining walls via a Weeks-Chandler-Anderson potential [219]. Because the theory ignores boundary effects, the density is shown for  $-28 < x < 28$ . Boundary effects could be included using the methods described in [220, 221]. Symbols show simulation results, and solid lines Eq. 6.10. With a highly mobile cargo particle (blue diamonds) the dimer accumulates in regions of low activity (anti-chemotactic like behavior). At  $q = 3/2$  a uniform density is found (black squares). With a less mobile cargo (circles) the dimer accumulates where the activity is high (chemotaxis). The dashed line shows the  $1 \rightarrow \infty$  limit, corresponding to the Born-Oppenheimer approximation. The dotted line shows the  $q \rightarrow 0$  limit.



and

$$D(\mathbf{R}) = \frac{1}{1+q} \frac{T}{\gamma} + \frac{1}{(1+q)^2} \frac{\tau}{d\gamma^2} f_s^2(\mathbf{R}), \quad (6.9)$$

is the coarse-grained space-dependent diffusion coefficient of the dimer. The theoretical results are validated by Brownian dynamics simulations [217, 218].

## 6.2 Chemotaxis of Active Dimers

Figure 6.2 shows the stationary density distribution of dimers with a different friction ratio  $q$ . As long as the cargo is highly mobile (small  $q$ ), the dimer accumulates in regions of low activity like a single ABP, which – being an orthokinetic swimmer – behaves like an antichemotactic particle. When the cargo has large friction (large  $q$ ), it exhibits chemotaxis and accumulates where the activity is high. The crossover from anti-chemotactic to chemotactic behavior is captured by the coarse-grained equations, which yields the following expression for the steady-state den-

sity of the dimer:

$$\rho(\mathbf{R}) \propto \left[ 1 + \frac{1}{1+q} \frac{\tau}{\gamma T d} f_s^2(\mathbf{R}) \right]^{-\frac{1}{2}\epsilon}. \quad (6.10)$$

For  $q < d/(d-1)$ ,  $\epsilon$  is positive, and the dimer is chemotactic. For  $q > d/(d-1)$ ,  $\epsilon$  is negative, and the dimer is anti-chemotactic. At the threshold  $q = d/(d-1)$ , the distribution of the dimer is uniform and independent of the swim force. Note that in the limit of  $q \rightarrow 0$  the density distribution of the dimer reduces to that of a single ABP, and it accumulates in the region of low activity. In general, the exponent  $\epsilon$  depends on the potential between the two particles.

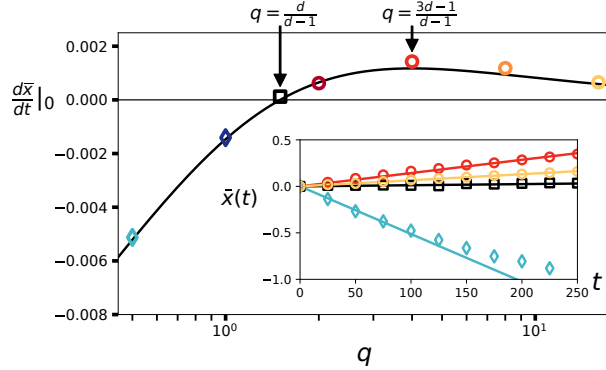
In order to understand the mechanism behind the switch from anti-chemotaxis to chemotaxis for increasing  $q$ , we consider the small and large  $q$  limits separately. When the friction coefficient of the cargo particle is much smaller than that of the ABP, the cargo relaxes to its quasi-steady state distribution at each position of the ABP. In this limit, one can consider the dimer to be a single ABP with an increased friction coefficient. Accordingly, the dimer accumulates in the low activity regions (antichemotactic like behavior). In the limit of large friction of the cargo particle, the ABP relaxes to a quasi-steady state distribution at each position of the load particle, and the ABP probes the neighborhood of the cargo particle. The activity gradient results in an effective force on the cargo particle in the direction of the activity gradient. In this limit, one observes the accumulation of the system in high activity regions (chemotaxis).

The steady-state density in the large friction limit can be obtained following an independent approach similar to the Born-Oppenheimer approximation in quantum mechanics [222]. When the cargo is large, one can consider it as immobile and the ABP as moving in a stationary potential. The ABP explores the environment around the load and exerts an effective force

$$\mathbf{F}_{eff}(\mathbf{r}_2) = \frac{d-1}{d} \frac{\tau}{2d\gamma} \nabla_2 f_s^2(\mathbf{r}_2) \quad (6.11)$$

on it, which is up the swim force gradient (see Fig. 6.1). This effective force can be considered as the driving force for the total system. The steady-state density of a passive Brownian particle with friction  $q\gamma$  in a

**Figure 6.3:** Time derivative at  $t = 0$  of the average position of the dimer in the same setup as Fig. 6.2 starting with a uniform distribution ( $d\bar{x}/dt$ ). Symbols show simulation results (colors as in Fig. 6.2). The line is the theoretical prediction  $d\bar{x}/dt \propto \epsilon/(1+q)^2$  with the proportionality constant fitted to the data (for details see App. 6.A.6). Inset:



initial time evolution of the average position ( $\bar{x}(t)$ ) for several values of  $q$ . The solid lines show the linear fit for short time from which the data in the main figure is extracted. For  $q < d/(d-1) = 3/2$  the dimers move to the left down the swim force gradient. For  $q > 3/2$  the dimers move to the right up the swim force gradient. As  $q$  increases beyond  $(3d-1)/(d-1) = 4$ , the dynamics start to slow down due to the increase in the friction of the dimer.

such an effective force field is

$$\rho(\mathbf{R}) \propto \exp \left[ \frac{1}{T} \frac{d-1}{d} \frac{\tau}{2d\gamma} f_s^2(\mathbf{R}) \right], \quad (6.12)$$

which shows that for large  $q$  the dimer moves preferentially to regions of high fuel concentration. For details of the calculations, see the Appendix. Note that this density is the  $q \rightarrow \infty$  limit of Eq. 6.10. This consideration shows that it is indeed the ability of the active particle to explore the activity gradient that causes the chemotaxis.

Whereas the steady-state distribution measures the chemotactic behavior of the dimer, it does not shed light on the ‘efficiency’ of the chemotactic transport of cargo particles by the ABPs. Though large  $q$  results in the strongest chemotactic behavior, it also slows down the transport of the cargo particle due to the increased friction of the dimer. In our case, this leads to an optimum  $q$  that yields the fastest transport to regions of high activity. To quantify this, we use the initial rate of change of the average position of the dimer, starting with a uniform distribution (see Fig. 6.3). For this setup, the displacement of the dimer is determined by



the convective velocity, which can be read off from Eq. 6.7,

$$\mathbf{V}(\mathbf{R}) = -\frac{1}{2}\epsilon\nabla D(\mathbf{R}) \propto \frac{\epsilon}{(1+q)^2}\nabla f_s^2. \quad (6.13)$$

Depending on the value of  $q$ , this is either up the swim force gradient (chemotaxis) or down the swim force gradient (anti-chemotaxis). The convective velocity has a maximum at  $q = (3d - 1)/(d - 1)$  which coincides with the simulation result. Note that for biased movement up the swim-force gradient, only a large enough cargo is necessary, and no memory [223], temporal integration of the fuel concentration [224], or an explicit coupling between the swim-force gradient and the orientation of the ABP [57, 225] is required.

### 6.3 Other Potentials

The same analysis can be done for a harmonic potential with zero rest length (that is,  $l_0 = 0$  and  $k$  is finite in Eq. 6.4). In this case the steady-state density is the same as that of a dimer with a rigid bond (Eq. 6.10), but with

$$\epsilon = 1 - \frac{q^2}{q + (1+q)\frac{\tau k}{\gamma}}. \quad (6.14)$$

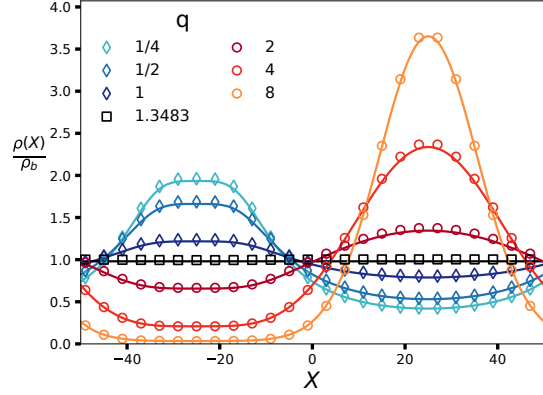
Note that in the limit  $k \rightarrow \infty$ ,  $\epsilon = 1$ , and the dimer behaves like a single active particle with a increased friction constant. This shows again the importance of the separations of time scales between the active and passive cargo particle for the emergence of chemotaxis. The value of  $q$  for which the density is flat, obtained by equating  $\epsilon$  to zero, is

$$q_0 = \frac{1}{2} \left( 1 + \frac{\tau k}{\gamma} \right) + \frac{1}{2} \sqrt{\left( 1 + \frac{\tau k}{\gamma} \right)^2 + 4 \frac{\tau k}{\gamma}}. \quad (6.15)$$

#### 6.3.1 Run-and-Tumble Dimer in One Dimension

The FPE corresponding to a one-dimensional dimer where the active particle is a run-and-tumble (RTP) particle can be solved numerically (see Section 6.A.8 for details). Because this is computationally less intensive than simulations, the following cases are explored using this one dimensional model.

**Figure 6.4:** Steady-state density of RTP dimers with different friction of the cargo ( $q$ ) in one dimension with periodic boundary conditions. The theoretical prediction (lines, Eqs. 6.10 and 6.14) agrees with the numerical solution (circles) to Eqs. 6.117 and 6.118. For clarity, every other data point is shown. The swim force is  $f_s(X) = 20(1 + \sin(X2\pi/L))$  with box size  $L = 100$ . The spring constant is  $k = 8$ . Dimers with a cargo with a small friction (small  $q$ , blue diamonds) are anti-chemotactic and accumulate where the swim force is small (left side of the box); dimers with a cargo with a large friction (large  $q$ , red circles) are chemotactic and accumulate where the swim force is small (right side of the box). The cross over happens at  $q \approx 1.3483$  (black squares) as predicted by Eq. 6.15. This behaviour is qualitatively the same as that of a dimer with a fixed bond discussed in the main text.



The orientation of an RT particle changes abruptly, that is, with rate  $\alpha$  it picks a random new direction (see Section 3.1.1). The autocorrelation function of the orientation decays exponentially.

If the ABP in the dimer is replaced by a run-and-tumble particle, the results of the previous section holds with  $d = 1$  (see Appendix 6.A.8). The case of a rigid bond results in a coarse-grained equation that is equal to that of a single run-and-tumble particle, as there is no internal degree of freedom and the two particles always move together, so there is no separation of time scales. Therefore, we only consider analytically the case of a harmonic bond.

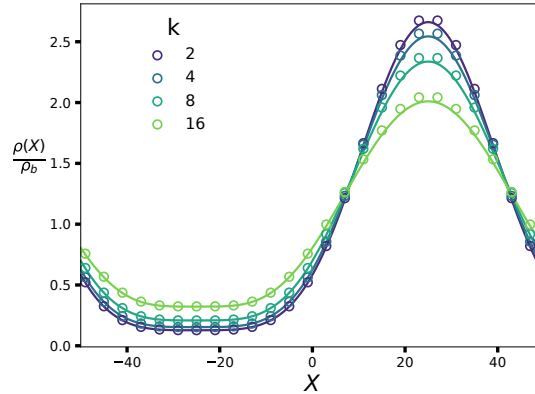
The equations of motion are

$$\partial_t x_1 = \frac{1}{\gamma} F + \frac{1}{\gamma} f_s(x_1) n + \sqrt{2T/\gamma} \zeta_1 \quad (6.16)$$

$$\partial_t x_2 = -\frac{1}{q\gamma} F + \sqrt{2T/\gamma} \zeta_2, \quad (6.17)$$

where  $x_1$  is the coordinate of the active particle with friction constant  $\gamma$  and swim force  $f_s$ ,  $x_2$  is the coordinate of the passive cargo particle with friction constant  $q\gamma$ , and  $\zeta_1$  and  $\zeta_2$  are white noise with zero mean and autocorrelation  $\langle \zeta_1(t) \zeta_1(t') \rangle = \langle \zeta_2(t) \zeta_2(t') \rangle = \delta(t - t')$ . The orientation

**Figure 6.5:** Steady-state density of RTP dimers with different spring constant ( $k$ ) in one dimension with periodic boundary conditions. The theoretical prediction (lines, Eqs. 6.10 and 6.14) agrees with the numerical solution (circles) to Eqs. 6.117 and 6.118. For clarity, every other data point is shown. The swim force is  $f_s(X) = 20(1 + \sin(X2\pi/L))$  with box size  $L = 100$ . The friction of the passive cargo particle is  $q = 4$  times that of the active RTP particle. For this value of  $q$  the dimer is chemotactic (accumulates in regions where the swim force is large). In creasing the spring constant ( $k$ ) decreases the chemotactic behaviour because it limits the ability of the active particle to explore the space around the passive cargo particle and thus limits the dimer's ability to sense gradients in the swim force.



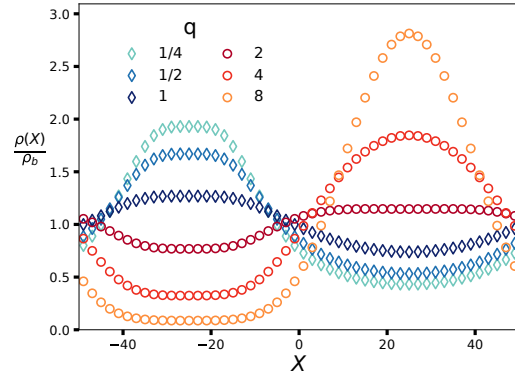
of the active particle is  $p \in \{+1, -1\}$ , which points either in the positive (right moving) or the negative (left moving) direction. With rate  $\alpha$  the active particle randomizes its orientation (so it changes direction with rate  $\alpha/2$ ). All results are shown here are for  $\gamma = 1$ ,  $T = 1$ , and  $\alpha = 1/\tau = 40$ .

Figure 6.4 shows the steady-state density of dimers with harmonic potential for different friction of the cargo particle. The behaviour is qualitatively the same as the of a three-dimensional dimer with a fixed bond: the dimer is chemotactic if the cargo has a large friction, and is anti-chemotactic if the cargo has a small friction.

If the spring constant  $k$  increases, the active particle is no longer able to explore the neighbourhood of the passive cargo particle and can therefore no longer sense the gradient in the swim force, which results in a decrease in the chemotaxis (see Fig. 6.5). The chemotactic behaviour is most pronounced in case of the weakest potential; however, the limit  $k \rightarrow 0$  is not possible, as it violates the assumption that the separation between the active particle and the cargo particle is small compared to gradients of the swim force.

To show that the transition from anti-chemotaxis to chemotaxis as the friction of the cargo increases is a general feature that happens for differ-

**Figure 6.6:** Steady-state density of RTP dimers with a ‘rope’ potential (Eq. 6.18) with  $l_0 = 2$  in one dimension with periodic boundary conditions. The swim force is  $f_s(X) = 20(1 + \sin(X2\pi/L))$  with box size  $L = 100$ . The symbols show the numerical solution to Eqs. 6.117 and 6.118. Note that even though the potential is very different compared to the harmonic potential in Fig. 6.4, the density profiles are very similar.



ent kinds of potentials, we consider the following potential:

$$U(x_1, x_2) = \begin{cases} 0 & \text{if } |x_1 - x_2| < l_0, \\ \infty & \text{else.} \end{cases} \quad (6.18)$$

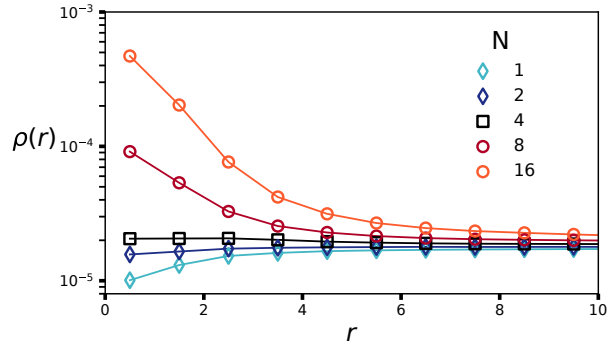
This potential corresponds to an active particle and a cargo particle bound by a rope, so the active particle can explore the space around the passive particle without exerting any force, as long as the separation is smaller than the length of the ‘rope’  $l_0$ . The behaviour of an active-passive dimer with such a potential is qualitatively similar to the cases shown before (see Fig. 6.6).

Because the FPE governing the dynamics of the one-dimensional run-and-tumble dimer (Eq. 6.131) are qualitatively the same as the FPE for the two and three-dimensional cases (Eq. 6.7), one can assume that the results for the one-dimensional dimer with a rope potential also hold for a two and three-dimensional dimer. In two dimensions, an active passive dimer with a rope potential (Eq. 6.18) corresponds to an active particle inside a movable ring, where the ring has the role of the passive particle. This provides a possible experimental setup to test the theory.

## 6.4 Chemotaxis of Active Polymers

Instead of coupling an ABP to a passive cargo, several ABPs can be combined to form chains or clusters of  $N$  ‘monomers’ [226, 227]. Then, each individual ABP may be regarded as an active pulling agent connected to a ‘cargo’ of  $N - 1$  particles because the other  $N - 1$  ABPs do not pull coherently in identical directions but rather in random directions. Fig-

**Figure 6.7:** Stationary concentrations of ABP-molecules inside a spherical container of radius  $r_{max} = 25$ . The symbols show simulation data, and the lines are a guide for the eye. The source of activity is at its center and the driving force decreases as  $f_s(r) = 15/r$  for  $r \geq 1$ , and remains constant  $f_s(r) = 15$  for  $r < 1$ .



This activity profile corresponds to a stationary fuel source emitting fuel by diffusion. The mono- and dimers are anti-chemotactic and are driven out of the region of high activity (blue diamonds). The quadromer is distributed uniformly (black squares). Longer polymers ( $N > 4$ , red circles) are chemotactic and accumulate near the peak of the fuel concentration.

Figure 6.7 displays the stationary radial density distribution profiles of the molecules inside the container. Short oligomers are anti-chemotactic and stay away from regions of high activity. Long polymers, on the other hand, are chemotactic and accumulate where activity is high. The crossover point is seen with the quadromer which is roughly uniformly distributed in the activity field.

Polymeric ABPs are therefore qualitatively similar to a single ABP coupled to a passive cargo. If either the cargo is sufficiently inert or the degree of polymerization sufficiently high, such that it inhibits the free motion of an individual ABP, then the situation of a single ABP inside an approximately stationary potential arises: Inside an activity gradient, the particle is running up the confining potential in the direction of increasing activity. This bias generates a net force which – if the system is mobile – drives the same up the activity gradient. If, however, the cargo is rather mobile, then the motion of the ABP remains approximately undisturbed and the complex runs down the activity gradient as an individual ABP does.

## 6.5 Discussion

ABPs are equivalent to other models of active matter (see Section 3.1), such as run-and-tumble [144, 228], active Ornstein-Uhlenbeck particles [134, 135], and the results shown here also apply to these models. We show in the Appendix that the chemotactic behavior observed in the active-

passive dimer cannot be reproduced in a system of dimers in which the active particle is replaced by a passive Brownian particle coupled to a spatially inhomogeneous thermostat

An interesting outlook is the development of artificial nano-machines which can locate origins of fuel gradients based on the design principle of coupling ABPs to passive cargo without a complex sensing and steering system. Furthermore, a natural progression of this work is to study how the behavior of a single active-passive dimer or more complex clusters in an activity gradient affect the collective properties of a system with a large number of such components [229–232].

The coupling of active bodies with or without passive bodies leads to effective sensing of gradients of activity (fuel) and can be generalized in several directions. First, the connectivity between the bodies does not need to be linear as in the studies presented in this letter. Virtually any kind of topology of connecting the active bodies leads to effective chemotaxis, given that the complex provides sufficient friction to single active bodies. Moreover, active bodies moving inside a container that is permeable for the fuel but not for the active bodies can give rise to chemotactic motion of the container, provided the activity gradient is present inside the container. Also in this case, it is the exploration of the active bodies in the gradient field which leads to a higher averaged pressure on the container walls located at the higher activity. Our results may shed light on the origin of prebiotic forms of life and how chemotactic sensing has emerged during evolution.

## 6.A Appendix

In this appendix details of the derivations are shown. All results hold for two and three dimensions and for both active Brownian particles (ABPs) and run-and-tumble particles (RTPs). Section 6.A.1 shows the derivation of the steady-state density of the active-passive dimer with a rigid bond in a swim force gradient (Eq. 6.10 in the main text), as well as the derivation for a dimer with a harmonic bond with zero rest length. Section 6.A.5 shows the derivation of the Born-Oppenheimer approximation for the  $q \rightarrow \infty$  limit (Eqs. 6.11 and 6.12 in the main text). Section 6.A.6 shows the derivation of the average position of the dimer in a rectangular box as in Fig. 6.3. In Section 6.A.7 we comment on how the model relates to a dimer with a passive Brownian particle in a temperature gradient instead of an ABP with a swim-force gradient. In Section 6.A.8 we show the derivation of the density for a dimer in one dimension and consider the effect of the spring constant of the potential between the active and passive particle on the steady-state density. Furthermore, we consider numerically a nonharmonic potential to show that the transition to chemotaxis exists for a wide range of potentials, and briefly discuss a possible experimental setup to test the theory.

### 6.A.1 Coarse Graining The Active-Passive Dimer

The derivations shown here rely on two coarse-graining steps. First, the orientational degrees of freedom are eliminated from the FPE by expanding in eigenfunctions of the Laplacian on the unit sphere. This results in a hierarchy of equations for functions that depend only on the position coordinates of the active particle and the cargo particle. This method is based on the adiabatic elimination by the eigenfunction expansion method developed in ref. [233] and has been used to study both interacting and noninteracting active Brownian particles [35, 144–146, 234]. Second, because we are interested in the large-scale behaviour of the system (that is, length scales much larger than the separation between the two particles), we integrate out the internal degrees of freedom. Because of this second coarse-graining step, one does not need to determine explicitly the expansion coefficients in the expansion in eigenfunctions of the Laplacian, and the combination of the two steps results in accurate predictions for the relevant quantities.

### 6.A.2 The Active-Passive Dimer Model

The equations of motion for an ABP [90] bound to a passive cargo particle are

$$\partial_t \mathbf{r}_1 = \frac{1}{\gamma} \mathbf{F} + \frac{1}{\gamma} f_s(\mathbf{r}_1) \mathbf{n} + \sqrt{2T/\gamma} \boldsymbol{\xi}_1, \quad (6.19)$$

$$\partial_t \mathbf{n} = \sqrt{2D_r} \mathbf{n} \times \boldsymbol{\eta} + \text{tumble}, \quad (6.20)$$

$$\partial_t \mathbf{r}_2 = -\frac{1}{q\gamma} \mathbf{F} + \sqrt{2T/q\gamma} \boldsymbol{\xi}_2, \quad (6.21)$$

where  $\mathbf{r}_1$  is the coordinate of the active particle and  $\mathbf{r}_2$  the coordinate of the (passive) cargo particle,  $\mathbf{p}$  is the orientation of the active particle, and  $\mathbf{F}$  is the force the cargo particle exerts on the active particle. The orientation vector changes because of orientational diffusion and because of tumbling, which means that with rate  $\alpha$  the orientation vector changes to a random position on the unit sphere.  $T$  is the temperature in units such that the Boltzmann constant  $k_b$  is unity. The friction of the active particle is  $\gamma$ . The friction of the passive cargo particle is  $q$  times that of the active particle. The swim force of the active particle is  $f_s$ . (The swim speed is  $v_s = f_s/\gamma$ .) The vectors  $\boldsymbol{\xi}_1$ ,  $\boldsymbol{\xi}_2$  and  $\boldsymbol{\eta}$  are random Gaussian vectors with zero mean and autocorrelation  $\langle \boldsymbol{\xi}_1(t) \boldsymbol{\xi}_1(t') \rangle = \langle \boldsymbol{\xi}_2(t) \boldsymbol{\xi}_2(t') \rangle = \langle \boldsymbol{\eta}(t) \boldsymbol{\eta}(t') \rangle = \mathbf{1} \delta(t - t')$ , where  $\mathbf{1}$  is the identity matrix.

The potential holding the two particles together is

$$U(\mathbf{r}_1, \mathbf{r}_2) = \frac{1}{2} k (|\mathbf{r}_1 - \mathbf{r}_2| - l_0)^2, \quad (6.22)$$

where  $k$  is the spring constant, and  $l_0$  is the rest length. We consider two cases: i) A rigid bond, which we model by taking the limit  $k \rightarrow \infty$ . ii) A harmonic spring with zero rest length ( $l_0 = 0$ ) and general spring constant  $k$ . The force on the active particle is  $\mathbf{F} = -\nabla_1 U = -k(r' - l_0) \hat{\mathbf{r}}'$ , where  $\mathbf{r}' = \mathbf{r}_1 - \mathbf{r}_2$ ,  $r' = |\mathbf{r}'|$ , and  $\hat{\mathbf{r}}' = \mathbf{r}'/r'$ . The force on the passive particle is  $-\mathbf{F}$ . Other kinds of potentials are considered in Section 6.A.8.

The FPE corresponding Eqs. 6.19, 6.20 and 6.21 is [235]

$$\begin{aligned} \frac{\partial}{\partial t} P(t) = & -\frac{1}{\gamma} \nabla_1 \cdot [\mathbf{F} P(t)] - \frac{1}{\gamma} \nabla_1 \cdot [f_s \mathbf{n} P(t)] + \frac{T}{\gamma} \nabla_1^2 P(t) \\ & + \frac{1}{q\gamma} \nabla_2 \cdot [\mathbf{F} P(t)] + \frac{T}{q\gamma} \nabla_2^2 P(t) \\ & + D_r \mathcal{R}^2 P(t) - \alpha P(t) + \alpha \phi(t), \end{aligned} \quad (6.23)$$



where  $P(t) = P(\mathbf{r}_1, \mathbf{r}_2, \mathbf{n}, t)$  and  $\mathcal{R} = \mathbf{n} \times \nabla_{\mathbf{n}}$  is the angular momentum operator in the space of  $\mathbf{n}$  [216], and  $\mathcal{R}^2$  is the Laplacian on the unit sphere. The last two terms account for tumbling with rate  $\alpha$  [35]. And  $\phi(t) = \phi(\mathbf{r}_1, \mathbf{r}_2, t) = \int d\Omega_d P(\mathbf{r}_1, \mathbf{r}_2, \mathbf{n}(\Omega_d), t)$ , with  $\Omega_d$  the  $d$ -dimensional solid angle.<sup>1</sup>

### 6.A.3 Eliminating the Orientational Degrees of Freedom

To find an equation for the density, the coarse-graining procedure described in Section 3.2.2 is used. In particular, we expand  $P(t)$  in eigenfunctions of the  $\mathcal{R}^2$  operator and integrate out the orientational degrees of freedom. The first three eigenfunctions of  $\mathcal{R}^2$  are  $1$ ,  $\mathbf{n}$ ,  $\mathbf{nn} - \mathbf{1}/d$ . The eigenvalues are, respectively,  $0$ ,  $-(d-1)$  and  $-2d$ . The probability can be expanded in the eigenfunctions of  $\mathcal{R}^2$  as [144, 145]

$$P(t) = \phi + \sigma \cdot \mathbf{n} + \omega : (\mathbf{nn} - \mathbf{1}/d) + \Theta(P(t)). \quad (6.24)$$

This is the Cartesian multipole expansion. One could equivalently use an angular multipole expansion, where  $P(t)$  is expanded in spherical harmonics (or circular harmonics for  $d = 2$ ) [236]. The functions  $\phi$ ,  $\sigma$  and  $\omega$  depend on  $\mathbf{r}_1$ ,  $\mathbf{r}_2$  and  $t$ .  $\sigma$  and  $\omega$  are the dipole and quadrupole moments, and are proportional to the polar and nematic order parameter [237]. Note that  $\omega$  can be made symmetric and traceless [145]. The expansion coefficients can be calculated using the integral over the orientations

$$\langle f(\mathbf{n}) \rangle = \frac{1}{\omega_d} \int d\Omega f(\mathbf{n}), \quad (6.25)$$

where  $\mathbf{n} = \mathbf{n}(\Omega_d)$ .

Because most operators in Eq. 6.23 do not depend on  $\mathbf{n}$ , we rewrite it as

$$\frac{\partial}{\partial t} P(t) = \mathcal{L}P(t) + \mathbf{L}_s \cdot [\mathbf{n}P(t)] + D_r \mathcal{R}^2 P(t) - \alpha P(t) + \alpha \phi, \quad (6.26)$$

---

<sup>1</sup>For two and three dimensions  $\Omega_2 = 2\pi$ ,  $\int d\Omega_2 = \int_0^{2\pi} d\theta \sin\theta$ ,  $\Omega_3 = 4\pi$ ,  $\int d\Omega_3 = \int_0^\pi d\phi \int_0^{2\pi} d\theta \sin\theta$ .

where

$$\begin{aligned} \mathcal{L}P(t) = & -\frac{1}{\gamma}\nabla_1 \cdot [\mathbf{F}P(t)] + \frac{T}{\gamma}\nabla_1^2 P(t) \\ & + \frac{1}{q\gamma}\nabla_2 \cdot [\mathbf{F}P(t)] + \frac{T}{q\gamma}\nabla_2^2 P(t), \end{aligned} \quad (6.27)$$

and

$$\mathbf{L}_s \cdot [\mathbf{p}P(t)] = -\nabla_1 \cdot \left[ \frac{1}{\gamma} f_s \mathbf{p}P(t) \right] \quad (6.28)$$

accounts for the swim force.

To get an equation for  $\phi$ , we integrate Eq. 6.26 over the orientational degrees of freedom, which gives

$$\partial_t \phi = \langle \partial_t P(t) \rangle = \mathcal{L}\phi + \frac{1}{d} \mathbf{L}_s \cdot \boldsymbol{\sigma}. \quad (6.29)$$

The integral over the orientational degrees of freedom of the product of  $\mathbf{n}$  with Eq. 6.26 gives an equation for  $\boldsymbol{\sigma}$ :

$$\begin{aligned} \partial_t \boldsymbol{\sigma} = & d \langle \mathbf{n} \partial_t P(t) \rangle \\ = & -\tau^{-1} \boldsymbol{\sigma} + \mathcal{L}\boldsymbol{\sigma} + \mathbf{L}_s \phi + \frac{2}{2+d} \mathbf{L}_s \cdot \boldsymbol{\omega} \end{aligned} \quad (6.30)$$

where  $\tau^{-1} = (d-1)D_r + \alpha$  is the inverse of the relaxation time of the  $\boldsymbol{\sigma}$  mode, which is equal to the autocorrelation time of the orientation vector  $\mathbf{n}$  (see Eqs. 1.82 and 3.4).

The integral over the orientational degrees of freedom of the product of  $\mathbf{nn} - \mathbf{1}/d$  with Eq. 6.26 gives an equation for  $\boldsymbol{\omega}$ :

$$\partial_t \boldsymbol{\omega} = -\tau_\omega^{-1} \boldsymbol{\omega} + \mathcal{L}\boldsymbol{\omega} + \mathbf{A} : \mathbf{L}_s \boldsymbol{\sigma} + \mathbf{L}_s \cdot \mathbf{Y}, \quad (6.31)$$

where  $\tau_\omega^{-1} = 2dD_r + \alpha$  is the inverse of the relaxation time of the  $\boldsymbol{\omega}$  mode, and

$$\mathbf{Y} = \frac{2d}{2+d} \langle \mathbf{n} (\mathbf{nn} - \mathbf{1}/d) \Theta (P(t)) \rangle, \quad (6.32)$$

involves higher order coefficients of the expansion in Eq. 6.24.

Equations 6.29, 6.30 and 6.31 are exact and form a hierarchy of equations. However, this hierarchy is not closed due to the  $\mathbf{Y}$  term in Eq. 6.31. Often the hierarchy is closed by assuming that the "nematic" order ( $\boldsymbol{\omega}$ ) in

the system is negligible [146], or that the projection onto the higher order modes is zero [238]. Here we do not do this as  $\omega$  is not small in general. However, as shown explicitly, below, on a coarse-grained level where one only considers the position of the dimer and not the positions of the two particles individually, it will turn out that the contribution to the flux from  $\omega$  and  $Y$  are of the order  $\sim \nabla^3$  and can therefore be ignored.

#### 6.A.4 Elimination of the Internal Degree of Freedom

Next we use the following coordinate transformation:

$$\mathbf{R} = \frac{1}{1+q}\mathbf{r}_1 + \frac{q}{1+q}\mathbf{r}_2, \quad \mathbf{r}' = \mathbf{r}_1 - \mathbf{r}_2, \quad (6.33)$$

where  $\mathbf{R}$  is the 'center-of-friction' coordinate, which we call the collective coordinate, and  $\mathbf{r}'$  is the internal degree of freedom. The gradient with respect to the  $\mathbf{R}$  coordinate is  $\nabla_{\mathbf{R}}$ , and the gradient with respect to the  $\mathbf{r}'$  coordinate is  $\nabla_{\mathbf{r}'}$ . With this, the equation for the density (Eq. 6.29) becomes

$$\begin{aligned} \partial_t \phi = & \frac{1}{1+q} \frac{T}{\gamma} \nabla_{\mathbf{R}}^2 \phi - \frac{1}{1+q} \frac{1}{d} \frac{1}{\gamma} \nabla_{\mathbf{R}} \cdot (f_s \sigma) \\ & - \nabla_{\mathbf{r}'} \cdot \left[ \frac{1}{\gamma} f_s \sigma + \frac{1+q}{q} \frac{1}{\gamma} \mathbf{F} \phi - \frac{1+q}{q} \frac{T}{\gamma} \nabla_{\mathbf{r}'} \phi \right]. \end{aligned} \quad (6.34)$$

We are interested in the large scale behaviour of the system, so we want to know

$$\rho(\mathbf{R}, t) = \int_V d^d r' \phi(\mathbf{R}, \mathbf{r}', t), \quad (6.35)$$

which obeys

$$\partial_t \rho = -\nabla_{\mathbf{R}} \cdot \mathbf{J}, \quad (6.36)$$

where  $\mathbf{J} = \mathbf{J}_D + \mathbf{J}_\sigma$ ,

$$\mathbf{J}_D = -\frac{1}{1+q} \frac{T}{\gamma} \nabla_{\mathbf{R}} \rho \quad (6.37)$$

is the flux due to passive diffusion, and

$$J_\sigma = \frac{1}{1+q} \frac{1}{d\gamma} \int_V d^d r' f_s \sigma, \quad (6.38)$$

is the flux due to the activity. In the new coordinates, the equations for  $\mathbf{p}$  and  $\omega$  become,

$$\begin{aligned} (1 + \tau \partial_t) \sigma = & - \left( \frac{1}{1+q} \nabla_{\mathbf{R}} + \nabla_{\mathbf{r}'} \right) \frac{\tau}{\gamma} (f_s \phi) - \frac{1+q}{q} \frac{\tau}{\gamma} \nabla_{\mathbf{r}'} \cdot (\mathbf{F} \sigma) \\ & + \tau \left( \frac{1}{1+q} \nabla_{\mathbf{R}}^2 + \frac{1+q}{q} \nabla_{\mathbf{r}'}^2 \right) \sigma \\ & - \frac{2}{2+d} \frac{\tau}{\gamma} \left( \frac{1}{1+q} \nabla_{\mathbf{R}} + \nabla_{\mathbf{r}'} \right) \cdot (f_s \omega), \end{aligned} \quad (6.39)$$

$$(1 + \tau_\omega \partial_t) \omega = - \tau_\omega \nabla_{\mathbf{R}} \cdot M_{\mathbf{R}} - \tau_\omega \nabla_{\mathbf{r}'} \cdot M_{\mathbf{r}'}. \quad (6.40)$$

The form of the tensors  $M_{\mathbf{R}}$  and  $M_{\mathbf{r}'}$  are not shown explicitly because these terms are only used to show that they have a contribution to  $\rho$  of the order of  $\sim \mathcal{O}(\nabla_{\mathbf{R}}^3)$  and can therefore be neglected.

The density  $\rho$  obeys a continuity equation, is therefore locally conserved and relaxes on a time scale  $\sim \mathcal{O}((\nabla_{\mathbf{R}})^{-1})$ . The  $\mathbf{p}$  and  $\omega$  modes relax on a time scale  $\tau$  and  $\tau_\omega$ , respectively. So  $\rho$  can be identified as the slow mode,  $\mathbf{n}$  and  $\omega$  are the fast modes; therefore, one can set the time derivatives in the two previous equations to zero.

Furthermore, we are interested in the limit where the gradient of the swim force is small compared to the separation between the two particles and small compared to the persistence length of the active particle ( $\tau f_s / \gamma$ ). The expansion coefficients are functions of  $\mathbf{R}$  and  $\mathbf{r}'$ . Gradients in  $\mathbf{R}$  of these functions are of the same order as gradients of the swim force and are therefore small. Gradients in  $\mathbf{r}'$  of the expansion coefficients, however, are not small, but these can be moved around in the integral by integration by parts and turned into gradients with respect to  $\mathbf{R}$  by using  $\nabla_{\mathbf{r}'} f_s = \nabla_{\mathbf{r}'} f_s(\mathbf{R} + \frac{q}{1+q} \mathbf{r}') = \frac{q}{1+q} \nabla_{\mathbf{R}} f_s$ . We will neglect terms  $\sim \mathcal{O}(\nabla_{\mathbf{R}}^3)$  in Eq. 6.36, which means that we neglect terms  $\sim \mathcal{O}(\nabla_{\mathbf{R}}^2)$  when calculating  $J_\sigma$ .

We can then use Eq. 6.39 to calculate  $J_\sigma$ :

$$\begin{aligned}
J_\sigma &= -\frac{1}{(1+q)^2} \frac{1}{d\gamma^2} \int_V d^d r' \tau f_s \nabla_{\mathbf{R}}(f_s \phi) \\
&\quad - \frac{1}{1+q} \frac{1}{d\gamma^2} \int_V d^d r' \tau f_s \nabla_{\mathbf{r}'}(f_s \phi) \\
&\quad - \frac{1}{q} \frac{1}{d\gamma^2} \int_V d^d r' \tau f_s \nabla_{\mathbf{r}'} \cdot (\mathbf{F}\sigma) \\
&\quad + \frac{1}{1+q} \frac{1}{d\gamma} \int_V d^d r' \tau f_s \left( \frac{1}{1+q} \nabla_{\mathbf{R}}^2 + \frac{1+q}{q} \nabla_{\mathbf{r}'}^2 \right) \sigma \\
&\quad + \frac{2}{2+d} \frac{1}{1+q} \frac{\tau \omega}{d\gamma^2} \int_V d^d r' df_s \left( \frac{\nabla_{\mathbf{R}}}{1+q} + \nabla_{\mathbf{r}'} \right) \cdot (f_s \omega). \quad (6.41)
\end{aligned}$$

In the last two integrals, one can use integration by parts to make the  $\nabla_{\mathbf{r}'}$ 's (also the ones in  $\omega$ , see Eq. 6.40) act on  $f_s$ , and  $\nabla_{\mathbf{r}'} f_s \propto \nabla_{\mathbf{R}} f_s$  to show that the last two integrals are second order in  $\nabla_{\mathbf{R}}$  and can be neglected. For the second and third integral we use integration by parts. This gives

$$\begin{aligned}
J_\sigma &= -\frac{1}{(1+q)^2} \frac{\tau}{d\gamma^2} \int_V d^d r' f_s \nabla_{\mathbf{R}}(f_s \phi) \\
&\quad + \frac{q}{(1+q)^2} \frac{\tau}{d\gamma^2} \int_V d^d r' \phi f_s \nabla_{\mathbf{R}} f_s + \frac{1}{1+q} \frac{\tau}{d\gamma^2} I, \quad (6.42)
\end{aligned}$$

where

$$I = \int_V d^d r' (\mathbf{F} \cdot \nabla_{\mathbf{R}} f_s) \sigma, \quad (6.43)$$

$$= -\frac{\tau}{\gamma} \int_V d^d r' \mathbf{F} \cdot (\nabla_{\mathbf{R}} f_s) \nabla_{\mathbf{r}'} \cdot \left( \mathbf{1} \phi f_s + \frac{1+q}{q} \mathbf{F} \sigma \right) \quad (6.44)$$

$$= \frac{\tau}{\gamma} \int_V d^d r' \left( \mathbf{1} \phi f_s + \frac{1+q}{q} \sigma \mathbf{F} \right) \cdot \nabla_{\mathbf{r}'} (\mathbf{F} \cdot \nabla_{\mathbf{R}} f_s). \quad (6.45)$$

Next we use

$$\nabla_{\mathbf{r}'} (\mathbf{F} \cdot \nabla_{\mathbf{R}} f_s) = (\nabla_{\mathbf{r}'} \mathbf{F}) \cdot \nabla_{\mathbf{R}} f_s + \mathcal{O}(\nabla_{\mathbf{R}}^2 f_s), \quad (6.46)$$

and

$$\nabla_{\mathbf{r}'} \mathbf{F} = -k \nabla_{\mathbf{r}'} [(r' - l_0) \hat{\mathbf{r}}'] = -k \mathbf{A}, \quad (6.47)$$

with  $\mathbf{A} = \hat{\mathbf{r}}' \hat{\mathbf{r}}' + (1 - r/r')(\mathbf{1} - \hat{\mathbf{r}}' \hat{\mathbf{r}}')$ , and  $r' = |\mathbf{r}'|$  and  $\hat{\mathbf{r}}' = \mathbf{r}'/r'$ . Note that

$\mathbf{F} \cdot \mathbf{A} = \mathbf{F}$ . With this,  $I$  becomes

$$I = -\frac{\tau k}{\gamma} \int_V d^d r' \phi f_s \mathbf{A} \cdot \nabla_{\mathbf{R}} f_s - \frac{1+q}{q} \frac{\tau k}{\gamma} \int_V d^d r' (\mathbf{F} \cdot \nabla_{\mathbf{R}} f_s) \sigma, \quad (6.48)$$

$$= -\frac{\tau k}{\gamma} \int_V d^d r' \phi f_s \mathbf{A} \cdot \nabla_{\mathbf{R}} f_s - \frac{1+q}{q} \frac{\tau k}{\gamma} I, \quad (6.49)$$

$$= -\frac{q\tau k/\gamma}{q + (1+q)\tau k/\gamma} \int_V d^d r' \phi f_s \mathbf{A} \cdot \nabla_{\mathbf{R}} f_s. \quad (6.50)$$

With this Eq. 6.42 becomes

$$\begin{aligned} J_\sigma = & -\frac{1}{(1+q)^2} \frac{\tau}{d\gamma^2} \int_V d^d r' f_s \nabla_{\mathbf{R}} (f_s \phi) + \frac{q}{(1+q)^2} \frac{\tau}{d\gamma^2} \int_V d^d r' \phi f_s \nabla_{\mathbf{R}} f_s \\ & - \frac{1}{(1+q)^2} \frac{\tau}{d\gamma^2} \frac{q(1+q)\tau k/\gamma}{q + (1+q)\tau k/\gamma} \int_V d^d r' \phi f_s \mathbf{A} \cdot \nabla_{\mathbf{R}} f_s. \end{aligned} \quad (6.51)$$

Next we consider two cases for the potential: First, a rigid bond modeled as a harmonic spring with infinite spring constant and a nonzero rest length. Second, a harmonic spring with zero rest length.

### Rigid Bond

If the force is infinitely strong, that is  $k \rightarrow \infty$ ,

$$\lim_{k \rightarrow \infty} \frac{q(1+q)\tau k/\gamma}{q + (1+q)\tau k/\gamma} = q. \quad (6.52)$$

Furthermore, we can approximate  $\phi(\mathbf{R}, \mathbf{r}', t) \approx \rho(\mathbf{R}, t) \delta(r' - l_0) l_0^{1-d} / \Omega_d$ , because  $r' \approx l_0$  as  $k \rightarrow \infty$ , and the deviation from a uniform distribution on a sphere (or circle for  $d = 2$ ) is proportional to gradients of the swim force and therefore contributes to the flux terms of the order  $\sim \mathcal{O}(\nabla_{\mathbf{R}}^2)$ . With this approximation the first two integrals in Eq. 6.51 become

$$\begin{aligned} & -\frac{1}{(1+q)^2} \frac{\tau}{d\gamma^2} \int_V d^d r' f_s \nabla_{\mathbf{R}} (f_s \phi) + \frac{q}{(1+q)^2} \frac{\tau}{d\gamma^2} \int_V d^d r' \phi f_s \nabla_{\mathbf{R}} f_s \\ = & -\frac{1}{(1+q)^2} \frac{\tau}{d\gamma^2} \left( f_s^2 \nabla_{\mathbf{R}} \rho - q\rho \frac{1}{2} \nabla_{\mathbf{R}} f_s^2 \right), \end{aligned} \quad (6.53)$$

where the swim force has been taken out of the integral because  $f_s = f_s(\mathbf{r}) = f_s(\mathbf{R} + \mathbf{r}'q/(1+q)) = f_s(\mathbf{R}) + \mathcal{O}(\nabla_{\mathbf{R}} f_s)$ . The last integral in Eq.

6.51 becomes

$$\begin{aligned}
& -\frac{q}{(1+q)^2} \frac{\tau}{d\gamma^2} \int_V d^d r' \phi f_s \mathbf{A} \cdot \nabla_{\mathbf{R}} f_s \\
&= -\frac{q}{(1+q)^2} \frac{\tau}{2d\gamma^2} \rho f_s (\nabla_{\mathbf{R}} f_s) \cdot \int_V d^d r' \frac{r'^{1-d}}{\Omega_d} \delta(r' - l_0) \mathbf{R}, \\
&= -\frac{q}{(1+q)^2} \frac{\tau}{d\gamma^2} \rho f_s (\nabla_{\mathbf{R}} f_s) \cdot \int d\Omega \frac{\hat{\mathbf{r}}'(\Omega) \hat{\mathbf{r}}'(\Omega)}{\Omega_d}, \\
&= -\frac{q}{(1+q)^2} \frac{\tau}{d\gamma^2} \rho \frac{1}{2d} \nabla_{\mathbf{R}} f_s^2, \tag{6.54}
\end{aligned}$$

where we used  $\int d\Omega_d \hat{\mathbf{r}}'(\Omega) \hat{\mathbf{r}}'(\Omega) = \Omega_d \mathbf{1}/d$ . With this, we find

$$J_\sigma = -\frac{1}{(1+q)^2} \frac{\tau}{d\gamma^2} f_s^2(\mathbf{R}) \nabla_{\mathbf{R}} \rho - \frac{\epsilon}{(1+q)^2} \frac{\tau}{d\gamma^2} \rho \frac{1}{2} \nabla_{\mathbf{R}} f_s^2(\mathbf{R}), \tag{6.55}$$

where

$$\epsilon = 1 - q \frac{d-1}{d}. \tag{6.56}$$

The total flux is

$$\begin{aligned}
J &= J_D + J_\sigma, \\
&= -\frac{1}{1+q} \frac{T}{\gamma} \nabla_{\mathbf{R}} \rho - \frac{1}{(1+q)^2} \frac{\tau}{d\gamma^2} f_s^2(\mathbf{R}) \nabla_{\mathbf{R}} \rho \\
&\quad - \frac{\epsilon}{(1+q)^2} \frac{\tau}{d\gamma^2} \rho \frac{1}{2} \nabla_{\mathbf{R}} f_s^2(\mathbf{R}), \\
&= \mathbf{V}(\mathbf{R}) \rho - D(\mathbf{R}) \nabla_{\mathbf{R}} \rho, \tag{6.57}
\end{aligned}$$

where

$$D(\mathbf{R}) = \frac{1}{1+q} \frac{T}{\gamma} + \frac{1}{(1+q)^2} \frac{\tau}{d\gamma^2} f_s^2(\mathbf{R}), \tag{6.58}$$

is the space-dependent diffusion coefficient, and

$$\mathbf{V}(\mathbf{R}) = -\frac{1}{2} \epsilon \frac{1}{(1+q)^2} \frac{\tau}{d\gamma^2} \nabla_{\mathbf{R}} f_s^2(\mathbf{R}), \tag{6.59}$$

$$= -\frac{1}{2} \epsilon \nabla_{\mathbf{R}} D(\mathbf{R}), \tag{6.60}$$

is the drift velocity.

The flux-free steady-state solution for  $\rho$  is

$$\rho \propto \left[ 1 + \frac{1}{1+q} \frac{\tau}{d\gamma T} f_s^2(\mathbf{R}) \right]^{-\frac{1}{2}\epsilon}. \quad (6.61)$$

For  $\epsilon = 0$  the density is flat and independent of the swim-force profile. This happens when  $q$  is equal to

$$q_0 = \frac{d}{d-1} = \begin{cases} 3/2 & \text{for } d = 3, \\ 2 & \text{for } d = 2. \end{cases} \quad (6.62)$$

In the limit of highly mobile cargo, that is  $q \rightarrow 0$ , the density becomes

$$\rho \propto \left[ 1 + \frac{\tau}{d\gamma T} f_s^2(\mathbf{R}) \right]^{-\frac{1}{2}}, \quad (6.63)$$

which is the density of a single active particle in a space dependent swim force [144, 153]

In the limit of high friction cargo ( $q \rightarrow \infty$ ) the density becomes

$$\rho \propto \exp \left[ \frac{d-1}{2d} \frac{\tau}{d\gamma T} f_s^2(\mathbf{R}) \right]. \quad (6.64)$$

Whether the drift velocity (Eq. 6.60) is up or down the swim force gradient, depends on the sign of  $\epsilon$ : when  $\epsilon > 0$  ( $q < d/(d-1)$ ) the drift velocity is down the swim force gradient, which corresponds to antichemotaxis; when  $\epsilon < 0$  ( $q > d/(d-1)$ ) the drift velocity is up the swim force gradient, which corresponds to chemotaxis. For the infinitely strong potential with nonzero rest length,  $\epsilon = 0$  for  $q = d/d-1$ , and decreases with increasing  $q$ , so with increasing friction of the cargo, the chemotactic behaviour increases. The maximum drift velocity is obtained for

$$q_{max} = \frac{3d-1}{d-1} = \begin{cases} 5 & \text{for } d = 2, \\ 4 & \text{for } d = 3. \end{cases} \quad (6.65)$$

### Harmonic Force With Zero Rest Length

We are interested in the range where the separation between the two particles is small compared to the gradients of the swim force. Because of this, for the first two integral in Eq. 6.51, we can use  $\phi(\mathbf{R}, \mathbf{r}', t) \approx \rho(\mathbf{R}, t) \delta^{(3)}(\mathbf{r}')$ .



This, together with  $A(l_0 = 0) = \mathbf{1}$ , gives

$$J_\sigma = -\frac{1}{(1+q)^2} \frac{\tau}{d\gamma^2} f_s^2(\mathbf{R}) \nabla_{\mathbf{R}} \rho - \frac{\epsilon}{(1+q)^2} \frac{\tau}{d\gamma^2} \rho \frac{1}{2} \nabla_{\mathbf{R}} f_s^2(\mathbf{R}), \quad (6.66)$$

where

$$\epsilon = 1 - \frac{q^2}{q + (1+q) \frac{\tau k}{\gamma}}. \quad (6.67)$$

The total flux and steady-state density are the same as for the rigid bond (Eq. 6.57 and Eq. 6.61), but with  $\epsilon$  given by the previous equation. Note that in the limit  $k \rightarrow \infty$ ,  $\epsilon = 1$ , and the dimer behaves like a single active particle with a increased friction constant. The  $k = 0$  limit cannot be captured by the theory, as it violates the assumption that the separation between the two particles is small compared to the gradients in the swim force. The value of  $q$  for which the density is flat, obtained by equating  $\epsilon$  to zero, is

$$q_0 = \frac{1}{2} \left( 1 + \frac{\tau k}{\gamma} \right) + \frac{1}{2} \sqrt{\left( 1 + \frac{\tau k}{\gamma} \right)^2 + 4 \frac{\tau k}{\gamma}}. \quad (6.68)$$

In the small  $q$  limit the dimer behaves the same as a single active particle with an increased friction constant, and the steady-state density is the same as for the rigid bond (Eq. 6.63). In the limit of large  $q$ , the steady-state density becomes

$$\rho(\mathbf{R}) \propto \exp \left[ \frac{1}{1 + \frac{\tau k}{\gamma}} \frac{\tau}{2d\gamma T} f_s^2(\mathbf{R}) \right]. \quad (6.69)$$

### 6.A.5 The Born-Oppenheimer Approximation

Here we derive the steady-state density in the limit  $q \rightarrow \infty$ . Only the derivation for the dimer with a rigid bond is shown; the derivation for the harmonic potential is similar. In this limit, the dynamics of the cargo particle are much slower than the dynamics of the active particle. Due to this separation of time scales, we can use a Born-Oppenheimer approximation [222]. In this approximation, we calculate the average force that the active particle exerts on the passive cargo particle that is fixed at the origin. To be more precise, we start by calculating the average force on the active particle due to a fixed potential  $U$ . The equations for an active

particle in a potential are

$$\partial_t \mathbf{r} = \frac{1}{\gamma} \mathbf{F} + f_s(\mathbf{r}) \mathbf{n} + \sqrt{2T/\gamma} \boldsymbol{\zeta}, \quad (6.70)$$

$$\partial_t \mathbf{n} = \sqrt{2D_r} \mathbf{n} \times \boldsymbol{\eta} + \text{tumbling}, \quad (6.71)$$

where  $\mathbf{F} = -\nabla_1 U(\mathbf{r})$  with  $U(\mathbf{r}) = \frac{1}{2}k(r_1 - l_0)^2$ . The corresponding FPE is

$$\begin{aligned} \partial_t W(\mathbf{r}, \mathbf{n}, t) = & -\nabla_1 \cdot \left[ \frac{1}{\gamma} \mathbf{F} W - \frac{T}{\gamma} \nabla_1 W \right] - \nabla_1 \cdot \left[ \frac{1}{\gamma} f_s \mathbf{n} W \right] \\ & + D_r \mathcal{R}^2 W - \alpha W + \alpha \phi, \end{aligned} \quad (6.72)$$

where the last two terms account for the tumbling and

$$\phi(\mathbf{r}, t) = \int d\Omega_d W(\mathbf{r}, \mathbf{p}(\Omega_d), t). \quad (6.73)$$

The probability density  $W$  can be expanded in the same way is  $P(t)$ :

$$W(t) = \phi + \boldsymbol{\sigma} \cdot \mathbf{n} + \boldsymbol{\omega} : (\mathbf{n}\mathbf{n} - \mathbf{1}/d) + \Theta(W(t)), \quad (6.74)$$

where  $\phi$ ,  $\boldsymbol{\sigma}$  and  $\boldsymbol{\omega}$  are functions of  $\mathbf{r}$  and  $t$ . The equation for the coefficients are obtained, as before, by taking scalar products. The equation for  $\phi$  is

$$\partial_t \phi = -\nabla_1 \cdot \mathbf{J}, \quad (6.75)$$

where

$$\mathbf{J} = \frac{1}{\gamma} \mathbf{F} \phi - \frac{T}{\gamma} \nabla_1 \phi + \frac{1}{d\gamma} f_s \boldsymbol{\sigma}. \quad (6.76)$$

The equation for  $\boldsymbol{\sigma}$  is

$$\begin{aligned} \partial_t \boldsymbol{\sigma} = & -\tau^{-1} \boldsymbol{\sigma} - \nabla_1 \cdot \left[ \frac{1}{\gamma} \mathbf{F} \boldsymbol{\sigma} - \frac{T}{\gamma} \nabla_1 \boldsymbol{\sigma} \right] \\ & - \nabla_1 \cdot \left[ \frac{1}{\gamma} f_s \phi \right] - \nabla_1 \cdot \left[ \frac{1}{\gamma} f_s \boldsymbol{\omega} \right]. \end{aligned} \quad (6.77)$$

The average force on the active particle due to the potential is

$$\mathbf{F}_{avg} = \int d^d r \mathbf{F}(\mathbf{r}) \phi(\mathbf{r}), \quad (6.78)$$

where  $\phi$  is the steady-state density. In steady state, the flux is zero, and

Eq. 6.76 can be used to rewrite the expression for the average force:

$$\mathbf{F}_{avg} = \int d^d r T \nabla_1 \phi - \int d^d r \gamma \frac{1}{d\gamma} f_s \sigma. \quad (6.79)$$

The first integral is zero because  $\phi(r = \infty) = 0$ , which shows that thermal diffusion does not contribute to the average force. In the second integral,  $\sigma$  can be replaced by the expression in Eq. 6.77 with  $\partial_t \sigma = 0$ . This gives

$$\begin{aligned} \mathbf{F}_{avg} &= \frac{1}{d\gamma} \int d^d r f_s \tau \nabla_1 (f_s \phi) + \frac{1}{d\gamma} \int d^d r f_s \tau \nabla_1 \cdot (\mathbf{F} \sigma) \\ &\quad - \frac{1}{d\gamma} T \int d^d r f_s \tau \nabla_1^2 \sigma + \frac{1}{d\gamma} \int d^d r f_s \tau \nabla_1 \cdot \boldsymbol{\omega}. \end{aligned} \quad (6.80)$$

The third and fourth integrals are second order in  $\nabla_1$  and can be neglected. This can be seen by integrating by parts twice (there is also a  $\nabla_1$  in  $\boldsymbol{\omega}$ ). For the first two integrals we use integration by parts. This gives

$$\mathbf{F}_{avg} = -\frac{\tau}{d\gamma} \int d^d r \phi f_s \nabla_1 f_s - \frac{\tau}{d\gamma} \int d^d r \sigma \mathbf{F} \cdot \nabla_1 f_s, \quad (6.81)$$

$$= -\frac{\tau}{d\gamma} \int d^d r \phi f_s \nabla_1 f_s - \frac{\tau}{d\gamma} I, \quad (6.82)$$

where

$$I \equiv \int d^d r \sigma \mathbf{F} \cdot \nabla_1 f_s, \quad (6.83)$$

$$= -\frac{\tau}{\gamma} \int d^d r \mathbf{F} \cdot (\nabla_1 f_s) [\nabla_1 \cdot (\mathbf{F} \sigma) + \nabla_1 (f_s \phi)], \quad (6.84)$$

$$= \frac{\tau}{\gamma} \int d^d r [\sigma \mathbf{F} + f_s \phi \mathbf{1}] \cdot \nabla_1 (\mathbf{F} \cdot \nabla_1 f_s), \quad (6.85)$$

where in the second line we ignored terms  $\mathcal{O}(\nabla_1^2 f_s, (\nabla_1 f_s)^2)$ , and used integration by parts to go to the last line. Next we use again that

$$\nabla_1 (\mathbf{F} \cdot \nabla_1 f_s) = (\nabla_1 \mathbf{F}) \cdot \nabla_1 f_s + \mathcal{O}(\nabla_1^2 f_s), \quad (6.86)$$

and

$$\nabla_1 \mathbf{F} = -k \nabla_1 [(r - l_0) \hat{\mathbf{r}}_1] = -k \mathbf{A}, \quad (6.87)$$

where  $\mathbf{A} \equiv \hat{\mathbf{r}}_1 \hat{\mathbf{r}}_1 + \left(1 - \frac{l_0}{r_1}\right) (\mathbf{1} - \hat{\mathbf{r}}_1 \hat{\mathbf{r}}_1)$ ,  $r_1 = |\mathbf{r}_1|$ , and  $\hat{\mathbf{r}}_1 = \mathbf{r}_1/r_1$ . With this  $I$  becomes

$$I = -\frac{\tau k}{\gamma} \int d^d r \phi f_s \mathbf{A} \cdot \nabla_1 f_s - \frac{\tau k}{\gamma} \int d^d r \sigma \mathbf{F} \cdot f_s, \quad (6.88)$$

$$= -\frac{\tau k}{\gamma} \int d^d r \phi f_s \mathbf{A} \cdot \nabla_1 f_s - \frac{\tau k}{\gamma} I, \quad (6.89)$$

$$= -\frac{\tau k/\gamma}{1 + \tau k/\gamma} \int d^d r \phi f_s \mathbf{A} \cdot \nabla_1 f_s, \quad (6.90)$$

where we used  $\mathbf{F} \cdot \mathbf{A} = \mathbf{F}$ .

The average force then becomes

$$\mathbf{F}_{avg} = -\frac{\tau}{d\gamma} \int d^d r \phi f_s \nabla_1 f_s + \frac{\tau k/\gamma}{1 + \tau k/\gamma} \frac{\tau}{d\gamma} \int d^d r \phi f_s \mathbf{A} \cdot \nabla_1 f_s. \quad (6.91)$$

For an infinitely stiff potential  $k \rightarrow \infty$ , and

$$\lim_{k \rightarrow \infty} \frac{\tau k/\gamma}{1 + \tau k/\gamma} = 1, \quad (6.92)$$

and we can approximate  $\phi(\mathbf{r}) \approx \frac{1}{\Omega_d} r_1^{1-d} \delta(r_1 - l_0)$ , because the deviation from a uniform distribution is proportional to gradients in the swim force, so it contributes to the second order term in the average force. Furthermore, if gradients in the swim force are small compared to  $r$ , the terms with swim force can be taken out of the integral, as the error is  $\sim \mathcal{O}(\nabla_{\mathbf{R}})$ . In this limit, the average force becomes

$$\begin{aligned} \mathbf{F}_{avg} &= -\frac{\tau}{2d\gamma} \left[ \nabla_1 f_s^2 \right]_{r_1=0} \int d^d r \phi + \frac{\tau}{2d\gamma} \left[ \nabla_1 f_s^2 \right]_{r_1=0} \cdot \int d\Omega_d \frac{1}{\Omega_d} \hat{\mathbf{r}}_1 \hat{\mathbf{r}}_1, \\ &= -\frac{d-1}{d} \frac{\tau}{2d\gamma} \left[ \nabla_1 f_s^2 \right]_{r_1=0}, \end{aligned} \quad (6.93)$$

where we used  $\int d\Omega_d \hat{\mathbf{r}}_1 \hat{\mathbf{r}}_1 = \mathbf{1}\Omega_d/d$ . Note that the average force on the cargo particle is  $-\mathbf{F}_{avg}$ .

Now consider the case where the position of the passive cargo particle is not fixed to the origin, but it moves slowly compared to the active particle. Then, if the cargo particle is at position  $\mathbf{r}_2$ , it experiences an effective force

$$\mathbf{F}_{eff} = \frac{d-1}{d} \frac{\tau}{2d\gamma} \nabla_2 f_s^2(\mathbf{r}_2), \quad (6.94)$$

which is minus  $\mathbf{F}_{avg}$  with the origin shifted to the location of the cargo particle. The equation of motion of a passive Brownian particle with friction  $q\gamma$  diffusing in a force field  $\mathbf{F}_{eff}$  is

$$\partial_t \mathbf{r}_2 = \frac{1}{q\gamma} \mathbf{F}_{eff} + \sqrt{2T/q\gamma\chi}. \quad (6.95)$$

The corresponding FPE is

$$\partial_t \rho(\mathbf{r}_2, t) = -\nabla_2 \cdot \mathbf{J}, \quad (6.96)$$

$$\mathbf{J} = \frac{1}{q\gamma} \mathbf{F}_{eff} \rho - \frac{T}{q\gamma} \nabla_2 \rho. \quad (6.97)$$

Equating the flux to zero gives the steady-state density distribution:

$$\rho(\mathbf{r}_2) \propto \exp \left[ \frac{d-1}{d} \frac{\tau}{2d\gamma T} f_s^2(\mathbf{r}_2) \right], \quad (6.98)$$

which is the same as Eq. 6.64. Note that to calculate the effective force (Eq. 6.94) and the flux (Eq. 6.97) in this limit it is not necessary to calculate the steady-state density of an active particle in a fixed potential, which is a difficult problem on its own [145, 148].

### 6.A.6 Average Position of the Dimer

In this section we show the derivation of the average position of the dimer in a box with length  $L$ . This is the theory shown in Fig. 3 in the main text. The simulations were done with a Weeks-Chandler-Anderson potential [219] for the walls. Here we ignore the details of the interaction of the dimer with the walls and model the walls as zero-flux boundary condition at the walls. The average position of the dimer in the box is

$$\bar{R} = \int_{-L/2}^{L/2} dR R \rho(R, t). \quad (6.99)$$

The time derivative of this is

$$\partial_t \bar{R} = - \int_{-L/2}^{L/2} dR R \partial_R J(R, t), \quad (6.100)$$

$$= \int_{-L/2}^{L/2} dR J(R, t), \quad (6.101)$$

where we used the zero-flux condition at the boundaries. If the system starts with a homogeneous bulk density  $\rho_b$ , and we substitute Eq. 6.57 for the flux, the time derivative at  $t = 0$  becomes

$$\partial_t \bar{R}|_{t=0} = -\frac{1}{2} \epsilon \rho_b \int_{-L/2}^{L/2} dR \partial_R D, \quad (6.102)$$

$$= -\frac{1}{2} \frac{\epsilon}{(1+q)^2} \frac{\tau}{d\gamma^2} \rho_b \int_{-L/2}^{L/2} dR \partial_R f_s^2. \quad (6.103)$$

The most important feature of this equation is

$$\partial_t \bar{R}|_{t=0} \propto \frac{\epsilon}{(1+q)^2}, \quad (6.104)$$

because it indicates the dependence of  $\partial_t \bar{R}|_{t=0}$  on  $q$  independent of the swim-force profile or the geometry of the container.

For the case in Fig. 3 in the main text  $f_s(R) = f_0 \sqrt{R + L/2}$ , with  $f_0 = \sqrt{6}$ . With this we get,

$$\partial_t \bar{R}|_{t=0} = -\frac{1}{2} \frac{\epsilon}{(1+q)^2} \frac{\tau}{d\gamma^2} f_0^2 \rho_b L, \quad (6.105)$$

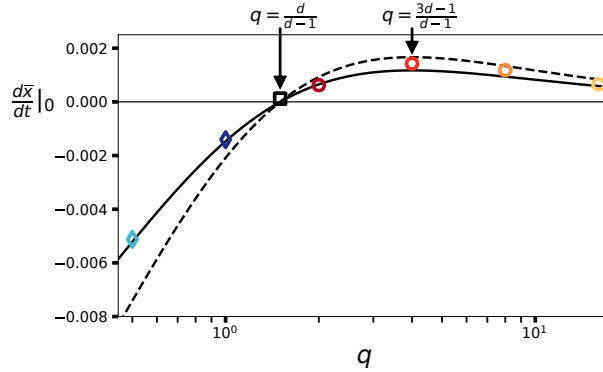
which is what is shown in Fig. 3 in the main text with  $\rho_b = 1/L$  and  $f_0 = \sqrt{6}$ . In Fig. 6.8 we show a comparison between the theoretical prediction (Eq. 6.105) and a fit of 6.104 to simulation data.

### 6.A.7 Comparison to Active Temperature

Because Brownian particles coupled to different thermostats have shown interesting behaviour [239–242], we consider here a modification of the active-passive dimer model where the dimer is made up from a passive particle and a particle with a space-dependent temperature. We do not consider this an approximate model for the active-passive dimer, where the activity is approximated by an effective temperature, as this concept, although useful in some contexts, is not well defined in general for far-from-equilibrium active-matter systems [243, 244]. Models where particles have different temperatures have recently received much attention [239–242].

The steady-state density of a single passive Brownian particle with a

**Figure 6.8:** The system setup is the same as Fig. 2 in the main text. The data (symbols) and theoretical prediction (dashed line, Eq. 6.105) for the initial change in the average position of the dimer in the box. The solid shows Eq. 6.104 with the prefactor fitted to the data (as in Fig. 3 of the main text). Even though there is a discrepancy between the theoretical prediction and the simulation results for small values of  $q$ , the dependence on  $q$  is accurately captured by the theory, as is indicated by the fit of Eq. 6.104 (solid line). The mismatch between the theoretical prediction and the data is likely due to boundary effects in the simulation, which are ignored in the theory.



space-dependent temperature is [27]

$$\rho(\mathbf{r}_1) \propto \frac{1}{T(\mathbf{r}_1)}, \quad (6.106)$$

see Section 1.3.2 Eq. 1.68. If a high temperature corresponds to a high activity, this corresponds to antichemotactic behaviour. If such a particle is bound to a heavy cargo particle, does it, as the active-passive dimer, become chemotactic?

If the persistence length of the active particle  $\delta = \tau f_s / \gamma$  is constant all the integration by parts for  $\nabla_{r'}$  in Eq. 6.41 yield zero, and up to first order in the gradient,  $J_\sigma$  becomes

$$J_\sigma = -\frac{1}{(1+q)^2} \frac{1}{d\gamma^2} \int_V d^d r' \tau f_s \nabla_{\mathbf{R}}(f_s \phi). \quad (6.107)$$

Using the same approximations as before yields for the total flux the same as Eq. 6.57 but with  $\epsilon = 1$ . The density of the dimer in this case is just that of a single active particle with friction  $(1+q)\gamma$ . So the only effect of increasing  $q$  is that it increases the friction of the dimer, and there is no  $q$  for which the dimer is chemotactic. Note that this holds for any  $\delta$ , not just in the "active temperature" limit.

This result can also be obtained from the Born-Oppenheimer approach. In this case all the integrals in Eq. 6.80 yield zero (this can be obtained

by integrating by parts), and the average force is zero. So again, this shows that if the persistence length is constant the dimer acts as a single active particle with increased friction and does not exhibit chemotactic behaviour for any  $q$ .

In the limit  $\delta \rightarrow 0$ , a self-propelled particle with space-dependent swim force but constant persistence length becomes equivalent to a passive Brownian particle with temperature  $T_{eff} = \frac{\tau f_s^2}{d\gamma} + T$  [35]. Therefore, the previous consideration shows that a dimer build from a passive Brownian particle in a temperature gradient attached to a passive cargo particle with a spatially independent temperature does not exhibit chemotactic behaviour for any value of  $q$ .

### 6.A.8 Run-and-Tumble Dimer in One Dimension

Because ABPs are not defined in one dimension, and RTPs in one dimension have a discrete orientation (either in the positive or in the negative direction), we show the derivation of the flux of the collective coordinate for this case separately. Because a fixed bond length in one dimension means that there is no internal degree of freedom, we only consider the case of a harmonic potential with different spring constants between the active and passive particle. The equations of motion are

$$\partial_t x_1 = \frac{1}{\gamma} F + \frac{1}{\gamma} f_s(x_1) n + \sqrt{2T/\gamma} \xi_1 \quad (6.108)$$

$$\partial_t x_2 = -\frac{1}{q\gamma} F + \sqrt{2T/\gamma} \xi_2, \quad (6.109)$$

where  $x_1$  is the coordinate of the active particle with friction constant  $\gamma$  and swim force  $f_s$ ,  $x_2$  is the coordinate of the passive cargo particle with friction constant  $q\gamma$ ,  $T$  is the temperature in units such that the Boltzmann constant is unity, and  $\xi_1$  and  $\xi_2$  are white noise with zero mean and auto-correlation  $\langle \xi_1(t) \xi_1(t') \rangle = \langle \xi_2(t) \xi_2(t') \rangle = \delta(t - t')$ . The orientation of the active particle is  $n \in \{+1, -1\}$ , which points either in the positive (right moving) or the negative (left moving) direction. With rate  $\alpha$  the active particle randomizes its orientation (so it changes direction with rate  $\alpha/2$ ). The force of the RTP on the passive cargo particle is  $\mathbf{F} = -\partial_1 U$ , where



$U = -\frac{1}{2}k(x_1 - x_2)^2$ . The corresponding FPE equation is [228]

$$\begin{aligned} \partial_t \phi_R(t) = & -\partial_1 \left[ v\phi_R(t) + \frac{1}{\gamma}F\phi_R(t) - \frac{T}{\gamma}\partial_1\phi_R(t) \right] \\ & -\partial_2 \left[ -\frac{1}{q\gamma}F\phi_R(t) - \frac{T}{q\gamma}\partial_2\phi_R(t) \right] \\ & -\frac{1}{2}\alpha\phi_R(t) + \frac{1}{2}\alpha\phi_L(t), \end{aligned} \quad (6.110)$$

$$\begin{aligned} \partial_t \phi_L(t) = & -\partial_1 \left[ -v\phi_L(t) + \frac{1}{\gamma}F\phi_L(t) - \frac{T}{\gamma}\partial_1\phi_L(t) \right] \\ & -\partial_2 \left[ -\frac{1}{q\gamma}F\phi_L(t) - \frac{T}{q\gamma}\partial_2\phi_L(t) \right] \\ & +\frac{1}{2}\alpha\phi_R(t) - \frac{1}{2}\alpha\phi_L(t), \end{aligned} \quad (6.111)$$

where  $\phi_R(t) = \phi_R(x_1, x_2, t)$  ( $\phi_L(t) = \phi_L(x_1, x_2, t)$ ) is the probability density of a right (left) moving RTP at  $x_1$  and a cargo particle at  $x_2$ .

Next we perform the same steps as in the two or three dimensional case. First we transform the equations using

$$\phi(t) = \phi_R(t) + \phi_L(t), \quad (6.112)$$

$$\sigma(t) = \phi_R(t) - \phi_L(t), \quad (6.113)$$

where  $\phi(t) = \phi(x_1, x_2, t)$  is the density and  $\sigma(t) = \sigma(x_1, x_2, t)$  is the excess of dimers with a right moving RTP. The equation density is

$$\partial_t \phi(t) = -\partial_1 \left[ v\sigma(t) + \frac{1}{\gamma}F\phi(t) - \frac{T}{\gamma}\partial_1\phi \right] - \partial_2 \left[ -\frac{1}{q\gamma}F\phi(t) - \frac{T}{q\gamma}\partial_2\phi \right], \quad (6.114)$$

and

$$\begin{aligned} \partial_t \sigma(t) = & -\alpha\sigma(t) - \partial_1 \left[ v\phi(t) + \frac{1}{\gamma}F\sigma(t) - \frac{T}{\gamma}\partial_1\sigma \right] \\ & -\partial_2 \left[ -\frac{1}{q\gamma}F\sigma(t) - \frac{T}{q\gamma}\partial_2\sigma \right]. \end{aligned} \quad (6.115)$$

We use the same coordinate transformation as before:

$$X = \frac{1}{1+q}x_1 + \frac{q}{1+q}x_2 \quad x' = x_1 - x_2. \quad (6.116)$$

In these coordinates, the equations for  $\phi$  and  $\sigma$  become

$$\begin{aligned} \partial_t \phi(t) = & -\frac{1}{1+q} \frac{1}{\gamma} X [f_s \sigma - TX\phi] \\ & - \frac{1}{\gamma} x' \left[ f_s \sigma + \frac{1+q}{q} F\phi - \frac{1+q}{q} Tx'\phi \right], \end{aligned} \quad (6.117)$$

$$\begin{aligned} \partial_t \sigma(t) = & -\alpha \sigma - \frac{1}{1+q} \frac{1}{\gamma} X [f_s \phi - TX\sigma] \\ & - \frac{1}{\gamma} x' \left[ f_s \phi + \frac{1+q}{q} F\sigma - \frac{1+q}{q} Tx'\sigma \right]. \end{aligned} \quad (6.118)$$

Note that, in contrast with the two or three-dimensional cases (Eqs. 6.29 and 6.30), the set of equations for  $\phi$  and  $\sigma$  is exact and closed.

### 6.A.9 Coarse Graining the RTP Dimer

Because we are interested in the large scale behaviour of the system, we want to know

$$\rho(X, t) = \int dx' \phi(X, x', t), \quad (6.119)$$

which obeys

$$\partial_t \rho = -\partial_X J, \quad (6.120)$$

where  $J = J_D + J_\sigma$ ,

$$J_D = -\frac{1}{1+q} \frac{T}{\gamma} \partial_X \rho \quad (6.121)$$

is the flux due to passive diffusion, and

$$J_\sigma = \frac{1}{1+q} \frac{1}{\gamma} \int dx' f_s \sigma \quad (6.122)$$

is the flux due to the activity. The density obeys a continuity equation (Eq. 6.119), so is locally conserved and relaxes on a time scale of the order  $\sim \mathcal{O}((\partial_X)^{-1})$ . From Eq. 6.117 it follows that  $\sigma$  relaxes on a time scale  $1/\alpha$ . So, as in the three dimensional case,  $\rho$  can be identified as the slow degree of freedom and  $\sigma$  as the fast degree of freedom; one can therefore neglect the time derivative in Eq. 6.118. Derivatives with respect to  $X$  of  $\rho$  and  $\sigma$  are of the same order as  $\partial_X f_s$ , which is small. Derivatives

with respect to  $x'$  of  $\rho$  and  $\sigma$  are not small, but they can be turned into derivatives with respect to  $X$  by integration by parts and using  $\partial_{x'} f_s = \partial_{x'} f_s(X + \frac{q}{1+q}x') = \frac{q}{1+q} \partial_X f_s$ . Because derivatives with respect to  $X$  are small, we neglect terms of the order  $\mathcal{O}(\partial_X^3)$  in Eq. 6.119, which means we can neglect terms of the order  $\mathcal{O}(\partial_X^2)$  in Eq. 6.122.

Using Eq. 6.118 and  $\partial_t \sigma \approx 0$  to replace  $\sigma$  in Eq. 6.122, we find

$$\begin{aligned} J_\sigma &= \frac{1}{(1+q)^2} \frac{T}{\gamma^2 \alpha} \int dx' f_s \partial_X^2 \sigma - \frac{1}{(1+q)^2} \frac{1}{\gamma^2 \alpha} \int dx' f_s \partial_X (f_s \phi) \\ &\quad - \frac{1}{1+q} \frac{1}{\gamma^2 \alpha} \int dx' f_s \partial_{x'} (f_s \phi) - \frac{1}{q} \frac{1}{\gamma^2 \alpha} \int dx' f_s \partial_{x'} (F \sigma) \\ &\quad - \frac{1}{q} \frac{T}{\gamma^2 \alpha} \int dx' f_s \partial_{x'}^2 \sigma. \end{aligned} \quad (6.123)$$

The first integral can be ignored because it is second order in derivatives with respect to  $X$ . The same holds for the last integral because one can integrate by parts twice. For the second and third integral we use integration by parts. This gives

$$\begin{aligned} J_\sigma &= - \frac{1}{(1+q)^2} \frac{1}{\gamma^2 \alpha} \int dx' f_s \partial_X (f_s \phi) + \frac{q}{(1+q)^2} \frac{1}{\gamma^2 \alpha} \int dx' \phi f_s \partial_X f_s \\ &\quad + \frac{1}{1+q} \frac{1}{\gamma^2 \alpha} I, \end{aligned} \quad (6.124)$$

where

$$I \equiv \int dx' \sigma F \partial_X f_s. \quad (6.125)$$

Using Eq. 6.118 again to replace  $\sigma$  and ignoring second order derivatives with respect to  $X$ , we find

$$I = - \frac{1}{\alpha \gamma} \int dx' F (\partial_X f_s) \partial_{x'} \left[ f_s \phi + \frac{1+q}{q} F \sigma \right], \quad (6.126)$$

$$= \frac{1}{\alpha \gamma} \int dx' \partial_{x'} [F (\partial_X f_s)] \left[ f_s \phi + \frac{1+q}{q} F \sigma \right]. \quad (6.127)$$

The force is  $F = -kx'$ , so  $\partial_{x'} [F (\partial_X f_s)] = -k \partial_X f_s + \mathcal{O}(\partial_X^2 f_s)$ . With this,  $I$

becomes

$$\begin{aligned}
I &= -\frac{k}{\alpha\gamma} \int dx' \phi f_s \partial_X f_s - \frac{k}{\alpha\gamma} \frac{1+q}{q} \int dx' \sigma F \partial_X f_s, \\
&= -\frac{k}{\alpha\gamma} \int dx' \phi f_s \partial_X f_s - \frac{k}{\alpha\gamma} \frac{1+q}{q} I, \\
&= -\frac{q^{\frac{k}{\alpha\gamma}}}{q + (1+q)^{\frac{k}{\alpha\gamma}}} \int dx' \phi f_s \partial_X f_s.
\end{aligned} \tag{6.128}$$

With the approximation  $\phi(X, x', t) \approx \rho(X, t) \delta(x')$  and the result for  $I$ ,  $J_\sigma$  becomes

$$J_\sigma = -\frac{1}{(1+q)^2} \frac{1}{\gamma^2 \alpha} f_s^2(X) \partial_X \rho - \frac{1}{(1+q)^2} \frac{1}{\gamma^2 \alpha} \frac{1}{2} \epsilon \rho \partial_X f_s^2(X), \tag{6.129}$$

where

$$\epsilon = 1 - \frac{q^2}{q + (1+q)^{\frac{k}{\gamma\alpha}}}. \tag{6.130}$$

The total flux is

$$J = J_D + J_\sigma = V(X) \rho - D(X) \partial_X \rho, \tag{6.131}$$

where

$$D(X) = \frac{1}{1+q} \frac{T}{\gamma} + \frac{1}{(1+q)^2} \frac{1}{\gamma^2 \alpha} f_s^2(X) \tag{6.132}$$

is the space-dependent diffusion constant, and

$$V(X) = -\frac{1}{2} \epsilon \partial_X D(X) \tag{6.133}$$

is the drift velocity. The zero-flux steady-state density is

$$\rho(X) \propto \left[ 1 + \frac{1}{1+q} \frac{1}{\gamma T \alpha} f_s^2(X) \right]^{-\frac{1}{2} \epsilon}. \tag{6.134}$$

Note that this is the same as the three dimensional case (Eq. 6.61 and  $\epsilon$  shown in Eq. 6.67) with  $d = 1$  and  $\tau = 1/\alpha$ , the autocorrelation time of the orientation of a one-dimensional RTP.

### 6.A.10 Numerical Solution

Equations 6.117 and 6.118 can be solved numerically by a first order discretization of the space and time coordinates. Because these equations are exact, the numerical solution can be used to test the theoretical prediction for the steady-state density distribution Eq. 6.134, as well as explore interparticle potentials for which there is no theoretical prediction.

# Chapter 7

## Active Colloidal Molecules

This chapter contains results which have been published in ref. [185].  
Reprinted (adapted) with permission from H.D. Vuijk, S. Klempahn, H. Merlitz, J.-U. Sommer, and A. Sharma. *Physical Review E* 106, 014617, 2022. Copyright (2018) by the American Physical Society.

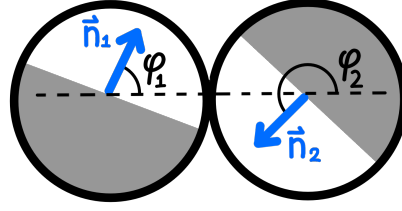
In this chapter, we consider a rigid assembly of two active Brownian particles (ABPs), forming a so called active colloidal dimer, in a gradient of activity. We show analytically that depending on the relative orientation of the two particles the active dimer accumulates in regions of either high or low activity, corresponding to, respectively, chemotaxis and antichemotaxis. Certain active dimers show both chemotactic and antichemotactic behavior, depending on the strength of the activity. Our coarse-grained Fokker-Planck approach yields an effective potential, which we use to construct a nonequilibrium phase diagram that classifies the dimers according to their tactic behavior. Moreover, we show that for certain dimers a higher persistence of the motion is achieved similar to the effect of a steering wheel in macroscopic devices. The results of this chapter could be useful for designing autonomous active colloidal structures which adjust their motion depending on the local activity gradients, without any feedback mechanism [116, 118, 119] or time-dependent activity [211, 225, 245–247].

Colloidal sized active Brownian particles (APBs) can be assembled into active colloidal molecules [125], for example, dimers and tadpole shaped particles [128, 129, 248], active polymers [127], or more complex structures [249, 250]. From a theoretical perspective, active particles connected in a chain to form polymers, have recently received much attention [185, 227, 251–257]. In contrast to Chapter 6, here we consider an active dimer where the orientation of the active particles that constitute the dimer are fixed with respect to the bond vector (see Fig. 7.1), which corresponds to the experimental systems in refs. [128, 129, 248]. In particular, we study the behaviour of active colloidal dimers with a space dependent swim force, and how the orientation of the active particles relative to the bond vector affects the dimer's behaviour, as proposed in Ref. [258]. With the recent advances in fabrication techniques, colloidal particles can now be assembled into desired structures [259–264]. Since structure determines the functionality of the active dimer our study could be important for the design of active matter for environmental and medical applications where, generally, one has little or no control over the external gradients [92].

## 7.1 The Model

We consider a two dimensional model consisting of two ABPs [90] attached to each other forming an active colloidal dimer, see Fig. 7.1. The motion of the dimer is governed by the following stochastic differential

**Figure 7.1:** A sketch of an active colloidal dimer consisting of two active Janus particles. The orientation vectors  $\mathbf{n}_1$  and  $\mathbf{n}_2$  of the active particles are shown in blue. The angles  $\phi_1$  and  $\phi_2$  are the angles between  $\mathbf{n}_1$  and  $\mathbf{n}_2$  and the vector connecting the centers of the particle.



equations (SDEs):

$$\partial_t \mathbf{r}_1 = 4\mathbf{F} + 4f_s(\mathbf{r}_1)\mathbf{n}_1 + 2\boldsymbol{\zeta}_1, \quad (7.1)$$

$$\partial_t \mathbf{r}_2 = -4\mathbf{F} + 4f_s(\mathbf{r}_2)\mathbf{n}_2 + 2\boldsymbol{\zeta}_2, \quad (7.2)$$

where  $\mathbf{r}_1$  and  $\mathbf{r}_2$  are the positions of particle 1 and 2, the vector  $\boldsymbol{\zeta}_1$  and  $\boldsymbol{\zeta}_2$  are random Gaussian vectors with  $\langle \boldsymbol{\zeta}_1(t) \rangle = \langle \boldsymbol{\zeta}_2(t) \rangle = 0$ ,  $\langle \boldsymbol{\zeta}_1(t)\boldsymbol{\zeta}_1(t') \rangle = \langle \boldsymbol{\zeta}_2(t)\boldsymbol{\zeta}_2(t') \rangle = \mathbf{1}\delta(t-t')$ ,  $f_s(\mathbf{r})$  is the active force at position  $\mathbf{r}$ , and  $\mathbf{n}_1$  ( $\mathbf{n}_2$ ) is the direction of the active force on particle one (two). The force  $\mathbf{F}$  holds the two particles together. In the following we take this force to be strong enough to keep the two particles at a fixed distance  $l$  from each other. Furthermore, this force fixes the orientation of the two ABPs relative to the bond vector. The unit of length and time are such that  $l = 1$  and the diffusion constant of the center-of-mass coordinate of the dimer is unity. The unit of force is  $2T/l$ , where  $T$  is the temperature in units such that the Boltzmann constant is unity. Note that in contrast to other theoretical studies [133, 153, 208, 265], the rotational diffusion constant is not a free parameter, but comes from the translational diffusion of the two particles. Note that, in order to keep our analysis general, we do not take into account the torque on the two active particles due to the activity gradient because this depends on the specific self-propulsion mechanism [266]. However, this torque can be included in the analysis presented here. We ignore the hydrodynamic interaction between the two particles, and their effect on the self-propulsion [93, 267–270] Because the distance between the two particles is constant, the two translational degrees of freedom of the two particles can be transformed to the center-of-mass coordinate of the dimer  $\mathbf{R} = (\mathbf{r}_1 + \mathbf{r}_2)/2$  and  $\theta$ , the angle between the bond vector  $\mathbf{n} = \mathbf{r}_1 - \mathbf{r}_2 = (\cos \theta, \sin \theta)$  and the x-axis. We call the bond vector



$\mathbf{n}$  the orientation of the dimer. The corresponding SDEs are

$$\partial_t \mathbf{R} = 2 [f_s(\mathbf{r}_1) \mathbf{n}_1 + f_s(\mathbf{r}_2) \mathbf{n}_2] + \sqrt{2} \boldsymbol{\zeta}, \quad (7.3)$$

$$\partial_t \theta = -4 \mathbf{n} \cdot \boldsymbol{\epsilon} \cdot [f_s(\mathbf{r}_1) \mathbf{n}_1 - f_s(\mathbf{r}_2) \mathbf{n}_2] + \sqrt{8} \eta, \quad (7.4)$$

where  $\mathbf{r}_1 = \mathbf{R} + \frac{1}{2} \mathbf{n}$ ,  $\mathbf{r}_2 = \mathbf{R} - \frac{1}{2} \mathbf{n}$ ,  $\epsilon_{yx} = -\epsilon_{xy} = 1$ ,  $\epsilon_{xx} = \epsilon_{yy} = 0$ ,  $\boldsymbol{\zeta}$  and  $\eta$  are a random Gaussian vector and number, respectively, with  $\langle \boldsymbol{\zeta}(t) \rangle = 0$ ,  $\langle \boldsymbol{\zeta}(t) \boldsymbol{\zeta}(t') \rangle = \mathbf{1} \delta(t - t')$ , and  $\langle \eta(t) \rangle = 0$ ,  $\langle \eta(t) \eta(t') \rangle = \delta(t - t')$ . The free parameters in this study are the swim force  $f_s(\mathbf{r})$  and the two angles  $\phi_1$  and  $\phi_2$ .

The Fokker-Planck equation (FPE) corresponding to the SDEs 7.3 and 7.4 governs the time evolution of the probability density  $P(\mathbf{R}, \theta, t)$  [235]. We coarse grain this equation by integrating out  $\theta$  and only retain terms up to order  $\sim \mathcal{O}(\nabla^2)$ . This results in an FPE for the probability density of the dimer  $\rho(\mathbf{R}, t) = \frac{1}{2\pi} \int d\theta P(\mathbf{R}, \theta, t)$ . In the following we only consider steady-state properties. From the FPE one can extract the steady-state density  $\rho(\mathbf{R})$ , flux  $\mathbf{J}(\mathbf{R})$  and polarization  $\mathbf{p}(\mathbf{R}) = \rho^{-1}(\mathbf{R}) \int d\theta \mathbf{n} P(\mathbf{R})$ . Details of the coarse graining procedure and the calculation of the steady-state properties are shown in App.7.A.1.

## 7.2 Results and Discussion

Before we discuss the solution to the FPE, we inspect Eqs. 7.3 and 7.4 to understand what kind of behavior one can expect from this system. To do this, we ignore terms  $\sim \mathcal{O}(\nabla^2 f_s)$ , and assume that the swim force only depends on the  $x$  coordinate. Equations 7.3 and 7.4 then become

$$\partial_t x = 2f_s(x) (c_+ n_x - s_+ n_y) - (c_- n_x - s_- n_y) n_x \partial_x f_s(x) + \sqrt{2} \zeta_x \quad (7.5)$$

$$\partial_t y = 2f_s(x) (s_+ n_x + c_+ n_y) - (s_- n_x + c_- n_y) n_x \partial_x f_s(x) + \sqrt{2} \zeta_y \quad (7.6)$$

$$\partial_t \theta = -4s_- f_s(x) - 2s_+ n_x \partial_x f_s(x) + \sqrt{8} \eta, \quad (7.7)$$

where  $x = \mathbf{R} \cdot \hat{\mathbf{e}}_x$ ,  $y = \mathbf{R} \cdot \hat{\mathbf{e}}_y$ ,  $c_{\pm} = \cos(\phi_1) \pm \cos(\phi_2)$ , and  $s_{\pm} = \sin(\phi_1) \pm \sin(\phi_2)$ .

Because of the torque on the orientation of the dimer, that is the  $-4s_- f_s$  term in Eq. 7.7, these dimers are chiral active particles [90, 271], and because of that they are odd diffusive [272], meaning that they have diffusive fluxes perpendicular to density gradients (see App. 7.A.3).

In order to get a better physical understanding of the different contributions to the equations of motion, a few illustrative examples are dis-

cussed. A dimer with  $\phi_1 = \phi_2 = 0$ , shown in the inset of Fig. 7.2 (a), is structurally similar to a single ABP. Accordingly, this dimer accumulates where the swim force is small. Dimers where the two active particles have opposite orientations along the orientation vector are shown in the insets of Fig. 7.2 (b) and (c). These dimers are symmetric under  $n_x \rightarrow -n_x$ . Since the swim-force varies only along the  $x$  coordinate, at any location, a dimer with  $\phi_1 = 0, \phi_2 = \pi$ , experiences a net force towards the region of small swim force (antichemotactic) whereas an dimer with  $\phi_1 = \pi, \phi_2 = 0$  experiences a net force towards the region of large swim force (chemotactic).

A particularly interesting structure is an dimer with  $\phi_1 = \phi_2 = \pi/2$  shown in the inset of Fig. 7.2 (f). In this case, the orientations of the two particles are parallel to each other and perpendicular to the orientation vector. The equations of motion are

$$\partial_t x = -4n_y f_s(x) + \sqrt{2}\tilde{\xi}_x, \quad (7.8)$$

$$\partial_t y = 4n_x f_s(x) + \sqrt{2}\tilde{\xi}_y, \quad (7.9)$$

$$\partial_t \theta = -4n_x \partial_x f_s(x) + \sqrt{8}\eta. \quad (7.10)$$

The first two of these equation are the same as that for a ABP with rotated orientation vector. In the equation of motion of the angle, however, a new feature appears. There is an active torque on the dimer prportional to  $n_x$  and the gradient in the swim force. This torque rotates the dimer, like a steering wheel, in such a way that the orientation vector points in the direction perpendicular to the gradient in the swim force, therefore, this torque stabilizes the dimer such that the active forces point in the direction opposite the gradient in the swim force. Accordingly, this dimer accumulates where the swim force is small.

Dimers in which the orientations of the two active particles have opposite orientations and perpendicular to the orientation vector are shown in the insets of Fig. 7.3 (a) and (b). For  $\phi_1 = \pi/2, \phi_2 = 3\pi/2$ , the equations of motion are

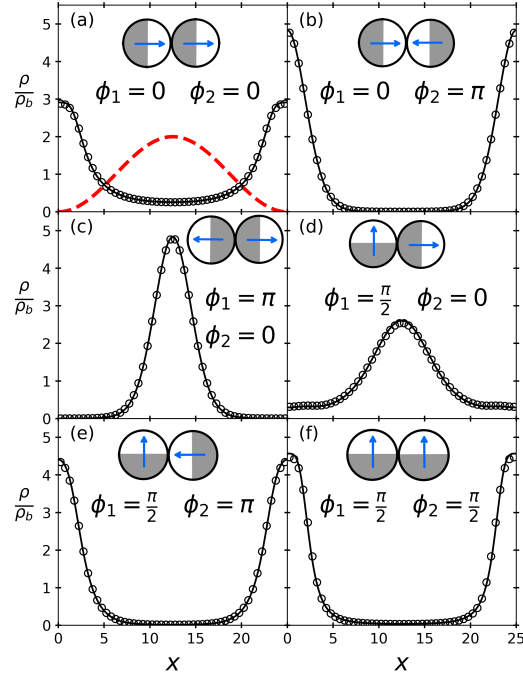
$$\partial_t x = 2n_y n_x \partial_x f_s(x) + \sqrt{2}\tilde{\xi}_x, \quad (7.11)$$

$$\partial_t y = -2n_x^2 \partial_x f_s(x) + \sqrt{2}\tilde{\xi}_y, \quad (7.12)$$

$$\partial_t \theta = -8f_s + \sqrt{8}\eta. \quad (7.13)$$

Two features of these equations are noteworthy. Firstly, there is an active torque acting on the dimer (the  $-8f_s$  part in the equation for the time evolution of the angle). This is equivalent to the active torque in case of an active chiral particle [55, 271, 273]. Secondly, the term  $-n_x^2 \partial_x f_s(x)$  in

**Figure 7.2:** Density for different dimers (see insets) relative to the bulk density  $\rho_b = \int_0^L dx \rho(x)/L$ , where  $L = 25$  is the simulation box with periodic boundary conditions. The orientations of the particles in the dimer are indicated in the figure. The symbols show the simulation of Eqs. 7.3 and 7.4, the solid line show the theoretical prediction (Eq. 7.15), and the red dashed line in (a) shows the shape of the swim-force profile  $f_s(x) = 8[1 + \sin(2\pi x/L + 3\pi/2)]$ . The orientation of the particles in the dimer can be used to control whether the dimer accumulates in regions where  $f_s$  is small (panels a,b, e and f), or in regions where  $f_s$  is large (panels c and d).

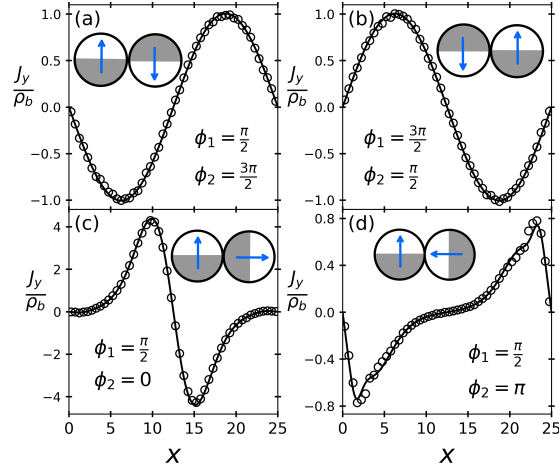


the time evolution equation for the  $y$  coordinate is nonzero on average for a fixed value of  $x$ . Since there is translational invariance in the  $y$  direction, this effective force, remains unbalanced giving rise to stationary fluxes perpendicular to the swim-force and density gradients. Note that since the dimer is symmetric under  $n_x \rightarrow -n_x$ , on average the  $x$  coordinate gets no contribution from the swim-force gradients. Accordingly, this dimer shows no preferential accumulation in a swim-force gradient. The behaviour of a dimer with  $\phi_1 = 3\pi/2, \phi_2 = \pi/2$  (inset of Fig. 7.3 (b)) is similar except that its chirality is reversed.

The structural properties of the dimer, namely net activity proportional to  $f_s$ , force proportional to  $\nabla f_s$ , torque proportional to  $f_s$ , and a torque proportional to  $\nabla f_s$ , are determined by the orientation of the two particles and result in two classes of steady-state behaviour. One could design the dimer in such a way that it preferentially moves towards regions with high or low swim force. Going beyond the examples above, for a generic structure of the dimer, the stationary density distribution can be obtained from the coarse grained Fokker Planck equation by setting the flux along the gradient of swim force to zero (for details of the derivation see App. 7.A.4). This yields

$$\rho(x) \propto \exp(-U), \quad (7.14)$$

**Figure 7.3:** Flux perpendicular to swim-force gradients. The bulk density is  $\rho_b = \int_0^L dx \rho(x)/L$  with  $L = 25$ . These transverse fluxes are reminiscent of, for instance, chemotactic sea urchin sperm swimming in the presence of a chemical source [274]. The swim force is  $f_s(x) = 8 [1 + \sin(2\pi x/L + 3\pi/2)]$  (same as Fig 7.2). The orientations of the particles in the dimer are shown in the figures.



with

$$U = \frac{c}{2d} f_s + \frac{b}{4d} \ln(1 + d f_s^2) + \frac{ad - c}{2d^{3/2}} \text{atan}(\sqrt{d} f_s), \quad (7.15)$$

where  $a = c_-$ ,  $b = c_+^2 + 2s_+^2$ ,  $c = s_-^2 c_- - s_- s_+ c_+$ , and  $d = \frac{1}{2}(2s_-^2 + c_+^2 + s_+^2)$ . Figure 7.2 shows the stationary density distribution of dimers with different structures obtained from simulations of Eqs. 7.3 and 7.4. Depending on the structure, dimers accumulate in the regions where swim force is small or large. The theoretical predictions (Eq. 7.15) are in agreement with the simulations.

The steady-state density distribution obtained from the coarse grained Fokker Planck equation is Boltzmann-like with an effective potential ( $U$ ). However, this does not imply that on this coarse-grained level the dynamics obey detailed balance; there are configurations of the dimer that result in steady-state fluxes in the direction perpendicular to gradients in the swim force (see Fig. 7.3). For instance, a dimer with  $\phi_1 = \pi/2$  and  $\phi_2 = 3\pi/2$  is a chiral particle that rotates clockwise whereas a dimer with  $\phi_1 = 3\pi/2$  and  $\phi_2 = \pi/2$  rotates anticlockwise. While these dimers show no preferential accumulation ( $U = 0$  in Eq. 7.15), the gradient in the swim force gives rise to a net force along the  $y$  direction that gives rise to fluxes  $J_y = -\rho_b \partial_x f_s$  for the clockwise dimer (Fig. 7.3(a)) and  $J_y = \rho_b \partial_x f_s$  for the anticlockwise dimer (Fig. 7.3(b)). In case of a generic dimer structure, for which the stationary distribution is not homogeneous (Fig. 7.3(c-d)), the flux along the  $y$  direction is perpendicular to the density gradient (along  $x$ ). Fluxes perpendicular to the density gradients is a characteristic

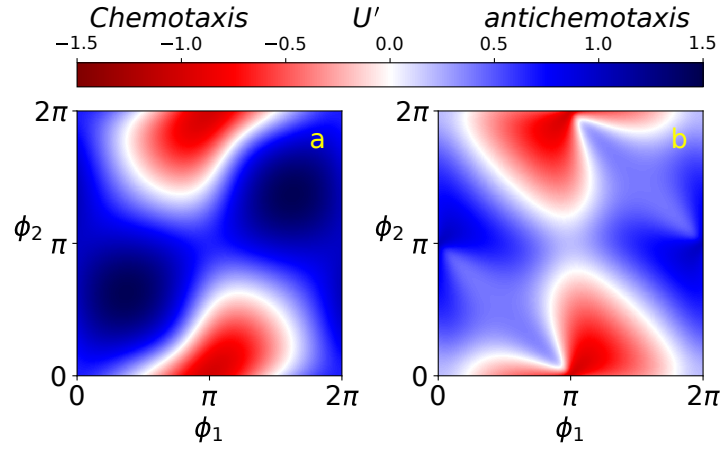
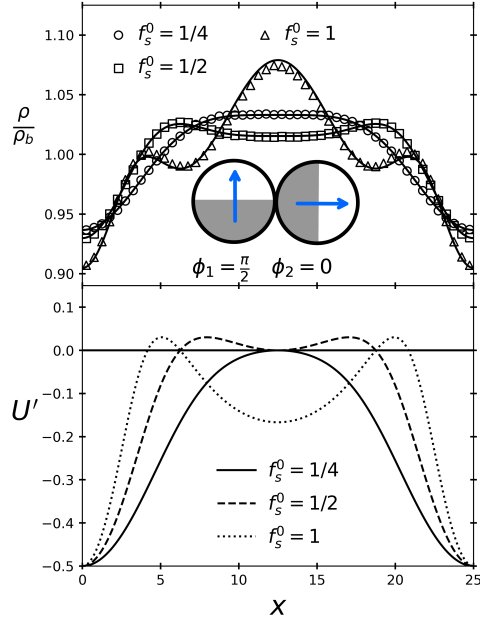


**Figure 7.4:** Phase diagrams for the tactic behaviour of dimers for  $f_s = 0.5$  in (a) and  $f_s = 5$  in (b). Every point in the  $\phi_1$ - $\phi_2$  plane corresponds to a different dimer structure. The blue region corresponds to antichemotactic dimers, which experience an effective force down the swim-force gradients ( $U' > 0$ ). The red region corresponds to chemotactic dimers ( $U' < 0$ ). These tactic regions are separated by white boundaries which correspond to dimers which show no preferential accumulation ( $U' = 0$ ). The phase behaviour is dependent on the magnitude of the swim force implying that the same dimer can be chemotactic or antochemotactic depending on the magnitude of the swim force.

property of odd-diffusive systems [234, 272, 275]. The odd-diffusive flux of active dimers can be obtained from the coarse grained Fokker Planck equation (see App. 7.A.4). These fluxes are a clear indication of broken detailed balance, and show that on this coarse-grained level not all properties of the dimer can be captured by the effective potential (Eq. 7.15) alone.

Whether a dimer accumulates in small or large swim-force regions is determined by the effective force that it experiences in swim-force gradients. The effective force can be obtained from the effective potential as  $-\nabla U = -U' \nabla f_s$ , where  $U' = \frac{dU}{df_s}$ . Wherever  $U' < 0$  ( $U' > 0$ ) the dimer moves up (down) the swim-force gradient, corresponding to chemotactic (antichemotactic) behaviour. Figure 7.4(a) shows a phase diagram in the  $\phi_1$ - $\phi_2$  plane that categorises different dimer structures according to their tactic behaviour for  $f_s = 0.5$ . Dimers which show no preferential accumulation in a swim-force gradient correspond to the white lines shown in Fig. 7.4(a) obtained as  $U' = 0$ .

**Figure 7.5:** Top: Density relative to the bulk density for a dimer with  $\phi_1 = \pi/2$  and  $\phi_2 = 0$  (see inset) for different values of the swim force. This is the same dimer as Fig. 7.2 d. The bulk density is  $\rho_b = \int_0^L dx \rho(x)/L$ , where  $L = 25$  is the simulation box with periodic boundary conditions. The swim force is  $f_s(x) = f_s^0 [1 + \sin(2\pi x/L + 3\pi/2)]$ , with the value of  $f_s^0$  as indicated in the legend. Bottom: Derivative of the effective potential  $U' = dU/df_s$ . Wherever  $U' < 0$  ( $U' > 0$ ) the dimer is chemotactic (antichemotactic). The density profile changes qualitatively when the swim force increases. In this case there is a single peak in the density where  $f_s$  is large for  $f_s^0 = 1/4$ , as the swim force increases ( $f_s^0 = 1/2$ ) the peak split in two, and if the swim force is increased further ( $f_s^0 = 1$ ) a third peak appears.



As can be seen in Fig. 7.4(b), the phase behaviour depends on the magnitude of the swim force. This means that a dimer can be antichemotactic in case of a small swim force and chemotactic in case of a large swim force, or vice versa. This can result in "local" (anti)chemotaxis, as shown in Fig. 7.5, where at low swim force there is a single peak in the density that coincides with the peak in  $f_s$ , as the swim force increases, the peak splits in two, and on further increasing the swim force a third peak appears. The density distribution has multiple peaks because  $U'$  is negative in some regions and positive in others which can be regarded as coexisting chemotactic and antichemotactic dynamic phases.

Using experimental values from Ref. [128] for dimers with a constant activity, we estimate the change in density relative to a passive region for the dimer shown in Fig. 7.2 (d) to be  $\rho_{active}/\rho_{passive} \approx 4$  (see App. 7.A.6 for details of the estimate). While this is a conservative estimate, it is likely possible to obtain much larger density changes, for example for the dimer in Fig. 7.2 (b), or by different experimental conditions. To obtain better predictions for experimental system, it would be interesting to include the effects of the specific self-propulsion mechanism [276] and the hydrodynamic interaction between the two particles in the dimer [268,



## 7.A Appendix

### 7.A.1 Active Dimer Model

The equations of motion for the dimer (see Fig. 7.2) are

$$\partial_t \mathbf{r}_1 = \frac{1}{\gamma} \mathbf{F} + \frac{1}{\gamma} f_s(\mathbf{r}_1) \mathbf{n}_1 + \sqrt{2T/\gamma} \boldsymbol{\xi}_1, \quad (7.16)$$

$$\partial_t \mathbf{r}_2 = -\frac{1}{\gamma} \mathbf{F} + \frac{1}{\gamma} f_s(\mathbf{r}_2) \mathbf{n}_2 + \sqrt{2T/\gamma} \boldsymbol{\xi}_2, \quad (7.17)$$

where  $\mathbf{r}_1$ ,  $\mathbf{n}_1$ ,  $\mathbf{r}_2$ , and  $\mathbf{n}_2$  are, respectively, the position and orientation vectors of particles 1 and 2,  $\gamma$  is the friction constant of a single particle in the dimer,  $f_s(\mathbf{r})$  is the swim force,  $T$  is the temperature in units such that the Boltzmann constant is unity, the vectors  $\boldsymbol{\xi}_1$  and  $\boldsymbol{\xi}_2$  are random Gaussian vectors with  $\langle \boldsymbol{\xi}_1(t) \rangle = \langle \boldsymbol{\xi}_2(t) \rangle = 0$  and  $\langle \boldsymbol{\xi}_1(t) \boldsymbol{\xi}_1(t') \rangle = \langle \boldsymbol{\xi}_2(t) \boldsymbol{\xi}_2(t') \rangle = \mathbf{1} \delta(t - t')$ . The force between the two active particles  $\mathbf{F}$  is always such that the distance between the two is constant and equal to  $l$ .

We make the equations dimensionless by  $\mathbf{r}_1 \rightarrow l\mathbf{r}_1$ ,  $\mathbf{r}_2 \rightarrow l\mathbf{r}_2$ ,  $t \rightarrow 2\gamma l^2 t/T$  and  $f_s(\mathbf{r}) \rightarrow 2T f_s(\mathbf{r})/l$ , so length is measured in units such that the distance between the two particles is unity, time is measured in units such that the dimer typically diffuses a unit length per unit time, and forces are measured in units of  $2T/l$ . The dimensionless equations corresponding to Eqs. 7.16 and 7.17 are

$$\partial_t \mathbf{r}_1 = 4\mathbf{F} + 4f_s(\mathbf{r}_1) \mathbf{n}_1 + 2\boldsymbol{\xi}_1, \quad (7.18)$$

$$\partial_t \mathbf{r}_2 = -4\mathbf{F} + 4f_s(\mathbf{r}_2) \mathbf{n}_2 + 2\boldsymbol{\xi}_2. \quad (7.19)$$

These equation can be rewritten using the center-of-mass coordinate  $\mathbf{R} = \frac{1}{2} (\mathbf{r}_1 + \mathbf{r}_2)$  and the relative coordinate  $\mathbf{r} = \mathbf{r}_1 - \mathbf{r}_2$ :

$$\partial_t \mathbf{R} = 2 [f_s(\mathbf{r}_1) \mathbf{n}_1 + f_s(\mathbf{r}_2) \mathbf{n}_2] + \sqrt{2} \boldsymbol{\xi}, \quad (7.20)$$

$$\partial_t \mathbf{r} = -8\mathbf{F} - 4 [f_s(\mathbf{r}_1) \mathbf{n}_1 - f_s(\mathbf{r}_2) \mathbf{n}_2] + \sqrt{8} \boldsymbol{\eta}, \quad (7.21)$$

where  $\langle \boldsymbol{\xi}(t) \rangle = \langle \boldsymbol{\eta}(t) \rangle = 0$  and  $\langle \boldsymbol{\xi}(t) \boldsymbol{\xi}(t') \rangle = \langle \boldsymbol{\eta}(t) \boldsymbol{\eta}(t') \rangle = \mathbf{1} \delta(t - t')$ . The second equation accounts for the relative movement of the two particles, which can be decomposed in a rotation of the unit vector pointing from  $\mathbf{r}_1$  to  $\mathbf{r}_2$ , and a change in the distance between the two particles (see Sec. 7.A.5).  $\mathbf{r} = r\mathbf{n}$ , with  $\mathbf{n} = (\cos(\theta), \sin(\theta))$ . The Langevin equation for the



change in the distance is

$$\partial_t r = -8\mathbf{n} \cdot \mathbf{F} - 4\mathbf{n} \cdot [f_s(\mathbf{r}_1)\mathbf{n}_1 - f_s(\mathbf{r}_2)\mathbf{n}_2] + \sqrt{8}\mathbf{n} \cdot \boldsymbol{\eta}. \quad (7.22)$$

Because the particles are connected by a stiff rod, the force due to the rod  $\mathbf{F}$  is always such that  $r = 1$  and  $\partial_t r = 0$ . The equation for the orientation is

$$\begin{aligned} \partial_t \mathbf{n} = & -8(\mathbf{1} - \mathbf{nn}) \cdot \mathbf{F} - 4(\mathbf{1} - \mathbf{nn}) \cdot [f_s(\mathbf{r}_1)\mathbf{n}_1 - f_s(\mathbf{r}_2)\mathbf{n}_2] \\ & + \sqrt{8}(\mathbf{1} - \mathbf{nn}) \cdot \boldsymbol{\eta}. \end{aligned} \quad (7.23)$$

This equation should be integrated with the Stratonovich rule. The first term on the right-hand side is zero because  $\mathbf{F} \propto \mathbf{n}$ , and the last term can be replaced by  $\boldsymbol{\epsilon} \cdot \mathbf{n} \boldsymbol{\eta}$  where  $\epsilon_{yx} = -\epsilon_{xy} = 1$  and  $\epsilon_{xx} = \epsilon_{yy} = 0$ , so

$$\partial_t \mathbf{n} = 4(\mathbf{1} - \mathbf{nn}) \cdot [f_s(\mathbf{r}_1)\mathbf{n}_1 - f_s(\mathbf{r}_2)\mathbf{n}_2] + \sqrt{8}\boldsymbol{\epsilon} \cdot \boldsymbol{\eta}. \quad (7.24)$$

The previous equation is equivalent to

$$\partial_t \theta = 4\mathbf{n} \cdot \boldsymbol{\epsilon} \cdot [f_s(\mathbf{r}_1)\mathbf{n}_1 - f_s(\mathbf{r}_2)\mathbf{n}_2] + \sqrt{8}\eta, \quad (7.25)$$

with  $\langle \eta(t) \rangle = 0$  and  $\langle \eta(t)\eta(t') \rangle = \delta(t - t')$ . This equation together with Eq. 7.20 describes the dynamics of the dimer and are used for the simulations.

## 7.A.2 Small Gradient Approximation

The orientation vectors of the active particles can be written as a rotation of the orientation vector of the dimer:  $\mathbf{n}_1 = R_1 \mathbf{n}$  and  $\mathbf{n}_2 = R_2 \mathbf{n}$ , where  $R_1 = R(\phi_1)$ ,  $R_2 = R(\phi_2)$  and

$$R(\phi) = \begin{bmatrix} \cos \phi & -\sin \phi \\ \sin \phi & \cos \phi \end{bmatrix}. \quad (7.26)$$

We define  $A = R_1 + R_2 = c_+ \mathbf{1} + s_+ \boldsymbol{\epsilon}$  and  $B = R_1 - R_2 = c_- \mathbf{1} + s_- \boldsymbol{\epsilon}$ , where  $c_{\pm} = \cos(\phi_1) \pm \cos(\phi_2)$  and  $s_{\pm} = \sin(\phi_1) \pm \sin(\phi_2)$ .

We assume gradients in the swimforce to be small, so we expand the

swim force in Eqs. 7.20 and 7.25:

$$\partial_t \mathbf{R} = 2f_s A \cdot \mathbf{n} - \mathbf{n} \cdot (\nabla f_s) B \cdot \mathbf{n} + \sqrt{2} \boldsymbol{\zeta} + \mathcal{O}(\nabla^2 f_s), \quad (7.27)$$

$$\begin{aligned} \partial_t \theta &= 4\mathbf{n} \cdot \boldsymbol{\epsilon} \cdot B \cdot \mathbf{n} f_s - 2\mathbf{n} \cdot \boldsymbol{\epsilon} \cdot A \cdot \mathbf{n} \mathbf{n} \cdot \nabla f_s + \sqrt{8} \eta + \mathcal{O}(\nabla^2 f_s), \\ &= -4s_- f_s + 2s_+ \mathbf{n} \cdot \nabla f_s + \sqrt{8} \eta + \mathcal{O}(\nabla^2 f_s), \end{aligned} \quad (7.28)$$

where  $f_s = f_s(\mathbf{R})$ , and  $\nabla$  is the gradient with respect to  $\mathbf{R}$ .

The motion of a single chiral active Brownian particle is described by [90, 271]

$$\partial_t \mathbf{r} = v_s \mathbf{n} + \sqrt{2D} \boldsymbol{\zeta}, \quad (7.29)$$

$$\partial_t \theta = \Omega + \sqrt{2D_r} \eta, \quad (7.30)$$

where  $v_s$  is the swim speed,  $D$  the thermal diffusion constant,  $\Omega$  the angular velocity of the orientation vector, and  $D_r$  is the rotational diffusion constant. Comparing with Eqs. 7.27 and 7.28 shows that, if the swim force is constant, the swim speed of the dimer is  $v_s = |2f_s A \cdot \mathbf{n}| = 2f_s \sqrt{c_+^2 + s_+^2}$ , its thermal diffusion constant is  $D = 1$ , its angular velocity is  $\Omega = -4s_- f_s$ , and its rotational diffusion constant is  $D_r = 4$ . The active diffusion constant is

$$D_a = \frac{v_s^2}{2D_r} = \frac{1}{2} f_s \left( c_+^2 + s_+^2 \right). \quad (7.31)$$

If  $\Omega \neq 0$  there is a torque on the particle and it swims in circles. These particles are called *circle swimmers* [55] or *chiral active particles* [273]. The chirality results in diffusive fluxes perpendicular to density gradients. This property is called odd diffusion (see App. 7.A.3). By tuning  $s_-$  one can tune the chirality and with that the odd diffusivity of these dimers.

The FPE corresponding to Eqs. 7.27 and 7.28 is

$$\begin{aligned} \partial_t P &= -2\nabla \cdot [f_s A \cdot \mathbf{n} P] + \nabla \cdot [B \cdot \mathbf{n} \mathbf{n} \cdot (\nabla f_s) P] \\ &\quad + \nabla^2 P + 4s_- f_s \mathcal{R} P - 2s_+ \mathcal{R} [\mathbf{n} \cdot (\nabla f_s) P] \\ &\quad + 4\mathcal{R}^2 P + \mathcal{O}(\nabla^3), \end{aligned} \quad (7.32)$$

$$\begin{aligned} &= -2A_{ij} \nabla_i [f_s n_j P] + B_{ij} \nabla_i [(\nabla_k f_s) n_j n_k P] \\ &\quad + \nabla^2 P + 4s_- f_s \mathcal{R} P - 2s_+ (\nabla_i f_s) \mathcal{R} [n_i P] \\ &\quad + 4\mathcal{R}^2 P + \mathcal{O}(\nabla^3), \end{aligned} \quad (7.33)$$

where  $\mathcal{R} = \frac{\partial}{\partial \theta} = n_x \frac{\partial}{\partial n_y} - n_y \frac{\partial}{\partial n_x}$ . The previous equation is valid up to third order in the gradient operator because the SDEs (Eq. 7.27 and 7.28) are only valid up to second order in the gradient.

We expand the probability density in eigenfunctions of  $\mathcal{R}^2$  (see Sec. 3.2.2):

$$P(\mathbf{R}, \mathbf{n}(\theta), t) = \rho(\mathbf{R}, t) + \sigma(\mathbf{R}, t) \cdot \mathbf{n} + \tau(\mathbf{R}, t) : (\mathbf{n}\mathbf{n} - \mathbf{1}/2) + \Theta,$$

where  $\rho(\mathbf{R}, t) = \frac{1}{2\pi} \int d\theta P(\mathbf{R}, t)$  is the density,  $\sigma$  and  $\tau$  are the coefficients of, respectively, the second and third moment, and  $\Theta$  is the projection onto higher-order moments. If the swim force is uniform ( $\nabla f_s = 0$ ), the system is isotropic and therefore  $\sigma = 0$ ,  $\tau = 0$  and  $\Theta = 0$ , all moments except the zeroth are at least proportional to  $\nabla$ . For the integral over the orientation  $\mathbf{n}(\theta)$  we write  $\langle \cdot \rangle = \frac{1}{2\pi} \int_0^{2\pi} d\theta \cdot$ . The equation for  $\rho$  can be obtained by averaging Eq. 7.33:

$$\begin{aligned} \partial_t \langle P(t) \rangle &= -2A_{ij} \nabla_i [f_s \langle n_j P \rangle] + B_{ij} \nabla_i [(\nabla_k f_s) \langle n_j n_k P \rangle] \\ &\quad + \nabla^2 \langle P \rangle + 4s_- f_s \langle \mathcal{R} P \rangle - 2s_+ (\nabla_i f_s) \langle \mathcal{R} P n_i \rangle \\ &\quad + 4 \langle \mathcal{R}^2 P \rangle + \mathcal{O}(\nabla^3). \end{aligned} \quad (7.34)$$

All averages with  $\mathcal{R}$  in this equation are zero. With  $\langle P \rangle = \rho$ ,  $\langle n_j P \rangle = \sigma_j / 2$  and  $\langle n_j n_k P \rangle = \delta_{jk} \langle P \rangle + \langle (n_j n_k - \delta_{jk} / 2) P \rangle = \delta_{jk} \rho / 2 + \tau_{jk} / 4$  the previous equation becomes

$$\partial_t \rho = -\nabla \cdot \mathbf{J}, \quad (7.35)$$

with

$$\begin{aligned} J_i &= A_{ij} f_s \sigma_j - \frac{1}{2} B_{ij} (\nabla_j f_s) \rho - \frac{1}{4} B_{ij} (\nabla_k f_s) \tau_{jk} - \nabla_i \rho + \mathcal{O}(\nabla^2), \\ &= A_{ij} f_s \sigma_j - \frac{1}{2} B_{ij} (\nabla_j f_s) \rho - \nabla_i \rho + \mathcal{O}(\nabla^2), \end{aligned} \quad (7.36)$$

where in the last step we ignored the term with  $\tau$  because if there is no gradient in the swim force, the system is isotropic, so there is no nematic ordering ( $\tau = 0$ ), and therefore  $\tau \sim \mathcal{O}(\nabla f_s)$  and  $\tau_{jk} \nabla_k f_s \sim \mathcal{O}(\nabla^2)$ .

To get an equation for  $\sigma$ , we multiply Eq. 7.33 by  $n_l$  and average over

**n:**

$$\begin{aligned}
2\partial_t \langle n_l P \rangle &= -2A_{ij} \nabla_i [f_s 2 \langle n_j n_l P \rangle] + B_{ij} \nabla_i [(\nabla_k f_s) 2 \langle n_j n_k n_l P \rangle] \\
&\quad + \nabla^2 2 \langle n_l P \rangle + 4s_- f_s 2 \langle n_l \mathcal{R} P \rangle - 2s_+ (\nabla_i f_s) 2 \langle n_l \mathcal{R} n_i P \rangle \\
&\quad + 8 \langle n_l \mathcal{R}^2 P \rangle + \mathcal{O}(\nabla^3). \tag{7.37}
\end{aligned}$$

With what we used before together with

$$2 \langle n_j n_k n_l P \rangle = 2\sigma_m \langle n_j n_k n_l n_m \rangle + \langle n_j n_k n_l \Theta \rangle = \sigma_m T_{jklm}^{(4)} + \chi_{jkl}$$

where  $T_{jklm}^{(4)} = (\delta_{jk} \delta_{lm} + \delta_{jl} \delta_{km} + \delta_{jm} \delta_{kl})$  and  $\chi_{jkl}$  is the projection of  $n_j n_k n_l$  on  $\Theta$ ,

$$2 \langle n_l \mathcal{R} P \rangle = -2 \langle (\mathcal{R} n_l) P \rangle = -\epsilon_{lm} 2 \langle n_m P \rangle = -\epsilon_{lm} \sigma_m,$$

$$\begin{aligned}
2 \langle n_l \mathcal{R} n_i P \rangle &= -2 \langle (\mathcal{R} n_l) n_i P \rangle = -\epsilon_{lm} 2 \langle n_m n_i P \rangle \\
&= -\epsilon_{lm} 2 \left( \frac{1}{2} \delta_{mi} \rho + \frac{1}{4} \tau_{mi} \right) = -\epsilon_{li} \rho - \frac{1}{4} \epsilon_{lm} \tau_{mi},
\end{aligned}$$

and

$$2 \langle n_l \mathcal{R}^2 P \rangle = 2 \langle (\mathcal{R}^2 n_l) P \rangle = -2 \langle n_l P \rangle = -\sigma_l,$$

the previous equation becomes

$$\begin{aligned}
\partial_t \sigma_l &= -2A_{il} \nabla_i [f_s \rho] - A_{ij} \nabla_i [f_s \tau_{jl}] \\
&\quad + B_{ij} \nabla_i \left[ (\nabla_k f_s) \left( \sigma_m T_{jklm}^{(4)} + \chi_{jkl} \right) \right] \\
&\quad + \nabla^2 \sigma_l - 4s_- f_s \epsilon_{lm} \sigma_m + 2s_+ \epsilon_{li} (\nabla_i f_s) \rho \\
&\quad + s_+ (\nabla_i f_s) \epsilon_{lm} \tau_{mi} - 4\sigma_l + \mathcal{O}(\nabla^3). \tag{7.38}
\end{aligned}$$

Equation 7.35 shows that the time scale of the time evolution in the density is  $\sim \mathcal{O}(\nabla^{-1})$ . The previous equation show that the time scale of the time evolution of  $\sigma$  is at least  $\sim 4$ , so compared to  $\rho$ ,  $\sigma$  is a fast degree of freedom, and therefore  $\partial_t \sigma \approx 0$ . With this together with  $\sigma \sim \mathcal{O}(\nabla)$ ,  $\tau \sim \mathcal{O}(\nabla)$ ,  $\chi \sim \mathcal{O}(\nabla)$ , we can re-arrange the previous equation:

$$\begin{aligned}
\sigma_j &= -\frac{1}{2} \frac{1}{1 + s_-^2 f_s^2} [\delta_{jl} - s_- f_s \epsilon_{jl}] \\
&\quad \times [A_{kl} \nabla_k (f_s \rho) - s_+ \epsilon_{lk} (\nabla_k f_s) \rho] + \mathcal{O}(\nabla^2). \tag{7.39}
\end{aligned}$$

Equations 7.35, 7.36 and 7.39 describe the coarse-grained dynamics of the dimer.

### 7.A.3 Odd Diffusion

Odd-diffusive systems have a diffusion tensor with antisymmetric components which can be written as [234, 272, 275, 277]

$$D_{ij} = D_{\parallel} \delta_{ij} + D_{\perp} \epsilon_{ij}. \quad (7.40)$$

Such a diffusion tensor appears in many different kinds of systems, as chiral active matter [271, 273, 278, 279] and diffusion under Lorentz force [272, 280–283]. The diagonal components of this tensor ( $D_{\parallel}$ ) are related to the diffusion along the density gradient; the antisymmetric components ( $D_{\perp}$ ) are related to the diffusion perpendicular to the density gradient.

The diffusion tensor of the dimers can be calculated from Eqs. 7.36 and 7.39 resulting in

$$D_{\parallel} = 1 + D_a \frac{1}{1 + \omega^2}, \quad (7.41)$$

$$D_{\perp} = D_a \frac{\omega}{1 + \omega^2}, \quad (7.42)$$

where  $\omega = \Omega/D_r = -s_- f_s$  is the active angular velocity divided by the rotational diffusion constant.

### 7.A.4 Steady State

#### Density

We calculate the steady-state density for  $f_s = f_s(x)$ , so  $\rho = \rho(x)$  and  $\sigma = \sigma(x)$ . In this case the flux in the  $x$ -direction is zero:

$$0 = J_x = f_s A_{xj} \sigma_j + \frac{1}{2} B_{xx} (\nabla_x f_s) \rho - \nabla_x \rho. \quad (7.43)$$

For the first term we use Eq. 7.39:

$$\begin{aligned} A_{xj} \sigma_j &= -\frac{1}{2} \frac{1}{1 + s_-^2 f_s^2} \left( c_+^2 + 2s_+^2 - s_- s_+ c_+ f_s \right) (\nabla_x f_s) \rho \\ &\quad - \frac{1}{2} \frac{f_s}{1 + s_-^2 f_s^2} \left( c_+^2 + s_+^2 \right) \nabla_x \rho. \end{aligned} \quad (7.44)$$

With this, the steady-state density becomes

$$\rho \propto e^{-U}, \quad (7.45)$$

where

$$\begin{aligned} \nabla_x U &= \frac{1}{2} (\nabla_x f_s) \\ &\times \frac{c_- + (c_+^2 + 2s_+^2) f_s + s_- (s_- c_- - s_+ c_+) f_s^2}{1 + \frac{1}{2} (c_+^2 + s_+^2 + 2s_-^2) f_s^2}, \end{aligned} \quad (7.46)$$

$$\begin{aligned} U &= \int dx \nabla_x U, \\ &= \frac{c}{2d} f_s + \frac{b}{4d} \ln(1 + d f_s^2) + \frac{ad - c}{2d^{3/2}} \operatorname{atan}(\sqrt{d} f_s), \end{aligned} \quad (7.47)$$

where  $a = c_-$ ,  $b = c_+^2 + 2s_+^2$ ,  $c = s_-^2 c_- - s_- s_+ c_+$ , and  $d = \frac{1}{2} (2s_-^2 + c_+^2 + s_+^2)$ .

### Polarization

The polarization is defined as the average orientation per particle:

$$\mathbf{p} = \frac{\langle \mathbf{n}P \rangle}{\langle P \rangle} = \frac{\boldsymbol{\sigma}}{2\rho}. \quad (7.48)$$

Together with Eq. 7.39, this gives

$$p_x = -\frac{1}{4} \frac{1}{1 + s_-^2 f_s^2} [(c_+ - 2s_- s_+ f_s) \nabla_x f_s - (c_+ - s_- s_+ f_s) f_s \nabla_x U], \quad (7.49)$$

and

$$p_y = \frac{1}{4} \frac{1}{1 + s_-^2 f_s^2} [(2s_+ + s_- c_+ f_s) \nabla_x f_s - (s_+ + s_- c_+ f_s) f_s \nabla_x U]. \quad (7.50)$$

### Flux

The flux in the y-direction (see Eqs. 7.36 and 7.39) is

$$J_y = f_s A_{yj} \sigma_j - \frac{1}{2} B_{yx} (\nabla_x f_s) \rho = 2f_s A_{yj} p_j \rho - \frac{1}{2} B_{yx} (\nabla_x f_s) \rho = V_y \rho, \quad (7.51)$$

where

$$\begin{aligned} V_y &= 2f_s A_{yx} p_x + 2f_s A_{yy} p_y - \frac{1}{2} B_{yx} (\nabla_x f_s), \\ &= 2f_s (s_+ p_x + c_+ p_y) - \frac{1}{2} s_- (\nabla_x f_s). \end{aligned} \quad (7.52)$$

### 7.A.5 Torque

The general Langevin equation for a vector  $\mathbf{r}$  is

$$\partial_t \mathbf{r} = \mathbf{F}(\mathbf{r}) + \sqrt{2}\boldsymbol{\eta}. \quad (7.53)$$

The vector  $\mathbf{r}$  can be decomposed in a length and a orientation:  $\mathbf{r} = r\mathbf{n}$ , with  $|\mathbf{n}| = 1$ . With Stratonovich integration one can use  $\mathbf{n} \cdot d\mathbf{n} = 0$  to find the equations of motion for  $\mathbf{n}$  and  $r$ :

$$\partial_t r = \mathbf{n} \cdot \partial_t \mathbf{r} = \mathbf{n} \cdot \mathbf{F} + \sqrt{2}\mathbf{n} \cdot \boldsymbol{\eta}, \quad (7.54)$$

$$\partial_t \mathbf{n} = \frac{1}{r} (\mathbf{1} - \mathbf{nn}) \cdot \mathbf{F} + \sqrt{2} \frac{1}{r} (\mathbf{1} - \mathbf{nn}) \cdot \boldsymbol{\eta}. \quad (7.55)$$

The Fokker-Planck equation corresponding to the last equation is

$$\begin{aligned} \partial_t P(\mathbf{n}, t) &= -\frac{1}{r} (n_x \partial_y - n_y \partial_x) [(n_x F_y - n_y F_x) P] \\ &\quad + \frac{1}{r^2} (n_x \partial_y - n_y \partial_x)^2 P, \end{aligned} \quad (7.56)$$

$$= -\frac{1}{r} \partial_\theta [(n_x F_y - n_y F_x) P] + \frac{1}{r^2} \partial_\theta^2 P, \quad (7.57)$$

where in the last step we used  $\mathbf{n} = (\cos(\theta), \sin(\theta))$ . The SDE for  $\mathbf{n}$  is equivalent to

$$\partial_t \mathbf{n} = \frac{1}{r} (\mathbf{1} - \mathbf{nn}) \cdot \mathbf{F} + \sqrt{2} \frac{1}{r} \boldsymbol{\epsilon} \cdot \mathbf{n} \boldsymbol{\eta}, \quad (7.58)$$

where  $\boldsymbol{\epsilon} = \begin{bmatrix} 0 & -1 \\ 1 & 0 \end{bmatrix}$ , and it is equivalent to

$$\partial_t \theta = \frac{1}{r} n_x F_y - \frac{1}{r} n_y F_x + \sqrt{2} \frac{1}{r} \boldsymbol{\eta} = -\frac{1}{r} \mathbf{n} \cdot \boldsymbol{\epsilon} \cdot \mathbf{F} + \sqrt{2} \frac{1}{r} \boldsymbol{\eta}. \quad (7.59)$$

### 7.A.6 Mapping to Experimental Dimer

Reference [128] reports experiments on dimers similar to the dimers in our work but with a constant swim force. Example c of Ref. [128] corresponds to  $\phi_1 = \pi/2$  and  $\phi_2 = \pi$ , which is shown in Fig. 2(e) of the main text.

The dynamics of this dimer can be described by the following Langevin equations

$$\partial_t \mathbf{r} = \tilde{v} \tilde{\mathbf{n}} + \sqrt{2\tilde{D}} \tilde{\boldsymbol{\zeta}}, \quad (7.60)$$

$$\partial_t \theta = \tilde{\omega} + \sqrt{2\tilde{D}_r} \tilde{\eta}, \quad (7.61)$$

see Eq. 1, 2 and 3 of Ref. [128]. The experimentally measured value of the parameters are  $\tilde{v} = 1.3 \mu\text{m}/\text{s}$ ,  $\tilde{D} = 0.15 \mu\text{m}^2/\text{s}$ ,  $\tilde{\omega} = 1.1 \text{s}^{-1}$ , and  $\tilde{D}_r = 1/16 \text{s}^{-1}$  (see Table I row c of Ref. [128]).

The difference between the dimer in Fig. 2(d) and 2(e) of the main text disappears if there is no activity gradient. The dynamics of the dimer in Fig. 2(e) with a constant activity are described by

$$\partial_t x = \frac{1}{2\gamma} f_s (n_x - n_y) + \sqrt{\frac{T}{\gamma}} \xi_x, \quad (7.62)$$

$$\partial_t y = \frac{1}{2\gamma} f_s (n_x + n_y) + \sqrt{\frac{T}{\gamma}} \xi_x, \quad (7.63)$$

$$\partial_t \theta = -\frac{1}{\gamma l} f_s + \sqrt{\frac{4T}{\gamma l^2}} \eta, \quad (7.64)$$

where we have put the dimensions back in order to compare with the experimental system.

The  $x$  component of the active force is  $\frac{1}{2\gamma} f_s (n_x - n_y)$ , which is equal to  $\frac{1}{\sqrt{2}\gamma} f_s \tilde{n}_x$ , and similarly, for the  $y$  component of the active force is  $\frac{1}{\sqrt{2}\gamma} f_s \tilde{n}_y$ , where  $\tilde{n}_x$  and  $\tilde{n}_y$  are the  $x$  and  $y$  components of the unit vector  $\tilde{\mathbf{n}}$  that points in the direction of the active force. By comparing the previous equations with Eqs. 7.60 and 7.61 shows that

$$\tilde{v} = \frac{f_s}{\sqrt{2}\gamma}, \quad \tilde{D} = \frac{T}{2\gamma}, \quad \tilde{\omega} = \frac{f_s}{\gamma l}, \quad \tilde{D}_r = \frac{2T}{\gamma l^2}. \quad (7.65)$$



The dimensionless swim force  $lf_s/(2T)$  can be calculated in two ways:

$$\frac{l}{2T}f_s = \frac{\tilde{v}^2}{2\tilde{D}\tilde{\omega}} \approx 5.1, \quad (7.66)$$

$$\frac{l}{2T}f_s = \frac{\tilde{v}}{\sqrt{2\tilde{D}\tilde{D}_r}} \approx 9.5. \quad (7.67)$$

The two ways to calculate the dimensionless force do not agree because in our model we ignore hydrodynamics and the fact that connecting the two ABPs has an effect on their activity.

The ratio of the density of the dimers in an active region and a region without activity  $\rho_{active}/\rho_{passive} \approx 4$ , or  $\rho_{active}/\rho_{passive} \approx 16$ , depending on which way the force is estimated.

## Chapter 8

# Active Brownian Particles in Time-Varying Activity Fields

This chapter contains results which have been published in: H. Merlitz, H.D. Vuijk, J. Brader, A. Sharma, and J.-U. Sommer. Linear response approach to active Brownian particles in time-varying activity fields. *The Journal of Chemical Physics*, 148(19), 2018.

The text has been rewritten and the simulation data has been regenerated with different parameters.

In this chapter the dynamics of an active Brownian particle (ABP) with a space and time dependent swim speed is studied. In particular, the polarization and density distribution are calculated for a sinusoidal swim speed. Furthermore, it is shown that the polarization is phase shifted with respect to the swim speed, which results in a drift velocity. As an application of this result an experimental set up is suggested where the drift velocity can be used to increase the density of an ABP near a boundary.

## 8.1 The Model

The motion of the ABP is modeled by the following stochastic differential equations (SDEs):

$$\partial_t \mathbf{r} = v_s(\mathbf{r}, t) \mathbf{n} + \sqrt{2D} \boldsymbol{\zeta}, \quad (8.1)$$

$$\partial_t \mathbf{n} = \sqrt{2D_r} \mathbf{n} \times \boldsymbol{\eta}, \quad (8.2)$$

where  $\mathbf{r}$  is the position of the ABP,  $v_s$  is the space and time-dependent swim speed,  $\mathbf{n}$  is the orientation of the ABP which is a function of the solid angle  $\Omega$ ,  $D$  its passive diffusion constant, and  $D_r$  its orientational diffusion constant. The stochastic vectors  $\boldsymbol{\zeta}$  and  $\boldsymbol{\eta}$  are random Gaussian white noise with  $\langle \boldsymbol{\zeta}(t) \rangle = \langle \boldsymbol{\eta}(t) \rangle = 0$  and  $\langle \boldsymbol{\zeta}(t) \boldsymbol{\zeta}(t') \rangle = \langle \boldsymbol{\eta}(t) \boldsymbol{\eta}(t') \rangle = \mathbf{1} \delta(t - t')$ . Note that there is no coupling between the gradient of the swim speed and the orientation vector  $\mathbf{n}$ . Throughout this chapter, the swim speed is taken to be

$$v_s(x, t) = v_0 [s + \sin(kx - ckt)], \quad (8.3)$$

where  $k$  is the wave number,  $c$  is the wave velocity, and  $s$  is the offset, which must be larger than 1 to make sure the swim speed is positive. In the following  $s = 1$ . With the exception of Sec. 8.5, bulk properties are studied, and therefore periodic boundaries are used.

The theory is tested with two different active particles with radius  $a = 1/2 \mu\text{m}$ , and  $a = 1/8 \mu\text{m}$ . The thermal diffusion constants at room temperature in water<sup>1</sup> are  $D = 2/(3\pi a) \mu\text{m}^2\text{s}^{-1}$ . We assume that the rotational correlation time is unaffected by the activity, and is therefore equal to its equilibrium value  $\tau = \pi a^3 s$ .

---

<sup>1</sup>At room temperature  $T \approx 4 \times 10^{-21} \text{ kg m}^2 \text{ s}^{-2}$ , and the viscosity of water  $\eta_s = 10^{-3} \text{ kg m}^{-1} \text{ s}^{-1}$ . These values together with the equations for thermal translational diffusion (the Stokes-Einstein relation Eq. A.31) and rotational diffusion (Eq. A.14, with  $\tau = 1/(2D_r)$ ) result in the values presented in the main text.

The Fokker-Planck equation (FPE) corresponding to Eqs. 8.1 and 8.2 is

$$\partial_t P(t) = (L_{eq} + \delta L_s) P(t), \quad (8.4)$$

with  $P(t) = P(\mathbf{r}, \mathbf{n}, t)$ ,  $\delta L_{eq} = L_D + L_R$  is the equilibrium Fokker-Planck operator where  $L_D = D\nabla^2$  accounts for the thermal diffusion,  $L_R = D_r \mathcal{R}^2$  accounts for the rotational diffusion, and  $\delta L_s = -\mathbf{n} \cdot \nabla v_s$  accounts for the nonequilibrium self-propulsion. In App. 8.A it is shown that when  $\delta L_s$  is treated as a perturbation, the nonequilibrium average of a generic function  $g(\mathbf{r}, \mathbf{n})$  can be calculated as

$$\begin{aligned} \langle g \rangle &= \langle g \rangle_{eq} + \\ &\int_{-\infty}^t dt' \int d^3 r' \int d\Omega' P_{eq} g(\mathbf{r}', \mathbf{n}') e^{-(L_D + L_R)(t' - t)} \mathbf{n}' \cdot \nabla' v_s(\mathbf{r}', t'), \end{aligned} \quad (8.5)$$

where  $\Omega$  is the solid angle in three dimensions,  $\mathbf{n}' = \mathbf{n}(\Omega')$ , the primed operators depend and act on the primed variables, and terms of order  $\sim \mathcal{O}(v_s^2)$  have been ignored.

## 8.2 Polarization

First, the polarization is calculated. The polarization is defined as the average orientation per particle:

$$\mathbf{p}(\mathbf{r}, t) = \frac{\langle \delta(\mathbf{r} - \mathbf{r}'(t)) \mathbf{n}'(t) \rangle}{\rho(\mathbf{r}, t)}, \quad (8.6)$$

where  $\mathbf{r}'(t)$  and  $\mathbf{n}'(t)$  denote the position and orientation of the active particle at time  $t$ , and the angle brackets indicate an average over the noise. Because the density does not have a linear response to the swim speed [153],  $\rho(\mathbf{r}, t)$  in the denominator can be replaced by the bulk density, as the error is second order in the swim speed. Using Eq. 8.5 with the function  $g$  replaced by  $\mathbf{n}$  for the remaining average in Eq. 8.6 gives

$$\mathbf{p}(\mathbf{r}, t) = \int_{-\infty}^t dt' \int d^3 r' v_s(\mathbf{r}', t') \chi(|\mathbf{r} - \mathbf{r}'|, |t - t'|), \quad (8.7)$$

where

$$\chi(|\mathbf{r} - \mathbf{r}'|, |t - t'|) = \frac{1}{3} \exp\left[-\frac{|t - t'|}{\tau}\right] \frac{\nabla' \exp\left[-\frac{|\mathbf{r} - \mathbf{r}'|^2}{4D|t - t'|}\right]}{(4\pi D|t - t'|)^{3/2}}, \quad (8.8)$$

is the response function for the polarization (see App. 8.A.1).

Using the swim speed in Eq. 8.3 and evaluating the integrals in Eq. 8.8 gives for the  $x$  component of the polarization

$$p(x, t) = \mathbf{p}_x(\mathbf{r}, t) = -\frac{v_0 k \cos(kx - kct + \psi)}{3\sqrt{(Dk^2 + 1/\tau)^2 + k^2 c^2}}, \quad (8.9)$$

with phase shift

$$\psi = \text{atan}\left(\frac{kc}{Dk^2 + 1/\tau}\right), \quad (8.10)$$

see App. 8.A.1 for details of the calculations. The  $y$  and  $z$  components of the polarization are zero because the swim speed only depends on the  $x$  coordinate. In the comoving frame,  $\tilde{x} = x - ct$ , the polarization is  $\tilde{p}(\tilde{x}) = p(x + ct, t)$ , where the tilde indicates coordinates and function in the comoving frame. With increasing velocity of the activity wave, the polarization decreases, and the phase shift increases and saturates at  $\pi/2$ . The decrease of the polarization for increasing  $c$  indicates the ABP does not have enough time to respond to the changing wave activity. A comparison between this result and simulations is shown in Fig. 8.1.

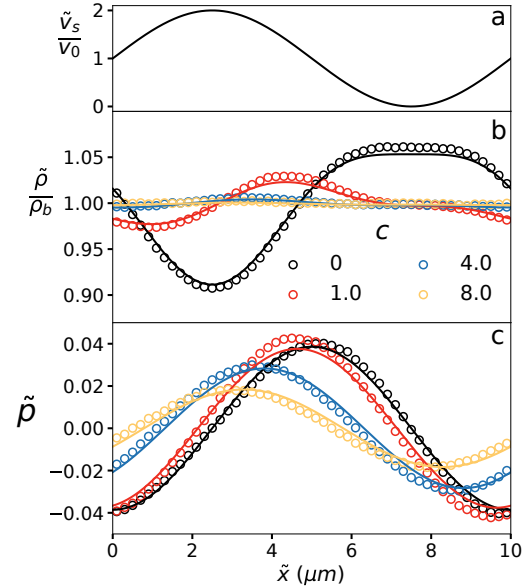
### 8.3 Density

As mentioned before, the density does not have a linear response to the swim speed [153]. However, the linear-response result for the polarization can be used to determine the density. Integrating the FPE in Eq. 8.4 over  $y, z$ , and the orientational degrees of freedom results in the equation for the density  $\rho(x, t) = \int dy \int dz \int d\Omega P(t)$ :

$$\partial_t \rho(x, t) = -\partial_x J(x, t), \quad (8.11)$$

$$J(x, t) = v_s(x, t) p(x, t) \rho(x, t) - D \partial_x \rho(x, t). \quad (8.12)$$

**Figure 8.1:** Density (panel b) normalized with the bulk density  $\rho_b = 1/10 \mu m^{-1}$ , and polarization (panel c) in the comoving frame for the swim speed shown in panel a. Symbols show simulation results and the solid lines the theoretical prediction (Eq. 8.9 in panel b, and Eq. 8.14 in panel c). The wave velocity  $c$  of the swim speed is indicated in the legend. The particles have radius  $a = 1/2 \mu m$ , and the systems size is  $10 \mu m$ . The theoretical predictions match the simulation data. As  $c$  increases, the density and polarization modulations decrease because the particle does not have enough time to respond to the changing swim speed. Note that for  $c \gtrsim 4 \mu m s^{-1}$  the density is almost flat. The polarization, on the other hand, is still inhomogeneous, indicating that even for high wave velocities the particles can respond to the changing swim speed.



From this the density in the comoving frame can be calculated:

$$\tilde{\rho}(\tilde{x}) \propto \int_0^\lambda d\tilde{x}' \exp\left(-\int_{\tilde{x}}^{\tilde{x}+\tilde{x}'} d\tilde{y} b(\tilde{y})\right), \quad (8.13)$$

where the tilde indicates functions and variables in the comoving frame,  $\lambda = 2\pi/k$  is the wave length of the activity wave,  $b(\tilde{y}) = (\tilde{v}_s(\tilde{y})\tilde{\rho}(\tilde{y}) - c) / D$ , and the proportionality constant is determined by the normalization  $\int_0^L d\tilde{x} \tilde{\rho}(\tilde{x}) = L\rho_b$ , where  $L$  is the system size, and  $\rho_b$  is the bulk density. The previous equation holds for a generic swim speed. If the swim speed is given by Eq. 8.3 the integrals can be evaluated up to second order in the swim speed. This results in

$$\tilde{\rho}(\tilde{x}) \propto e^{-\tilde{U}(\tilde{x})}, \quad (8.14)$$

with

$$\tilde{U}(\tilde{x}) = -\frac{v_0^2 k}{3D\sqrt{(Dk^2 + 1/\tau)^2 + k^2 c^2}} \times \left[ \frac{\sin(k\tilde{x} + \psi_1)}{\sqrt{c^2/D^2 + k^2}} - \frac{\cos(2k\tilde{x} + \psi_2)}{2\sqrt{c^2/D^2 + 4k^2}} \right] \quad (8.15)$$

for the swim force in Eq. 8.3, and where  $\psi_1 = \psi + \text{atan}\left(\frac{c}{Dk}\right)$ , and  $\psi_2 = \psi + \text{atan}\left(\frac{c}{2Dk}\right)$ . See App. 8.A.2 for details of the calculations. Note that the density modulation decreases as the wave velocity of the activity increases. However, as shown in Fig. 8.1, for values of  $c$  for which the density modulation is almost zero, there can still be a significant modulation in the polarization, as shown in Fig. 8.1. The reason for this is that the density is a conserved quantity and relaxes on times scales inversely proportional to gradients (see Eq. 8.11). The polarization, on the other hand, is not a conserved quantity and relaxes on a time scale  $\tau$ , which is, in the cases shown in Fig. 8.1 much shorter than the times scales of the density relaxation.

## 8.4 Drift Velocity

Due to the moving activity wave, the active particle is "dragged" along with the wave. The drift velocity of the active particles is

$$\begin{aligned} v_d &= \lim_{t \rightarrow \infty} \langle x \rangle / t = \frac{J}{\rho_b}, \\ &= \frac{1}{\rho_b} \frac{1}{\lambda} \int_0^\lambda dx v_s(x) p(x) \rho(x) = \frac{1}{\lambda} \int_0^\lambda dx v_s(x) p(x) + \mathcal{O}(v_s^3), \\ &= \frac{1}{6} v_0^2 \frac{k^2 c}{(Dk^2 + 1/\tau)^2 + k^2 c^2}, \end{aligned} \quad (8.16)$$

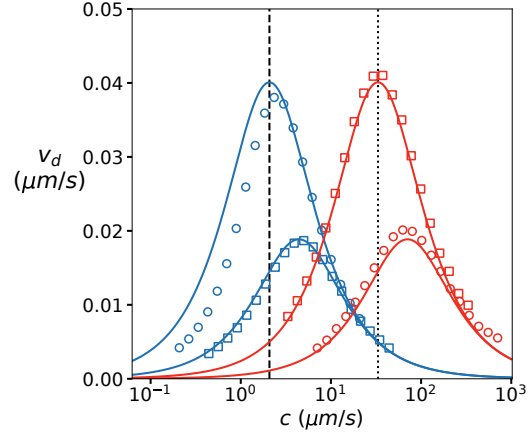
where the last equality holds for the swim speed in Eq. 8.3 with  $s = 1$ . Note that if there is no phase shift in the polarization  $p(x) \propto \partial_x v_s$ , and because of that  $v_d = 0$ .

The drift velocity has a maximum as a function of  $k$  at

$$k_m = \frac{1}{\sqrt{D\tau}}. \quad (8.17)$$

As a function of  $c$  it has a maximum at  $c_m = Dk + 1/(k\tau)$ , which, evalu-

**Figure 8.2:** Drift velocity due to a swim speed wave (Eq. 8.3). The symbols correspond to simulation result and the solid line shows the theoretical prediction (Eq. 8.16). The blue lines and symbols correspond to the “blue” particle with radius  $a = a^{(b)} = 1/2 \mu\text{m}$  and swim speed  $v_0 = 1 \mu\text{m/s}$ . The red lines and symbols correspond to the “red” particle with  $a = a^{(r)} = 1/8 \mu\text{m}$  and  $v_0 = 4 \mu\text{m/s}$ . The circles correspond to the wave number such that the peak in the drift



velocity is maximal for the blue particle:  $k = k_m(a = a^{(b)})$ . Likewise the squares correspond to  $k = k_m(a = a^{(r)})$ . Note that for  $k = k_m(a = a^{(b)})$  (circles),  $c = c_m(a = a^{(b)})$  (dashed line), the drift velocity of the blue particle is an order of magnitude larger than that of the red particle. Similarly for  $k = k_m(a = a^{(r)})$  (squares),  $c = c_m(a = a^{(r)})$  (dotted line), the drift velocity of the red particle is much larger than that of the blue particle. The discrepancy between the theory and the simulations of the blue particle with  $k = k_m(a = a^{(b)})$  (circles) indicates the break down of the linear-response domain.

ated at  $k_m$  is

$$c_m = 2\sqrt{\frac{D}{\tau}}. \quad (8.18)$$

The maximum value of the drift velocity is

$$v_d(k_m, c_m) = \frac{1}{24}v_0^2\sqrt{\frac{\tau}{D}}. \quad (8.19)$$

Note that  $k_m$  and  $c_m$  depend on  $D$  and  $\tau$ , which are both functions of the particle radius. Using the equilibrium values for  $\tau = 1/(2D_r) = 4\pi\eta_s a^3/T$  and  $D = T/(6\pi\eta_s a)$ , where  $a$  is the radius of the particle, gives  $k_m \sim a^{-1}$ ,  $c_m \sim a^{-2}$ , and  $v_d(k_m, c_m) \sim v_0^2 a^2$ . The self-propulsion velocity of self-diffusiophoretic particles (see Section 2.2.1) scales inversely with the size of the particle,  $v_s \sim a^{-1}$  (see Sec. 2.2.1). In that case, the maximum drift velocity is independent of the size of the particle,  $v_d(k_m, c_m) \sim a^0$ . The drift velocity as a function of  $c$  for two different particles sizes are shown in Fig. 8.2.



## 8.5 Confined Particles

On a time scale larger than  $1/(kc)$  the effect of the activity can be captured by an effective force  $F_e = \gamma v_d$ . This is the equivalent conservative force that is needed to move a passive particle with friction constant  $\gamma$  with velocity  $v_d$ . The effective potential corresponding to this force is  $U_e = -\int^x dx F_e = -\gamma v_d x$ . One cannot have a linear potential and periodic boundary conditions. Therefore, in this section the particle is confined between walls at  $x = 0$  and  $x = L$ .

In the low activity limit the effect of the active motion is to increase the diffusion constant of the ABP. To take this into account an effective temperature is used. In equilibrium the temperature is equal to  $\gamma D$ . By analogy, the effective temperature is  $T_e = \gamma(D + \overline{D}_a)$ , where

$$\overline{D}_a = \frac{1}{\lambda} \int_0^\lambda dx D_a(x) = \frac{1}{2} \tau v_0^2, \quad (8.20)$$

where  $D_a(x) = \tau v_s^2(x)/3$  is the active diffusion constant (see Eq. 3.19), and the last equality holds for the swim speed given in Eq. 8.3.

The steady-state density is given by the Boltzmann distribution

$$\rho(x) \propto e^{-U_e(x)/T_e} = e^{x/\lambda}, \quad (8.21)$$

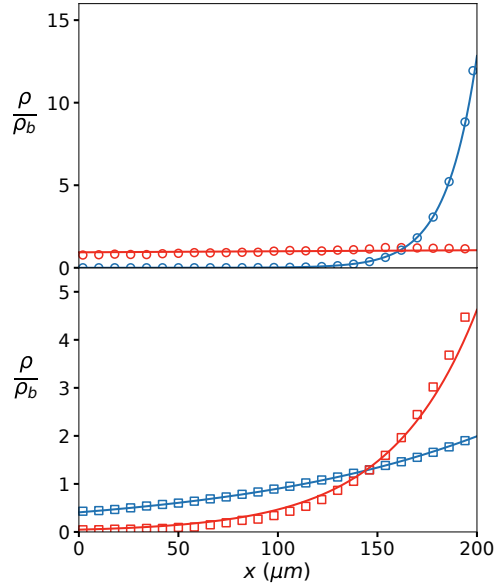
where

$$\lambda = \frac{T + \tau v_0^2/2}{\gamma v_d} = \frac{D + \overline{D}_a}{v_d}, \quad (8.22)$$

is the length scale of the exponential decay of the density. Note the similarity of this density and length scale and the density and length scale of the sedimentation problem (Eqs. 3.64 and 3.66). The relative minus sign in the exponential compared with the sedimentation problem, is there because in this case the "sedimentation" velocity ( $v_d$ ) is in the positive  $x$  direction instead of the negative  $z$  direction.

As shown in Fig. 8.3, the particle size determines the drift velocity for a given activity wave. The drift velocity of a particle with radius  $a = 1/2$ , with a swim speed wave tuned to the optimal values ( $k = k_m$  and  $c = c_m$ ) for a particle with radius  $a = 1/8$ , is orders of magnitude smaller than the drift velocity of a particle of radius  $a = 1/8$  with the same swim speed wave. This results in a different effective potential for the two particles, and with that a different density distribution. In particular, one can change the properties of the swim speed wave ( $k$  and  $c$ ) and selectively

**Figure 8.3:** Accumulation of active particles at the right wall due to the induced drift velocity. The particles are contained between two walls at  $x = 0$  and  $x = 200 \mu\text{m}$ . The symbols represent simulation results, and the solid line show the theoretical prediction (Eq. 8.21). The red and blue colors correspond to the "blue" ( $a = a^{(b)} = 1/2 \mu\text{m}$ ,  $v_0 = v_0^{(b)} = 1 \mu\text{m/s}$ ) and "red" ( $a = a^{(r)} = 1/8 \mu\text{m}$ ,  $v_0 = v_0^{(r)} = 4 \mu\text{m/s}$ ) particles in Fig. 8.2. The top panel corresponds to  $k = k_m(a = a^{(b)})$  (circles in Fig. 8.2) and  $c = c_m(a = a^{(b)})$  (dashed line in Fig. 8.2). The bottom panel corresponds to  $k = k_m(a = a^{(r)})$  (squares in Fig. 8.2) and  $c = c_m(a = a^{(r)})$  (dotted line in Fig. 8.2). By choosing the wave number and wave speed appropriately one can enrich particles with a specific size at the boundary. This can possibly be used to separate particles by their size.



enrich the density of particles with a certain size at one of the boundaries of the container; see Fig 8.3.

## 8.6 Conclusion

In this chapter it was shown how active particles orient in a time- and space-dependent activity field, without a coupling between the gradient in the activity and the orientation of the particle. In particular, it was shown how this results in a drift velocity in the direction of the activity wave. These results could be used to transport active particles, either synthetic or biological, or their cargo to a desired location, which has a wide range of applications [175, 182, 197, 198, 284, 285]

## 8.A Appendix: Linear-Response Theory

The FPE corresponding to the SDEs 8.1 and 8.2 is

$$\partial_t P(t) = (L_{eq} + \delta L_s) P(t), \quad (8.23)$$

with  $P(t) = P(\mathbf{r}, \mathbf{n}, t)$ ,  $\delta L_{eq} = L_D + L_R$  is the equilibrium Fokker-Planck operator where  $L_D = D\nabla^2$  accounts for the thermal diffusion and  $L_R = D_r \mathcal{R}^2$  accounts for the rotational diffusion, and  $\delta L_s = -\mathbf{n} \cdot \nabla v_s$  accounts for the nonequilibrium self-propulsion<sup>2</sup>. The probability can be written as  $P(t) = P_{eq} + \delta P(t)$ , where  $P_{eq}$  is the equilibrium probability density, that is, the probability density for  $v_s = 0$ . In equilibrium the translational and orientational degrees of freedom are not coupled:

$$P_{eq} = \frac{\rho_b}{\Omega_d}, \quad (8.24)$$

where  $\rho_b$  is the bulk density.

Because  $\partial_t P(t) = \partial_t \delta P(t)$ , the time evolution of the nonequilibrium part ( $\delta P(t)$ ) of the probability is

$$\partial_t \delta P(t) = (L_D + L_R + \delta L_s) (P_{eq} + \delta P(t)) \quad (8.25)$$

$$= (L_D + L_R) \delta P(t) + \delta L_s P_{eq} + \mathcal{O}(v_s^2), \quad (8.26)$$

where the  $\delta L_s \delta P(t)$  term is ignored because it is second order in the swim speed. The previous equation can be integrated with an integrating factor, resulting in

$$\delta P(t) = e^{-(L_D + L_R)(t_i - t)} \delta P(t_i) + \int_{t_i}^t dt' e^{-(L_D + L_R)(t' - t)} \delta L_s(t') P_{eq}, \quad (8.27)$$

where  $t_i$  an arbitrary initial time, the nonequilibrium operator is written as  $\delta L_s(t')$  to indicate that the swim speed should be evaluated at  $t'$ . One can take the initial probability to be  $P_{eq}$ , such that  $\delta P(t_i) = 0$ , and the

---

<sup>2</sup>Note that this is an operator equality meaning that  $\delta L_s f(\mathbf{r}, \mathbf{n}, t) = -\mathbf{n} \cdot \nabla [v_s(\mathbf{r}, t) f(\mathbf{r}, \mathbf{n}, t)]$  for a generic function  $f$ .

initial time to be  $t_i = -\infty$ . With this,

$$\begin{aligned}
P(t) &= P_{eq} + \delta P(t), \\
&= P_{eq} + \int_{-\infty}^t dt' e^{-(L_D+L_R)(t'-t)} \delta L_S(t') P_{eq}, \\
&= P_{eq} - \int_{-\infty}^t dt' P_{eq} e^{-(L_D+L_R)(t'-t)} \mathbf{n} \cdot \nabla v_s(\mathbf{r}, t'), \quad (8.28)
\end{aligned}$$

where in the last line  $\delta L_S(\mathbf{r}, \mathbf{n}, t') P_{eq} = -P_{eq} \mathbf{n} \cdot \nabla v_s(\mathbf{r}, t')$  was used.

The probability density can be used to calculate the average of a generic function  $f(\mathbf{r}, \mathbf{n})$ :

$$\begin{aligned}
\langle g \rangle &= \langle g \rangle_{eq} + \\
&\int_{-\infty}^t \int d^3 r' \int d\Omega' P_{eq} g(\mathbf{r}', \mathbf{n}') e^{-(L'_D+L'_R)(t'-t)} \mathbf{n}' \cdot \nabla' v_s(\mathbf{r}', t'), \quad (8.29)
\end{aligned}$$

where  $\langle g \rangle_{eq}$  indicates an average with respect to the equilibrium probability density, and the primes indicate that the operators act on the primed coordinates. Using that

$$\begin{aligned}
\int d^3 r' \int d\Omega' h(\mathbf{r}', \mathbf{n}') e^{-(L'_D+L'_R)(t'-t)} f(\mathbf{r}', \mathbf{n}') &= \\
\int d^3 r' \int d\Omega' f(\mathbf{r}', \mathbf{n}') e^{-(L'_D+L'_R)(t'-t)} h(\mathbf{r}', \mathbf{n}'), \quad (8.30)
\end{aligned}$$

the average can be written as

$$\begin{aligned}
\langle g \rangle &= \langle g \rangle_{eq} + \\
&\int_{-\infty}^t \int d^3 r' \int d\Omega' P_{eq} [\mathbf{n}' \cdot \nabla' v_s(\mathbf{r}', t')] e^{-(L'_D+L'_R)(t'-t)} g(\mathbf{r}', \mathbf{n}'), \quad (8.31)
\end{aligned}$$

where the square brackets indicate that the operator  $\nabla'$  only acts on  $v_s$ .

### 8.A.1 Polarization

The polarization, that is the average orientation per particles, is

$$\mathbf{p}(\mathbf{r}, t) = \frac{\langle \delta(\mathbf{r} - \mathbf{r}'(t)) \mathbf{n}'(t) \rangle}{\langle \delta(\mathbf{r} - \mathbf{r}'(t)) \rangle} = \frac{\langle \delta(\mathbf{r} - \mathbf{r}'(t)) \mathbf{n}'(t) \rangle}{\rho(\mathbf{r}, t)}. \quad (8.32)$$

Because the density does not have a linear response to the swim speed, it can be replaced by the bulk density [153]. The remaining average can be calculated using Eq. 8.31:

$$\begin{aligned}
p_i(\mathbf{r}, t) &= -\frac{1}{\rho_b} \int_{-\infty}^t dt' \int d^3 r' \int d\Omega' P_{eq} \left[ n'_j \cdot \nabla'_j v_s(\mathbf{r}', t') \right] \\
&\quad e^{-(L'_D + L'_R)(t'-t)} \delta(\mathbf{r} - \mathbf{r}') n'_i \\
&= -\frac{1}{\rho_b} \int_{-\infty}^t dt' \int d^3 r' \rho_b \left[ n'_j \cdot \nabla'_j v_s(\mathbf{r}', t') \right] e^{-L'_D(t'-t)} \delta(\mathbf{r} - \mathbf{r}') \\
&\quad \int d\Omega' \frac{1}{\Omega_3} n'_j e^{-L'_R(t'-t)} n'_i, \tag{8.33}
\end{aligned}$$

where  $P_{eq} = \rho_b / \Omega_3$  was used. For the last integral one can use

$$\begin{aligned}
e^{-L_R(t'-t)} n_i &= \sum_{k=0}^{\infty} \frac{[-(t'-t)]^k}{k!} (D_r \mathcal{R}^2)^k n_i \\
&= \sum_{k=0}^{\infty} \frac{[-(t'-t)]^k}{k!} \left( \frac{-1}{\tau} \right)^k n_i \\
&= e^{-(t'-t)/\tau} n_i, \tag{8.34}
\end{aligned}$$

where  $D_r \mathcal{R}^2 \mathbf{n} = -2D_r \mathbf{n} = -\mathbf{n}/\tau$  was used, and  $\tau = 1/(2D_r)$  is the orientational correlation time. Using this, together with  $\int d\Omega \mathbf{n} \mathbf{n} = \Omega_3 \mathbf{1}/3$  (see Sec. 3.2.2), the polarization becomes

$$\begin{aligned}
p_i(\mathbf{r}, t) &= -\frac{1}{3\rho_b} \int_{-\infty}^t dt' e^{-(t'-t)/\tau} \\
&\quad \int d^3 r' \rho_b \left[ \nabla'_i v_s(\mathbf{r}', t') \right] e^{-L'_D(t'-t)} \delta(\mathbf{r} - \mathbf{r}'). \tag{8.35}
\end{aligned}$$

Using  $\nabla'_i v_s(\mathbf{r}', t') = \int d^3 r'' \delta(\mathbf{r}'' - \mathbf{r}') \nabla''_i v_s(\mathbf{r}'', t')$  the polarization can be written as

$$\begin{aligned}
p_i(\mathbf{r}, t) &= -\frac{1}{3\rho_b} \int_{-\infty}^t dt' e^{-(t'-t)/\tau} \int d^3 r'' \left[ \nabla''_i v_s(\mathbf{r}'', t') \right] \\
&\quad \int d^3 r' \rho_b \delta(\mathbf{r}'' - \mathbf{r}') e^{-L'_D(t'-t)} \delta(\mathbf{r} - \mathbf{r}') \\
&= \frac{1}{3\rho_b} \int_{-\infty}^t dt' \int d^3 r'' e^{-(t'-t)/\tau} v_s(\mathbf{r}'', t') \nabla''_i G(|\mathbf{r} - \mathbf{r}''|, |t' - t|), \tag{8.36}
\end{aligned}$$

where for the  $\nabla''$  operator integration by parts was used, and

$$\begin{aligned} G(|\mathbf{r} - \mathbf{r}''|, |t' - t|) &= \int d^3 r' \delta(\mathbf{r}'' - \mathbf{r}') e^{-L'_D(t'-t)} \delta(\mathbf{r} - \mathbf{r}') \\ &= \frac{\exp\left[-\frac{|\mathbf{r}'' - \mathbf{r}'|^2}{4D|t-t'|}\right]}{(4\pi D|t-t'|)^{3/2}} \end{aligned} \quad (8.37)$$

is the probability that a particle starts at  $\mathbf{r}$  and diffuses to  $\mathbf{r}''$  in time  $t' - t$ . With this, the polarization can be expressed as

$$\mathbf{p}(\mathbf{r}, t) = \int_{-\infty}^t dt' \int d^3 r' v_s(\mathbf{r}', t') \chi(|\mathbf{r} - \mathbf{r}'|, |t' - t|), \quad (8.38)$$

where

$$\chi(|\mathbf{r} - \mathbf{r}'|, |t' - t|) = \frac{1}{3} e^{-(t'-t)/\tau} \nabla' G(|\mathbf{r} - \mathbf{r}'|, |t' - t|), \quad (8.39)$$

is the response function for the polarization.

In order to calculate the polarization it is more convenient to use Eq. 8.36 and use integration by parts to let the operator  $\nabla''$  act on the swim speed:

$$\begin{aligned} \mathbf{p}(\mathbf{r}, t) &= -\frac{1}{3} \int_{-\infty}^t e^{-(t'-t)/\tau} \int d^3 r' [\nabla' v_s(\mathbf{r}', t')] G(|\mathbf{r} - \mathbf{r}'|, |t - t'|) \\ &= -\frac{1}{3} \int_0^\infty e^{-t'/\tau} \int d^3 r' [\nabla' v_s(\mathbf{r}', t - t')] \frac{\exp\left[-\frac{|\mathbf{r}'' - \mathbf{r}'|^2}{4Dt'}\right]}{(4\pi Dt')^{3/2}}. \end{aligned} \quad (8.40)$$

For the swim speed profile in the main text  $v_s = v_0 [1 + \sin(kx - kct)]$ , only the  $x$  component of the polarization is nonzero. Evaluating the integrals with this swim speed results in

$$p(x, t) = -\frac{v_0 k \pi}{3} \frac{\cos(kx - kct + \psi)}{\sqrt{(Dk^2 + 1/\tau)^2 + c^2 k^2}}, \quad (8.41)$$

where  $p(x, t)$  is the  $x$  component of  $\mathbf{p}(x, t)$ , and the phase shift is

$$\psi = \text{atan}\left(\frac{kc}{Dk^2 + 1/\tau}\right), \quad (8.42)$$

and  $\tau = 1/(2D_r)$  is the orientational correlation time.

### 8.A.2 Density

The equation for the particle density

$$\rho(x, t) = \int dy \int dz \int d\Omega P(\mathbf{r}, \mathbf{n}, t) \quad (8.43)$$

can be obtained by integrating the FPE 8.23 over the orientational degrees of freedom, and using  $\int d\Omega \mathcal{R}^2 P(x, t) = 0$ :

$$\partial_t \rho(x, t) = -\partial_x J(x, t), \quad (8.44)$$

$$J(x, t) = v_s(x, t) p(x, t) \rho(x, t) - D \partial_x \rho(x, t), \quad (8.45)$$

where the polarization comes from  $\int d\Omega \mathbf{n} P(x, t) = \rho(x, t) \mathbf{p}(x, t)$ .

In the comoving frame,  $\tilde{x} = x - ct$ , this equation becomes

$$\partial_t \rho(\tilde{x}, t) = -\partial_{\tilde{x}} J(\tilde{x}, t), \quad (8.46)$$

$$\tilde{J}(\tilde{x}, t) = [\tilde{v}_s(\tilde{x}) \tilde{p}(\tilde{x}, t) - c] \tilde{\rho}(\tilde{x}, t) - D \partial_{\tilde{x}} \tilde{\rho}(\tilde{x}, t), \quad (8.47)$$

where  $\tilde{\rho}(\tilde{x}, t) = \rho(\tilde{x} + ct, t)$ ,  $\tilde{p}(\tilde{x}, t) = p(\tilde{x} + ct, t)$ ,  $\tilde{J}(\tilde{x}, t) = J(\tilde{x} + ct, t)$ , and  $\tilde{v}_s(\tilde{x}) = v_s(\tilde{x} + ct, t)$ , are, respectively, the density, polarization, flux and swim speed in the comoving frame.

In the steady state in the comoving frame  $\partial_t \tilde{\rho} = 0$ , and therefore the flux in the comoving frame must be a constant. Integrating the flux over one period  $\lambda = 2\pi/k$  gives

$$\tilde{J} = \frac{1}{\lambda} \int_0^\lambda d\tilde{x} \tilde{J} = -\rho_b c + \frac{1}{\lambda} \int_0^\lambda d\tilde{x} \tilde{v}_s(\tilde{x}) \tilde{p}(\tilde{x}) \tilde{\rho}(\tilde{x}), \quad (8.48)$$

where the time variable is no longer written because in the comoving frame the functions do not depend on time.

To obtain an equation for the density, Eq. 8.47 is rewritten as

$$\frac{\tilde{J}}{D} \exp\left(-\int_{\tilde{x}_0}^{\tilde{x}} d\tilde{y} b(\tilde{y})\right) = -\partial_{\tilde{x}} \left[ \exp\left(-\int_{\tilde{x}_0}^{\tilde{x}} d\tilde{y} b(\tilde{y})\right) \tilde{\rho}(\tilde{x}) \right], \quad (8.49)$$

where  $\tilde{x}_0$  is an arbitrary constant. Integrating this from  $\tilde{x}$  to  $\tilde{x} + \lambda$ , and

using that  $\tilde{\rho}$  and  $b$  are periodic, gives

$$\frac{\tilde{J}}{D} \int_0^\lambda d\tilde{x}' \exp\left(-\int_{\tilde{x}}^{\tilde{x}+\tilde{x}'} d\tilde{y} b(\tilde{y})\right) = \left[1 - \exp\left(-\int_0^\lambda d\tilde{y} b(\tilde{y})\right)\right] \tilde{\rho}(\tilde{x}), \quad (8.50)$$

after  $\tilde{x}' \rightarrow \tilde{x}' + \tilde{x}$ . Integrating over  $\tilde{x}$  from 0 to  $L$  and rearranging results in

$$\frac{\tilde{J}}{\rho_b} = DL \frac{1 - \exp\left(-\int_0^\lambda d\tilde{y} b(\tilde{y})\right)}{\int_0^\lambda d\tilde{x} \int_0^\lambda d\tilde{x}' \exp\left(-\int_{\tilde{x}}^{\tilde{x}+\tilde{x}'} d\tilde{y} b(\tilde{y})\right)}, \quad (8.51)$$

which gives, in addition to Eq. 8.48, another expression for the flux. Using Eq. 8.50 to replace  $\tilde{J}$  in the previous expression, gives an equation for the density in the comoving frame:

$$\frac{\tilde{\rho}(\tilde{x})}{\rho_b} = \lambda \frac{\int_0^\lambda d\tilde{x}' \exp\left(-\int_{\tilde{x}}^{\tilde{x}+\tilde{x}'} d\tilde{y} b(\tilde{y})\right)}{\int_0^\lambda d\tilde{x} \int_0^\lambda d\tilde{x}' \exp\left(-\int_{\tilde{x}}^{\tilde{x}+\tilde{x}'} d\tilde{y} b(\tilde{y})\right)}. \quad (8.52)$$

Up to second order in the swim speed, the integrals can be evaluated:

$$\begin{aligned} \tilde{\rho}(\tilde{x}) &\propto \int_0^\lambda d\tilde{x}' \exp\left[-\int_{\tilde{x}}^{\tilde{x}+\tilde{x}'} d\tilde{y} b(\tilde{y})\right] \\ &\propto \int_0^\lambda d\tilde{x}' e^{c\tilde{x}'/D} \left[1 - \int_{\tilde{x}}^{\tilde{x}+\tilde{x}'} d\tilde{y} \tilde{v}_s(\tilde{y}) \tilde{p}(\tilde{y})\right] + \mathcal{O}(v_s^4). \\ &\propto 1 - \frac{c/D}{e^{c\lambda/D} - 1} \int_0^\lambda d\tilde{x}' e^{c\tilde{x}'/D} \int_{\tilde{x}}^{\tilde{x}+\tilde{x}'} d\tilde{y} \tilde{v}_s(\tilde{y}) \tilde{p}(\tilde{y}) + \mathcal{O}(v_s^4). \end{aligned} \quad (8.53)$$

Resulting in

$$\tilde{\rho}(\tilde{x}) \propto e^{-\tilde{U}(\tilde{x})}, \quad (8.54)$$



where in the comoving frame

$$\begin{aligned} \tilde{U}(\tilde{x}) &= \frac{c/D}{e^{c\lambda/D} - 1} \int_0^\lambda d\tilde{x}' e^{c\tilde{x}'/D} \int_{\tilde{x}}^{\tilde{x}+\tilde{x}'} d\tilde{y} \tilde{v}_s(\tilde{y}) \tilde{p}(\tilde{y}) + \mathcal{O}(v_s^4). \quad (8.55) \\ &= - \frac{v_0^2 k}{3D \sqrt{(Dk^2 + 1/\tau)^2 + k^2 c^2}} \times \\ &\quad \left[ \frac{\sin(k\tilde{x} + \psi_1)}{\sqrt{c^2/D^2 + k^2}} - \frac{\cos(2k\tilde{x} + \psi_2)}{2\sqrt{c^2/D^2 + 4k^2}} \right] \quad (8.56) \end{aligned}$$

for the swim force in Eq. 8.3, and where  $\psi_1 = \psi + \text{atan}\left(\frac{c}{Dk}\right)$ , and  $\psi_2 = \psi + \text{atan}\left(\frac{c}{2Dk}\right)$ .

**Part III**  
**Appendix**



# Appendix A

## Hydrodynamics

This chapter reviews basic fluid dynamics. The main results are the rotational and translational friction of a sphere (Sections A.3 and A.4), the friction of a rod (Section A.5), and Lorentz's reciprocal theorem (Section A.6).

### A.1 The Navier-Stokes Equation

The dynamics of fluids are governed by the Navier-Stokes equation. This equation is a consequence of mass conservation and Newton's equations of motion applied to an infinitesimal fluid element. Because the mass of the fluid is locally conserved, the change in density of an infinitesimal fluid element at position  $\mathbf{r}$  at time  $t$  is equal to minus the flow of mass through the boundary of that element. This condition results in a continuity equation for the time evolution of the mass density:

$$\partial_t \rho(\mathbf{r}, t) + \nabla \cdot [\mathbf{u}(\mathbf{r}, t) \rho(\mathbf{r}, t)] = 0, \quad (\text{A.1})$$

where  $\rho(\mathbf{r}, t)$  and  $\mathbf{u}(\mathbf{r}, t)$  are, respectively, the mass density and the velocity of the fluid at position  $\mathbf{r}$  at time  $t$ . That the second term in the continuity equation is equal to the flow of mass through the boundary follows from the divergence theorem.

In many applications the fluid is incompressible<sup>1</sup>. This means that the

---

<sup>1</sup>Whether a fluid can be considered as incompressible depends both on the properties of the fluid as on its flow. For example, air is highly compressible; however, when the velocities are small compared to the speed of sound, it can be considered as incompressible.

density an observer moving along with the fluid measures is constant. So if  $\mathbf{r}(t)$  is the position of the observer,  $d\mathbf{r}/dt = \mathbf{u}(\mathbf{r}(t), t)$ . The equation corresponding to this statement is

$$0 = \frac{d}{dt}\rho(\mathbf{r}(t), t) = \frac{\partial}{\partial t}\rho + \mathbf{u} \cdot \nabla\rho. \quad (\text{A.2})$$

In this case the continuity equation for the mass density (Eq. A.1) becomes

$$\nabla \cdot \mathbf{u} = 0, \quad (\text{A.3})$$

which is called the incompressibility equation. In the following it is not only assumed that the fluid is incompressible, but also that it has a constant density.

Newton's equations of motion applied to an infinitesimal volume element gives the Navier-Stokes equation

$$\rho (\partial_t \mathbf{u} + \mathbf{u} \cdot \nabla \mathbf{u}) = \nabla \cdot \Sigma + \mathbf{f}_e, \quad (\text{A.4})$$

where  $\Sigma = \Sigma(\mathbf{r}, t)$  is the stress tensor, and  $\mathbf{f}_e = \mathbf{f}_e(\mathbf{r}, t)$  is an external force per unit volume acting on the fluid (e.g. a force coming from the interaction with a boundary or colloid in the fluid). The left-hand side represents the inertial forces. The stress tensor accounts for the forces due to gradients in the pressure and due to viscous forces. This tensor has units of force per unit area, so  $d\mathbf{S} \cdot \Sigma = dS \hat{\mathbf{n}} \cdot \Sigma$ , where  $d\mathbf{S}$  is an infinitesimal area with area  $dS$  and normal vector  $\hat{\mathbf{n}}$ , is the force on a infinitesimal area. For an incompressible fluid with constant shear viscosity, the stress tensor is [286]

$$\Sigma = -p(\mathbf{r}, t)\mathbf{1} + \eta_s \left[ \nabla \mathbf{u} + (\nabla \mathbf{u})^T \right], \quad (\text{A.5})$$

where  $p(\mathbf{r}, t)$  is the pressure,  $\eta_s$  is the shear viscosity,  $[\nabla \mathbf{u}]_{ij} = \partial_i u_j$ , and the superscript  $T$  indicates a transpose. The second term on the right hand side of the previous equation represent shear stresses. They are stresses due to spatial inhomogeneities in the velocity field. These stresses result in forces perpendicular to the normal vector of an area element called shear forces. The expression for the shear stress comes from a lowest order expansion in  $\partial_i u_j$ , because the shear stress vanishes if the flow field is independent of space, and the requirement that shear stress vanishes when  $\mathbf{u} = \boldsymbol{\Omega} \times \mathbf{r}$ , where  $\boldsymbol{\Omega}$  is the angular velocity, because this corresponds to a rotation of the fluid [13, 287]. With this stress tensor the

Navier-Stokes equation becomes

$$\rho (\partial_t \mathbf{u} + \mathbf{u} \cdot \nabla \mathbf{u}) = -\nabla p + \eta_s \nabla^2 \mathbf{u} + \mathbf{f}_e, \quad (\text{A.6})$$

where  $\nabla^2 \mathbf{u}$  is the vector Laplacian acting on the flow field. For a more rigorous derivation of the Navier-Stokes equation see for example Ref. [288]. The force of the fluid acting on a object in the fluid is  $-\int_{\partial} d\mathbf{S} \cdot \Sigma$ , where integral is over the surface of the object and  $d\mathbf{S}$  is in the direction of the normal vector that points out of the object.

The goal of many problems in hydrodynamics is to solve Eqs. A.3 and A.6 for  $p(\mathbf{r}, t)$  and  $\mathbf{u}(\mathbf{r}, t)$  given certain boundary conditions. The Navier-Stokes equation for an incompressible fluid (Eqs. A.3 and A.6) applies to a vast range of problems. This equation is a nonlinear, second-order partial differential equation, and cannot be solved for most systems. However, in some case not all terms in the equation are important. In most biological micro- and nano-scale systems (such as biological or artificial microswimmers), inertial forces are negligible. In this case the Navier-Stokes equation reduces to the Stokes equation, which is the topic of the next section.

## A.2 The Stokes Equation

To quantify the importance of the inertial forces in the Navier-Stokes equation, one can nondimensionalize it by scaling distances by the typical length scale  $L$  (e.g. the size of a colloid or length of a rod-like particle), and velocities by the characteristic velocity  $V$ . The dimensionless quantities are  $\tilde{\mathbf{r}} = \mathbf{r}/L$ ,  $\tilde{\mathbf{u}} = \mathbf{u}/V$ ,  $\tilde{t} = tV/L$ ,  $\tilde{p} = L/(\eta_s V)$ , and  $\tilde{\mathbf{f}}_e = \mathbf{f}_e L^2/(\eta_s V)$ . With this the nondimensionalized Navier-Stokes equation (Eq. A.6) becomes

$$Re (\partial_{\tilde{t}} \tilde{\mathbf{u}} + \tilde{\mathbf{u}} \cdot \tilde{\nabla} \tilde{\mathbf{u}}) = -\tilde{\nabla} \tilde{p} + \tilde{\nabla}^2 \tilde{\mathbf{u}} + \tilde{\mathbf{f}}_e, \quad (\text{A.7})$$

where  $Re = \rho VL/\eta_s$  is called the Reynolds number [289]. Note that both  $\tilde{\mathbf{u}} \cdot \tilde{\nabla} \tilde{\mathbf{u}}$  and  $\tilde{\nabla}^2 \tilde{\mathbf{u}}$  are of the order unity. The Reynolds number quantifies the importance of inertial forces (left-hand-side of the previous equation) compared to viscous forces  $\eta_s \nabla^2 \mathbf{u}$ . When the Reynolds number is small the Navier-Stokes equation reduces to the Stokes equation:

$$\nabla p - \eta_s \nabla^2 \mathbf{u} = -\nabla \cdot \Sigma = \mathbf{f}_e, \quad (\text{A.8})$$

which is also called the creeping-flow equation. The absence of a time derivative in the Stokes equation does not necessarily mean that the solutions are independent of time, as the boundary conditions can be time dependent. When the boundary conditions are time dependent, the system is called quasi-steady, and time only plays the role of a parameter. In this case the momentum of the fluid diffuses instantaneously to its quasi-steady state, and there is no lag when the boundary conditions change in time [77]. Note that one still needs to complement this equation with the incompressibility equation (Eq. A.3) to solve for the pressure and the flow field.

### A.3 Friction of a Rotating Sphere

Because the Stokes equation is linear, the relation between the torque on the sphere and the angular velocity of the surrounding fluid is linear  $\tau = \gamma_{rot}\Omega$ , where  $\tau$  is the torque,  $\gamma_{rot}$  is the rotational friction constant and  $\Omega$  is the angular velocity. To determine this constant, consider a sphere with radius  $a$ , with its center at the origin, rotating about the  $z$ -axis. The force of the fluid on an infinitesimal area of the sphere is  $d\mathbf{S} \cdot \Sigma$ , so the torque about the  $z$ -axis per unit area that must be applied to the sphere is minus the  $\phi$  component of that force (minus because this is the force on the fluid) times the distance to the origin  $d\tau(\theta) = -a \sin \theta \Sigma_{r\phi}(a, \theta) dS$ .

Due to the symmetry of the problem, the velocity field can be written as  $\mathbf{u} = \hat{\mathbf{e}}_\phi u(r, \theta)$ , where  $r$  is the radial distance,  $\theta$  is the polar angle, and  $\phi$  is the azimuthal angle. There is no external force, and the pressure is independent of  $\phi$ , so the  $\phi$  component of the Stokes equation for this problem is

$$\begin{aligned} 0 &= \left[ \nabla^2 \mathbf{u} \right]_\phi, \\ &= \frac{1}{r^2} \frac{\partial}{\partial r} \left[ r^2 \frac{\partial u}{\partial r} \right] + \frac{1}{r^2 \sin \theta} \frac{\partial}{\partial \theta} \left[ \sin \theta \frac{\partial u}{\partial \theta} \right] - \frac{u}{r^2 \sin \theta}. \end{aligned} \quad (\text{A.9})$$

The fluid at the boundary of the sphere move along with the sphere with the same velocity, therefore the so called no-slip boundary condition is used [290]:  $u(a, \theta) = a\Omega \sin \theta$ . Far away from the sphere the fluid is at rest:  $\lim_{r \rightarrow \infty} u(r, \theta) = 0$ . The boundary condition at the surface of the sphere suggests a solution of the form  $R(r) \sin \theta$ . The previous equation

then becomes

$$0 = r^2 \frac{d^2 R}{dr^2} + 2r \frac{dR}{dr} - 2R, \quad (\text{A.10})$$

which has solutions  $R = r$  and  $R = 1/r^2$ . Together with the boundary conditions, this gives for the flow field

$$u(r, \theta) = a^3 \Omega r^{-2} \sin \theta. \quad (\text{A.11})$$

The  $r\phi$ -component of the stress tensor is  $\Sigma_{r\phi} = \eta_s \left[ \nabla \mathbf{u} + (\nabla \mathbf{u})^T \right]_{r\phi} = -3\eta_s \Omega a^3 r^{-3} \sin \theta$ . With this the total torque about the  $z$ -axis becomes

$$\begin{aligned} \tau &= \int d\tau = 3\eta_s \Omega a \int_0^{2\pi} d\phi \int_0^\pi d\theta \sin \theta a^2 \sin^2 \theta \\ &= 8\pi \eta_s a^3 \Omega. \end{aligned} \quad (\text{A.12})$$

The rotational friction constant is

$$\gamma_{rot} = 8\pi \eta_s a^3. \quad (\text{A.13})$$

This also gives the rotational-diffusion constant

$$D_r = \frac{T}{\gamma_{rot}} = \frac{T}{8\pi \eta_s a^3}, \quad (\text{A.14})$$

so the rotational diffusion constant is inversely proportional to the cube of the radius.

## A.4 Friction of a Translating Sphere

The drag force on a translating sphere with radius  $a$  is proportional to its velocity:

$$\mathbf{F}_d = \gamma \mathbf{V}, \quad (\text{A.15})$$

where  $\gamma$  is the friction constant of the sphere. The force is equal to minus the integral of the stress on the boundary of the sphere  $\mathbf{F}_d = - \int d\mathbf{S} \cdot \Sigma$ . Without loss of generality, the velocity is taken to be in the  $z$ -direction,



$V = V\hat{\mathbf{e}}_z$ . The  $z$ -component of the force is

$$F_{dz} = - \int d\mathbf{S} \cdot \boldsymbol{\Sigma} \cdot \hat{\mathbf{e}}_z = \int dS \Sigma_{r\theta} \sin \theta - \Sigma_{rr} \cos \theta. \quad (\text{A.16})$$

Due to the symmetry, the flow field can be written as  $\mathbf{u} = \hat{\mathbf{e}}_r u_r(r, \theta) + \hat{\mathbf{e}}_\theta u_\theta(r, \theta)$ . The equations are solved most easily in the comoving frame with its origin coinciding with the center of the sphere. The boundary conditions for the flow field in the comoving frame are  $\mathbf{u}(\mathbf{r}, t) = -\mathbf{V}$  for  $r \rightarrow \infty$ , and no-slip boundary conditions [290] for  $r = a$ ,  $\mathbf{u}(a, \theta) = 0$ .

It is convenient to define a so called Stokes stream function  $\psi(r, \theta)$  such that the incompressibility equation is always satisfied [286]. For

$$u_r = \frac{1}{r^2 \sin \theta} \frac{\partial \psi}{\partial \theta}, \quad u_\theta = -\frac{1}{r \sin \theta} \frac{\partial \psi}{\partial r}, \quad (\text{A.17})$$

$\nabla \cdot \mathbf{u} = 0$ , and the problem is reduced to finding the scalar function  $\psi$ . The boundary conditions for  $\psi$  are  $\psi = -\frac{1}{2} V r^2 \sin^2 \theta$  as  $r \rightarrow \infty$ , and  $\partial_r \psi = \partial_\theta \psi = 0$  for  $r = a$ . The Stokes equation for this problem is

$$\nabla p = \eta_s \nabla^2 \mathbf{u} = -\eta_s \nabla \times (\nabla \times \mathbf{u}), \quad (\text{A.18})$$

where the second equality holds when  $\nabla \cdot \mathbf{u} = 0$ . The equations for the  $r$  and  $\theta$  components are

$$\frac{\partial p}{\partial r} = \frac{\eta_s}{r^2 \sin \theta} \frac{\partial}{\partial \theta} E^2 \psi, \quad \frac{\partial p}{\partial \theta} = -\frac{\eta_s}{\sin \theta} \frac{\partial}{\partial r} E^2 \psi, \quad (\text{A.19})$$

where

$$E^2 = \frac{\partial^2}{\partial r^2} + \frac{\sin \theta}{r^2} \frac{\partial}{\partial \theta} \left( \frac{1}{\sin \theta} \frac{\partial}{\partial \theta} \right). \quad (\text{A.20})$$

Equating the  $\theta$  derivative of  $\partial_r p$  with the  $r$  derivative of  $\partial_\theta p$  gives

$$E^2 (E^2 \psi) = 0. \quad (\text{A.21})$$

The boundary condition for  $r \rightarrow \infty$  suggests a trial solution of the form  $\psi = R(r) \sin^2 \theta$ . This trial solution together with the boundary conditions for  $\psi$  gives

$$\psi = -\frac{1}{4} \sin^2 \theta V (a^3 r^{-1} - 3ar + 2r^2). \quad (\text{A.22})$$

From this solution and Eqs. A.19, one finds

$$dp(r, \theta) = \frac{3}{2} Va\eta_s d \left[ \cos \theta r^{-2} \right], \quad (\text{A.23})$$

so the pressure, up to an arbitrary constant, is

$$p(r, \theta) = \frac{3}{2} Va\eta_s \frac{\cos \theta}{r^2}. \quad (\text{A.24})$$

The components of the velocity vector are

$$u_r = -\frac{1}{2} V \cos \theta \left[ 2 - 3\frac{a}{r} + \left(\frac{a}{r}\right)^3 \right], \quad (\text{A.25})$$

$$u_\theta = \frac{1}{4} V \sin \theta \left[ 4 - 3\frac{a}{r} - \left(\frac{a}{r}\right)^3 \right], \quad (\text{A.26})$$

from which one can calculate the relevant components of the stress tensor:

$$\begin{aligned} \Sigma_{rr}(a, \theta) &= -p(a, \theta) + 2\eta_s \left. \frac{\partial u_r}{\partial r} \right|_{r=a} \\ &= -\frac{3V\eta_s}{2a} \cos \theta, \end{aligned} \quad (\text{A.27})$$

$$\begin{aligned} \Sigma_{r\theta}(a, \theta) &= \eta_s \left. \frac{\partial u_\theta}{\partial r} \right|_{r=a} - \eta_s \left. \frac{u_\theta}{r} \right|_{r=a} + \eta_s \left. \frac{1}{r} \frac{\partial u_r}{\partial \theta} \right|_{r=a} \\ &= \frac{3V\eta_s}{2a} \sin \theta, \end{aligned} \quad (\text{A.28})$$

and  $\Sigma_{r\phi} = 0$ . Note that

$$\hat{\mathbf{e}}_r \cdot \Sigma(a, \theta) = \Sigma_{rr}(a, \theta) \hat{\mathbf{e}}_r + \Sigma_{r\theta}(a, \theta) \hat{\mathbf{e}}_\theta = -\frac{3\eta_s}{2a} \mathbf{V} \quad (\text{A.29})$$

is a constant on the surface of the sphere. With this the force becomes  $F_{dz} = \gamma V$ , with

$$\gamma = 6\pi\eta_s a, \quad (\text{A.30})$$

which is called Stoke's law [8]. Using Einstein's result for the translational diffusion constant (Eq. 1.4), one obtains the diffusion constant

$$D = \frac{T}{\gamma} = \frac{T}{6\pi\eta_s a}, \quad (\text{A.31})$$

which shows that the translational diffusion constant is inversely proportional to the radius of the sphere.

## A.5 Friction of a Rod

In order to calculate the friction of a rod, a different approach is used than in the previous two cases. For this problem the Green's function method explained in Refs. [13, 291] is used.

The Green's function of the Stokes equation are the tensor  $T$  called the Oseen tensor, which gives the response of the fluid flow due to a external force density  $\mathbf{f}_e$ :

$$\mathbf{u}(\mathbf{r}) = \int d\mathbf{r}' T(\mathbf{r} - \mathbf{r}') \cdot \mathbf{f}_e(\mathbf{r}'), \quad (\text{A.32})$$

and the vector  $\mathbf{g}$ , which gives the response of the pressure to an external force:

$$p(\mathbf{r}) = \int d\mathbf{r}' \mathbf{g}(\mathbf{r} - \mathbf{r}') \mathbf{f}_e(\mathbf{r}'). \quad (\text{A.33})$$

These Green's functions satisfy

$$\nabla \cdot T(\mathbf{r}) = 0, \quad (\text{A.34})$$

$$\nabla \mathbf{g}(\mathbf{r}) - \eta_s \nabla^2 T(\mathbf{r}) = \mathbf{1} \delta(\mathbf{r}). \quad (\text{A.35})$$

One can easily check, by using Eqs. A.32 and A.33, that these equations are equivalent to the Stokes equation (Eq. A.8). These equations can be solved using Fourier transform methods [13], which give

$$T(\mathbf{r}) = \frac{1}{8\pi\eta_s r} [\mathbf{1} + \hat{\mathbf{r}}\hat{\mathbf{r}}], \quad (\text{A.36})$$

where  $r = |\mathbf{r}|$  and  $\hat{\mathbf{r}} = \mathbf{r}/r$ .

To calculate the friction of a rod with length  $L$  and radius  $R$ , one can model the rod as a rigid chain of  $N = L/(2R)$  spheres with radius  $R$ . When the rod is dragged, the resulting velocity field is

$$\mathbf{u}(\mathbf{r}) = \int_{\partial_N} dS' T(\mathbf{r} - \mathbf{r}') \cdot \mathbf{f}(\mathbf{r}'), \quad (\text{A.37})$$

where  $\partial_N$  indicates the surface of all the beads, and  $\mathbf{f}(\mathbf{r}')$  is the force per unit area that the rod exerts on a fluid element. Due to the force, the rod

moves with a constant velocity  $\mathbf{u}_0$ , so the boundary condition is  $\mathbf{u}(\mathbf{r}) = \mathbf{u}_0$  for  $\mathbf{r} \in \partial_N$ .

Defining the new coordinate  $\mathbf{x} = \mathbf{r} - \mathbf{r}_i$  where  $\mathbf{r}_i$  is the position of the center of bead  $i$ , the equation for the velocity field can be written as

$$\mathbf{u}(\mathbf{x} + \mathbf{r}_i) = \sum_{j=1}^N \int_{\partial} dS' T(\mathbf{x} - \mathbf{x}' + \mathbf{r}_{ij}) \cdot \mathbf{f}_j(\mathbf{x}'), \quad (\text{A.38})$$

where the integral is over the surface of a single bead,  $\mathbf{f}_j(\mathbf{x}')$  is the force per unit area on a surface element of bead  $j$ , and  $\mathbf{r}_{ij} = \mathbf{r}_i - \mathbf{r}_j = (i - j)2R\hat{\mathbf{t}}$ , where  $\hat{\mathbf{t}}$  is a unit vector along the rod. The boundary condition becomes

$$\mathbf{u}_0 = \sum_{j=1}^N \int_{\partial} dS' T(\mathbf{x} - \mathbf{x}' + \mathbf{r}_{ij}) \cdot \mathbf{f}_j(\mathbf{x}') \quad \text{for } |\mathbf{x}| = R. \quad (\text{A.39})$$

This holds for all  $i$ . Integrating both sides over the surface of the rod removes the  $i$  dependence:

$$\mathbf{u}_0 = \frac{1}{2\pi RL} \sum_{i,j=1}^N \int_{\partial} dS' \left[ \int_{\partial} dS T(\mathbf{x} - \mathbf{x}' + \mathbf{r}_{ij}) \right] \cdot \mathbf{f}_j(\mathbf{x}'). \quad (\text{A.40})$$

The integral in the square brackets can be evaluated using a Fourier transformation and complex integration (see Ref. [13]). For  $i = j$  the integral is  $2R\mathbf{1}/(3\eta_s)$ . For  $i \neq j$  one can use the approximation  $T(\mathbf{x} - \mathbf{x}' + \mathbf{r}_{ij}) \approx T(\mathbf{r}_{ij})$  because the error is of the order of the diameter of the rod, which is assumed to be small.

With this, the integral in the square brackets becomes independent of  $\mathbf{x}'$  and the primed integral only acts on  $\mathbf{f}_j(\mathbf{x}')$ . The total hydrodynamic force on bead  $j$  is  $\mathbf{F}_j^h = - \int_{\partial} dS' \mathbf{f}_j(\mathbf{x}')$ . The total hydrodynamic force on the rod is the sum of the hydrodynamic forces on the beads  $\mathbf{F}^h = \sum_{i=1}^N \mathbf{F}_i^h$ . For a long rod one can approximate the hydrodynamic force on bead  $j$  by  $\mathbf{F}_j^h = \mathbf{F}^h/N$ . All together this gives

$$\mathbf{u}_0 = -\frac{1}{3\pi\eta_s L} \mathbf{F}^h - \frac{4R^2}{L^2} \left[ \sum_{\substack{i,j=1 \\ i \neq j}}^N T(\mathbf{r}_{ij}) \right] \cdot \mathbf{F}^h. \quad (\text{A.41})$$

The sum in the square brackets is

$$\begin{aligned} \sum_{\substack{i,j=1 \\ i \neq j}}^N T(\mathbf{r}_{ij}) &= \frac{1}{16\pi\eta_s R} [\mathbf{1} + \hat{\mathbf{t}}\hat{\mathbf{t}}] \sum_{\substack{i,j=1 \\ i \neq j}}^N \frac{1}{|i-j|}, \\ &\approx \frac{1}{8\pi\eta_s R} [\mathbf{1} + \hat{\mathbf{t}}\hat{\mathbf{t}}] \frac{L}{2R} \ln\left(\frac{L}{2R}\right), \end{aligned} \quad (\text{A.42})$$

where in the last line the double sum was approximated by integrals. The velocity becomes

$$\begin{aligned} \mathbf{u}_0 &= -\frac{1}{3\pi\eta_s L} \mathbf{F}^h - \frac{\ln\left(\frac{L}{2R}\right)}{4\pi\eta_s L} [\mathbf{1} + \hat{\mathbf{t}}\hat{\mathbf{t}}] \cdot \mathbf{F}^h \\ &\approx -\frac{\ln\left(\frac{L}{2R}\right)}{4\pi\eta_s L} [\mathbf{1} + \hat{\mathbf{t}}\hat{\mathbf{t}}] \cdot \mathbf{F}^h. \end{aligned} \quad (\text{A.43})$$

Inverting this relation gives the friction tensor:  $\mathbf{F}^h = -\gamma \cdot \mathbf{u}_0$ , with

$$\gamma = \gamma_{\parallel} \hat{\mathbf{t}}\hat{\mathbf{t}} + \gamma_{\perp} [\mathbf{1} - \hat{\mathbf{t}}\hat{\mathbf{t}}], \quad (\text{A.44})$$

and

$$\gamma_{\parallel} = \frac{2\pi\eta_s L}{\ln\left(\frac{L}{2R}\right)}, \quad \gamma_{\perp} = \frac{4\pi\eta_s L}{\ln\left(\frac{L}{2R}\right)}, \quad (\text{A.45})$$

are the parallel and perpendicular friction coefficients. For more accurate calculations using different methods, see for example Refs. [289, 292, 293].

## A.6 Lorentz's Reciprocal Theorem

The reciprocal theorem is useful to find solutions to the Stokes equation if one already has a solution for the same geometry, but different boundary conditions [73, 289, 294]. Let  $(\mathbf{u}, \Sigma)$  and  $(\mathbf{u}', \Sigma')$  be solutions to the Stokes equation, that is  $\nabla \cdot \mathbf{u} = 0$ ,  $\nabla \cdot \Sigma = 0$ , and  $\nabla \cdot \mathbf{u}' = 0$ ,  $\nabla \cdot \Sigma' = 0$ . The domain is all space outside a body with boundary  $\partial$ . Then, because both are solution to the Stokes equation

$$0 = \mathbf{u}' \cdot (\nabla \cdot \Sigma) - \mathbf{u} \cdot (\nabla \cdot \Sigma'), \quad (\text{A.46})$$

$$= \nabla \cdot [\mathbf{u}' \cdot \Sigma - \mathbf{u} \cdot \Sigma'] - (\nabla \mathbf{u}') : \Sigma + (\nabla \mathbf{u}) : \Sigma'. \quad (\text{A.47})$$

where the nabla operator does not act on anything outside of the brackets. By using  $\Sigma = -p\mathbf{1} + \eta_s \nabla \mathbf{u} + \eta_s (\nabla \mathbf{u})^T$ ,  $\nabla \cdot \mathbf{u} = 0$ , with the equivalent equations for the primed system, and the tensor identities  $(\nabla \mathbf{u}) : (\nabla \mathbf{u}') = (\nabla \mathbf{u}') : (\nabla \mathbf{u})$ , and  $(\nabla \mathbf{u}) : (\nabla \mathbf{u}')^T = (\nabla \mathbf{u}') : (\nabla \mathbf{u})^T$ , one can show that the last two terms of the previous equation cancel. Integrating the remaining part over the total volume  $V$  gives

$$0 = \int_V d^3r \nabla \cdot (\mathbf{u}' \cdot \Sigma - \mathbf{u} \cdot \Sigma') \quad (\text{A.48})$$

$$= \int_{\partial_\infty} d\mathbf{S} \cdot (\mathbf{u}' \cdot \Sigma - \mathbf{u} \cdot \Sigma') + \int_{\partial} d\mathbf{S} \cdot (\mathbf{u}' \cdot \Sigma - \mathbf{u} \cdot \Sigma'), \quad (\text{A.49})$$

where  $\partial_\infty$  means a surface at infinity with a normal vector pointing out of the enclosing volume. Assuming that the velocity and stress decay sufficiently fast such that the integral over the surface at infinity vanishes, this can be written as

$$\int_{\partial} d\mathbf{S} \cdot \Sigma \cdot \mathbf{u}' = \int_{\partial} d\mathbf{S} \cdot \Sigma' \cdot \mathbf{u}, \quad (\text{A.50})$$

which is the reciprocal theorem.



# Bibliography

- [1] S. G. Brush. A History of Random Processes I. Brownian Movement from Brown to Perrin. *Archive for history of exact sciences*, 5(1):1–36, 1968.
- [2] M. Smoluchowski. Zur kinetischen theorie der brownschen molekularbewegung und der suspensionen. *Annalen der Physik*, 326 (14):756–780, 1906.
- [3] M. Smoluchowski. On the mean path of molecules of gas and its relationship to the theory of diffusion. *Bulletin International de l'Académie Sciences de Cracovie, Classe des Sciences Mathématiques et Naturelles*, pages 202–213, 1906.
- [4] A. Fick. Ueber Diffusion. *Annalen der Physik und Chemie*, 170(1): 59–86, 1855.
- [5] A. Einstein. über die von der molekularkinetischen Theory der Wärme geforderte Bewegung von in ruhenden Flüssigkeiten suspendierten Teilchen. *Annalen der Physik*, 32(8):549–560, 1905.
- [6] A. Einstein. Elementare Theorie der Brownschen Bewegung. *Z. für Electrochemie und angewandte physikalische Chemie*, 14(17):235–239, 1908.
- [7] A. Einstein. *Investigations on the Theory of the Brownian Movement by Albert Einstein*. Dover, 1956.
- [8] G. G. Stokes. On the effect of the internal friction of fluids on the motion of pendulums. *Transactions of the Cambridge Philosophical Society*, 9:8–106, 1851.
- [9] M. P. Langevin. Sur la theorie du mouven Brownien. *C. R. Acad. Sci. (Paris)*, 1946:530–533, 1908.



- [10] D. S. Lemons and A. Gythiel. Paul Langevin's 1908 paper "On the Theory of Brownian Motion" ["Sur la théorie du mouvement brownien," C. R. Acad. Sci. (Paris) **146**, 530–533 (1908)]. *American Journal of Physics*, 65(11):1079–1081, 1997.
- [11] G. E. Uhlenbeck and L. S. Ornstein. On the theory of Brownian motion. *Physical review*, 36(5):823, 1930.
- [12] A. P. Philipse. *Brownian Motion: Elements of Colloid Dynamics*. Undergraduate Lecture Notes in Physics. Springer, 2018.
- [13] J. K. G. Dhont. *An Introduction to Dynamics of Colloids*. Elsevier, 1996.
- [14] C. Gardiner. *Stochastic Methods: A Handbook for the Natural and Social Sciences*. Springer, fourth edition, 2009.
- [15] N. G. Van Kampen. *Stochastic Processes in Physics and Chemistry*. Elsevier, third edition, 2007.
- [16] P. C. Bressloff. *Stochastic Processes in Cell Biology*, volume 41 of *Interdisciplinary Applied Mathematics*. Springer International Publishing, Cham, 2014.
- [17] W. Coffey and Y. P. Kalmykov. *The Langevin Equation: With Applications to Stochastic Problems in Physics, Chemistry and Electrical Engineering*, volume 27. World Scientific, third edition, 2012.
- [18] H. C. Berg. *Random Walks in Biology*. Princeton University press, 1993.
- [19] R. Kubo, M. Toda, and N. Hashitsume. *Statistical Physics II: Nonequilibrium Statistical Mechanics*. Springer, 1991.
- [20] A. Libchaber. From Biology to Physics and Back: The Problem of Brownian Movement. *Annual Review of Condensed Matter Physics*, 10 (1):275–293, 2019.
- [21] R. N. Mantegna and H. E. Stanley. *An Introduction to Econophysics: Correlations and Complexity in Finance*. Cambridge University Press, 1999.
- [22] A. A. Gushchin. *Stochastic Calculus for Quantitative Finance*. Elsevier, 2015.
- [23] S. E. Shreve. *Stochastic Calculus for Finance I The Binomial Asset Pricing Model*. Springer Science & Business Media, 2005.

- [24] D. S. Dean. Stochastic Density Functional Theory – Bangalore School on Statistical Physics 2018, 2018.
- [25] L. Isserlis. On a Formula for the Product-Moment Coefficient of any Order of a Normal Frequency Distribution in any Number of Variables. *Biometrika*, 12(1/2):134, 1918.
- [26] G. Volpe and G. Volpe. Simulation of a Brownian particle in an optical trap. *American Journal of Physics*, 81(3):224–230, 2013.
- [27] N. G. van Kampen. Diffusion in inhomogeneous media. *Zeitschrift für Physik B Condensed Matter*, 68(2):135–138, 1987.
- [28] N. G. Van Kampen. Diffusion in inhomogeneous media. *Journal of physics and chemistry of solids*, 49(6):673–677, 1988.
- [29] N. G. van Kampen. Explicit calculation of a model for diffusion in nonconstant temperature. *Journal of Mathematical Physics*, 29(5):1220–1224, 1988.
- [30] G. Volpe and J. Wehr. Effective drifts in dynamical systems with multiplicative noise: A review of recent progress. *Reports on Progress in Physics*, 79(5):053901, 2016.
- [31] S. Hottovy, A. McDaniel, G. Volpe, and J. Wehr. The Smoluchowski-Kramers Limit of Stochastic Differential Equations with Arbitrary State-Dependent Friction. *Communications in Mathematical Physics*, 336(3):1259–1283, 2015.
- [32] S. Hottovy, G. Volpe, and J. Wehr. Noise-Induced Drift in Stochastic Differential Equations with Arbitrary Friction and Diffusion in the Smoluchowski-Kramers Limit. *Journal of Statistical Physics*, 146(4):762–773, 2012.
- [33] D. P. Herzog, S. Hottovy, and G. Volpe. The Small-Mass Limit for Langevin Dynamics with Unbounded Coefficients and Positive Friction. *Journal of Statistical Physics*, 163(3):659–673, 2016.
- [34] A. W. C. Lau and T. C. Lubensky. State-dependent diffusion: Thermodynamic consistency and its path integral formulation. *Physical Review E*, 76(1):011123, 2007.
- [35] M. J. Schnitzer. Theory of continuum random walks and application to chemotaxis. *Physical Review E*, 48(4):2553, 1993.

- [36] M. C. Marchetti, J. F. Joanny, S. Ramaswamy, T. B. Liverpool, J. Prost, M. Rao, and R. A. Simha. Hydrodynamics of soft active matter. *Reviews of Modern Physics*, 85(3):1143–1189, 2013.
- [37] S. Ramaswamy. The mechanics and statistics of active matter. *Annual Review of Condensed Matter Physics*, 1(1):323–345, 2010.
- [38] F. Jülicher, S. W. Grill, and G. Salbreux. Hydrodynamic theory of active matter. *Reports on Progress in Physics*, 81(7):076601, 2018.
- [39] F. Jülicher, K. Kruse, J. Prost, and J. Joanny. Active behavior of the Cytoskeleton. *Physics Reports*, 449(1-3):3–28, 2007.
- [40] F. Jülicher, A. Ajdari, and J. Prost. Modeling molecular motors. *Reviews of Modern Physics*, 69(4):1269–1282, 1997.
- [41] A. B. Kolomeisky and M. E. Fisher. Molecular Motors: A Theorist’s Perspective. *Annual Review Physical Chemistry*, 58:675–695, 2007.
- [42] M. Feng and M. K. Gilson. Enhanced Diffusion and Chemotaxis of Enzymes. *Annual Review of Biophysics*, 49(1):87–105, 2020.
- [43] S. Ghosh, A. Somasundar, and A. Sen. Enzymes as Active Matter. *Annual Review of Condensed Matter Physics*, 12(1):177–200, 2021.
- [44] S. Sengupta, K. K. Dey, H. S. Muddana, T. Tabouillot, M. E. Ibele, P. J. Butler, and A. Sen. Enzyme Molecules as Nanomotors. *Journal of the American Chemical Society*, 135(4):1406–1414, 2013.
- [45] A.-Y. Jee, Y.-K. Cho, S. Granick, and T. Trusty. Catalytic enzymes are active matter. *Proceedings of the National Academy of Sciences*, 115(46):E10812–E10821, 2018.
- [46] J. Agudo-Canalejo, P. Illien, and R. Golestanian. Phoresis and Enhanced Diffusion Compete in Enzyme Chemotaxis. *Nano Letters*, 18(4):2711–2717, 2018.
- [47] T. Vicsek and A. Zafeiris. Collective motion. *Physics Reports*, 517(3-4):71–140, 2012.
- [48] J. Elgeti, R. G. Winkler, and G. Gompper. Physics of microswimmers—single particle motion and collective behavior: A review. *Reports on Progress in Physics*, 78(5):056601, 2015.
- [49] J. L. Moran and J. D. Posner. Phoretic Self-Propulsion. *Annual Review of Fluid Mechanics*, 49(1):511–540, 2017.

- [50] R. Dreyfus, J. Baudry, M. L. Roper, M. Fermigier, H. A. Stone, and J. Bibette. Microscopic artificial swimmers. *Nature*, 437(7060):862–865, 2005.
- [51] B. J. Williams, S. V. Anand, J. Rajagopalan, and M. T. A. Saif. A self-propelled biohybrid swimmer at low Reynolds number. *Nature Communications*, 5(1):3081, 2014.
- [52] S. Palagi and P. Fischer. Bioinspired microrobots. *Nature Reviews Materials*, 3(6):113–124, 2018.
- [53] J. Palacci, S. Sacanna, A. P. Steinberg, D. J. Pine, and P. M. Chaikin. Living Crystals of Light-Activated Colloidal Surfers. *Science*, 339(6122):936–940, 2013.
- [54] I. Buttinoni, G. Volpe, F. Kümmel, G. Volpe, and C. Bechinger. Active Brownian motion tunable by light. *Journal of Physics: Condensed Matter*, 24(28):284129, 2012.
- [55] F. Kümmel, B. ten Hagen, R. Wittkowski, I. Buttinoni, R. Eichhorn, G. Volpe, H. Löwen, and C. Bechinger. Circular Motion of Asymmetric Self-Propelling Particles. *Physical Review Letters*, 110(19):198302, 2013.
- [56] I. Buttinoni, J. Bialké, F. Kümmel, H. Löwen, C. Bechinger, and T. Speck. Dynamical Clustering and Phase Separation in Suspensions of Self-Propelled Colloidal Particles. *Physical Review Letters*, 110(23):238301, 2013.
- [57] C. Lozano, B. ten Hagen, H. Löwen, and C. Bechinger. Phototaxis of synthetic microswimmers in optical landscapes. *Nature Communications*, 7(1):12828, 2016.
- [58] J. Arlt, V. A. Martinez, A. Dawson, T. Pilizota, and W. C. K. Poon. Painting with light-powered bacteria. *Nature Communications*, 9(1):768, 2018.
- [59] E. Gaffney, H. Gadêlha, D. Smith, J. Blake, and J. Kirkman-Brown. Mammalian Sperm Motility: Observation and Theory. *Annual Review of Fluid Mechanics*, 43(1):501–528, 2011.
- [60] E. H. Harris. *Chlamydomonas* as a Model Organism. *Annual Review of Plant Physiology and Plant Molecular Biology*, 52(1):363–406, 2001.

- [61] U. Ruffer and W. Nultsch. High-speed cinematographic analysis of the movement of *Chlamydomonas*. *Cell motility*, 5(3):251–263, 1985.
- [62] H. C. Berg. *E. Coli in Motion*. Springer Science & Business Media, first edition, 2008.
- [63] H. C. Berg. The Rotary Motor of Bacterial Flagella. *Annual Review of Biochemistry*, 72(1):19–54, 2003.
- [64] B. Alberts, A. Johnson, J. Lewis, D. Morgan, M. Raff, K. Roberts, P. Walter, J. Wilson, and T. Hunt. *Molecular Biology of the Cell*. Garland Science, Taylor and Francis Group, New York, NY, sixth edition, 2015.
- [65] J. Lighthill. Flagellar Hydrodynamics. *SIAM Review*, 18(2):161–230, 1976.
- [66] D. Bray. *Cell Movements: From Molecules to Motility*. Garland, New York, NY, 2. ed edition, 2001.
- [67] I. S. Aranson, editor. *Physical Models of Cell Motility*. Biological and Medical Physics, Biomedical Engineering. Springer International Publishing, Cham, 2016.
- [68] L. Pismen. *Active Matter Within and Around Us: From Self-Propelled Particles to Flocks and Living Forms*. Springer, 2021.
- [69] E. M. Purcell. Life at Low Reynolds number. *American Journal of Physics*, 45(1):3–11, 1977.
- [70] E. Lauga. *The Fluid Dynamics of Cell Motility*. Cambridge University Press, first edition, 2020.
- [71] E. Lauga. Life around the scallop theorem. *Soft Matter*, 7(7):3060–3065, 2011.
- [72] E. Lauga. Bacterial Hydrodynamics. *Annual Review of Fluid Mechanics*, 48(1):105–130, 2016.
- [73] O. S. Pak and E. Lauga. Theoretical models in low-Reynolds-number locomotion. *arXiv:1410.4321 [cond-mat, physics:physics]*, 2014.
- [74] J. Gray and G. Hancock. The propulsion of sea-urchin spermatozoa. *Journal of Experimental Biology*, 32(4):802–814, 1955.

- [75] E. Lauga and T. R. Powers. The hydrodynamics of swimming microorganisms. *Reports on Progress in Physics*, 72(9):096601, 2009.
- [76] R. G. Winkler and G. Gompper. Hydrodynamics in Motile Active Matter. In W. Andreoni and S. Yip, editors, *Handbook of Materials Modeling*, pages 1–21. Springer International Publishing, Cham, 2018.
- [77] S. Childress. *Mechanics of Swimming and Flying*. Cambridge Studies in Mathematical Biology. Cambridge University Press, first edition, 1981.
- [78] M. J. Lighthill. *Mathematical Biofluidynamics: A Treatment in Book Form of the Material in the Lecture Course Delivered to the "Mathematical Biofluidynamics" Research Conference of the National Science Foundation Held from July 16-20, 1973 at Rensselaer Polytechnic Inst., Troy, New York*. Number 17 in Regional Conference Series in Applied Mathematics. Soc. for Industrial and Applied Mathematics, Philadelphia, Pa, nachdr. edition, 1997.
- [79] H. C. Berg and D. A. Brown. Chemotaxis in *Escherichia coli* analysed by Three-dimensional Tracking. *Nature*, 239(5374):500–504, 1972.
- [80] M. Polin, I. Tuval, K. Drescher, J. P. Gollub, and R. E. Goldstein. *Chlamydomonas* Swims with Two "Gears" in a Eukaryotic Version of Run-and-Tumble Locomotion. *Science*, 325(5939):487–490, 2009.
- [81] J. L. Anderson. Colloid Transport by Interfacial Forces. *annual review fluid mechanics*, 21:61–99, 1989.
- [82] J. L. Anderson and D. C. Prieve. Diffusiophoresis: Migration of Colloidal Particles in Gradients of Solute Concentration. *Separation and Purification Methods*, 13(1):67–103, 1984.
- [83] S. Marbach, H. Yoshida, and L. Bocquet. Local and global force balance for diffusiophoretic transport. *Journal of Fluid Mechanics*, 892:A6, 2020.
- [84] J. L. Anderson. Transport Mechanisms of Biological Colloids. *Annals of the New York Academy of Sciences*, 469(1 Biochemical E):166–177, 1986.

- [85] M. N. Popescu, W. E. Uspal, and S. Dietrich. Self-diffusiophoresis of chemically active colloids. *The European Physical Journal Special Topics*, 225(11-12):2189–2206, 2016.
- [86] J. F. Brady. Particle motion driven by solute gradients with application to autonomous motion: Continuum and colloidal perspectives. *Journal of Fluid Mechanics*, 667:216–259, 2011.
- [87] R. Golestanian, T. B. Liverpool, and A. Ajdari. Propulsion of a Molecular Machine by Asymmetric Distribution of Reaction Products. *Physical Review Letters*, 94(22):220801, 2005.
- [88] R. Golestanian. Phoretic Active Matter. *arXiv:1909.03747 [cond-mat, physics:physics]*, 2019.
- [89] A. Domínguez, M. N. Popescu, C. M. Rohwer, and S. Dietrich. Self-Motility of an Active Particle Induced by Correlations in the Surrounding Solution. *Physical Review Letters*, 125(26):268002, 2020.
- [90] C. Bechinger, R. Di Leonardo, H. Löwen, C. Reichhardt, G. Volpe, and G. Volpe. Active Particles in Complex and Crowded Environments. *Reviews of Modern Physics*, 88(4):045006, 2016.
- [91] S. Michelin and E. Lauga. Phoretic self-propulsion at finite Péclet numbers. *Journal of Fluid Mechanics*, 747:572–604, 2014.
- [92] R. Golestanian, T. B. Liverpool, and A. Ajdari. Designing phoretic micro- and nano-swimmers. *New Journal of Physics*, 9(5):126–126, 2007.
- [93] M. N. Popescu, W. E. Uspal, Z. Eskandari, M. Tasinkevych, and S. Dietrich. Effective squirmer models for self-phoretic chemically active spherical colloids. *The European Physical Journal E*, 41(12):145, 2018.
- [94] J. R. Howse, R. A. L. Jones, A. J. Ryan, T. Gough, R. Vafabakhsh, and R. Golestanian. Self-Motile Colloidal Particles: From Directed Propulsion to Random Walk. *Physical Review Letters*, 99(4):048102, 2007.
- [95] S. Ebbens, M.-H. Tu, J. R. Howse, and R. Golestanian. Size dependence of the propulsion velocity for catalytic Janus-sphere swimmers. *Physical Review E*, 85(2):020401, 2012.

- [96] R. Kapral. Perspective: Nanomotors without moving parts that propel themselves in solution. *The Journal of Chemical Physics*, 138(2):020901, 2013.
- [97] G. Volpe, I. Buttinoni, D. Vogt, H.-J. Kuehmerer, and C. Bechinger. Microswimmers in Patterned Environments. *Soft Matter*, 7(19):8810, 2011.
- [98] M. E. Cates and J. Tailleur. Motility-Induced Phase Separation. *Annual Review of Condensed Matter Physics*, 6(1):219–244, 2015.
- [99] A. Zöttl and H. Stark. Emergent behavior in active colloids. *Journal of Physics: Condensed Matter*, 28(25):253001, 2016.
- [100] A. P. Solon, Y. Fily, A. Baskaran, M. E. Cates, Y. Kafri, M. Kardar, and J. Tailleur. Pressure is not a state function for generic active fluids. *Nature Physics*, 11(8):673–678, 2015.
- [101] C. O. Reichhardt and C. Reichhardt. Ratchet Effects in Active Matter Systems. *Annual Review of Condensed Matter Physics*, 8(1):51–75, 2017.
- [102] R. Phillips, J. Kondev, J. Theriot, and G. G. Hernan. *Physical Biology of the Cell*. CRC Press, Boca Raton London New York, second edition, first issued in paperback edition, 2019.
- [103] M. Almonacid, W. W. Ahmed, M. Bussonnier, P. Mailly, T. Betz, R. Voituriez, N. S. Gov, and M.-H. Verlhac. Active diffusion positions the nucleus in mouse oocytes. *Nature Cell Biology*, 17(4):470–479, 2015.
- [104] M. Almonacid, M.-E. Terret, and M.-H. Verlhac. Control of nucleus positioning in mouse oocytes. *Seminars in Cell & Developmental Biology*, 82:34–40, 2018.
- [105] A. Colin, G. Letort, N. Razin, M. Almonacid, W. Ahmed, T. Betz, M.-E. Terret, N. S. Gov, R. Voituriez, Z. Gueroui, and M.-H. Verlhac. Active diffusion in oocytes nonspecifically centers large objects during prophase I and meiosis I. *Journal of Cell Biology*, 219(3):e201908195, 2020.
- [106] N. Razin, R. Voituriez, J. Elgeti, and N. S. Gov. Generalized Archimedes’ principle in active fluids. *Physical Review E*, 96(3):032606, 2017.



- [107] M. D. Manson, P. Tedesco, H. C. Berg, F. M. Harold, and C. Van der Drift. A protonmotive force drives bacterial flagella. *Proceedings of the National Academy of Sciences*, 74(7):3060–3064, 1977.
- [108] M. D. Manson. Bacterial Motility and Chemotaxis. In *Advances in Microbial Physiology*, volume 33, pages 277–346. Elsevier, 1992.
- [109] O. Béjà, L. Aravind, E. V. Koonin, M. T. Suzuki, A. Hadd, L. P. Nguyen, S. B. Jovanovich, C. M. Gates, R. A. Feldman, J. L. Spudich, E. N. Spudich, and E. F. DeLong. Bacterial Rhodopsin: Evidence for a New Type of Phototrophy in the Sea. *Science*, 289(5486):1902–1906, 2000.
- [110] J. M. Walter, D. Greenfield, C. Bustamante, and J. Liphardt. Light-powering *Escherichia coli* with proteorhodopsin. *Proceedings of the National Academy of Sciences*, 104(7):2408–2412, 2007.
- [111] G. Frangipane, D. Dell’Arciprete, S. Petracchini, C. Maggi, F. Saglimbeni, S. Bianchi, G. Vizsnyiczai, M. L. Bernardini, and R. Di Leonardo. Dynamic density shaping of photokinetic *E. coli*. *eLife*, 7:e36608, 2018.
- [112] J. Arlt, V. A. Martinez, A. Dawson, T. Pilizota, and W. C. K. Poon. Dynamics-dependent density distribution in active suspensions. *Nature Communications*, 10(1):2321, 2019.
- [113] Y. Hong, N. M. K. Blackman, N. D. Kopp, A. Sen, and D. Velegol. Chemotaxis of Nonbiological Colloidal Rods. *Physical Review Letters*, 99(17):178103, 2007.
- [114] S. Jahanshahi, C. Lozano, B. Liebchen, H. Löwen, and C. Bechinger. Realization of a motility-trap for active particles. *Communications Physics*, 3(1):127, 2020.
- [115] M. N. Popescu, W. E. Uspal, C. Bechinger, and P. Fischer. Chemotaxis of Active Janus Nanoparticles. *Nano Letters*, 18(9):5345–5349, 2018.
- [116] N. A. Söker, S. Auschra, V. Holubec, K. Kroy, and F. Cichos. How Activity Landscapes Polarize Microswimmers without Alignment Forces. *Physical Review Letters*, 126(22):228001, 2021.
- [117] S. Auschra, V. Holubec, N. A. Söker, F. Cichos, and K. Kroy. Polarization-Density Patterns of Active Particles in Motility Gradients. *Physical Review E*, 103(6):062601, 2021.

- [118] T. Mano, J.-B. Delfau, J. Iwasawa, and M. Sano. Optimal run-and-tumble-based transportation of a Janus particle with active steering. *Proceedings of the National Academy of Sciences*, 114(13):E2580–E2589, 2017.
- [119] B. Qian, D. Montiel, A. Bregulla, F. Cichos, and H. Yang. Harnessing Thermal Fluctuations for Purposeful Activities: The Manipulation of Single Micro-swimmers by Adaptive Photon Nudging. *Chemical Science*, 4(4):1420–1429, 2013.
- [120] V. N. Manoharan, M. T. Elsesser, and D. J. Pine. Dense Packing and Symmetry in Small Clusters of Microspheres. *Science*, 301(5632):483–487, 2003.
- [121] A. van Blaaderen. Colloidal Molecules and Beyond. *science*, 301(5632):470–472, 2003.
- [122] W. Li, H. Palis, R. Mérindol, J. Majimel, S. Ravaine, and E. Duguet. Colloidal molecules and patchy particles: Complementary concepts, synthesis and self-assembly. *Chemical Society Reviews*, 49(6):1955–1976, 2020.
- [123] G.-R. Yi, D. J. Pine, and S. Sacanna. Recent progress on patchy colloids and their self-assembly. *Journal of Physics: Condensed Matter*, 25(19):193101, 2013.
- [124] D. Morpew, J. Shaw, C. Avins, and D. Chakrabarti. Programming Hierarchical Self-Assembly of Patchy Particles into Colloidal Crystals *via* Colloidal Molecules. *ACS Nano*, 12(3):2355–2364, 2018.
- [125] H. Löwen. Active colloidal molecules. *EPL (Europhysics Letters)*, 121(5):58001, 2018.
- [126] D. Li, S. Banon, and S. L. Biswal. Bending dynamics of DNA-linked colloidal particle chains. *Soft Matter*, 6(17):4197, 2010.
- [127] J. Yan, M. Han, J. Zhang, C. Xu, E. Luijten, and S. Granick. Reconfiguring active particles by electrostatic imbalance. *Nature Materials*, 15(10):1095–1099, 2016.
- [128] S. Ebbens, R. A. L. Jones, A. J. Ryan, R. Golestanian, and J. R. Howse. Self-assembled autonomous runners and tumblers. *Physical Review E*, 82(1):015304, 2010.

- [129] J. N. Johnson, A. Nourhani, R. Peralta, C. McDonald, B. Thiesing, C. J. Mann, P. E. Lammert, and J. G. Gibbs. Dynamic stabilization of Janus sphere trans-dimers. *Physical Review E*, 95(4):042609, 2017.
- [130] A. Villa-Torrealba, C. Chávez-Raby, P. de Castro, and R. Soto. Run-and-tumble bacteria slowly approaching the diffusive regime. *Physical Review E*, 101(6):062607, 2020.
- [131] M. Doi and S. Edwards. *The Theory of Polymer Dynamics*, volume 73. Oxford University Press, 1988.
- [132] P.-G. de Gennes. *Scaling Concepts in Polymer Physics*. Cornell university press, 1979.
- [133] T. F. F. Farage, P. Krinninger, and J. M. Brader. Effective interactions in active Brownian suspensions. *Physical Review E*, 91(4):042310, 2015.
- [134] É. Fodor, C. Nardini, M. E. Cates, J. Tailleur, P. Visco, and F. van Wijland. How Far from Equilibrium Is Active Matter? *Physical Review Letters*, 117(3):038103, 2016.
- [135] D. Martin, J. O’Byrne, M. E. Cates, É. Fodor, C. Nardini, J. Tailleur, and F. van Wijland. Statistical mechanics of active Ornstein-Uhlenbeck particles. *Physical Review E*, 103(3):032607, 2021.
- [136] É. Fodor and M. Cristina Marchetti. The statistical physics of active matter: From self-catalytic colloids to living cells. *Physica A: Statistical Mechanics and its Applications*, 504:106–120, 2018.
- [137] L. Caprini and U. M. B. Marconi. Time-dependent properties of interacting active matter: Dynamical behavior of one-dimensional systems of self-propelled particles. *Physical Review Research*, 2(3):033518, 2020.
- [138] L. Caprini, U. M. B. Marconi, R. Wittmann, and H. Löwen. Dynamics of active particles with space-dependent swim velocity. *arXiv:2111.10304 [cond-mat]*, 2021.
- [139] L. Caprini, A. R. Sprenger, H. Löwen, and R. Wittmann. The Parental Active Model: A unifying stochastic description of self-propulsion. *The Journal of Chemical Physics*, 156(7):071102, 2022.

- [140] T.-C. Lee, M. Alarcón-Correa, C. Miksch, K. Hahn, J. G. Gibbs, and P. Fischer. Self-Propelling Nanomotors in the Presence of Strong Brownian Forces. *Nano Letters*, 14(5):2407–2412, 2014.
- [141] Y. Zhang and H. Hess. Chemically-powered swimming and diffusion in the microscopic world. *Nature Reviews Chemistry*, 5(7):500–510, 2021.
- [142] G. B. Arfken and H. J. Weber. *Mathematical Methods for Physicists*. American Association of Physics Teachers, 1999.
- [143] S. Hess. *Tensors for Physics*. Springer, Berlin, 2015.
- [144] M. E. Cates and J. Tailleur. When are active Brownian particles and run-and-tumble particles equivalent? Consequences for motility-induced phase separation. *EPL (Europhysics Letters)*, 101(2):20010, 2013.
- [145] A. P. Solon, M. E. Cates, and J. Tailleur. Active brownian particles and run-and-tumble particles: A comparative study. *The European Physical Journal Special Topics*, 224(7):1231–1262, 2015.
- [146] A. Duzgun and J. V. Selinger. Active Brownian particles near straight or curved walls: Pressure and boundary layers. *Physical Review E*, 97(3):032606, 2018.
- [147] N. Nikola, A. P. Solon, Y. Kafri, M. Kardar, J. Tailleur, and R. Voituriez. Active Particles with Soft and Curved Walls: Equation of State, Ratchets, and Instabilities. *Physical Review Letters*, 117(9):098001, 2016.
- [148] J. Tailleur and M. E. Cates. Sedimentation, trapping, and rectification of dilute bacteria. *EPL (Europhysics Letters)*, 86(6):60002, 2009.
- [149] M. Enculescu and H. Stark. Active Colloidal Suspensions Exhibit Polar Order under Gravity. *Physical Review Letters*, 107(5):058301, 2011.
- [150] S. Hermann and M. Schmidt. Active ideal sedimentation: Exact two-dimensional steady states. *Soft Matter*, 14(9):1614–1621, 2018.
- [151] J. Vachier and M. G. Mazza. Dynamics of sedimenting active Brownian particles. *The European Physical Journal E*, 42(1):11, 2019.

- [152] J. Palacci, C. Cottin-Bizonne, C. Ybert, and L. Bocquet. Sedimentation of active colloidal suspensions. *Physical Review Letters*, 105(8):088304, 2010.
- [153] A. Sharma and J. M. Brader. Brownian systems with spatially inhomogeneous activity. *Physical Review E*, 96(3):032604, 2017.
- [154] M. Eisenbach and J. W. Lengeler. *Chemotaxis*. Imperial College Press, London, 2004.
- [155] H. C. Berg. Chemotaxis in Bacteria. *Annual Review of Biophysics*, 4:119–136, 1975.
- [156] L. Alvarez, B. M. Friedrich, G. Gompper, and U. B. Kaupp. The computational sperm cell. *Trends in Cell Biology*, 24(3):198–207, 2014.
- [157] P. J. M. Van Haastert and P. N. Devreotes. Chemotaxis: Signalling the way forward. *Nature Reviews Molecular Cell Biology*, 5(8):626–634, 2004.
- [158] B. Liebchen and H. Löwen. Modelling chemotaxis of microswimmers: From individual to collective behavior. In *Chemical Kinetics: Beyond the Textbook*, pages 493–516. World Scientific, 2020.
- [159] H. Berg and E. Purcell. Physics of chemoreception. *Biophysical Journal*, 20(2):193–219, 1977.
- [160] P. C. Bressloff. *Stochastic Processes in Cell Biology: Volume I*, volume 41 of *Interdisciplinary Applied Mathematics*. Springer International Publishing, Cham, 2021.
- [161] D. J. Webre, P. M. Wolanin, and J. B. Stock. Bacterial chemotaxis. *Current Biology*, 13(2):R47–\$49, 2003.
- [162] P.-G. de Gennes. Chemotaxis: The role of internal delays. *European Biophysics Journal*, 33(8):691–693, 2004.
- [163] A. Celani and M. Vergassola. Bacterial strategies for chemotaxis response. *Proceedings of the National Academy of Sciences*, 107(4):1391–1396, 2010.
- [164] T. Jakuszeit, J. Lindsey-Jones, F. J. Peaudecerf, and O. A. Croze. Migration and accumulation of bacteria with chemotaxis and chemokinesis. *The European Physical Journal E*, 44(3):32, 2021.

- [165] J. E. Segall, S. M. Block, and H. C. Berg. Temporal comparisons in bacterial chemotaxis. *Proceedings of the National Academy of Sciences*, 83(23):8987–8991, 1986.
- [166] S. M. Block, J. E. Segall, and H. C. Berg. Impulse responses in bacterial chemotaxis. *Cell*, 31(1):215–226, 1982.
- [167] S. L. Porter, G. H. Wadhams, and J. P. Armitage. Signal processing in complex chemotaxis pathways. *Nature Reviews Microbiology*, 9(3):153–165, 2011.
- [168] G. Micali and R. G. Endres. Bacterial chemotaxis: Information processing, thermodynamics, and behavior. *Current Opinion in Microbiology*, 30:8–15, 2016.
- [169] U. B. Kaupp, N. D. Kashikar, and I. Weyand. Mechanisms of Sperm Chemotaxis. *Annual Review of Physiology*, 70(1):93–117, 2008.
- [170] P. Lertsethtakarn, K. M. Ottemann, and D. R. Hendrixson. Motility and Chemotaxis in *Campylobacter* and *Helicobacter*. *Annual Review of Microbiology*, 65(1):389–410, 2011.
- [171] G. H. Wadhams and J. P. Armitage. Making sense of it all: Bacterial chemotaxis. *Nature Reviews Molecular Cell Biology*, 5(12):1024–1037, 2004.
- [172] Y. Tu. Quantitative Modeling of Bacterial Chemotaxis: Signal Amplification and Accurate Adaptation. *Annual Review of Biophysics*, 42(1):337–359, 2013.
- [173] P. C. Bressloff. *Stochastic Processes in Cell Biology: Volume II*, volume 41 of *Interdisciplinary Applied Mathematics*. Springer International Publishing, Cham, 2021.
- [174] B. Jurado-Sánchez, M. Pacheco, R. Maria-Hormigos, and A. Escarpa. Perspectives on Janus micromotors: Materials and applications. *Applied Materials Today*, 9:407–418, 2017.
- [175] W. Duan, W. Wang, S. Das, V. Yadav, T. E. Mallouk, and A. Sen. Synthetic Nano- and Micromachines in Analytical Chemistry: Sensing, Migration, Capture, Delivery, and Separation. *Annual Review of Analytical Chemistry*, 8(1):311–333, 2015.

- [176] F. Wong, K. K. Dey, and A. Sen. Synthetic Micro/Nanomotors and Pumps: Fabrication and Applications. *Annual Review of Materials Research*, 46(1):407–432, 2016.
- [177] V. Yadav, W. Duan, P. J. Butler, and A. Sen. Anatomy of Nanoscale Propulsion. *Annual Review of Biophysics*, 44(1):77–100, 2015.
- [178] D. Needleman and Z. Dogic. Active matter at the interface between materials science and cell biology. *Nature Reviews Materials*, 2(9):1–14, 2017.
- [179] J. Parmar, D. Vilela, K. Villa, J. Wang, and S. Sánchez. Micro- and Nanomotors as Active Environmental Microcleaners and Sensors. *Journal of the American Chemical Society*, 140(30):9317–9331, 2018.
- [180] B. Jurado-Sánchez and J. Wang. Micromotors for environmental applications: A review. *Environmental Science: Nano*, 5(7):1530–1544, 2018.
- [181] M. Zarei and M. Zarei. Self-Propelled Micro/Nanomotors for Sensing and Environmental Remediation. *Small*, 14(30):1800912, 2018.
- [182] X. Ma, K. Hahn, and S. Sanchez. Catalytic Mesoporous Janus Nanomotors for Active Cargo Delivery. *Journal of the American Chemical Society*, 137(15):4976–4979, 2015.
- [183] L. Baraban, M. Tasinkevich, M. N. Popescu, S. Sanchez, S. Dietrich, and O. Schmidt. Transport of cargo by catalytic Janus micro-motors. *Soft Matter*, 8(1):48–52, 2012.
- [184] H. Merlitz, C. Wu, and J.-U. Sommer. Directional transport of colloids inside a bath of self-propelling walkers. *Soft Matter*, 13(20):3726–3733, 2017.
- [185] H. D. Vuijk, H. Merlitz, M. Lang, A. Sharma, and J.-U. Sommer. Chemotaxis of Cargo-Carrying Self-Propelled Particles. *Physical Review Letters*, 126(20):208102, 2021.
- [186] J. Wang and W. Gao. Nano/Microscale Motors: Biomedical Opportunities and Challenges. *ACS Nano*, 6(7):5745–5751, 2012.
- [187] M. Mathesh, J. Sun, and D. A. Wilson. Enzyme catalysis powered micro/nanomotors for biomedical applications. *Journal of Materials Chemistry B*, 8(33):7319–7334, 2020.

- [188] S. Wang, X. Liu, Y. Wang, D. Xu, C. Liang, J. Guo, and X. Ma. Biocompatibility of artificial micro/nanomotors for use in biomedicine. *Nanoscale*, 11(30):14099–14112, 2019.
- [189] M. Mathesh, J. Sun, F. van der Sandt, and D. A. Wilson. Supramolecular nanomotors with “pH taxis” for active drug delivery in the tumor microenvironment. *Nanoscale*, 12(44):22495–22501, 2020.
- [190] L. Reinišová, S. Hermanová, and M. Pumera. Micro/nanomachines: What is needed for them to become a real force in cancer therapy? *Nanoscale*, 11(14):6519–6532, 2019.
- [191] K. Kim, J. Guo, Z. Liang, and D. Fan. Artificial Micro/Nanomachines for Bioapplications: Biochemical Delivery and Diagnostic Sensing. *Advanced Functional Materials*, 28(25):1705867, 2018.
- [192] B.-W. Park, J. Zhuang, O. Yasa, and M. Sitti. Multifunctional Bacteria-Driven Microswimmers for Targeted Active Drug Delivery. *ACS Nano*, 11(9):8910–8923, 2017.
- [193] B. E.-F. de Ávila, P. Angsantikul, J. Li, M. Angel Lopez-Ramirez, D. E. Ramírez-Herrera, S. Thamphiwatana, C. Chen, J. Delezuk, R. Samakapiruk, V. Ramez, M. Obonyo, L. Zhang, and J. Wang. Micromotor-enabled active drug delivery for in vivo treatment of stomach infection. *Nature Communications*, 8(1):272, 2017.
- [194] M. Xuan, J. Shao, X. Lin, L. Dai, and Q. He. Self-Propelled Janus Mesoporous Silica Nanomotors with Sub-100 nm Diameters for Drug Encapsulation and Delivery. page 6, 2014.
- [195] F. Qiu, S. Fujita, R. Mhanna, L. Zhang, B. R. Simona, and B. J. Nelson. Magnetic Helical Microswimmers Functionalized with Lipoplexes for Targeted Gene Delivery. *Advanced Functional Materials*, 25(11):1666–1671, 2015.
- [196] W. Gao and J. Wang. Synthetic micro/nanomotors in drug delivery. *Nanoscale*, 6(18):10486–10494, 2014.
- [197] A. Ghosh, W. Xu, N. Gupta, and D. H. Gracias. Active matter therapeutics. *Nano Today*, 31:100836, 2020.
- [198] S. Ebbens. Active colloids: Progress and challenges towards realising autonomous applications. *Current Opinion in Colloid & Interface Science*, 21:14–23, 2016.



- [199] Y. Hong, D. Velegol, N. Chaturvedi, and A. Sen. Biomimetic behavior of synthetic particles: From microscopic randomness to macroscopic control. *Phys. Chem. Chem. Phys.*, 12(7):1423–1435, 2010.
- [200] H. D. Vuijk, A. Sharma, D. Mondal, J.-U. Sommer, and H. Merlitz. Pseudochemotaxis in inhomogeneous active Brownian systems. *Physical Review E*, 97(4):042612, 2018.
- [201] A. Szabo, K. Schulten, and Z. Schulten. First passage time approach to diffusion controlled reactions. *The Journal of Chemical physics*, 72(8):4350–4357, 1980.
- [202] Y. Fily and M. C. Marchetti. Athermal Phase Separation of Self-Propelled Particles with No Alignment. *Physical Review Letters*, 108(23):235702, 2012.
- [203] R. Wittmann and J. M. Brader. Active Brownian particles at interfaces: An effective equilibrium approach. *EPL (Europhysics Letters)*, 114(6):68004, 2016.
- [204] C. Maggi, U. M. B. Marconi, N. Gnan, and R. Di Leonardo. Multidimensional stationary probability distribution for interacting active particles. *Scientific Reports*, 5(1):10742, 2015.
- [205] U. Marini Bettolo Marconi and C. Maggi. Towards a statistical mechanical theory of active fluids. *Soft Matter*, 11(45):8768–8781, 2015.
- [206] R. F. Fox. Functional-calculus approach to stochastic differential equations. *Physical Review A*, 33(1):467–476, 1986.
- [207] R. F. Fox. Uniform convergence to an effective Fokker-Planck equation for weakly colored noise. *Physical Review A*, 34(5):4525–4527, 1986.
- [208] A. Sharma, R. Wittmann, and J. M. Brader. Escape rate of active particles in the effective equilibrium approach. *Physical Review E*, 95(1):012115, 2017.
- [209] F. Peng, Y. Tu, J. C. M. van Hest, and D. A. Wilson. Self-Guided Supramolecular Cargo-Loaded Nanomotors with Chemotactic Behavior towards Cells. *Angewandte Chemie International Edition*, 54(40):11662–11665, 2015.

- [210] P. K. Ghosh, Y. Li, F. Marchesoni, and F. Nori. Pseudo-Chemotactic Drifts of Artificial Microswimmers. *Physical Review E*, 92(1):012114, 2015.
- [211] A. Geiseler, P. Hänggi, F. Marchesoni, C. Mulhern, and S. Savel'ev. Chemotaxis of artificial microswimmers in active density waves. *Physical Review E*, 94(1):012613, 2016.
- [212] D. T. Gillespie. *Markov Processes: An Introduction for Physical Scientists*. Academic Press, 1991.
- [213] I. Richard Lapidus. "Pseudochemotaxis" by micro-organisms in an attractant gradient. *Journal of Theoretical Biology*, 86(1):91–103, 1980.
- [214] H. Merlitz, H. D. Vuijk, R. Wittmann, A. Sharma, and J.-U. Sommer. Pseudo-chemotaxis of active Brownian particles competing for food. *PLOS ONE*, 15(4):e0230873, 2020.
- [215] H. D. Vuijk, S. Klempahn, H. Merlitz, J.-U. Sommer, and A. Sharma. Active colloidal molecules in activity gradients. *Physical Review E*, 106(1):014617, 2022.
- [216] P. M. Morse and H. Feshbach. *Methods of Theoretical Physics: Part 1*, volume 1. McGraw-Hill, 1953.
- [217] A. Iniesta and J. García de la Torre. A second-order algorithm for the simulation of the Brownian dynamics of macromolecular models. *The Journal of Chemical Physics*, 92(3):2015–2018, 1990.
- [218] K. Klenin, H. Merlitz, and J. Langowski. A Brownian Dynamics Program for the Simulation of Linear and Circular DNA and Other Wormlike Chain Polyelectrolytes. *Biophysical Journal*, 74(2):780–788, 1998.
- [219] J. D. Weeks, D. Chandler, and H. C. Andersen. The role of repulsive forces in determining the equilibrium structure of simple liquids. *The Journal of Chemical physics*, 54(12):5237–5247, 1971.
- [220] J. Elgeti and G. Gompper. Wall accumulation of self-propelled spheres. *EPL (Europhysics Letters)*, 101(4):48003, 2013.
- [221] J. Elgeti and G. Gompper. Run-and-tumble dynamics of self-propelled particles in confinement. *Europhysics Letters*, 101(5):58003, 2015.

- [222] M. Born and R. Oppenheimer. Zur Quantentheorie der Molekeln. *Annalen der Physik*, 389(20):457–484, 1927.
- [223] J. A. Kromer, N. de la Cruz, and B. M. Friedrich. Chemokinetic scattering, trapping, and avoidance of active Brownian particles. *Physical Review Letters*, 124(11):118101, 2020.
- [224] M. E. Cates. Diffusive transport without detailed balance in motile bacteria: Does microbiology need statistical physics? *Reports on Progress in Physics*, 75(4):042601, 2012.
- [225] C. Lozano and C. Bechinger. Diffusing wave paradox of phototactic particles in traveling light pulses. *Nature Communications*, 10(1):2495, 2019.
- [226] A. Kaiser, S. Babel, B. ten Hagen, C. von Ferber, and H. Löwen. How does a flexible chain of active particles swell? *The Journal of Chemical Physics*, 142(12):124905, 2015.
- [227] R. G. Winkler and G. Gompper. The physics of active polymers and filaments. *The Journal of Chemical Physics*, 153(4):040901, 2020.
- [228] J. Tailleur and M. E. Cates. Statistical Mechanics of Interacting Run-and-Tumble Bacteria. *Physical Review Letters*, 100(21):218103, 2008.
- [229] B. Liebchen and H. Löwen. Synthetic Chemotaxis and Collective Behavior in Active Matter. *Accounts of Chemical Research*, 51(12):2982–2990, 2018.
- [230] S. Saha, R. Golestanian, and S. Ramaswamy. Clusters, asters, and collective oscillations in chemotactic colloids. *Physical Review E*, 89(6):062316, 2014.
- [231] O. Pohl and H. Stark. Dynamic Clustering and Chemotactic Collapse of Self-Phoretic Active Particles. *Physical Review Letters*, 112(23):238303, 2014.
- [232] B. Nasouri and R. Golestanian. Exact Phoretic Interaction of Two Chemically Active Particles. *Physical Review Letters*, 124(16):168003, 2020.
- [233] K. Kaneko. Adiabatic Elimination by the eigenfunction Expansion method. 66(1), 1981.

- [234] H. D. Vuijk, J. U. Sommer, H. Merlitz, J. M. Brader, and A. Sharma. Lorentz forces induce inhomogeneity and flux in active systems. *Physical Review Research*, 2(1):013320, 2020.
- [235] H. Risken. *The Fokker-Planck Equation*. Springer, 1996.
- [236] M. te Vrugt and R. Wittkowski. Relations between angular and Cartesian orientational expansions. *AIP Advances*, 10(3):035106, 2020.
- [237] P. G. de Gennes and J. Prost. *The Physics of Liquid Crystals*. Number 83 in International Series of Monographs on Physics. Oxford University Press, 1993.
- [238] A. Baskaran and M. C. Marchetti. Hydrodynamics of self-propelled hard rods. *Physical Review E*, 77(1):011920, 2008.
- [239] A. Y. Grosberg and J.-F. Joanny. Nonequilibrium statistical mechanics of mixtures of particles in contact with different thermostats. *Physical Review E*, 92(3):032118, 2015.
- [240] S. N. Weber, C. A. Weber, and E. Frey. Binary Mixtures of Particles with Different Diffusivities Demix. *Physical Review Letters*, 116(5):058301, 2016.
- [241] E. Ilker and J.-F. Joanny. Phase separation and nucleation in mixtures of particles with different temperatures. *Physical Review Research*, 2(2):023200, 2020.
- [242] M. Wang and A. Y. Grosberg. Three-body problem for Langevin dynamics with different temperatures. *Physical Review E*, 101(3):032131, 2020.
- [243] D. Levis and L. Berthier. From single-particle to collective effective temperatures in an active fluid of self-propelled particles. *EPL (Europhysics Letters)*, 111(6):60006, 2015.
- [244] G. Szamel. Self-propelled particle in an external potential: Existence of an effective temperature. *Physical Review E*, 90(1):012111, 2014.
- [245] A. Geiseler, P. Hänggi, and F. Marchesoni. Self-Polarizing Microswimmers in Active Density Waves. *Scientific Reports*, 7(1):41884, 2017.

- [246] C. Maggi, L. Angelani, G. Frangipane, and R. Di Leonardo. Currents and flux-inversion in photokinetic active particles. *Soft Matter*, 14(24):4958–4962, 2018.
- [247] H. Merlitz, H. D. Vuijk, J. Brader, A. Sharma, and J.-U. Sommer. Linear response approach to active Brownian particles in time-varying activity fields. *The Journal of Chemical Physics*, 148(19):194116, 2018.
- [248] A. Nourhani, S. J. Ebbens, J. G. Gibbs, and P. E. Lammert. Spiral diffusion of rotating self-propellers with stochastic perturbation. *Physical Review E*, 94(3):030601, 2016.
- [249] S. A. Mallory, F. Alarcon, A. Cacciuto, and C. Valeriani. Self-assembly of active amphiphilic Janus particles. *New Journal of Physics*, 19(12):125014, 2017.
- [250] F. Schmidt, B. Liebchen, H. Löwen, and G. Volpe. Light-controlled Assembly of Active Colloidal Molecules. *The Journal of Chemical Physics*, 150(9):094905, 2019.
- [251] R. G. Winkler, J. Elgeti, and G. Gompper. Active Polymers — Emergent Conformational and Dynamical Properties: A Brief Review. *Journal of the Physical Society of Japan*, 86(10):101014, 2017.
- [252] S. M. Mousavi, G. Gompper, and R. G. Winkler. Active Brownian ring polymers. *The Journal of Chemical Physics*, 150(6):064913, 2019.
- [253] A. Martin-Gomez, T. Eisenstecken, G. Gompper, and R. G. Winkler. Active Brownian filaments with hydrodynamic interactions: Conformations and dynamics. *Soft Matter*, 15(19):3957–3969, 2019.
- [254] T. Eisenstecken and R. G. Winkler. Path integral description of semiflexible active Brownian polymers. *The Journal of Chemical Physics*, 156(6):064105, 2022.
- [255] J. Smrek, I. Chuback, C. N. Likos, and K. Kremer. Active topological glass. *Nature Communications*, 11(26), 2020.
- [256] I. Chubak, C. N. Likos, K. Kremer, and J. Smrek. Emergence of active topological glass through directed chain dynamics and nonequilibrium phase segregation. *Physical Review Research*, 2(4):043249, 2020.

- [257] J. Smrek and K. Kremer. Small activity differences drive phase separation in active-passive polymer mixtures. *Physical Review Letters*, 118(9):098002, 2017.
- [258] P. Attard. Design of Chemotaxis Devices Using Nano-Motors. *arXiv:1209.1448 [cond-mat, physics:physics]*, 2012.
- [259] Q. Chen, S. C. Bae, and S. Granick. Directed self-assembly of a colloidal kagome lattice. *Nature*, 469(7330):381–384, 2011.
- [260] E. Bianchi, R. Blaak, and C. N. Likos. Patchy colloids: State of the art and perspectives. *Physical Chemistry Chemical Physics*, 13(14):6397, 2011.
- [261] S. Sacanna, W. T. M. Irvine, P. M. Chaikin, and D. J. Pine. Lock and key colloids. *Nature*, 464(7288):575–578, 2010.
- [262] S. C. Glotzer and M. J. Solomon. Anisotropy of building blocks and their assembly into complex structures. *Nature Materials*, 6(8):557–562, 2007.
- [263] J. Zhang, J. Yan, and S. Granick. Directed Self-Assembly Pathways of Active Colloidal Clusters. *Angewandte Chemie*, 128(17):5252–5255, 2016.
- [264] M. N. Popescu. Chemically Active Particles: From One to Few on the Way to Many. *Langmuir*, 36(25):6861–6870, 2020.
- [265] L. Caprini, U. M. B. Marconi, C. Maggi, M. Paoluzzi, and A. Puglisi. Hidden velocity ordering in dense suspensions of self-propelled disks. *Physical Review Research*, 2(2):023321, 2020.
- [266] R. Golestanian. Anomalous Diffusion of Symmetric and Asymmetric Active Colloids. *Physical Review Letters*, 102(18):188305, 2009.
- [267] M. N. Popescu, M. Tasinkevych, and S. Dietrich. Pulling and pushing a cargo with a catalytically active carrier. *EPL (Europhysics Letters)*, 95(2):28004, 2011.
- [268] S. Y. Reigh and R. Kapral. Catalytic dimer nanomotors: Continuum theory and microscopic dynamics. *Soft Matter*, 11(16):3149–3158, 2015.
- [269] S. Y. Reigh, P. Chuphal, S. Thakur, and R. Kapral. Diffusiophoretically induced interactions between chemically active and inert particles. *Soft Matter*, 14(29):6043–6057, 2018.

- [270] A. Majee. Rotational motion of dimers of Janus particles. *The European Physical Journal E*, 40(3):30, 2017.
- [271] H. Löwen. Chirality in microswimmer motion: From circle swimmers to active turbulence. *The European Physical Journal Special Topics*, 225(11-12):2319–2331, 2016.
- [272] C. Hargus, J. M. Epstein, and K. K. Mandadapu. Odd Diffusivity of Chiral Random Motion. *Physical Review Letters*, 127(17):178001, 2021.
- [273] L. Caprini and U. Marini Bettolo Marconi. Active chiral particles under confinement: Surface currents and bulk accumulation phenomena. *Soft Matter*, 15(12):2627–2637, 2019.
- [274] B. M. Friedrich and F. Jülicher. Chemotaxis of sperm cells. *Proceedings of the National Academy of Sciences*, 104(33):13256–13261, 2007.
- [275] I. Abdoli, E. Kalz, H. D. Vuijk, R. Wittmann, J.-U. Sommer, J. M. Brader, and A. Sharma. Correlations in multithermostat Brownian systems with Lorentz force. *New Journal of Physics*, 22(9):093057, 2020.
- [276] S. Sánchez, L. Soler, and J. Katuri. Chemically Powered Micro- and Nanomotors. *Angewandte Chemie International Edition*, 54(5):1414–1444, 2015.
- [277] E. Kalz, H. D. Vuijk, I. Abdoli, J.-U. Sommer, H. Löwen, and A. Sharma. Collisions enhance self-diffusion in odd-diffusive systems. *arXiv:2206.13566*, 2022.
- [278] M. Mijalkov and G. Volpe. Sorting of chiral microswimmers. *Soft Matter*, page 7, 2013.
- [279] P. L. Muzzeddu, H. D. Vuijk, H. Lowen, J.-U. Sommer, and A. Sharma. Active chiral molecules in activity gradients. *arXiv*, 2022.
- [280] H. D. Vuijk, J. M. Brader, and A. Sharma. Anomalous fluxes in overdamped Brownian dynamics with Lorentz force. *Journal of Statistical Mechanics: Theory and Experiment*, 2019(6):063203, 2019.
- [281] I. Abdoli, H. D. Vuijk, J. U. Sommer, J. M. Brader, and A. Sharma. Nondiffusive fluxes in a Brownian system with Lorentz force. *Physical Review E*, 101(1):012120, 2020.

- [282] I. Abdoli, H. D. Vuijk, R. Wittmann, J. U. Sommer, J. M. Brader, and A. Sharma. Stationary state in Brownian systems with Lorentz force. *Physical Review Research*, 2(2):023381, 2020.
- [283] C. Hargus, K. Klymko, J. M. Epstein, and K. K. Mandadapu. Time reversal symmetry breaking and odd viscosity in active fluids: Green–Kubo and NEMD results. *The Journal of Chemical Physics*, 152(20):201102, 2020.
- [284] J. Katuri, X. Ma, M. M. Stanton, and S. Sánchez. Designing Micro- and Nanoswimmers for Specific Applications. *Accounts of Chemical Research*, 50(1):2–11, 2017.
- [285] D. Yamamoto and A. Shioi. Self-Propelled Nano/Micromotors with a Chemical Reaction: Underlying Physics and Strategies of Motion Control. *KONA Powder and Particle Journal*, 32(0):2–22, 2015.
- [286] D. Acheson. *Elementary Fluid Dynamics*. Oxford Applied Mathematics and Computing Science Series. Oxford University Press, first edition, 2009.
- [287] L. D. Landau and E. M. Lifshits. *Fluid Mechanics*, volume 6 of *Course of Theoretical Physics*. Butterworth-Heinemann, second edition, 1987.
- [288] C. Pozrikidis. *Fluid Dynamics*. Springer US, Boston, MA, 2017.
- [289] J. Happel and H. Brenner. *Low Reynolds Number Hydrodynamics*, volume 1 of *Mechanics of Fluids and Transport Processes*. Springer Netherlands, Dordrecht, 1981.
- [290] E. Lauga, M. P. Brenner, and H. A. Stone. Microfluidics: The no-slip boundary condition. *arXiv:cond-mat/0501557*, 2005.
- [291] J. K. G. Dhont and W. J. Briels. Rod-like Brownian Particles in Shear Flow. In *Soft Matter: Complex Colloidal Suspensions*, volume 2, pages 147–283. John Wiley & Sons, Ltd, 2005.
- [292] R. G. Cox. The motion of long slender bodies in a viscous fluid Part 1. General theory. *Journal of Fluid Mechanics*, 44(04):791, 1970.
- [293] J. P. K. Tillett. Axial and transverse Stokes flow past slender axisymmetric bodies. *Journal of Fluid Mechanics*, 44(3):401–417, 1970.
- [294] H. A. Stone and A. D. T. Samuel. Propulsion of Microorganisms by Surface Distortions. *Physical Review Letters*, 77(19):4102–4104, 1996.





# List of Publications

## Publications used in this Thesis:

- Chapter 5: H.D. Vuijk, A. Sharma, D. Mondal, J.-U. Sommer, and H. Merlitz. Pseudochemotaxis in inhomogeneous active systems. *Physical Review E*, 97(4), 2018.
- Chapter 6: H.D. Vuijk, H. Merlitz, M. Lang, A. Sharma, and J.-U. Sommer. Chemotaxis of cargo-carrying active particles. *Physical Review Letters*, 126(20), 2021.
- Chapter 7: H.D. Vuijk, S. Klempahn, H. Merlitz, J.-U. Sommer, and A. Sharma. Active colloidal molecules in activity gradients. *Physical Review E*, 106(1), 2022.
- Chapter 8: H. Merlitz, H. Vuijk, J. Brader, A. Sharma, J.-U. Sommer. Linear response approach to active Brownian particles in time-varying activity fields. *The Journal of Chemical Physics*, 148(19), 2018.

## Publications not discussed in this thesis:

- Odd-diffusive systems
  - E. Kalz\*, H.D. Vuijk\*, I. Abdoli, J.-U. Sommer, H. Löwen, A. Sharma. Collisions enhance self-diffusion in odd-diffusive systems. Accepted for publication in *Physical Review Letters*.  
\* Joint first author.
  - H.D. Vuijk, J.-U. Sommer, H. Merlitz, J.M. Brader, A. Sharma. Lorentz forces induce inhomogeneity and flux in active systems. *Physical Review Research*, 2(1), 2020.
  - H.D. Vuijk, J.M. Brader, and A. Sharma. Anomalous fluxes in overdamped Brownian dynamics with Lorentz force. *Journal of Statistical Mechanics: Theory and Experiment*, 2019(6), 2019.

- I. Abdoli, H.D. Vuijk, R. Wittmann, J.-U. Sommer, J.M. Brader, and A. Sharma. Correlations in multithermostat Brownian systems with Lorentz force. *New Journal of Physics*, 22(9), 2020.
- I. Abdoli, H.D. Vuijk, R. Wittmann, J.-U. Sommer, J.M. Brader, and A. Sharma. Stationary state in Brownian systems with Lorentz force. *Physical Review Research*, 2(2), 2020.
- I. Abdoli, H.D. Vuijk, J.-U. Sommer, J.M. Brader, and A. Sharma. Nondiffusive fluxes in a Brownian system with Lorentz force. *Physical Review E*, 101(1), 2020.
- E. Kalz, H.D. Vuijk, J.M. Brader, J.-U. Sommer, A. Sharma. Force autocorrelation function of odd-diffusive Brownian particles. *In preparation*
- Statistical Mechanics of Fluids:
  - H.D. Vuijk, J.M. Brader, A. Sharma. Effect of anisotropic diffusion on spinodal decomposition. *Soft Matter*, 15(6), 2019.
  - S.M. Tschopp, H.D. Vuijk, A. Sharma, J.M. Brader. Mean-Field theory of inhomogeneous fluids. *Physical Review E*, 102(4), 2020.
- Inhomogeneous Activity:
  - P.L. Muzzeddu, H.D. Vuijk, H. Löwen, J.-U. Sommer, and A. Sharma. Active Chiral Molecules in activity gradients. Submitted to *The Journal of Chemical Physics*.
  - H. Merlitz, H.D. Vuijk, R. Wittmann, A. Sharma, and J.-U. Sommer. Pseudo-chemotaxis of active Brownian particles competing for food. *PLOS ONE*, 15(4), 2020.

# Eidesstattliche Erklärung

Hiermit versichere ich, dass ich die vorliegende Arbeit ohne unzulässige Hilfe Dritter und ohne Benutzung anderer als der angegebenen Hilfsmittel angefertigt habe; die aus fremden Quellen direkt oder indirekt übernommenen Gedanken sind als solche kenntlich gemacht. Die Arbeit wurde bisher weder im Inland noch im Ausland in gleicher oder ähnlicher Form einer anderen Prüfungsbehörde vorgelegt.

Diese Dissertation wurde am Leibniz-Institut für Polymerforschung Dresden e.V. im Institut Theorie der Polymere unter wissenschaftlicher Betreuung von Prof. Dr. Jens-Uwe Sommer (betreuender Hochschullehrer) angefertigt.

Ich erkenne die Promotionsordnung des Bereichs Mathematik und Naturwissenschaften der Technischen Universität Dresden vom 23.02.2011 an.

Unterschrift:

Datum: